University of Wisconsin Milwaukee
UWM Digital Commons

Theses and Dissertations

August 2018

Graphene-Based Lubrication for Tribological Applications: Nanolubricants and Self-lubricating Nanocomposites

Emad Omrani
University of Wisconsin-Milwaukee

Follow this and additional works at: https://dc.uwm.edu/etd

Part of the Materials Science and Engineering Commons, and the Mechanical Engineering Commons

Recommended Citation

Omrani, Emad, "Graphene-Based Lubrication for Tribological Applications: Nanolubricants and Self-lubricating Nanocomposites" (2018). *Theses and Dissertations*. 1890.
https://dc.uwm.edu/etd/1890

GRAPHENE-BASED LUBRICATION FOR TRIBOLOGICAL APPLICATIONS: NANOLUBRICANTS AND SELF-LUBRICATING NANOCOMPOSITES

by

Emad Omrani

A Dissertation Submitted in

Partial Fulfillment of the

Requirements for the Degree of

Doctor of Philosophy

in Engineering

at

The University of Wisconsin-Milwaukee

August 2018

ABSTRACT

GRAPHENE-BASED LUBRICATION FOR TRIBOLOGICAL APPLICATIONS: NANOLUBRICANTS AND SELF-LUBRICATING NANOCOMPOSITES

by

Emad Omrani

The University of Wisconsin-Milwaukee, 2018
Under the Supervision of Professor Pradeep K. Rohatgi

In this work, the effects of graphene nanoplatelets (GNPs) additives on tribological properties of aluminum are investigated. The objective of this research is to investigate and explain the enhancement mechanisms of GNPs at the contact surface during tribological testing. The graphene nanoplatelets are studied both as an oil additive (Chapter I) and as a reinforcement (Chapter II) experimentally. The coefficient of friction (COF) and wear rate were identified using a pin-on-disk test setup.

Mineral, organic, and synthetic oils are not always efficient enough to satisfy the demands of a high-performance lubricant; therefore, mixing additives with base fluids is an approach to improve the lubrication ability and to reduce friction and wear. In chapter I, GNPs are used as lubricant additives to make nanolubricants. Then, the combined effect of the material's variables (GNPs loading, size, and dispersion stability) and tribo test's variable (applied normal load) are investigated on COF and wear rate of aluminum. Tribological studies are all carried out in the boundary lubrication regime. Three-

dimensional surface metrology is performed using an optical profilometer. Various surface analyses, including Scanning Electron Microscope (SEM), Energy-Dispersive X-ray Spectroscopy (EDX), and Raman Spectroscopy are performed to assess the chemical elements on the tested surfaces. The experimental and theoretical analyses show that GNPs are effective in reducing friction and wear, although, this positive effect is more influential at higher loads. Also, it is demonstrated that there is a critical concentration of GNPs, below which a reduced wear rate is not sustained. The proposed mechanism to describe the effect of GNPs in boundary lubrication condition is "reduced direct metal-metal contact area" at the contact surface. In other words, a material which has low shear strength layers sits between two contacting surfaces and separates the two sliding metal surfaces with no actual contact between them. This means that there is less formation of asperity junctions between the two surfaces.

Although liquid-based lubricants are efficient enough in most tribological applications, there are circumstances, such as extreme environmental conditions such as high or low temperatures, vacuum, radiation, and high contact pressure in some aerospace applications, where no liquid lubricants can be present. In addition, interminable providing of lubricant at the contact surface is another challenge ahead. In order to respond to these challenges of using liquid oil at extreme environmental conditions, in chapter II of this dissertation, the synthesis and performance of self-lubricating aluminum matrix nanocomposite are evaluated (Chapter II). Aluminum powder is mixed with varying concentrations of GNPs and alumina nanoparticles to form a hybrid metal matrix nanocomposite. High-energy ball milling is conducted at room temperature while powders are immersed and protected by benzene bath. Degassing is accomplished by heating to 135ºC. Consolidation of the powders is conducted by single

action cold compaction and single action hot compaction. Pin-on-disk experiments are conducted to investigate the tribological behavior of aluminum matrix composites reinforced by GNPs and compare them with unreinforced aluminum. Then, the combined effect of material's variables (reinforcement type and loading) and tribo test's variable (applied normal load) were investigated on COF and wear rate of aluminum. SEM and EDX were performed to assess the stoichiometry of the elements on the tribo surfaces. In addition, Raman Spectroscopy and Transmission Electron Microscopy (TEM) were also performed to identify the bonding/interactions between the phases on the surface. Results imply that the COF and wear rate of composites decrease by embedding graphene nanoparticles due to reduction the real contact area between the mating surfaces by forming the lubricant. Besides, the addition of alumina particles in Aluminum/GNPs composites can further improve COF and wear rate because of rolling effect of alumina nanoparticles.

Increasing the loading of GNPs reduces the COF, while there is an optimum concentration of GNPs, above and below which the wear rate is increased. In addition, the COF and wear of all composites decreases by increasing normal load. Based on the observations, multiple mechanisms are proposed to describe the improved tribological behavior of the synthesized self-lubricating nanocomposites. In addition to the reduced direct metal-metal contact area at the contact surface, the fact that the layered GNPs structure is exposed to at the contact surface keeps the surface lubricated. In other words, under sliding conditions, the transfer layer formation of the GNPs on the tribo surfaces acts as a solid lubricant film, which prevents direct contact between the mating surfaces. Additionally, it is experimentally confirmed that GNPs prevent the surface from oxygen diffusion, thereby reducing the amount of oxides which are harder and more abrasive at

the contact surface. "Load bearing" of added alumina nanoparticles, in addition to the increased hardness of the matrix, is another proposed mechanism of wear resistance enhancement. It has been shown that an effective lubricant layer forms when the solid lubricant has a strong adhesion to the bearing surface; otherwise, this lubricant layer can be easily rubbed away and tends to have a very short service life. Raman data confirms the formation of Al_4C_3 bonds on the tribo layer under certain test conditions.

I dedicate this research work to my lovely wife

Afsaneh

FOR HER UNCONDITIONAL LOVE AND SUPPORT.

I LOVE YOU.

also

This is dedicated to my beloved parents who spent their life dedicated to their

children by their endless love, support, and encouragements, may you find your path.

TABLE OF CONTENTS

LIST OF FIGURES

xiii

LIST OF TABLES

ACKNOWLEDGMENTS

I would like to thank my advisor Distinguished Professor Pradeep K. Rohatgi for the invaluable chance to pursue research under him. All guidance, motivation, advice, and patience from him have been channeled properly. He has inspired me to become an independent researcher and helped me realize the power of critical reasoning. He also demonstrated what a brilliant and hard-working scientist can accomplish.

My sincere thanks must also go to the members of my thesis advisory and exam committee: Prof. Lopez, Dr. Church, Dr. Menezes, and Dr. Nosonovsky for their helpful career advice and suggestions in general. In particular, Dr. Menezes showed me the great power and potential of myself.

Valuable help from Dr. Hardcastle for advanced analysis and characterization is greatly appreciated.

Special thanks to Dr. Sohn and Abhishek Mehta at the University of Florida for their TEM work, as well as to Mr. Rasoulian at Marquette University to help for using a viscometer.

There is no way to express how much it meant to me to have been a member of the Center for Composite Materials. These brilliant friends and colleagues inspired me over many years. Thank you, the students of the Center for Composite Materials.

I gratefully acknowledge the support of the UWM IAC Center, Dr. Yuan and Dr. Amano for supporting me financially during my Ph.D. program. Special thanks to Dr. Nasiri, Dean of Graduate office of Engineering Department for supporting me during my course of graduate studies.

Words cannot express how grateful I am to my family who support me in all areas of life. I deeply thank my parents.

I cannot forget friends who went through hard times with me, cheered me on, and celebrated each accomplishment.

Last but certainly not least, I would like to thank my colleague and my wife, Afsaneh, who helped me in all of the stages of the work. Afsaneh has been my best friend and great companion who loved, supported, encouraged, entertained, and helped me get through this agonizing period in the most positive way.

1 CHAPTER I: EFFECT OF GRAPHENE AS OIL ADDITIVE

1.1 INTRODUCTION

Friction and wear is a problem that affects practically every field of engineering. Wear has the effect of reducing the life of materials and causing eventual failures of the mechanical systems. A common example is the internal combustion engine, where the wear in engine cylinders reduces the effectiveness of piston ring seals, thereby reducing the combustion pressure and engine power. In practically any mechanical system, all friction ends up as lost energy, reducing the overall efficiency. Finally, friction can cause runaway heating that can damage or destroy mechanical components.

Base oils (vegetable oils, mineral oils, and synthetic oils) cannot always satisfy the demands of a high-performance lubricant by themselves [1]. For this reason, additives are mixed with base fluids to improve upon the lubricant's ability to reduce friction and wear, increase viscosity, improve viscosity index, resist corrosion and oxidation, increase component and lubricant lifetime, and minimize contamination [2]. Additives are synthetic chemical substances mixed with base oils to improve various characteristics of lubricants, so, the oils can placate the higher demand placed on them and satisfy specification requirements. Additives often improve existing properties, suppress undesirable properties, and introduce new properties to the base oils. One of the most important properties that additives enhance is a lubricant's ability to form protective films, which is especially important in boundary lubrication conditions. The use of additives has a large influence on the performance of lubricants that makes it possible to fulfill the increasingly complex demands placed on lubricants. When blending additives with base oils, it is important to have a well-balanced and optimized composition to improve the performance of the lubricant.

1.1.1 OBJECTIVE FOR GREEN OILS

It has been reported that 50% of all lubricants worldwide end up in the environment through usage, spillage, volatility, or improper disposal [3]. These oils typically are not environmentally friendly or biodegradable and are toxic to the environment by contaminating soil, air, and drinking water. Moreover, concerns for the depletion of crude oil reserves and increases in the price of oil have had an impact on the use of petroleum-based oils. These factors have caused the lubrication industry to develop and implement environmentally friendly lubricants. These 'green' lubricants are typically derived from organic materials that are non-toxic, renewable, and provide feasible and economic alternatives to traditional lubricants [4, 5]. For this reason, there has been a revival in the development of environmentally friendly or environmentally benign lubricants that satisfy the combination of environmental, health, economic, and performance challenges of modern lubricants.

Vegetable oils meet many of the requirements as alternatives to traditional petroleum-based lubricants because they are renewable, biodegradable, non-toxic, and have minimal environmental pollution and production costs [6]. Vegetable oils also exhibit higher lubricity, lower volatility, higher shear stability, higher viscosity index, higher load carrying index, and superior detergency and dispersancy when compared with mineral and synthetic oils [7, 8]. Despite the environmental advantages to using pure natural oils, they do suffer from poor thermal and oxidative stability, biological (bacterial) deterioration, hydrolytic instability, poor fluid flow behavior, solidification at low temperatures, and, occasionally, high wear rates [9-12]. They are also susceptible to

3

oxidative degradation due to the presence of free fatty acids and the presence of double bonds in the carbon chain.

1.1.2 OBJECTIVE FOR OIL ADDITIVE

Lubricant additives have an important influence on the performance of lubricants. These additives are active ingredients which can be added during a blending process to base oils in order to either enhance the existing performance of the base fluids or impart new properties that the base fluids lack.

Most of the lubricant oils at present contain several critical lubricant additives, including antiwear additives, dispersants, detergents, friction modifiers, viscosity index improvers, and antioxidants. Traditionally, oils are presented as a single-phase material to maintain a good consistency and dispersibility of the lubricant additives in the base oil. However, a great amount of research has been focused on introducing solid particles as a friction reduction or antiwear lubricant additive over recent years due to a number of incomparable advantages of the two-phase lubricant oils (liquid-solid), such as the superior thermal conductivity, high pressure standing ability, high resistance to decomposition at temperature, low environmental impact, etc. [13-15]. Some of the solid lubricant additives, particularly in nano or submicron size, have demonstrated even better tribological performances than the traditional organic additives, Zinc dialkyldithiophosphates (ZDDP) for instance.

Due to the diversity of the materials, there are still many controversies about their behavior in a base lubricant and their lubricating mechanisms, although many potential candidates have been tested as solid lubricant additives and have shown excellent tribological properties [16-18]. The major drawback of solid lubricant additives, the intrinsic poor

4

stability in liquid base lubricant systems, has considerably restrained them from applications. Therefore, the research on exploring novel solid lubricant additives and the techniques that would improve their dispersibility in base lubricants is certainly required.

1.1.3 WHY SOLID LUBRICANT ADDITIVES?

The good friction and wear reduction performances of solid lubricants were observed due to the low shear strength of the materials because of their intrinsic crystal structure. However, the introduction of a solid lubricant additive in lubricant oil caused another problem: stability. Solid particles are generally not stable in liquid media, especially for large particles. The agglomeration of the solid lubricant particles causes them to separate from the lubricant by sedimentation, thereby reducing or removing the additive content from the base lubricant so that the benefits gained from the introduction of solid particles in the lubricant are lost.

Outstanding performance in friction and wear reduction was observed in some applications of the solid inorganic lubricant additives [19-22]. Some of the solid inorganic lubricant additives even outperform the traditional organic lubricant additive ZDDP [23]. Lamellar or layered solid lubricants are some of the most widely used class of lubricants by engineers. A significant amount of research and development has been performed to understand the tribological characteristics of these lubricants, as well as determining the optimal lubricant for specific applications. A few examples of lamellar lubricants are graphite, molybdenum disulfide (MoS_2), hexagonal boron nitride (hBN), gallium selenium (GaSe), and boric acid (H_3BO_3). These lamellar solid powders all have similar molecular structures composed of layers of covalently bonded atoms. These layers are

5

held together by the weak van der Waals force, and maintain different distances between the layers for different molecules. Solid lubricants offer many advantages over liquid lubricants in applications (Table 1) involving high vacuum, high temperature, cryogenic temperature, radiation, extreme dust, or corrosive environments [24].

Table 1 Advantages and Disadvantages of Solid Lubricants[25]

Advantages	Disadvantages
□□Are highly stable in high-temperature, cryogenic temperature, vacuum, and high-pressure environments	□□Have higher coefficients of friction and wear than hydrodynamic lubrication
□□Have high heat dissipation with high thermally conductive lubricants, such as diamond films	□□Have poor heat dissipation with low thermally conductive lubricants, such as polymer-based films
□□Have high resistance to deterioration in high-radiation environments	□□Have poor self-healing properties so that a broken solid film tends to shorten the useful life of the lubricant (however, a solid film, such as a carbon nanotube film, may be readily reapplied to extend the useful life.)
□□Have high resistance to abrasion in high-dust environments	
□□Have high resistance to deterioration in reactive environments	□□May have undesirable color, such as with graphite and carbon nanotubes
□□Are more effective than fluid lubricants at intermittent loading, high loads, and high speeds	
□□Enable equipment to be lighter and simpler because lubrication distribution systems and seals are not required	
□□Offer a distinct advantage in locations where access for servicing is difficult	
□□Can provide translucent or transparent coatings, such as diamond and diamond-like carbon films, where desirable	

The lubrication mechanisms that govern solid lubricants are controlled by intrinsic properties, such as the layered crystal structure, interlayer distance, electrostatic attraction, and extrinsic parameters such as humidity, temperature, and environment. The interlayer distance between layers is also important because as the interlayer distance increases, the ability of the van der Waals force to hold adjacent layers together decreases; thus, the shearing resistance between layers weakens enhancing lubricity. The interlayer distances for graphite are 0.335 nm. There are no solid lubricants that can provide both low friction and low wear in all environments. For graphite and MoS_2, the interlayer distances are 0.335 nm and 0.296 nm, respectively. The friction and wear performance of solid lubricants is influenced by inherent properties, environmental parameters, and application usage. In humid air, graphite can have a lower friction coefficient than MoS_2; however, in dry and vacuum environments, MoS_2 has the lower coefficient of friction. They are used as additives in oils and greases where their physical properties prevail, and in coatings in which physiochemical reactions and adherence become critical. In these situations, the solid lubricant develops into a thin lubricating transfer film that can protect a surface by accommodating the relative motion by easily shearing and carrying a portion of the asperity contact load, thus decreasing friction and minimizing wear. This physical behavior allows lamellar solids to be used as solid lubricants whether they are in the form of a granular powder, compressed pellet, or colloidal solution.

1.1.4 THE ROLES OF SOLID LUBRICANT ADDITIVES

Lamellar powder lubricants are known for their crystal structure, in which atoms lying on the same layer are closely packed and strongly bonded together by covalent

www.manaraa.com

bonds, and the layers are relatively far apart due to the weak van der Waals force. When entrained between sliding surfaces, the lamellar powders can adhere to the surface, forming a protective boundary layer that minimizes contact between opposing surface asperities to prevent wear. The protective boundary acts as a lubricant in sliding contacts by accommodating relative surface velocities. The lamellar powder lubricants accomplish this by aligning their layers parallel to the direction of motion and sliding over one another to minimize friction. Moreover, these powder lubricants can lubricate in extreme conditions, such as high or low temperatures and pressures [26, 27].

The excellent tribological property of solid inorganic lubricant additives can be attributed to four mechanisms:

Tribochemical reactions -- Solid lubricant additives may interact with the surface material of friction pairs and form a surface protection film [28, 29].

Ball effect -- Small spherical nano-particles enable rolling between friction pairs. These particles introduce a partial rolling friction into a pure sliding friction [29].

Mending effect -- in most of the cases, the surface roughness is greater than the mean diameter of nano-particles. Nano-particles can be deposited on the surface and form a physical tribofilm, which compensates for the mass loss of materials [30, 31].

Third body effect -- a large number of nanoparticles helps to reduce compressive stress concentrations associated with high contact pressure by bearing the compressive force depressively [31, 32].

1.2 LITERATURE REVIEW

Inorganic solid lubricant additives have recently been developed. The utilization of nanosized or submicron sized particles as an inorganic lubricant additive is gradually earning their attention in industrial applications, owing to their outstanding tribological properties and good environmentally friendly features compared with the traditional organic lubricant additives that contain P, S, and Cl elements [33-35]. Like the traditional lubricant additives, some of the inorganic solid lubricant additives are also capable of forming a boundary film through so-called 'tribochemical' reactions to protect the rubbing surfaces. This boundary film may contain the materials from lubricant additives, lubricant, and substrate surface [36, 37].

1.2.1 EFFECT OF GRAPHENE AS AN OIL ADDITIVE

For tribology applications, nanoparticles as additives in base oil have been widely investigated [18, 38, 39]. These studies refer to synthesis and preparation of nanoscale particles and their tribological properties and mechanisms. It was observed that when the nanoparticles were added to the base oil, the extreme-pressure property and load-carrying capacity were improved, and the friction coefficient was decreased. At present, the viewpoint about mechanisms of nanoparticle additives is as follows: 1) ball effect [29, 40]; 2) tribochemical reactions [41, 42]; and 3) adsorption film theory [43]. The results of previous studies indicate that nanoparticles used as lubricating oil additive can improve the tribological properties of base oils. Commercially layered compound powders, usually as solid lubricants dispersed in oil, were also included [44]. The addition of nanomaterials as additives in base lubricant oil is a rapidly progressing field of research

because nanomaterials are different from traditional bulk materials due to their extremely small size and high specific surface area [45-47]. Amongst nanoparticles, the solid lubricants such as molybdenum disulfide (MoS_2) [48] and nano-graphite [49, 50] dispersed in oil exhibited beneficial effects by reducing friction and wear.

Graphite and graphene were used to enhance the tribological properties of materials as reinforcements [51-53] or as oil additives [35, 54]. It is reported that a layer of solid lubricant continuously forms on the tribosurface during dry sliding of the metal-graphite composites [55-57]. Composites reinforced with graphite particles at proper concentrations have better tribological properties because graphite particles act as a solid lubricant on worn surfaces [58-60], to graphite particles as an additive in oil [35, 49, 61, 62]. Lee et al. [49] separated graphite nanoparticles into industrial gear oil, and the results indicated graphite nanoparticles can improve the lubrication properties significantly. Huang et al. [35] used graphite nanosheets as an additive in paraffin oil to analyze the tribological behavior with a four-ball and a pin-on-disk friction and wear tester. It proved that the graphite nanosheets as an additive in oil at proper concentrations can improve tribological properties, load-carrying capacity, and antiwear ability, to decrease the friction coefficient. Aranganathan et al. [61] compared the effect of natural graphite (NG) and thermo-graphite (TG) contained in NAO friction materials (FMs). The tribo-performance of TG-based FM proved superior to NG-based ones, excluding recovery performance.

Graphene platelets (GNPs) [62] are a fascinating fundamental component of graphite due to their excellent lubricative properties. With increasing thickness of GNPs over several layers, the frictional force between an AFM tip and graphene decreases and is independent of the substrate [63]. The very low friction coefficient and high pressure

11

resistance of graphene make it a prospective reinforcement for lubricant and antiwear coatings [64-67]. Recently, GNPs as additives in base lubricants became a hotspot. Eswaraiah et al. [54] manufactured Ultrathin graphene-based engine oil nanolubricants and observed a reduction in frictional coefficient. They also found the frictional characteristics and wear scar diameter increases with increasing concentration of graphene. Arwin and Rashmi [68] detected NGPs as an additive for two different biolubricant base stocks resulted in a reduction of the coefficient of friction and a negative effect at a higher temperature. Some experiments showed the modification of GNPs can improve the dispersion of graphene platelets in base oil. The wear resistance and load-carrying capacity of the machine also reduce the resistance to shear and wear scar diameter [50, 69, 70].

The tribological behavior of nano graphite nanosheets as an additive in paraffin oil was investigated by Huang at al. [35] with a four-ball and a pin-on-disk tribo tester. The graphite nanosheets with an average diameter of 500 nm and a thickness of 15 nm were prepared by stirring ball milling. The maximum nanosized loads of the lubricating oil were determined according to the ASTM D2783 standard method. As a lubricant additive in oil, graphite nanosheets demonstrated better tribological properties than in pure paraffin oil when an appropriate additive concentration was used. The low shear strength between the sliding surfaces resulting from the employment of graphite nanosheets with the layered structure is responsible for the observed improvement on tribological properties. 1% was found to be the optimal concentration for the application of this type of solid lubricant additive. Gansheimer [71], Rapoport [72], and Kimura [73] also reported a similar improvement on tribological properties, such as friction and wear

reduction, and the improvement on maximum non-seizure load, by using MoS$_2$, WS$_2$ and BN as solid lubricant additives correspondingly.

1.2.2 SUMMARY

The present chapter has reviewed previous studies regarding the application of solid lubricant additives. Various types of solid lubricant additives have demonstrated outstanding tribological properties such as friction reduction, wear resistance, and improvement on maximum non-seizure load.

In general, it can be categorized into three ways by which solid lubricant additives can improve the tribological performance of a lubrication system. The first approach is to employ their easy shear crystal structure. Solid lubricant additives that have such lubricating mechanism such as graphite. These solid lubricant additives create a layer of material with low shear strength and, therefore, reduce the force required to activate the sliding and, consequently, reduce friction. The second approach is by mending or third body effect. Solid lubricant additives that have such lubricating mechanisms include metal nanoparticles, metal oxide nanoparticles, and other inert solid particles with small particle sizes. These particles may deposit onto the contact surfaces, fill valleys, and work as the separation material, ultimately reducing direct substrate to substrate contact and protecting contact surfaces. Finally, the third approach is associated with tribochemical reactions. Solid lubricant additives that have such lubricating mechanisms include borates, sulfides, chlorides and other materials that contain active elements such as Sulfur (S), Phosphorus (P), Chlorine (Cl), and Fluorine (F). These lubricant additives react with base oil and substrate materials and form a protective film (tribo film) with low shear

strength on contact surfaces. Exfoliation and replenishment of tribo film are the typical phenomena involved in tribo chemical reactions.

Although many materials have been tested as solid lubricant additives and have shown good tribological properties, there are still many controversies about their lubricating mechanisms. Therefore, research looking for new materials that are potentially suitable for a lubricant additive need to be continued. It is well known in literatures that dispersion of the additives in the base oil in the application of solid lubricant additives plays an important role on the tribological performance. Exploitation of new modification techniques is also an essential part of the research on solid lubricant additives.

1.3 MATERIALS AND EXPERIMENTS

In this chapter, the tribological properties of graphene nanoplatelets as an additive to synthesize a nanolubricant is studied. The experimental procedure which was applied to study the tribological performance of solid lubricant additives in the lubricant base oil begins with dispersing of the solid lubricant in the base media to prepare the so-called " Nano lubricant". Subsequently, the prepared nanolubricants were used to lubricate the sliding contact during a pin-on-disc tribo test. Friction and wear are evaluated at several parameters including volume friction of graphene and applied load. To understand the mechanism of the enhancement in presence of graphene nanoplatelets additives, several test rigs were also employed to analyze the worn surface of the pins. The key test equipment involved in the study are introduced in this chapter. This work is carried out in 3 phases:

1. Study the tribological properties of nanolubricant (base oil with graphene additive) to understand the effects of these solid lubricant additives on tribological performances,

2. Investigate different parameter on the wear and the friction behavior of composites.

3. Characterize worn surface of nanocomposites to understand wear mechanism and characterize the tribofilm on the surface to understand the reason for the change in wear and COF.

In the present investigation, canola oil with graphene nanoplatelets powder additives was studied using a pin-on-disk tribometer to determine its feasibility as a biolubricant. The primary materials used in this investigation were a) Al2024 as the pin (Speedy Metal, New Berlin, WI), b) 440C stainless steel as the disk (Speedy Metal, New Berlin, WI) and c) nano27 graphene nanoplatelets (GNPs) as the oil additive (Asbury, Asbury, NJ) with average thickness of approximately 10 nm and average platelet diameter of ~1 μm. Canola oil has a viscosity and surface tension like the functional fluids used in industrial applications such as metal-stamping and metal-forming operations. It has been speculated to serve as an automotive lubricant for gears or bearings [74]. In this study, canola oil was specifically chosen because it is readily available, inexpensive, environmentally benign, and tested previously by the authors [27]. Graphene nanoplatelets are ball milled for 3 hours before mixing with oil to reduce the thickness of graphene nanoplatelets. Additionally, 2024 aluminum alloy is used to manufacture components for metal-forming, drilling, and machining operations as well as extensive use in a broad set of applications within the manufacturing and automotive industries.

1.3.1 NANOLUBRICANTS

To make the nanolubricants, graphene nanoplatelets (GNPs) are dispersed in the canola oil for desired a volume fraction of GNPs (0.05, 0.10, 0.15, 0.20, 0.25, 0.30, 0.35 and 0.40 vol.%). Three methods of dispersing were employed to make the nanolubricants; Mechanical Shaker (IKA MS3), Ultrasonic mixer (Powersonic P1100 Ultrasonic Cleaner) and the combination of Shaker/Ultrasonic. The ball milled graphene was poured on top of the oil container and was shaked for 20 minutes with a speed of 10k rpm to have a homogenous nanolubricant. In ultrasonic mixer method, graphene was added to the top of oil container and mixed for 2 hours at 60 °C. The last method is mixing graphene for 20 minutes with a shaker at first and then using an ultrasonic mixer for 2 hours at 60 °C.

1.3.2 TRIBOLOGICAL TESTS

To perform the experiments, a disk-on-disk test setup is used that measures the friction coefficient using torque and load sensors, as well as the temperature of the lubricant. The surface samples are submerged in a small reservoir of the nano-lubricant. Base lubricants with no additives have been used as the base solvents to isolate the results and investigate the effect of particles explicitly.

Throughout this experimental investigation 2024 aluminum alloy (T4 heat treated) with HRB of 73 was consistently used for the construction of the pins and disks is 440C stainless steel with HRC of 60 in the tribo-interface. The pins were machined to dimensions of 6mm in diameter and 20 mm in length with a hemispherical tip. The disks were made having dimensions of 55 mm in diameter and 10 mm in thickness. The disks were originally machined and polished to a surface roughness having an arithmetic

16

average, S_a, of 0.15 ± 0.05 μm. Pin-on-disk tests at ambient conditions were conducted to characterize the tribological properties of the various nanolubricants. The schematic of the pin-on-disk test was shown in Figure 1. Table 2 presents the basic testing conditions used throughout each experiment. A thermocouple is also deployed to determine the temperature of the lubricant at the end of wear test. This test setup is designed for conducting boundary lubrication experiments with a small volume of lubricant.

Table 2 Test parameters

Parameter	Selected Values
Normal load (N)	5, 10, 15 and 20
Sliding velocity (mm/s)	25
Distance traveled (m)	1000
Environment	Ambient
Lubricant quantity (mL)	8
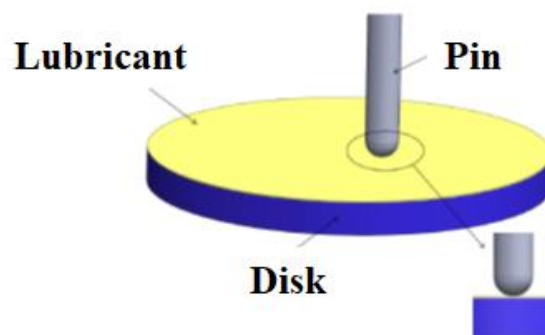
Figure 1 Schematic of pin-on-disk interface with a lubricant film covering the disk

17

Investigating the lubrication regime for the following experiments is an important preliminary step when characterizing the friction mechanisms between the pin and the disk surfaces. This can be achieved by utilizing the elastohydrodynamic minimum film thickness equation developed by Hamrock and Dowson, which is applicable in many material combinations for a variety of contact geometries including point contact of a hemisphere on a flat surface as is the geometry for the pin-on-disk testing. The numerically derived formula for the minimum film thickness is expressed in the following form:

$$\frac{h_o}{R'} = 3.63 \left(\frac{U\eta_o}{E'R'}\right)^{0.68} (\alpha E')^{0.49} \left(\frac{w}{E'R'^2}\right)^{-0.073} \left(1 - e^{-0.68k}\right)$$

h_o is the minimum film thickness (m);

U   is the entraining surface velocity (m/s), i.e. $U = \frac{(U_a + U_b)}{2}$, where the subscripts 'a' and 'b' refer to the velocities of bodies 'a' and 'b' respectively;

η_o is the viscosity at atmospheric pressure of the lubricant (Pa s);

E'   is the reduced Young's modulus (Pa), i.e. $\frac{1}{E'} = \frac{1}{2}\left(\frac{1-v_a^2}{E_a} + \frac{1-v_b^2}{E_b}\right)$ where v is Poisson's ratio and E is Young's modulus for the respective pin and disk specimen;

R'   is the reduced radius of curvature (m) for a pin on flat, i.e. $\frac{1}{R'} = \left(\frac{1}{R_{ax}} + \frac{1}{R_{ay}}\right)$, where R_a is the radius of curvature for the pin in the x and y directions

A   is the pressure-viscosity coefficient (m2/N), i.e. $\alpha = (0.6 + 0.965 \log_{10} \eta_o) \times 10^{-8}$

w   is the normal load (N)

k   is the ellipticity parameter defined as k = a/b, where 'a' is the semiaxis of the contact ellipse in the transverse direction (m) and 'b' is the semiaxis in the direction of motion (m), however in this calculation the value of the ellipticity parameter for point contact is k = 1.

In the present experimental conditions, the pin tip radius is 3mm, the sliding speed is 25mm/s, and the normal load is 5-20N. Hamrock and Dowson's elastohydrodynamic film thickness equation predicted a minimum film thickness ratio of 5.1×10^{-6} or less. These values are significantly less than unity and place the current experimental investigation in the boundary lubrication regime. It can be inferred that for the variety of testing conditions presented in this experimental study the lubricating regime will remain in the boundary lubrication.

During each of the tests the surface of the disk was partially submerged by the nanolubricant mixture, thereby continually lubricating the pin-disk interface throughout the duration of the test. The pin and disk specimens were cleaned before and after each test using an ultrasonic cleaner with soap, acetone, and hexane solutions. Each test has repeated a minimum of three times to ensure repeatability and accuracy of the results. The normal load and friction force measurements were monitored for each test using a two-beam type load cells that read the normal load from a static hanging mass and the friction force as the tangential force of the pin holder. The linear wear-loss was acquired through a linear variable differential transducer (LVDT) with an encoder, which recorded the vertical displacement of the pin.

The COF (coefficient of friction) value presented for each test was the average of the friction values. In addition, the linear wear-loss was acquired through a linear variable differential transducer (LVDT) with an encoder, which recorded the vertical displacement

of the pin. The linear wear loss of each pin was converted into a volumetric wear loss using Eq. (1) derived from the geometry of a spherical cap.

$$V = \frac{\pi h^2}{3}(3r - h) \qquad\qquad (1)$$

1.3.3 CHARACTERIZATION

The worn surfaces of the samples are investigated to understand the wear mechanism. Comprehensive characterization tests were designed for the nanolubricants to understand and explain the relationship between different parameters using the following techniques.

Two different scanning electron microscopes (SEM) (Hitachi S-4800 Ultra High-Resolution Cold Cathode Field Emission Scanning Electron Microscope (FE-SEM), JEOL JSM-6460 LV were used for characterization of the worn surfaces. Elemental analysis is performed using an Oxford Energy Dispersive Spectroscopy detector attached to the SEM. The thin window silicon drift detector (SDD) allows for the detection of the elements carbon and higher.

X-ray diffraction (XRD) data gathered by a D8 Bruker diffractometer with Cu Kα1 radiation (λ= 0.15406 nm) (scanning from 2θ = 15° to 2θ =85°, step size of 0.02°, counting time of 0.3s per step).

A LEXT OLS4100 3-D Laser Confocal Microscopy is used for 2-D and 3-D imaging and dimensional measurements with a surface feature observation resolution of 20 nm.

A Renishaw Inc. 1000B Raman spectroscopy (Helium neon laser (633nm)) is used to determine the formation of tribofilm on the worn surfaces.

20

1.4 RESULTS AND DISCUSSIONS

1.4.1 BALL MILLING OF GRAPHENE NANOPLATELETS

As discussed earlier, GNPs (Few layer graphene) offers better antifriction effect than a single layer graphene and graphite [75, 76]. The shear force acting on a few layer graphene helps its exfoliation [77, 78] thereby contributing to the lubrication effect of the oil. However, at the same GNPs loading, the number of layered graphene sheets present at the contact surface increases inversely by number of layers. One can say that, in case of very few layers of graphene, the repeated exfoliation due to shear forces could form several single layer graphene sheets which cover the contact surface and reduce metal-metal interaction. One approach to reducing the number of layers in GNPs is mechanical milling. During milling, the shear forces intercalate/exfoliate graphite. Graphite layers have the weak van der Waals bonding and strong bonds in basal plane. As a result, the shear force during milling can potentially reduce the number of layers in GNPs.

Figure 2 compares the Raman spectra of graphite, graphene nanoplatelets (GNPs), and ball-milled GNPs. Figure 3 illustrates the D- and G-band and Figure 4 shows the 2D-bands. In general, the D-band appears in graphite only in defective/disordered samples or at the edges. In GNPs, the 2D-band changes from a doublet peak profile to a single peak. In a perfectly A-B stacked few layer graphene, by about 5 – 6 layers, the 2D-peak starts exhibiting a two-peak profile. From top down point of view, this indicates that the 2D-band in graphite maintains a two-peak profile down to 5 or 6 layers. However, in samples with high c-axis disorder, the two-peak profile of graphite is not maintained. Cancado et al. [79] have shown that as disorder increases, the 2D2 shoulder shift upwards

and finally merges into the 2D1 band. However, this type of analysis and comparison is only valid when less than 5 or 6 layers of graphitic planes are under study. High 2D FWHM and the doublet structure of 2D bands in both Graphite and GNPs indicated the higher than 6 later c-axis disorders. According to Ferrari et al. [80], for a transition from graphite to nanocrystalline graphite, one can compare the ratio of the D-peak intensity to that of the G-peak which varies inversely with average inter defect distance as well as increasing of FWHM. Here, the I_D/I_G value changes from 0.32 to 0.52 in graphite to GNPs. In addition, the downshift of the 2D peaks from 2674 to 2651 in graphite to GNPs indicates the decrease in number of layers [81]. The ball-milling procedure breaks the large crystallites into smaller particles and introduces a significant number of defects. According to Kaniyoor et al. [82], a high amount of defect can suppress the 2D-band and a bump like region emerges. Since no chemical treatments were given here, the peculiar 2D-band shape cannot be due to functional groups and must be due to defects.

22
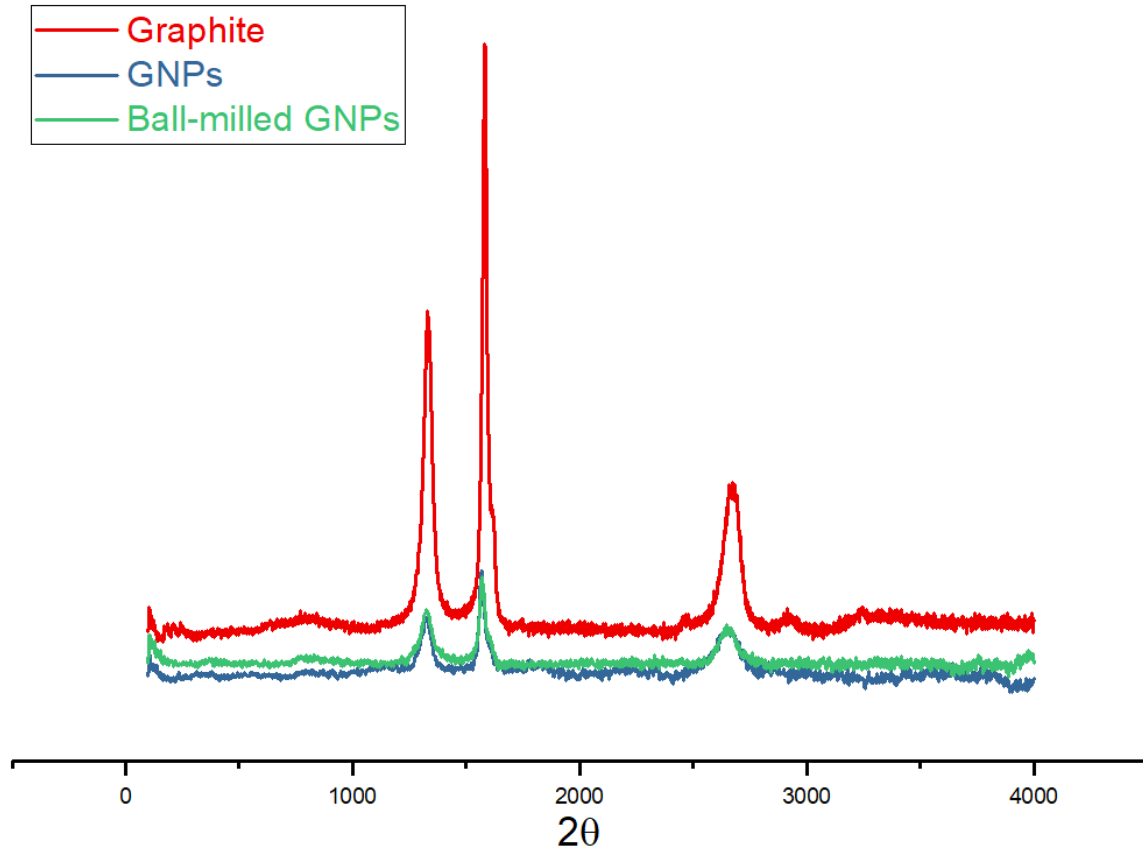
Figure 2 Raman spectra of graphite, GNP, and ball-milled GNPs
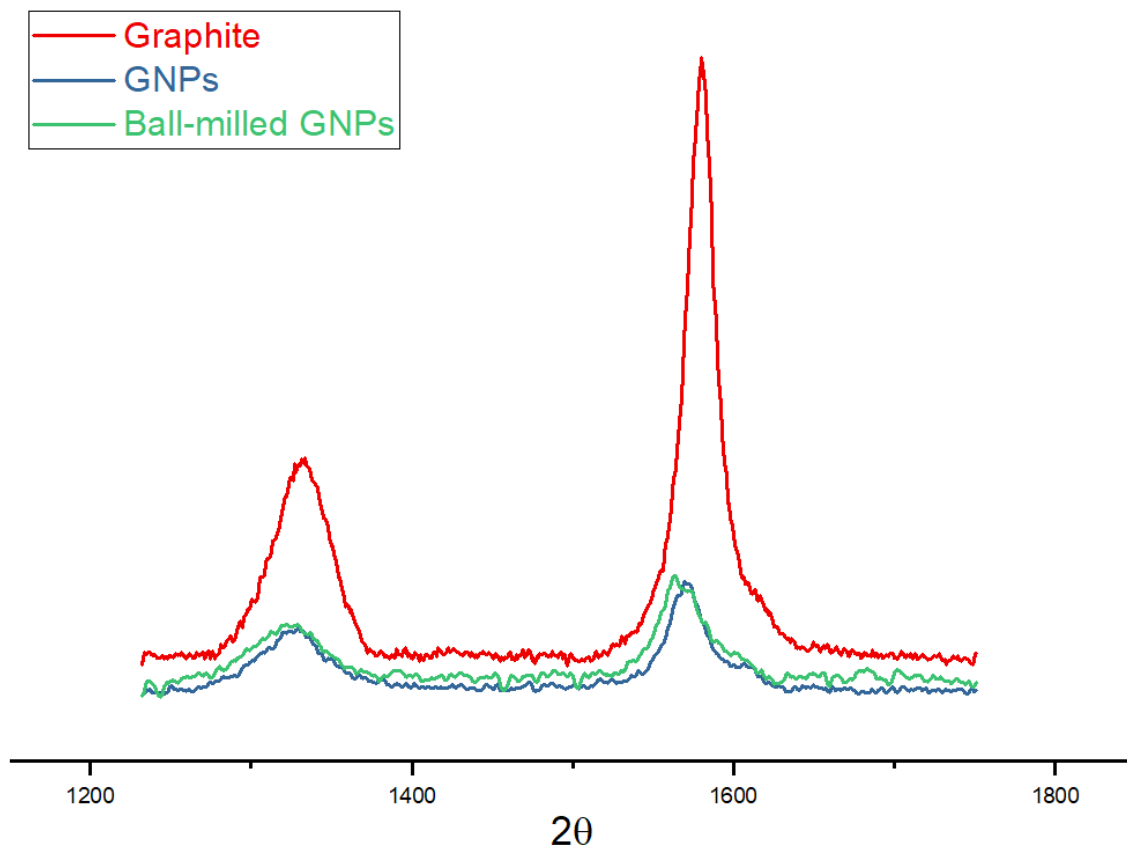
Figure 3 D- and G-band of graphite, GNPs, and ball-milled GNPs

24
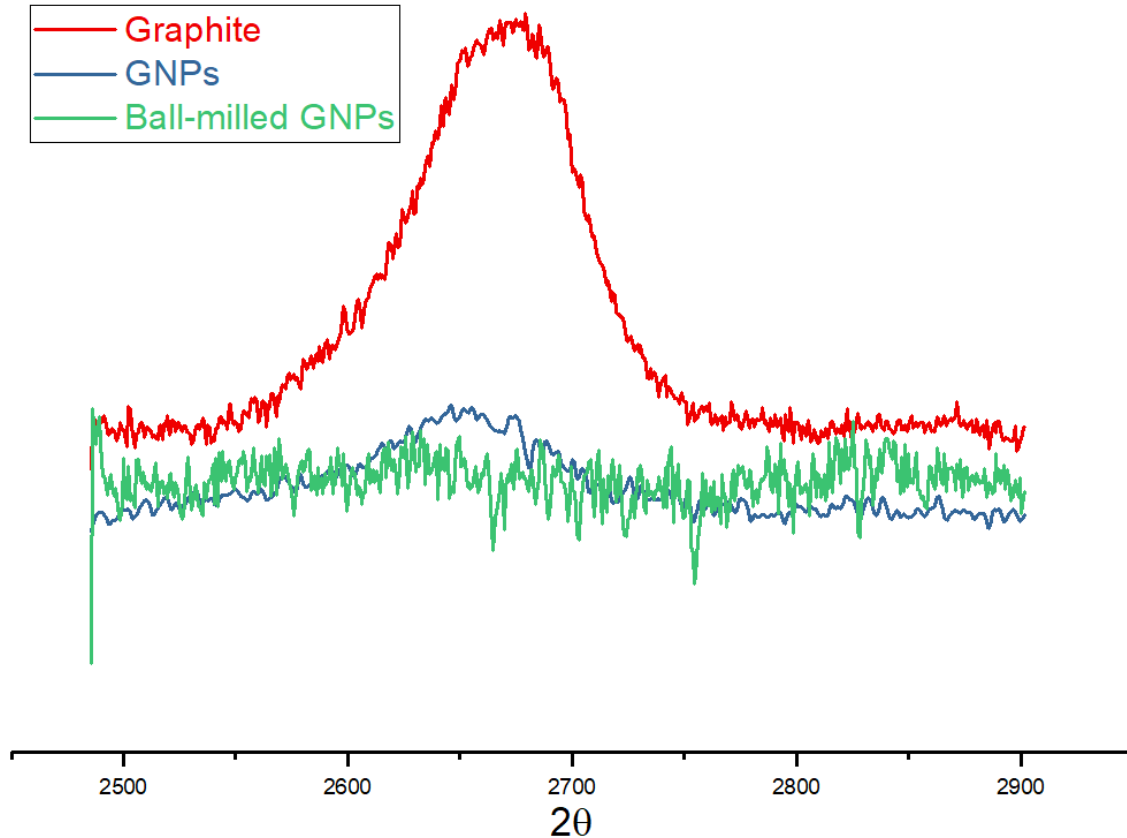
Figure 4 2D-band of graphite, GNPs, and ball-milled GNPs

XRD patterns of the graphene nanoplatelets (GNPs), and ball-milled GNPs (for 1,2,3,6 hours of milling time) samples are displayed in Figure 5. As shown in Figure 5, as-received GNPs exhibits a basal reflection (002) peak at 2θ =26.6∘ which corresponds to a d-spacing of 0.335 nm and represents the interlayer distance. Results shows that the diffraction peaks of the milled samples become weaker and broader, and the diffraction angle shifts downward as the milling time increases, indicating a gradual disordering process and d-spacing increase (intercalating process). The disordering process of GNPs seems to be complete after 3 hours of milling as only one single and board diffraction peak is observed in the corresponding XRD pattern. No further change can be seen from the XRD patterns for the samples milled for longer periods of time. One can say, when

graphite is completely exfoliated to single layer graphene, this diffraction peak disappears.
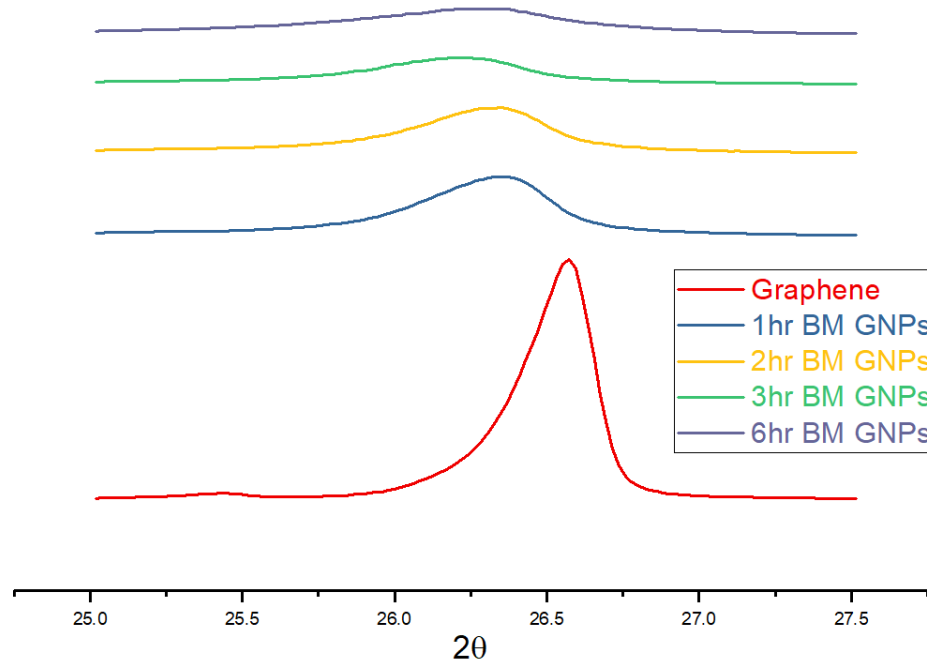
Figure 5 XRD patterns of the GNPs and ball-milled GNPs (for 1,2,3 and 6 hours milling time)

1.4.2 DISPERSION STABILITY

Graphene nanoplatelets strongly hydrophilic and easy to coagulate in oil. Hence, when graphene platelets are added to the base oil as a lubricant additive, it is necessary to ensure uniform dispersion without any agglomeration of graphene platelets in the base oil. All three methods described in 1.3.1 (Pg. 16) show a good dispersion appearance of particles into the oil. Figure 6 illustrates the dispersion of 0.1 vol.% graphene into the oil. Observations of the experiments reveal that after one day of mixing, the ultrasonic/shaker method started settling the particles from the top while two other methods were still well

26

dispersed (Figure 6b). After 5 days, the settlement of particles was observed in the shaking method while the ultrasonic mixing methods were still homogenized (Figure 6c). After 13 days, most of the graphene particles had settled to the bottom of the containers for shaking and shaking/ultrasonic mixing methods, even though graphene tended to settle at the bottom of container for the ultrasonic mixing method (Figure 6d). Therefore, the ultrasonic mixing method was selected for 2 hours at 60°C to use for mixing due to more stability of dispersion of solid lubricant particles. It should be noted that the stability of the nano-lubricants is crucial to avoid any aggregation, settling, sinking, and clustering effects.
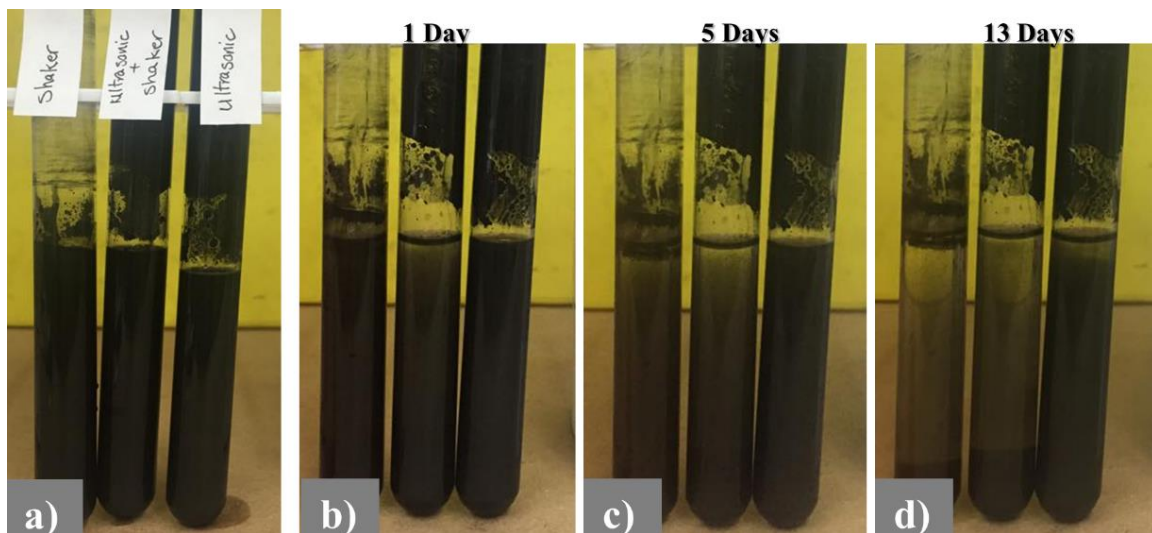
Figure 6 Compression of stability of mixing methods in several days

1.4.3 TRIBOLOGICAL PERFORMANCE

1.4.3.1 COF

In this work, the base lubricant without any additives has been used as the base oil to isolate the results and investigate the effect of particles explicitly. In general, the

27

concentration of the additive in lubricating oil plays an important role to determine lubricative characteristics. So, the effect of different concentrations of nanolubricants on the friction and wear properties of the lubricant is investigated.

Figure 7 shows the effect of volume fraction of nanolubricants on the COF and compared with neat oil. By adding graphene into the oil, the COF decreases because the graphene nanoplatelets can reduce the real contact area between two surfaces. Thus, these results reveal the important role that the GNPs play in filling the inter-asperity valleys. The graphene can more easily penetrate into the interface and form a continuous film in concave of rubbing face and align themselves parallel to the relative motion and slide over one another which can decrease shearing stress with relative ease providing lubrication. the COF gradually decreases by increasing the volume fraction of graphene, Therefore, at a high volume percentage of graphene, more graphene nanoplatelets present in the nanolubricant and between mating surfaces and, consequently, decreasing the direct contact area between worn surfaces. Moreover, with adding more graphene nanoplatelets into oil and increasing its concentration, more and more graphene deposit on the worn surface and thus greatly reduce the roughness of the surface and direct contact surface-to-surface, and the corresponding lubrication state gradually goes up to a good lubrication regime. A schematic illustration of the graphene nanoplatelets in the tribo-interface is shown in Figure 8. This figure demonstrates how the particles fill the inter-asperity valleys to establish a thin powder transfer film in the contact zone.

The lowest COF value is for nanolubricant with more than 0.3 vol.% of GNPs while neat oils have the highest COF value. Generally, the influence of the more graphene particles to lower the COF is far greater than the low amount of graphene particles. For example,

28

the presence of the 0.1 and 0.3 vol.% of graphene nanoplatelets at 15N applied load lowers the COF by 39% and 73% improvement, respectively when compared to the neat oil.

Figure 9 presents the results of the tests for base oil and several concentrations of nanolubricants at different loads. Results indicate that the effect of nanoparticles is more influential at higher loads and nanoparticle concentrations. The system works in the boundary lubrication regime which is the case where the lubricant film thickness between surfaces approaches the surface roughness. In this lubrication regime, there is substantial contact between surfaces but also some parts of the surfaces are separated by the lubricant film. Therefore, an increase in the normal load would squeeze more lubricant out of the contact region which reduces the lubricant film thickness between surfaces. This would escalate the probability of contact between surfaces and hence, increases the probability of particle engagement in the contact, therefore, the particles are more influential further in the boundary lubrication regime.
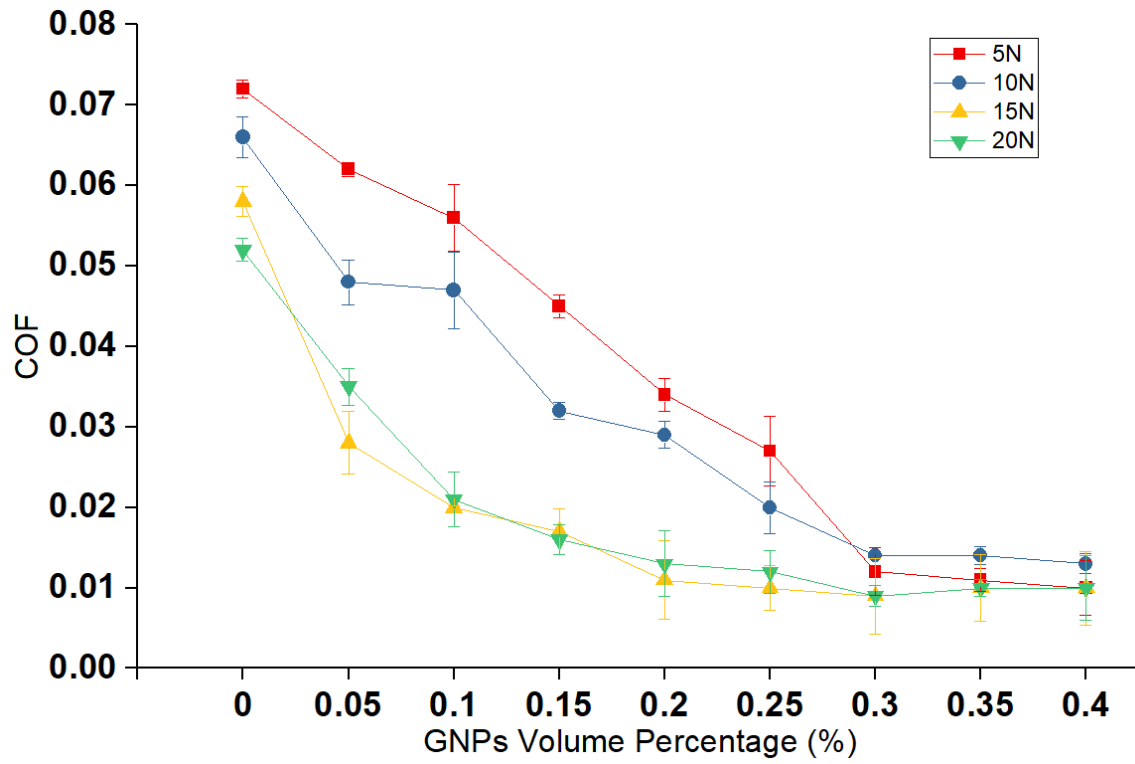
Figure 7 The variation of COF in different volume percentage of graphene at several loads.
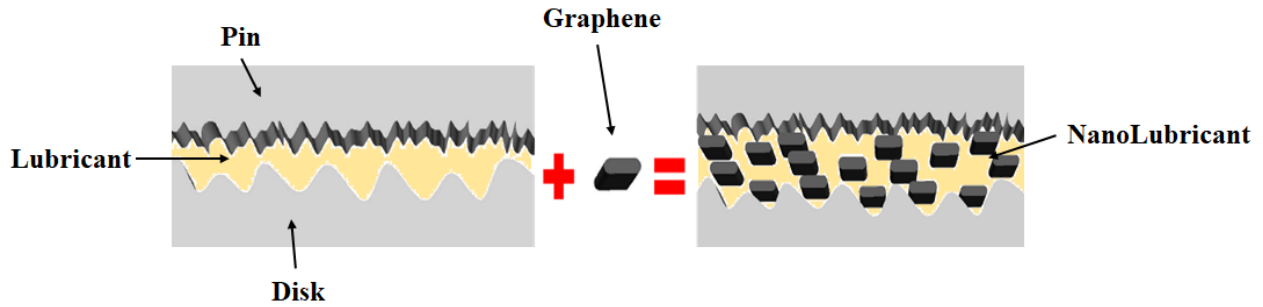
Figure 8 Schematic of the role of graphene as an oil additive in reducing COF
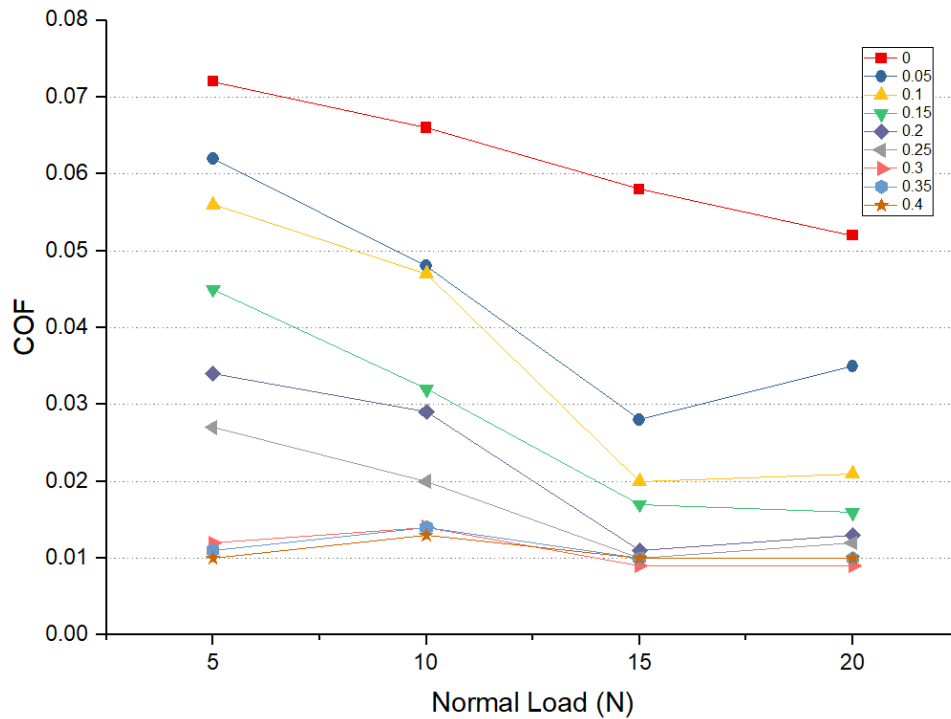
Figure 9 The variation of COF in different loads at several volume percentage of graphene

Figure 10 compares the worn surface of aluminum pins at 5N for neat oil and nanolubricant with 0.1 vol.% and 0.3 vol.% of graphene. There is no evidence for the presence of graphene on the worn surface using a neat oil wear test (Figure 10a) while they can be observed for samples lubricated by nanolubricant where the worn surfaces are covered by a lubricant graphene tribolayer as shown in Figure 10 (b) and (c). In conclusion, the real contact area between two surfaces reduced and so the COF is less than

neat oil. By comparing the worn surface of nanolubricant with 0.1 and 0.3 vol.% of graphene in Figure 10, it is obvious that more area of the worn surface is covered by graphene tribolayer for nanolubricant with 0.3 vol.% of graphene. Therefore, there is less real contact area between pin and disk and protect more asperities, so the COF of 0.30 vol.% nanolubricant is less than 0.1 vol.% nanolubricant.

generally, the nanoparticles usually form a thin transfer layer on the surface of the tribocontacts that can support partial hydrodynamic forces, therefore, reducing surface-to-surface contact of the asperities resulting in less friction, wear, and surface damage. It can be concluded that adding graphene particles into oil can be effective. As shown in Figure 10, surface characterization of samples shows some black spot on the contact surface for both samples in lubrication condition of nanolubricant. These are graphene nanoplatelets which is good evidence for reduced real contact area between pin and disk. Consequently, the reduction of the COF in presence of additives is attributed to this phenomenon.
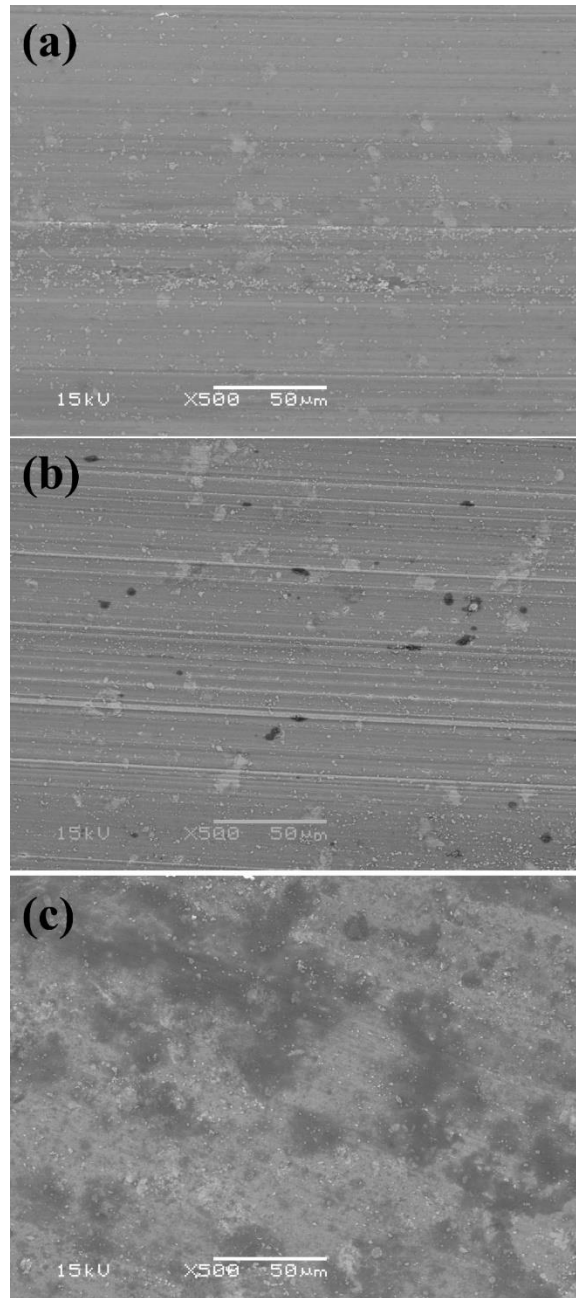
Figure 10 Worn surface of aluminum pins in presence of a) neat oil, b) nanolubricant with 0.1 vol.% graphene and c) nanolubricant with 0.3 vol.% of graphene at 5N applied load

Figure 11 shows the steady state temperature of the lubricant at the end of the experiment. In the case of lubricants, a lower friction coefficient results in less heat production and consequently the final temperature is lower. the graphene nanoparticles

33

also have proven to affect the thermal properties of the solution such as conduction which could result in better heat dissipation. Therefore, this effect appears to result in a significant reduction in the temperature in comparison to the lubricant without nanoparticles.
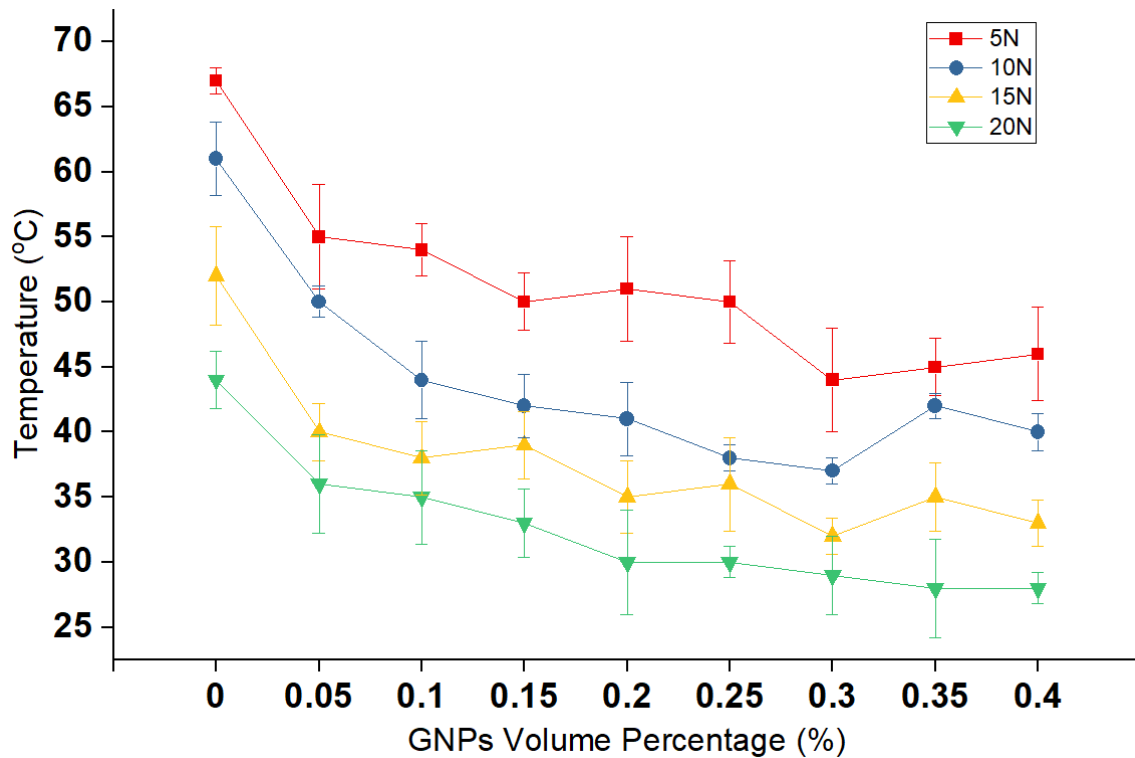
Figure 11 The variation of surface temperature in different volume percentages of graphene at several load

The fluid flow pattern is affected in the presence of the graphene suspended in the liquid that results in an increase in dissipated energy and an increase in the viscosity of the nanolubricants. Figure 12 and Figure 13 shows the results of viscometer for different concentrations of graphene at several temperatures. Figure 12 shows that the viscosity of graphene nanolubricants significantly reduces with temperature. The viscosity drops due to the inter-molecular and inter-particle adhesion forces. The inter-particle adhesion

34

forces become weak with the increase in temperature, causing a decrease in viscosity. Moreover, increased Brownian diffusion at elevated temperatures can reduce viscosity. Nguyen et al. [83] found that the dynamic viscosity of nanofluids increases considerably with particle volume fraction but clearly decreases with a temperature increase.

The increase in viscosity of mineral oil samples after the addition of graphene is insignificant. The reason for this behavior remains unclear as most of the existing explanations seem to be speculative [84, 85]. However, Heine et al. [86] showed through the molecular dynamics simulations of equilibrium structure and the response to imposed shear on suspensions of spheres, rods, plates, and jacks, that the rod and plate systems show noticeable particle alignment, which helps to minimize the frequency of particle collisions. Similarly, it is expected that the graphene having sheet structure could align itself along the shear direction. Nevertheless, this claim requires experimental validation. It can be concluded from Figure 13 that nanolubricant behave as a Newtonian fluid where viscosity remains constant, no matter the amount of shear applied for a constant temperature. Therefore, these fluids have a linear relationship between viscosity and shear stress.
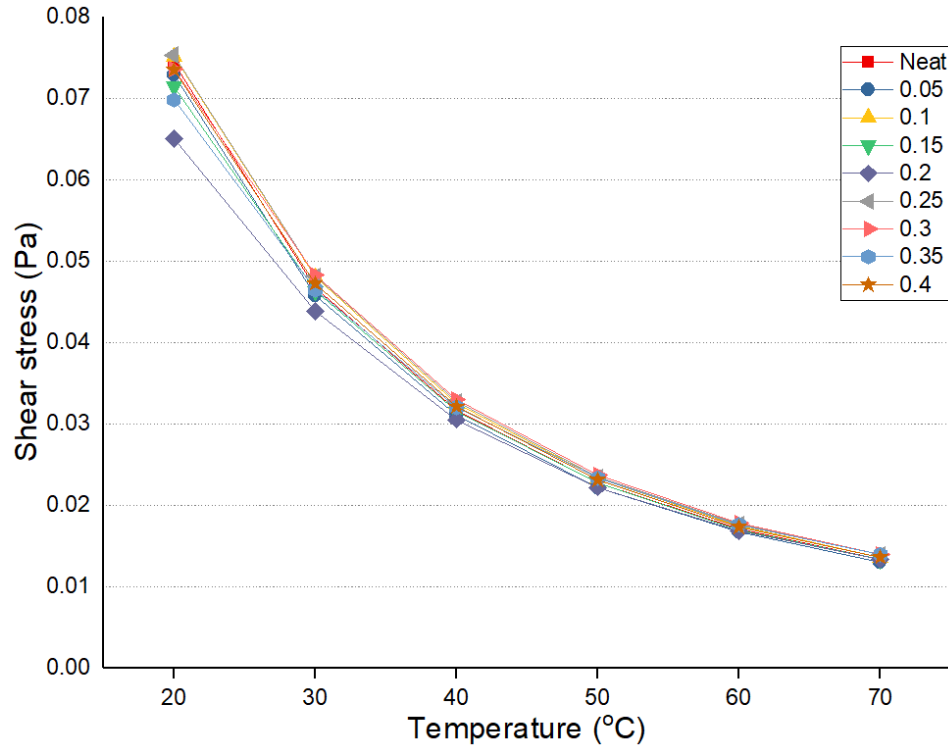
Figure 12 Viscosity versus temperature for different concentrations of

nanolubricants
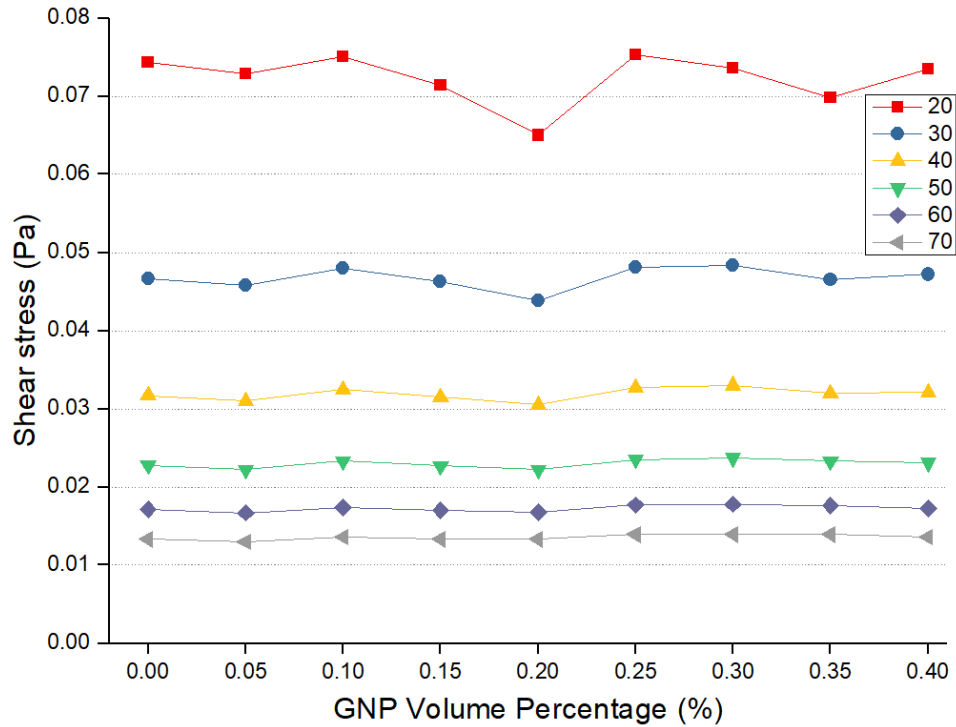
Figure 13 Viscosity versus volume percentage of graphene for different loads

The data from the friction and viscosity measurements are collapsed into the widely used Stribeck curve [87] in an attempt to develop generalized observations (Figure 14). P, η, and ω are the average contact pressure, viscosity and rotating speed, respectively in the x-axis of Figure 14. The Stribeck curve can account for the effect of changes in COF due to viscosity (temperature rise and particle concentration), along with pressure in one combined plot. The change of COF versus the average contact pressure, viscosity and rotating speed is considered in Figure 14 using the data shown in Figure 11 and Figure 12. The coefficient of friction decreases as more graphene are introduced in the lubricant and as contact pressure increases. As contact pressure increases, more asperities in the contact region yield and undergo plastic deformation. Lower resistance to the applied tangential load is exhibited, causing the overall friction coefficient to drop in accordance with existing friction theories [88-92]. Therefore, graphene nanoplatelet additives

37

decrease friction coefficient deep into the boundary lubrication regime (on the far left of the curve).
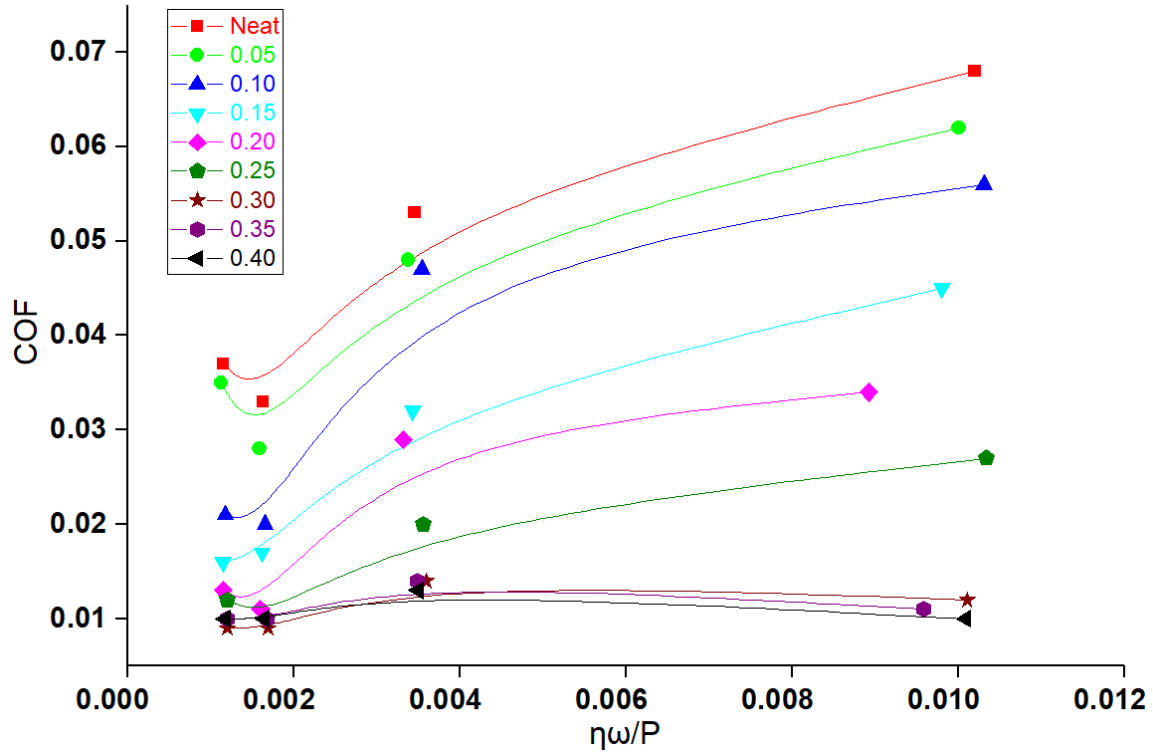
Figure 14 Stribeck curve for different volume percentage of graphene

1.4.3.2 Wear

Figure 15 shows the variation of the pin wear volumes rate with the load for all the nanolubricants. It is evident that wear rate of samples lubricated with nanolubricants significantly improved where the wear rate of nanolubricants is less than neat oil at different normal load. Besides, the pin wear volume rate decreases with the increasing graphene nanoplatelets volume fraction as an oil additive for various applied loads. Thus, the nanolubricants with a high number of particles have the lower wear volumes and the

lower particulate mixtures have the highest wear volumes; these results are like the trends seen in the coefficient of friction behavior.

The larger wear of neat oil can result from a real contacting area of the rubbing surface owing to wear. Therefore, this enhanced in wear of nanolubricant can be attributed to the layered structure of graphene mixed with based oil and due to its lubrication nature. When ultrathin graphene was added to the base oil, it fills up the micro- and nano-gaps of the rubbing surfaces and form lubricant graphene tribofilm which can smooth the surfaces, so that it avoids direct contact of the two surfaces and reduces the wear. The influence of the more graphene particles to lower the wear is far greater than the low amount of graphene particles. For example, by examining neat oil, the presence of the 0.1 and 0.3 vol.% of graphene nanoplatelets at 15N applied load lowers the wear volume by 78% and 99% improvement, respectively when compared to the neat oil.

Nevertheless, the wear rate versus GNPs volume percentage is U-shape. Consequently, there is an optimum amount of nano additive. The optimum amount of graphene as an oil additive for canola oil is 0.3 vol.% that the wear rate has the lowest value amongst nanolubricants. Adding more graphene in the oil beyond this optimum point (0.30 vol.% GNPs) cause to increases the wear rate. On contrary, less than 0.30 vol.% graphene, number of graphene particles is not sufficient to cover the majority of surface and reduce the contact between the mating surface to reduce the wear rate. In addition, particle additive concentrations below the optimum concentration result in insufficient load carrying capacity. When the particle additive concentration is above the optimum concentration, this results in the excessive additive in the base oil lead decreasing the load carrying capacity due to the formation of lumps in the interface which

39

will result in worse lubricating efficacy. Accordingly, the reason for increasing the wear rate after an optimum point is that graphene particles can easily aggregate in the oil mixture and during the wear process, resulting in the increase of the wear rate. aggregated graphene particles are considered to behave more like a third-body abrasive particle when sliding along the aluminum pin, because of their plate-like geometry, which damages the pin surface by plastic deformation, resulting in the high wear volume rate. Moreover, an excessive concentration of graphene nanoplatelets in oil will lead to graphene piling up between friction pairs, thus blocking the oil film, and the oil film will become much more discontinuous, even causing a dry friction [69]. As a result, the wear will increase beyond the bottom point of the curves (0.30 vol. %).

Generally, graphene nanoplatelets were two-dimensional nanosheets and could be easily dispersed in the base oil. Therefore, two contact surfaces were filled with the dispersed graphene nanoplatelets during the wear process, and then graphene nanoplatelets on wear surface could serve as spacers, preventing rough contact between the two mating wear surfaces. In addition, the two-dimensional sheet shape of graphene nanoplatelets could provide very easy shear and more easily a slider between the two contact surfaces. Consequently, the wear rate of the aluminum pin in nanolubricants samples dramatically drops.

Figure 16 depicts the variation of wear rate of pins at different loads in several volume percentages of graphene nanoplatelets. By increasing the load, the wear rate of aluminum in presence of nanolubricants decreased while the wear rate of neat oil increases. The wear rate slightly shows higher wear rate at higher normal load.
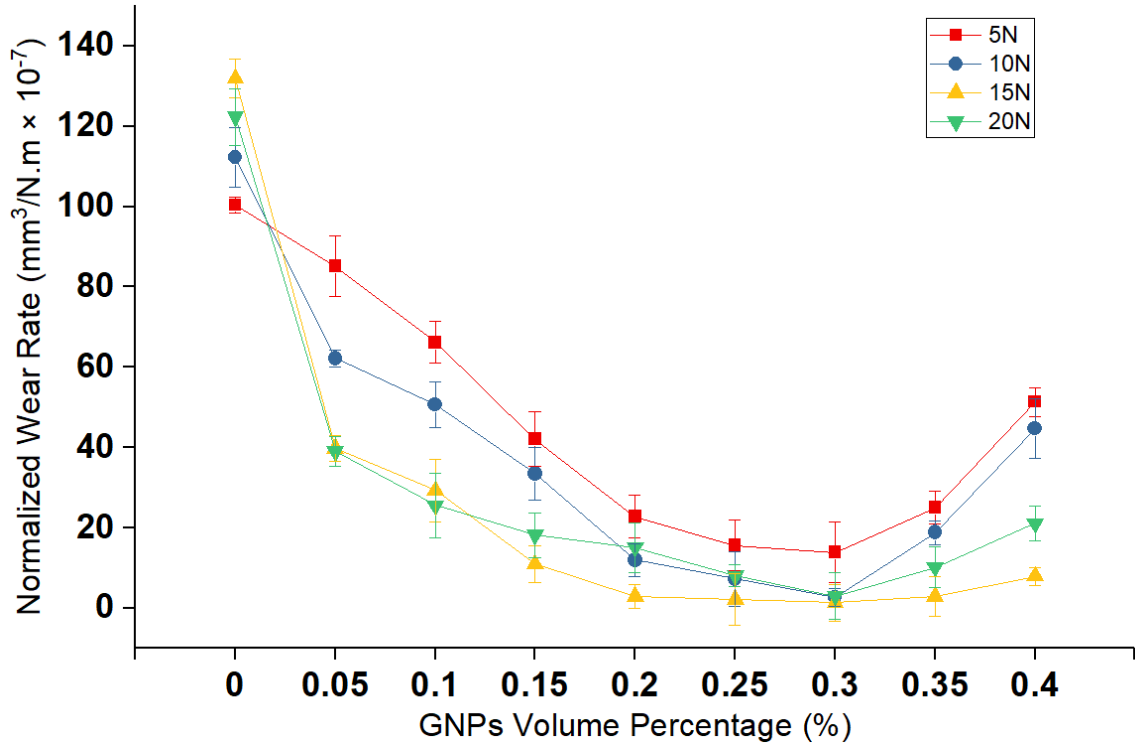
***Figure 15 The variation of wear rate in different volume percentage of graphene at
several loads.***
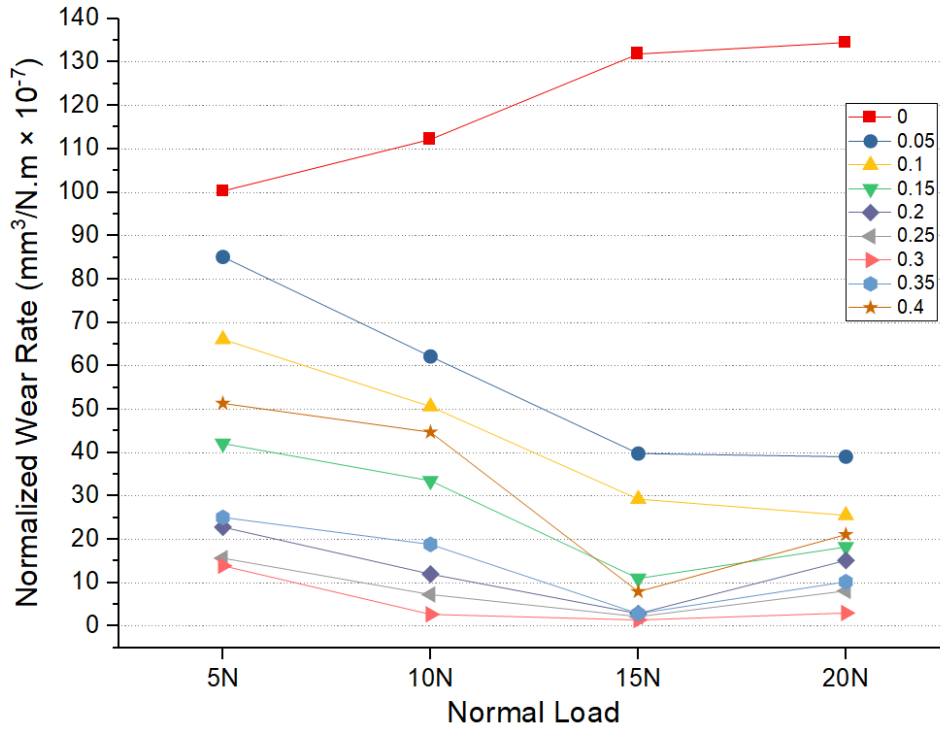
*Figure 16 The variation of wear rate in different loads at several volume percentages of graphene*

Figure 17 compares the worn surface of aluminum pins at 15N for neat oil and nanolubricant with 0.1 vol.% and 0.3 vol.% of graphene. There is no evidence for the presence of graphene on the worn surface for neat oil wear test (Figure 17a) while the black spots on the worn surfaces that expected to be a graphene tribolayer can be observed as shown in Figure 17 (b) and (c). Therefore, the real contact area between two surfaces reduced and so the wear rate of nanolubricants is less than neat oil. As explained in 1.4.3.1 (Pg. 27), with increasing the volume fraction of graphene, the larger area of the worn surface is deposited with graphene and thus greatly reduce the roughness of the surface and direct contact surface-to-surface, and have better lubrication regime. Consequently, less contact between asperities and less failure and deformation are occurred and as well as less wear rate is expected.

By comparing the worn surface of nanolubricant with 0.1 and 0.3 vol.% of graphene, it is obvious that the more surface area of aluminum pins tested with 0.3 vol.% nanolubricant covered by graphene tribolayer in comprising with nanolubricant with 0.1 vol.% of graphene. Therefore, there is less real contact area between pin and disk and so the wear rate is less than 0.1 vol.% nanolubricant. Generally, the geometry of the graphene is planar and therefore, the graphene can more easily penetrate the interface because on nano-sized and cause two important reasons for reducing friction and wear: 1) forming a nano-bearing between moving surfaces and 2) forming tribofilm in concave of rubbing face which can decrease shearing stress, therefore, give a low friction coefficient and wear. Generally, when adding additives to base oil allows it to act as a mechanical reinforcing element during friction and can strengthen the load carrying capacity of the lubricant.
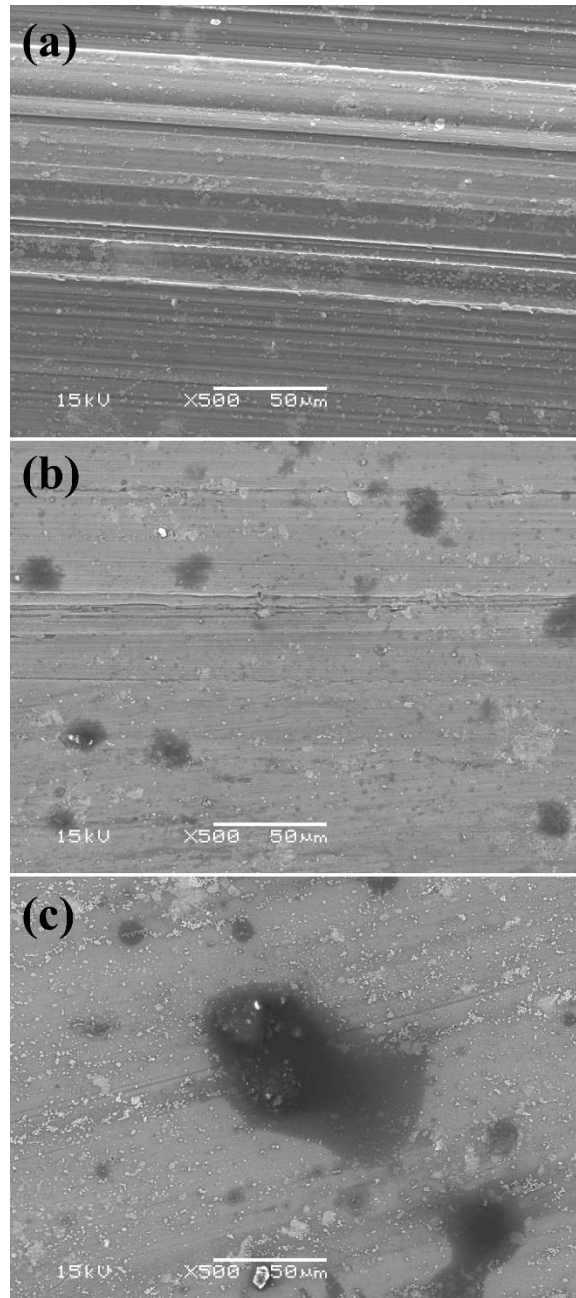
Figure 17 Worn surface of aluminum pins in presence of a) neat oil, b) nanolubricant with 0.1 vol.% graphene and c) nanolubricant with 0.3 vol.% of graphene at 15N applied load

Several enhancing and modification mechanisms have been proposed for nanoparticle lubricants in the boundary lubrication regime in the literature, such as: viscosity alteration, thermal stability enhancement, mending worn surfaces, the rolling effect and load bearing of nanoparticles. Viscosity and thermal properties are affected by the graphene nanoparticles.

44

However, the effect of these two mechanisms is minimal in the boundary lubrication regime where tribology is dominated by the contact of asperities. Particle deposition and forming a lubricant tribolayer is evident as shown in Figure 17 and the element of carbon is present at all the sample surfaces tested with the nanolubricant. The dispersion of particles and lubricant film on the surface is random and is sufficient to replace a significant portion of the worn material. Therefore, the mending mechanism is one of dominant in tribological tests. Moreover, the other mechanism is nanoparticles rolling and bearing and acting as nano bearings implies that the use of a nanolubricant should result in minimal wear. It is proven that nanoparticles can roll in between surfaces in contact [93]. Particles of the stable nanolubricant can exist as individual particles and don't form clusters in the suspension up to 0.30 vol.%. As more concentrated nanolubricant are used, more particles would be engaged in the contact and make larger and thicker lubricant tribofilm which explains the reduction in the wear rate versus particle concentration. On the other hand, at higher graphene concentration more than 0.30 vol.%, these particles would cluster and induce abrasive wear by plowing on the surface, therefore, increasing at wear rate happened. Due to the scaling effect on material strength, nanoparticles exhibit higher hardness than bulk materials which potentially makes them a source of abrasive wear. To avoid these effects, the concentration of nanolubricants is limited to 0.30 vol.%. However, it is reported in the literature [38-40] that the nanoparticle effect on wear and friction would saturate at a certain concentration. The saturation concentration depends on the type and size of the particle, as well as the properties of the base oil.

Based on the all the results, we would like to suggest the nanoparticles reduce the real area of contact and therefore reduce friction in the boundary lubrication. This theory implies that particles engaged in contact would keep surfaces apart around the particles which results in the reduction of the real area of contact. A decrease in the real area of contact translates to

a reduction of the friction coefficient and wear. As more concentrated nanolubricants are used, more particles would be engaged in the mating surfaces which explains the monotonic reduction in the friction coefficient versus particle concentration. In addition, these particles would bear high.

It is noteworthy to compare the wear on the aluminum pins and the stainless-steel disks, the influence of the crystal structure affects the wear rate, for example the steel disk has a body-centered cubic (BCC) crystal structure with a lower number of slip systems when compared with the aluminum pin, which has a face-centered cubic (FCC) crystal structure. Here, the BCC crystal structure has 48 possible slip systems, but since the planes are not so closely packed, they require higher amounts of stress to cause slip. On the contrary, the FCC crystal structure is closely packed and has 12 possible slip systems that require less stress than the BCC to cause slip. The limited number of slip systems in the steel decreases the occurrence of plastic deformation in the material, thereby severely limiting the real area of contact in the pin-disk interface; for this reason, less wear occurs with the steel disk when compared with the aluminum pin.

1.4.3.3 Surface Studies

1.4.3.3.1 Three-dimensional confocal microscope

To further evaluate the influence of the volume fraction on the wear, an optical profilometer was used to analyze the worn pin surfaces. An optical profilometer was used to measure surface roughness parameters. Figure 18 - Figure 21 shows three-dimensional worn surfaces of pins recorded by the optical profilometer at different loads. Surface analysis shows that the worn surfaces in presence of graphene nanoplatelets into the oil are smoother than neat oil. As it is expected from wear rate data (Figure 15), the worn

46

surfaces of neat oil samples are rougher than the worn surface of nanolubricant if compare Figure 18 - Figure 21(a) with other worn surfaces. Generally, it can be found that the worn surface lubricated only by the neat oil is rougher with many thick and deep grooves, but the worn surfaces lubricated by oil with graphene is comparably smoother and the grooves are shallower.
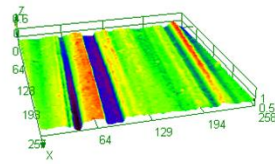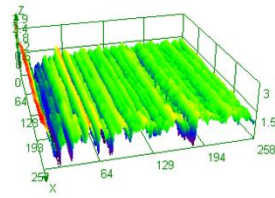
(a)　　　　　　　**(b)**　　　　　　　**(c)**
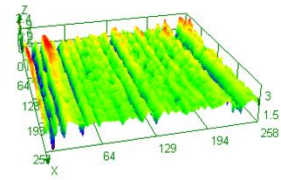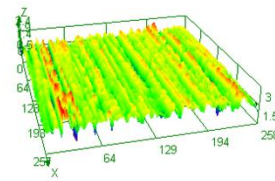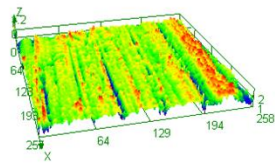
(d)　　　　　　　**(e)**　　　　　　　**(f)**
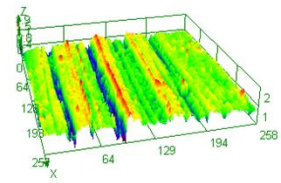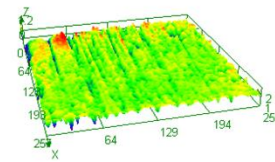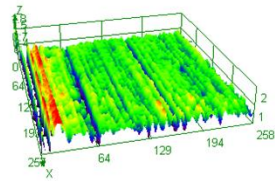
(g)　　　　　　　**(h)**　　　　　　　**(i)**
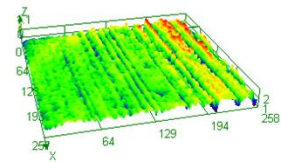
Figure 18 The 3D Optical profilometer images of worn surface of the pin at 5N for the a) neat oil b)0.05 vol.% nanolubricant c)0.10 vol.% nanolubricant d) 0.15 vol.% nanolubricant, e) 0.20 vol.% nanolubricant, f) 0.25 vol.% nanolubricant, g) 0.30 vol.% nanolubricant, h) 0.35 vol.% nanolubricant and i) 0.40 vol.% nanolubricant

(a)　　　　　　　**(b)**　　　　　　　**(c)**

(d)　　　　　　　**(e)**　　　　　　　**(f)**

(g)　　　　　　　**(h)**　　　　　　　**(i)**
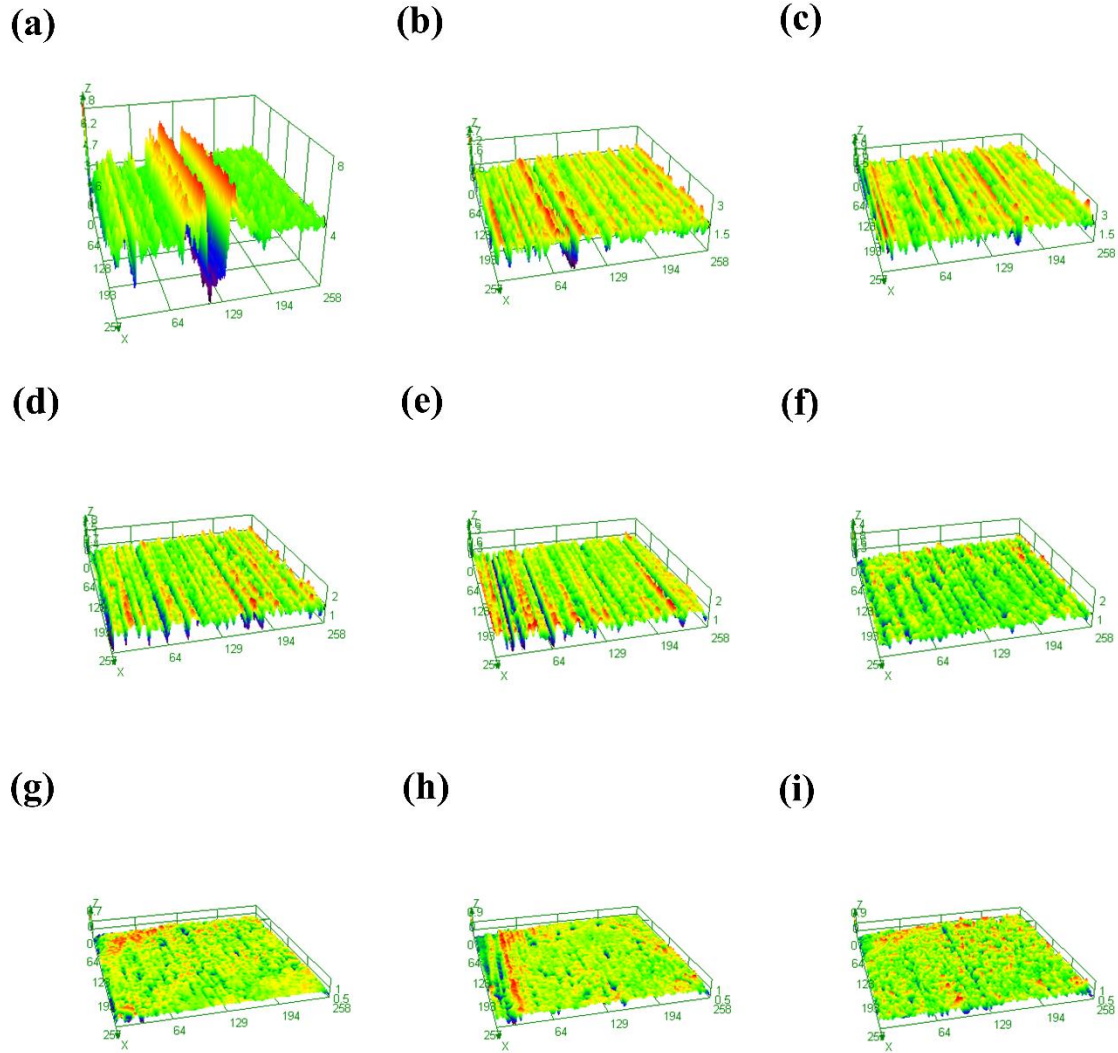
Figure 19 The 3D Optical profilometer images of worn surface of the pin at 10N for the a) neat oil b)0.05 vol.% nanolubricant c)0.10 vol.% nanolubricant d) 0.15 vol.% nanolubricant, e) 0.20 vol.% nanolubricant, f) 0.25 vol.% nanolubricant, g) 0.30 vol.% nanolubricant, h) 0.35 vol.% nanolubricant and i) 0.40 vol.% nanolubricant

(a)　　　　　　　　**(b)**　　　　　　　　**(c)**

(d)　　　　　　　　**(e)**　　　　　　　　**(f)**

(g)　　　　　　　　**(h)**　　　　　　　　**(i)**
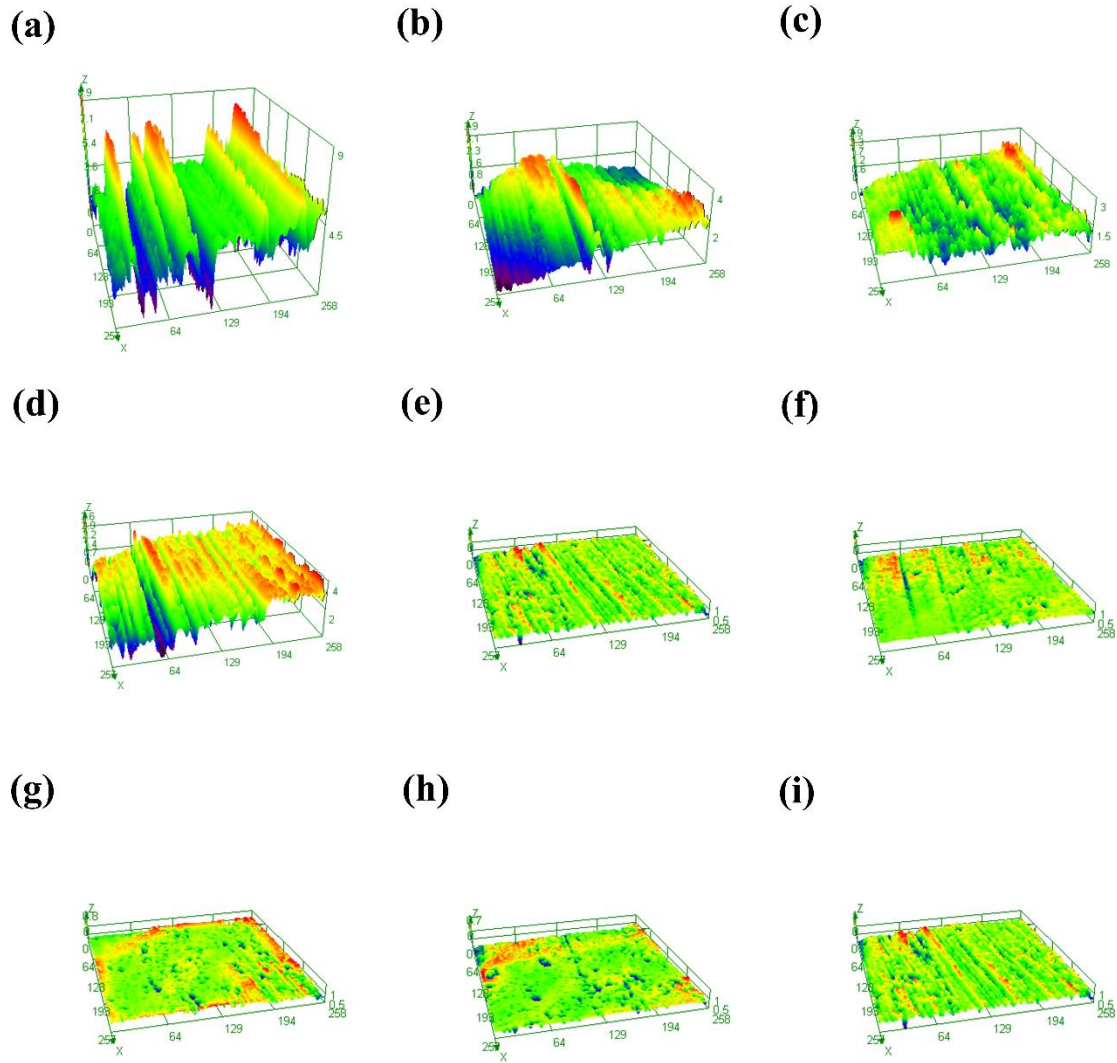
Figure 20 The 3D Optical profilometer images of worn surface of the pin at 15N for the a) neat oil b)0.05 vol.% nanolubricant c)0.10 vol.% nanolubricant d) 0.15 vol.% nanolubricant, e) 0.20 vol.% nanolubricant, f) 0.25 vol.% nanolubricant, g) 0.30 vol.% nanolubricant, h) 0.35 vol.% nanolubricant and i) 0.40 vol.% nanolubricant
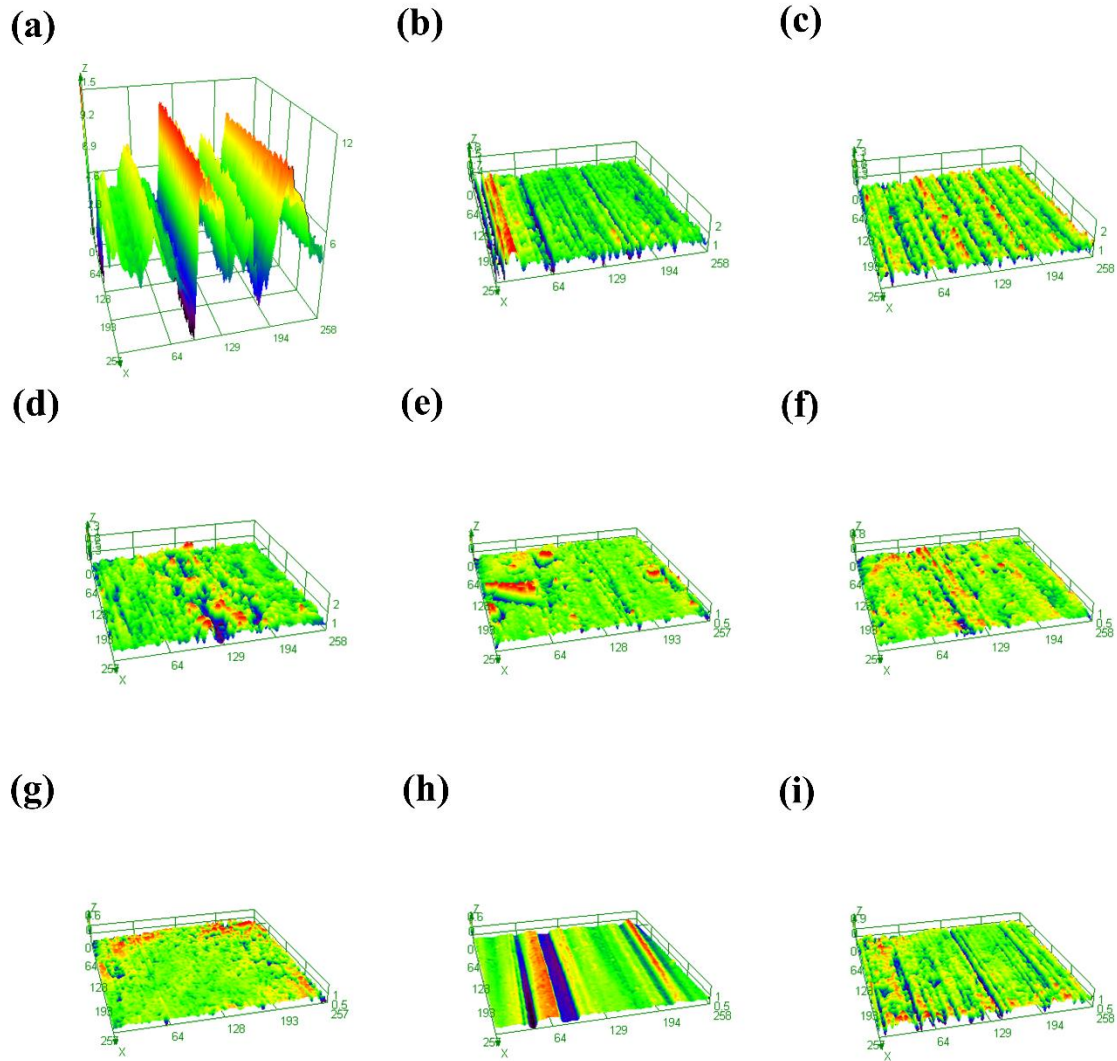
Figure 21 The 3D Optical profilometer images of worn surface of the pin at 20N for the a) neat oil b)0.05 vol.% nanolubricant c)0.10 vol.% nanolubricant d) 0.15 vol.% nanolubricant, e) 0.20 vol.% nanolubricant, f) 0.25 vol.% nanolubricant, g) 0.30 vol.% nanolubricant, h) 0.35 vol.% nanolubricant and i) 0.40 vol.% nanolubricant

The S_a values for the worn pin surfaces for various nanolubricants at different normal load are depicted in Figure 22, which shows a relationship between the surface roughness and volume fraction of graphene nanoplatelets. By comparing the roughness number of neat oil tested sample with nanolubricants, it is obvious that nanolubricants

are effective to enhance the wear rate due less damage and failure on the surface by having less surface roughness number. Moreover, the roughness number of the worn surface decreases by increasing the volume percentage of graphene in nanolubricants up to 0.30 vol.% the same trend of wear rate. Hence, amongst the nanolubricants, the lowest roughness belongs 0.30 vol.% nanolubricants as it is expected from wear data from Figure 16. Therefore, it can confirm the claim that GNPs can fills up the valleys of asperities to smooth the surfaces and avoids direct contact of the two surfaces and reduces the wear. Besides, nanolubricant with higher graphene volume percentage can fill up more gaps and then cover more area of surfaces and then more protection on the surfaces occurs. Therefore, the finish surface is smoother for nanolubricants with more graphene particles. On the other hand, adding graphene nanoplatelets more than 0.30 vol.% have negative effect as the surface roughness increases due to agglomerated graphene behave more like a third-body abrasive particle because of their plate-like geometry, which damages the pin surfaces by plastic deformation, resulting in the high wear volume rate and consequently, rougher surfaces.

It can be concluded from Figure 22 that surface roughness of samples at higher load is smoother as it is expected from wear rate as shown in Figure 16. Hence, adding graphene in nanolubricant is more effective at higher load because of lower wear rate and roughness. generally, there is a correlation between wear rate and roughness after the test. Hence, the wear rate is low, the surface roughness is low.

Figure 23 shows the relationship between wear rate and surface roughness at 15N. A direct relationship between S_a and wear rate and a sharp reduction in wear rate and S_a by adding 0.5 wt.% graphene can be observed. Moreover, the surface roughness increment from 0.35 wt.% to 0.40 vol.% graphene is in line with the increasing wear rate.

Therefore, all samples are corresponding to a direct relationship between wear rate and surface roughness.
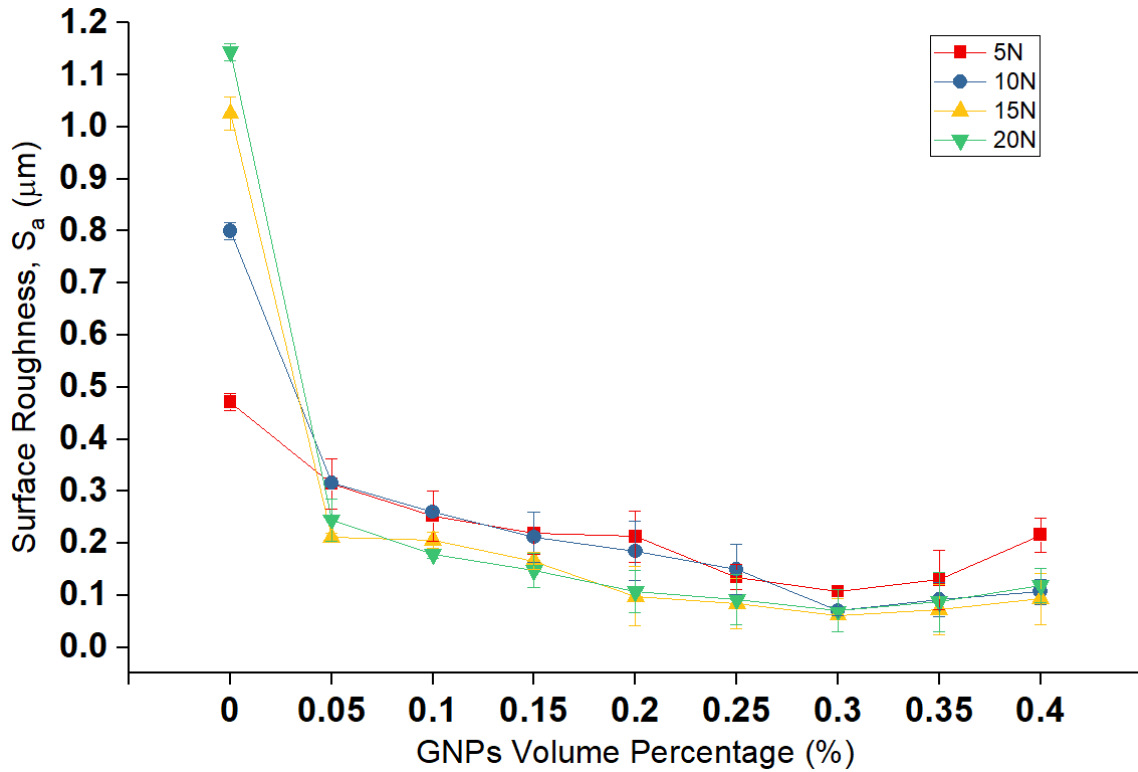
Figure 22 Surface roughness of worn surfaces of pins in several graphene nanoplatelets

at different loads
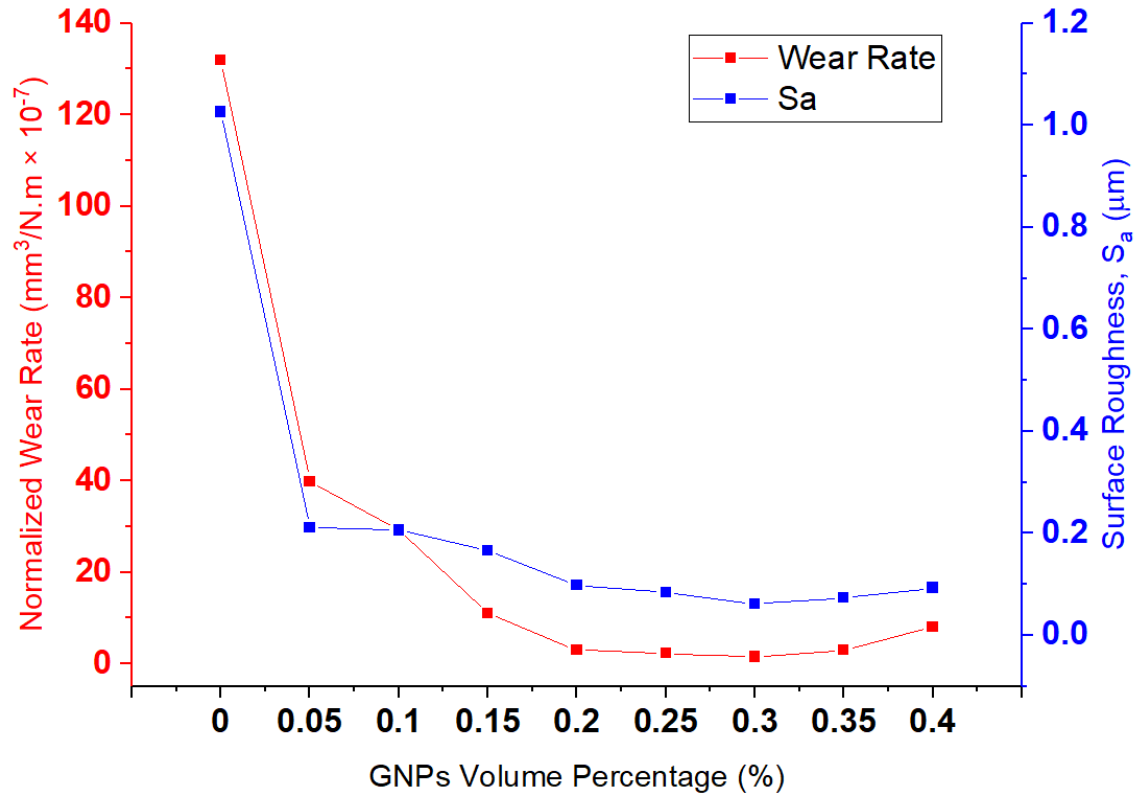
Figure 23 The relationship between Wear rate, the surface roughness (S_a) and GNPs concentration at 15N

1.4.3.3.2   Wear Scar Diameter

After each test, the worn surface is flat, and each worn pin has a unique wear scar diameter that related to wear rate of samples. Figure 24 depicts the scar diameter of the pin at 15N applied load for neat oil and nanolubricants. As shown in Figure 24, the diameter of the pin is larger for the sample tested with neat oil (Figure 24a) in comparison with nanolubricant (Figure 24 b and c) as it is expected because of the higher wear rate for neat oil sample. In addition, it is concluded that the scar diameter of the pin at different applied load for 0.30 vol.% nanolubricant is less than 0.10 vol.% nanolubricant (Figure 25) that confirm the wear rate results which lower wear rate occur in 0.30 vol.% nanolubricant rather than 0.10 vol.% nanolubricant. Moreover, the wear rate is lower at

a higher load, consequently, the scar diameter of pins is smaller as shown in Figure 25 (b), (d) and (f) in comparison with Figure 25 (a), (c) and (e). Figure 26 exhibit the correlation between scar diameter and graphene nanoplatelets volume percentage at different loads. The trend of wear scar diameter versus volume fraction of GNPs is the same trend of wear rate and surface roughness as expected.
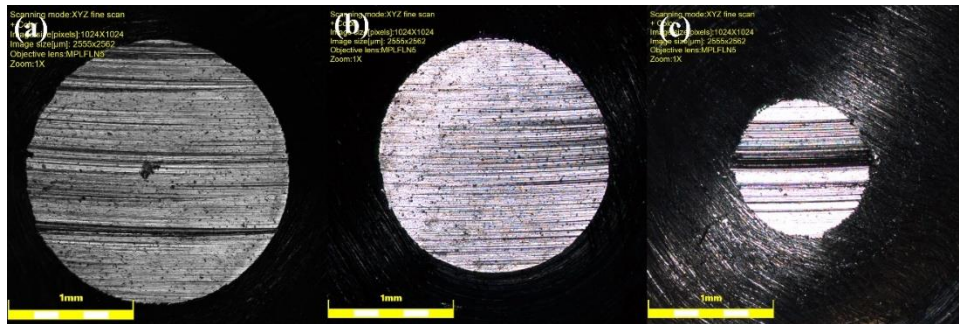
Figure 24 Wear Scar diameter of pins at 15N for samples tested with a) neat oil, b) 0.10 vol.% nanolubricant and c) 0.30 vol.% nanolubricant.

0.10 vol.% nanofluid   **0.30 vol.% nanofluid**
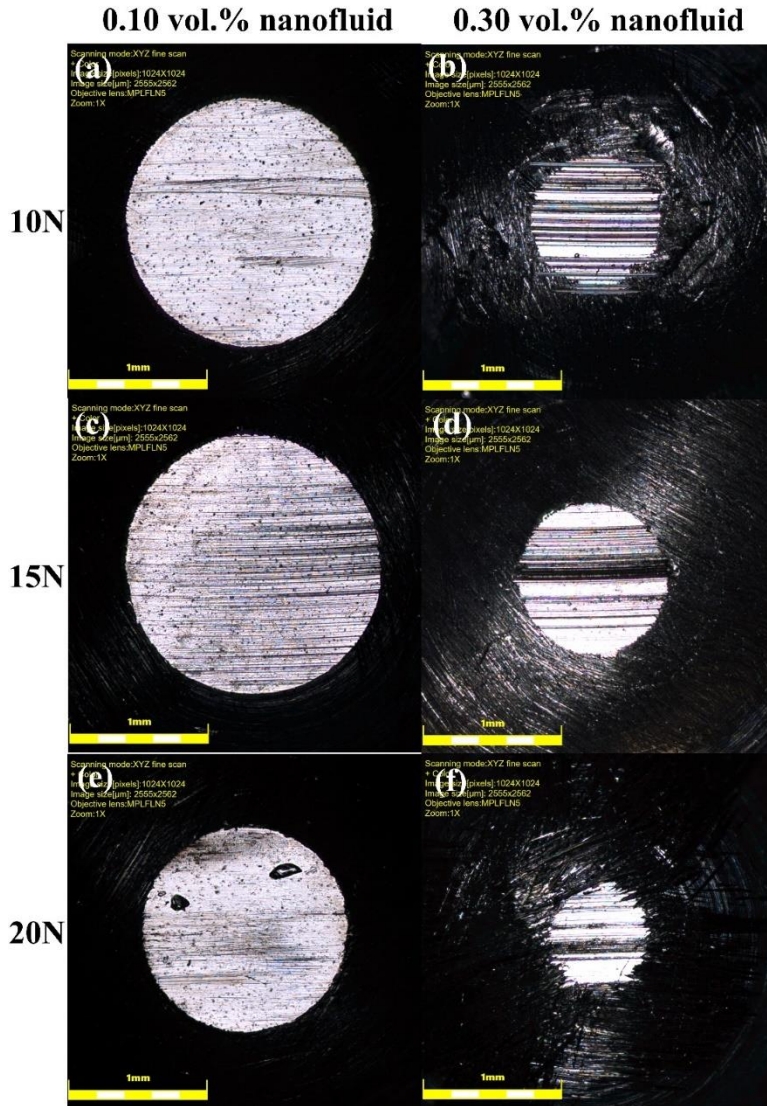
Figure 25 Wear Scar diameter of pins at differ load and graphene volume percentage in nanolubricant
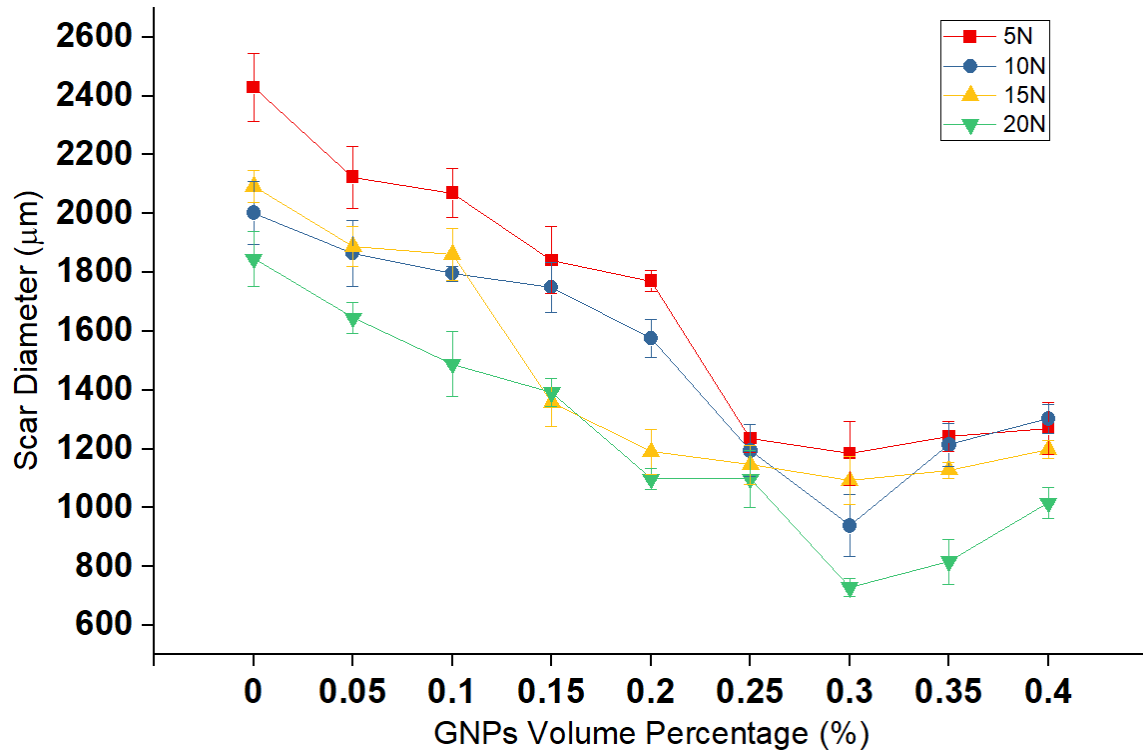
Figure 26 Correlation of wear scar diameter pin with graphene volume percentage of nanolubricant at different applied load

1.4.3.3.3   SEM Analysis

The evidence of reducing the friction and wear in presence of graphene nanoplatelets dispersed in nanolubricant can be confirmed by the results of SEM and EDX. Figure 27 shows scanning electron micrographs of worn pin surfaces for the particulate nanolubricants containing graphene nanoplatelets at different loads. If compare with the worn surface of neat oil (first row) with the worn surface of nanolubricants, it is obvious that the surface is rougher with many thick and deep crack due to no protective layer deposited to protect the worn surface for more damage and abrasive wear. The pin surface used in the neat oil is severely abraded, having a high S_a (Figure 22) value, which is significantly rougher than nanolubricant tests. On contrary, SEM investigations show that graphene nanoplatelets appeared on the worn surfaces of

57

nanolubricants as lubricant tribofilm (Figure 27), unevenly distributed over the texture of the surface. These particles or agglomerated particles as a lubricant tribofilm can be rolled up and are likely to act as nano-rolling and nano-bearing elements, which explains low friction coefficients and wear during the test. A graphene tribofilm is formed on the worn surface of nanolubricants as shown in the second, third and fourth row of Figure 27. This is consistent with the friction and wear results that show lower COF and wear rate for nanolubricants in compression with neat oil samples. In addition, this may suggest that the particles fill the inter-asperity valleys and create a smoother surface finish.

The problem is that these particles are not uniformly distributed over the contact surfaces, producing a preferential wear on the particle-free areas. As the particles migrate in motion, these areas prone to direct contact. This may be the explanation for the variation of the friction coefficient and wear at a different volume percentage of graphene nanoplatelets. Amongst the nanolubricant, more area of the surface covered by graphene tribolayer that can reduce real contact area more and more between two surfaces and consequently, reduce more in the value of COF and wear rate by increasing the number of graphene particles in nanolubricants. In the other word, the surface of worn pin samples covered enough by a graphene tribolayer can reduce the contact of surface-to-surface and then reduce COF and wear rate.

For each applied load from top to bottom in Figure 27, it can be revealed that the surface becomes smoother and roughness number of the worn surface decreases at a higher volume fraction of graphene nanoplatelets. The smoothest surface was observed in 0.30 vol.% nanolubricant. In fact, in this trial the presence of the 0.30 vol.% graphene particles lowered the COF by 82, 74, 73 and 76%, the pin wear volume by 86, 98, 99 and 98%, and the surface roughness by 77, 91, 94 and 94% at 5, 10, 15 and 20 N, respectively.

Therefore, adding 0.30 vol.% graphene is the optimum amount of graphene can cover and form a good distribution of graphene layer on the surface to preserve the pin surface from wear and damage. On the contrary, increasing more on graphene particles cause to have more wear due to agglomeration of particles and act as some third-party abrasive particles that more scratches were observed on the worn surfaces of samples with 0.40 vol.% nanolubricant.

Generally, these results further verify that nanolubricants can form a protective coating on a surface that lowers the coefficient of friction, wear volume, and surface roughness. Besides, the coverage of tribolayer play an important role to enhance the tribological properties.
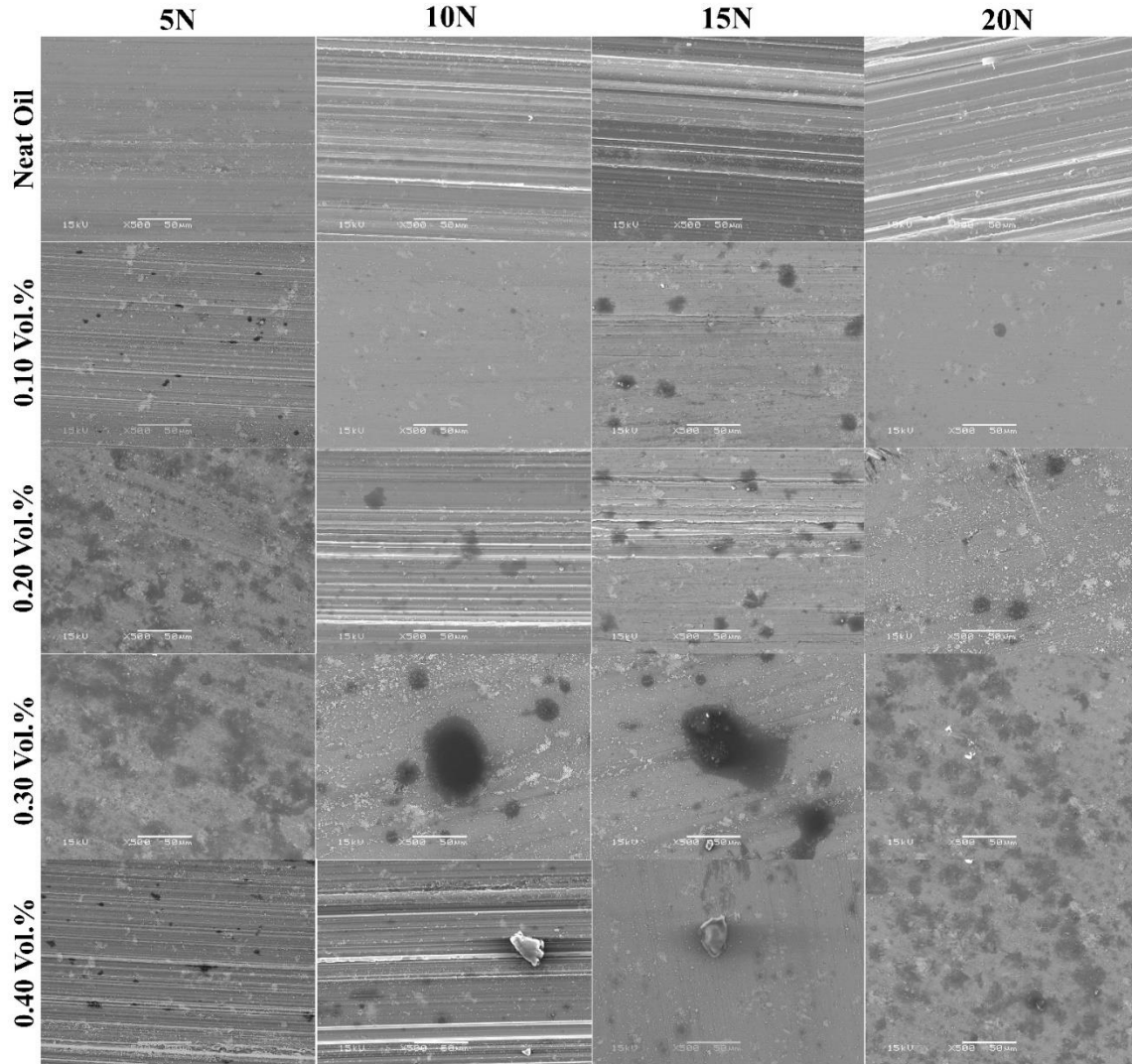
Figure 27 Scanning electron micrographs of worn pin surfaces for various nanolubricant at different loads

1.4.3.3.4 EDX Analysis

Figure 28 presents the EDX spectrum of test surfaces before performing any wear test. As one expects, the majority of the unworn test surfaces are aluminum. The sample surfaces studied in this work are the 2024 aluminum pin, therefore, a comparative study of the surface composition yields more insight on the particle-surface interaction. That is why the analysis of the original surface (Figure 28) shows that the majority of the surface is made of aluminum

with some minor trace of the copper and magnesium. Whereas, EDX results show that the majority of the samples worn under a pure base oil are composed of aluminum and a trace of iron and chromium on the surface and inside the wear grooves was observed (Figure 29). It is also evident in Figure 29 that there is no trace of the carbon element on the surface samples used in this work, prior to surfaces being exposed to graphene nanoplatelets exists in the nanolubricants.
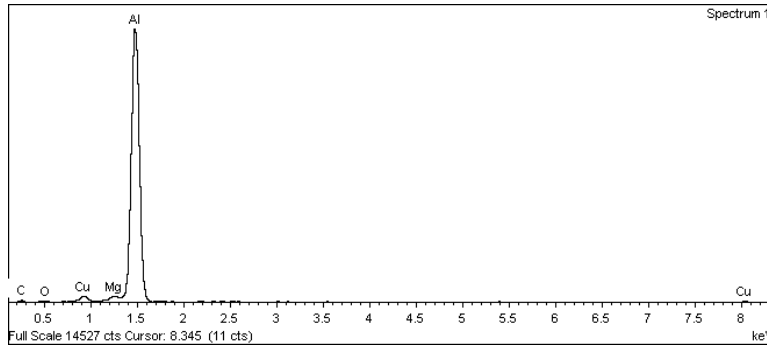
Figure 28 EDX spectrum of unworn aluminum samples before test
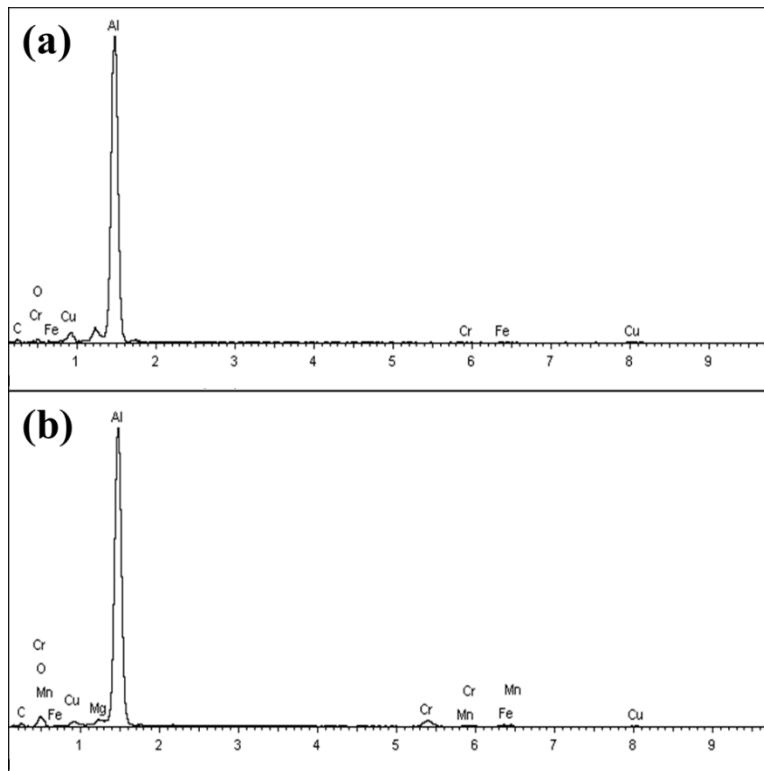
Figure 29 EDX spectrum of worn surfaces of aluminum pin samples for neat oil after test at a) 10N and b) 20N

As mentioned earlier, the addition of graphene lead to enhanced friction and wear because graphene nanoplatelets are brought in between contact areas as the graphene in oil is more stable. This is evident from the EDX analysis which confirms graphene's presence on the surfaces comparatively higher than other neat oil that doesn't contain graphene. It is noteworthy that the addition of 0.30 vol.% graphene has negligible effect

on overall behavior of the base oil due to more graphene flakes are brought in between contact surfaces. As shown in SEM images earlier, there are some black spots on the worn surfaces of pins that it is speculated that graphene particles form a lubricant tribofilm. To confirm these spots containing carbon or graphene, EDX was employed to determine the composition for these spots on the tribofilm. Figure 30 - Figure 33 depicts the EDX analysis for a sample surface tested with nanolubricants at different loads. The EDX analysis indicates that traces of the element carbon exist on the surfaces after being exposed to the nanolubricant during the test that nanoparticles play a significant role in acting upon the tribological contacts. The high concentration of carbon on the surface suggests that the graphene nanoparticles at the SEM/EDS analysis is still largely intact on the surface. This is also made more apparent by comparing to the EDX analysis of the control sample (Figure 29). It can be concluded that the graphene nanoplatelets particles could also be deposited on the worn surfaces for tested samples with nanolubricant containing graphene nanoparticles. This is in contrast to the surfaces worn while submerged in a base lubricant with no graphene particles because they have no signs of carbon. Figure 30 - Figure 33 (c), shows the carbon element mapping of the worn surface and indicates a distribution of nanoparticles adhering to the surface in and outside of the wear grooves. The same arguments stand for other samples and the carbon element trace appears to also be randomly distributed. Using EDX the average weight fraction of carbon detected on the surfaces exposed to the nanolubricant was measured to be 12-95 % at depending on the volume fraction of graphene into nanolubricants. It can be concluded that the graphene particles form a physical deposition film on the rubbing surface and prevent surfaces from direct contact. These results further indicate that graphene nanoplatelets increased the wear resistance of the oil and showed excellent antiwear properties. Generally, the darker areas in the SEM images had higher

63

concentrations of carbon, suggesting that graphene may be adsorbed in these dark areas and form a tribofilm on the worn surfaces that the notable improvements in friction and wear are achieved.

By comparing the composition of a surface tested with the 0.30 vol.% graphene nanolubricant with 0.10 vol.% nanolubricant, high traces of carbon and low traces of iron are observed that this is a relatively lower wear rate. In addition, high traces of iron and low traces of carbon suggest at the lower load that this is a relatively deep grooves where there are more damage and wear on the surface. Therefore, the overall conclusion of Figure 30 - Figure 33 is that particles are adhered to the surfaces in all cases regardless of the depth of the grooves. This suggests that the adherence of the particles does not depend on the high pressures within the asperity contacts as is theorized to be the case with many lubricant additives and the difference is an area that covered by graphene tribolayer. Therefore, it is evident that particles are dispersed randomly throughout the contact zone and can infiltrate the contact regions. This would disregard the hypothesis that the majority of particles fill up valleys and are not engaged in contact. Alternatively, the reduction of friction monotonically continues as more nanoparticles are dispersed in the lubricant. Also, wear seems to be a function of nanoparticle concentration.

Element	Weight%	Atomic%
C	5.27	11.65
O	3.37	5.59
Mg	1.04	1.14
Al	75.51	74.37
Si	0.49	0.46
Cr	5.84	2.98
Mn	1.09	0.53
Fe	3.17	1.51
Cu	4.23	1.77
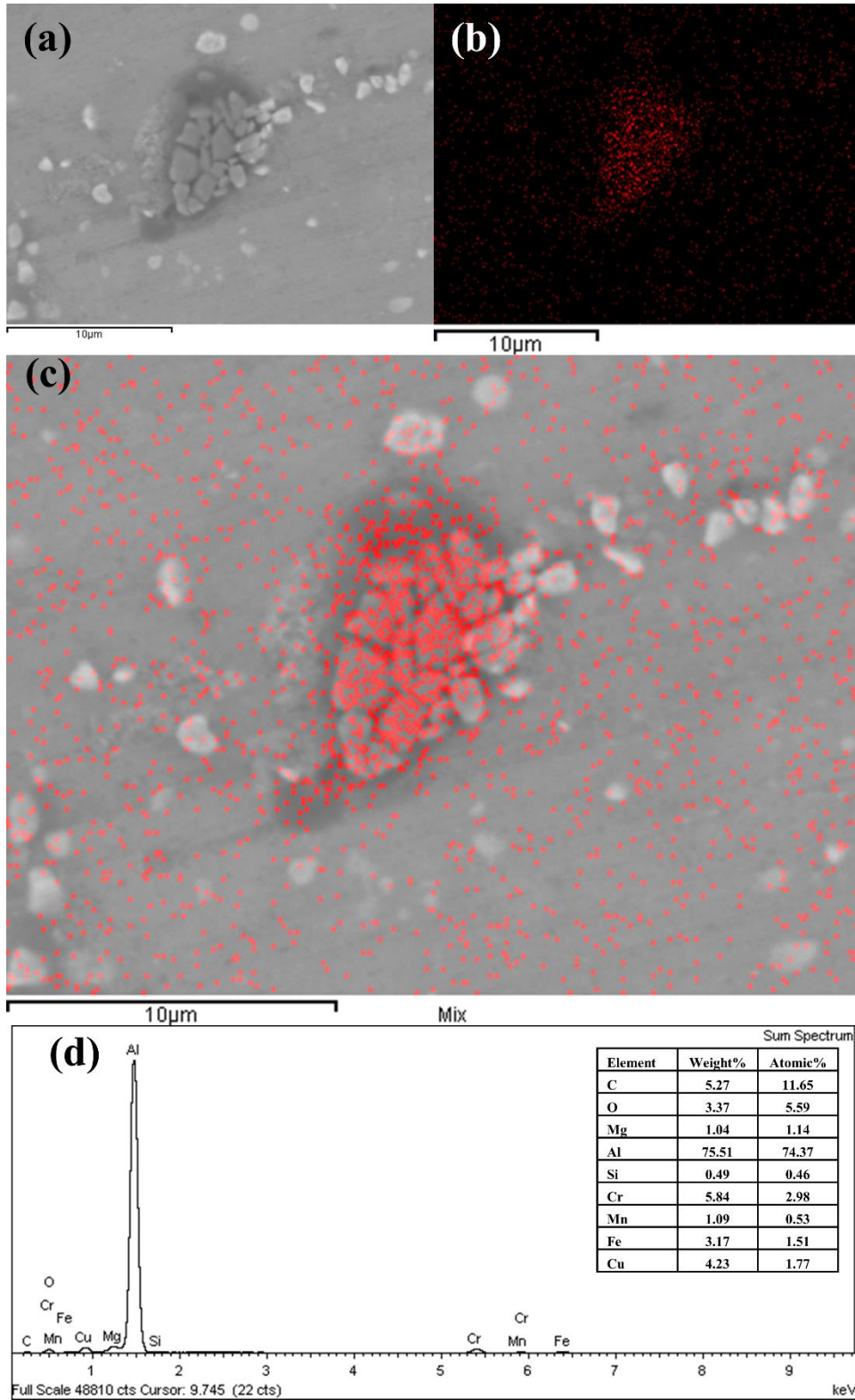
Figure 30 SEM image and elemental mapping for the surfaces tested with 0.10

vol.% nanolubricant at 20N and its material composition using EDX.

65

Element	Weight%	Atomic%
C	80.89	90.34
O	0.88	0.74
Al	17.75	8.82
Cu	0.48	0.10
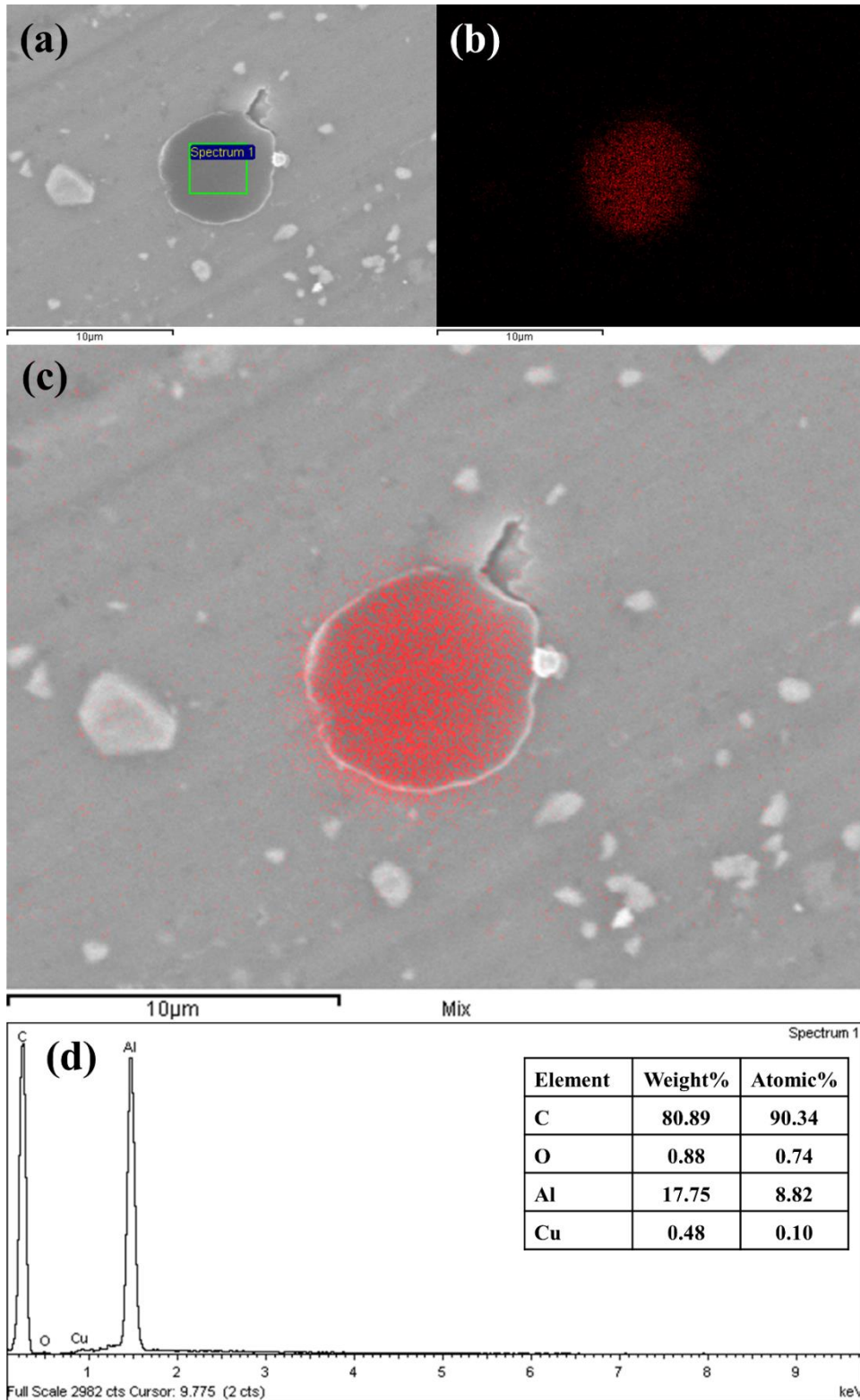
Figure 31 SEM image and elemental mapping for the surfaces tested with 0.30 vol.% nanolubricant at 20N and its material composition using EDX.
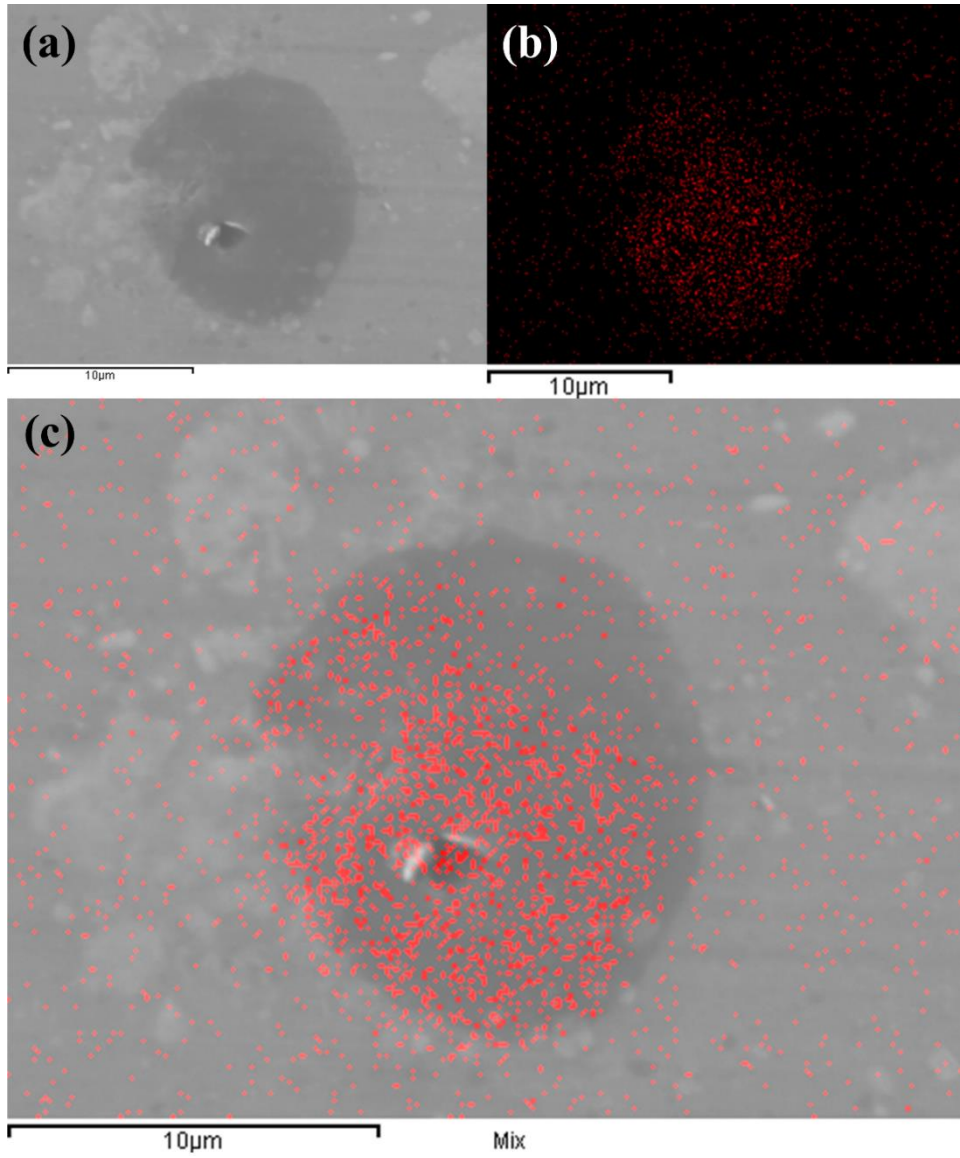
Figure 32 SEM image and elemental mapping for the surfaces tested with 0.10 vol.% nanolubricant at 10N and its material composition using EDX.
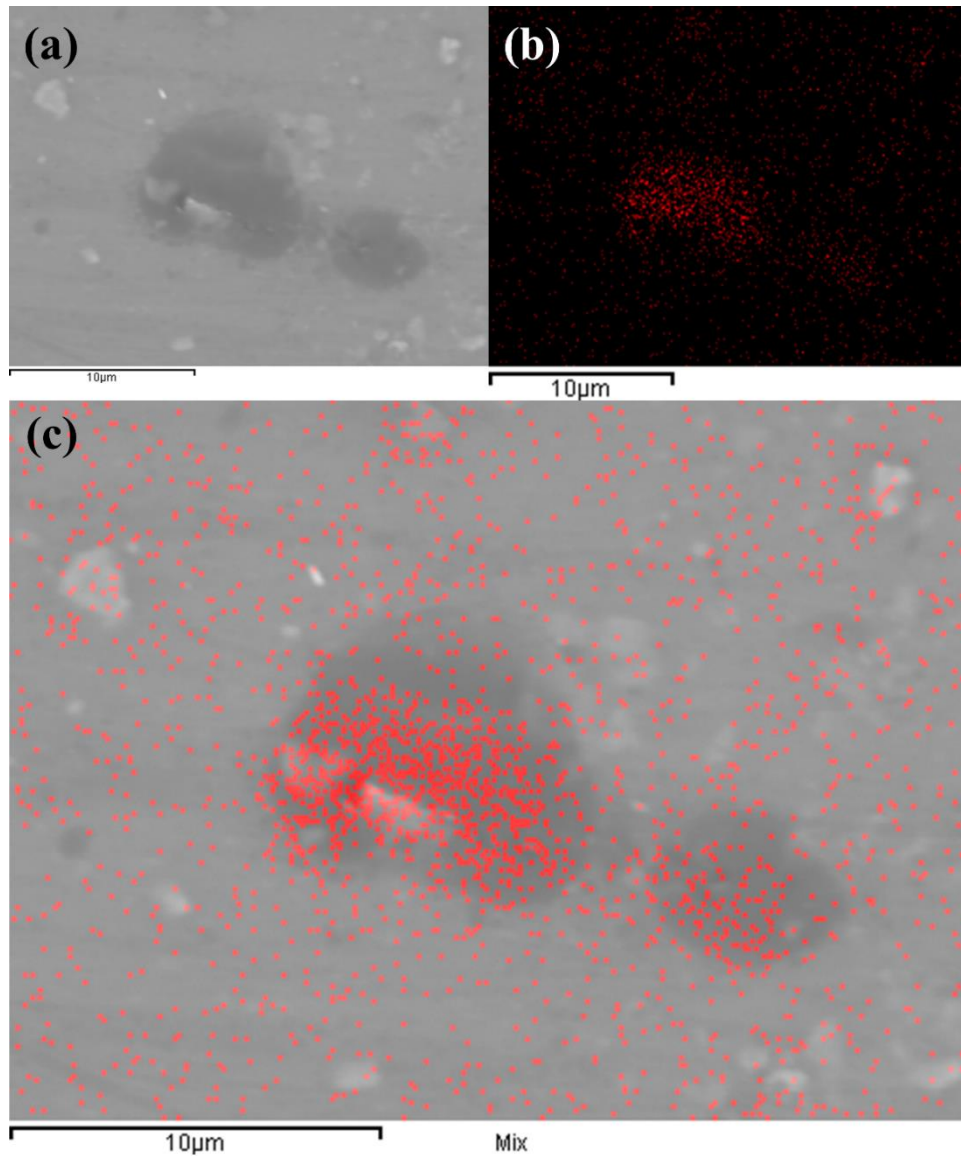
Figure 33 SEM image and elemental mapping for the surfaces tested with 0.30 vol.% nanolubricant at 10N and its material composition using EDX.

The mechanism of reduction in the real area of contact needs further investigation and study to be fully proven. One helpful study could be the characterization of the size of nanoparticles prior to and after the tests which can prove the abrasive nature of the particle-surface contact. It should be added that various nanoparticles behave differently based on

their mechanical behavior as governed by chemical and physical properties and arguments raised in this chapter are currently limited to the graphene nanoparticles studied.

1.4.3.3.5   Raman Spectra

The full Raman Spectra of worn surface of sample lubricated by neat oil and nanolubricant with 0.30 vol.% graphene is shown in Figure 34. The Raman spectra of the aluminum pin surface on the wear track surface lubricated by the neat oil prove no existence of graphene because of no existence of D- and G-band in the Raman spectra. On the other hand, the wear track surface lubricated with the nanolubricant exhibits strong D- and G-band of graphene in the Raman spectrum that confirms worn surface at least partly covered with graphene, however, with a disordered structure due to the presence of the D-peak in the Raman spectra. Therefore, the analysis result verifies the deposition of graphene nanoplatelets on the worn surface during the wear process, and the wear track surface is almost covered by the graphene after the tribological test (Figure 27). Consequently, the addition of GNPs into the oil clearly gives a positive effect on fraction and wear as can be seen in Figure 7 and Figure 15.
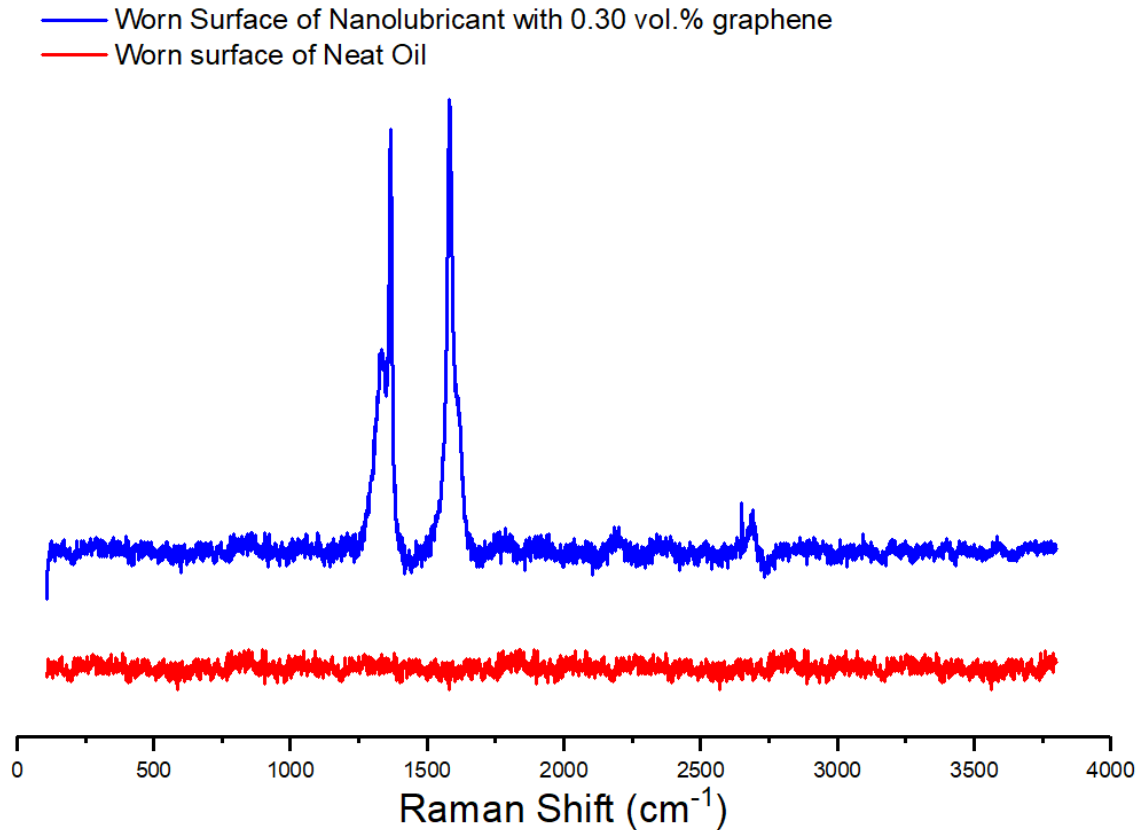
Figure 34 The Raman spectrum of the worn surface of nanolubricants with neat oil and 0.30 vol.% nanolubricants

1.4.3.3.6 Wear Mechanism

Several mechanisms have been proposed for various tribological enhancements using graphene as an additive. Zhang et al. [69] used liquid phase exfoliated graphene modified by oleic acid as additives (0.02–0.06 wt.%) in lubricant oil which showed enhanced performance, with friction coefficient and wear scar diameter reduced by 17% and 14%, respectively. Similarly, Lin et al. [50] found that the surface modified graphene enhances the wear resistance and load-carrying capacity of the machine. Their SEM and EDX results show that the enhancement might be due to extremely thin laminated structure, allowing the graphene to easily enter the contact area. Micro-tribological

studies by Ou et al. [94] showed that the reduced graphene oxide possesses good friction reduction and antiwear ability. They attributed the enhancement to graphene's intrinsic structure and self-lubricating property. Miura et al. [95] claimed that the grease with this graphene was providing better lubricating performance than all the other existing additives. Moreover, atomic force microscopy (AFM) based friction studies of graphene substrates have been instrumental in explaining various possible mechanisms [75, 96]. Electron-phonon coupling [97], puckering effect [76] and interplay of surface attractive forces [98] in graphene have a major role in reducing friction.

Based on the experimental observations and review of the existing literature, it was understood that the occurrence of several morphological transformations of graphene simultaneously or subsequently could be the key. The large variation in flake size exists when graphene is synthesized and dispersed in fluids using sonication techniques [99]. Therefore, the graphene-based suspension should be a poly dispersed graphene-oil mixture [100]. Small flakes could easily deposit in the valleys and prevent the deepening of the same. Large flakes could provide coating effect by sliding, buckling, bending or by turning into semi tubes as the shear forces act on them.

Graphene slides between the contacts [54], especially during mixed and hydrodynamic lubrication, thereby furthering the formation of a protective film [50] could be mainly possible due to its planar structure. As discussed, SEM images show that the graphene is deposited in valleys and ridges and EDX analysis further confirmed high carbon deposition in wear tracks as shown in Figure 37 - Figure 39.

The lubrication models of the pure neat oil and the nanolubricant are illustrated in Figure 35. In this study, in case of lubrication with the neat oil, two contact surfaces scratch each other, and many abrasive particles are produced because of the friction force.

71

The abrasive particles slide under high friction stress, leading to the contact surface becoming extremely rough. Once the surface roughness exceeds the oil film thickness, the dry contact will happen, and wide and deep grooves and furrows are formed on the wear surface. But as graphene are added to neat oil, the graphene with oil can penetrate the interface of contact pairs and gradually deposit and accumulate in the original. Quickly, these grooves are filled up, and the contact surfaces become flat and smooth, resulting in a decrease in frictional force. The surface roughness of the rubbing surfaces is largely decreased compared with that lubricated with the neat oil. Finally, the deposited graphene nanoplatelets form a deposition lubricant tribofilm and cover the worn surface, as confirmed by SEM and Raman, which results in fewer abrasive particles produced. The reduction of abrasive particles is helpful for maintaining the smooth contact surfaces and reducing the wear volume of friction pairs.

In addition, this performance can be described as the lubrication regime transition [69] as shown in Figure 36, where h is the thickness of the lubrication film, and R_a is the roughness of the solid surface. The lubrication in neat oil belongs to the mixed lubrication regime which contains dry contact (DC) and boundary lubrication (BL). Graphene coating on the surface reduces the roughness of the surface, resulting in an increase in h/R_a, thus the lubrication goes up into the BL regime. When the higher concentration of graphene is added into neat oil, graphene sheets will pile up between friction pairs, blocking the oil film. As h/R_a declines, the lubrication falls down to the mixed lubrication regime again.

Moreover, when the load increases, elastic deformation of the graphene takes place and it will reduce the buffering friction. And also, since the thickness of graphene layers in the present case is less in nanosized, this can form a nanobearing between moving surfaces. This may result in sliding when the excess load is applied. Hence, added additive

72

to the base oil can act as a mechanical reinforcing element during friction and can, therefore, strengthen the load carrying capacity of the nanolubricants.
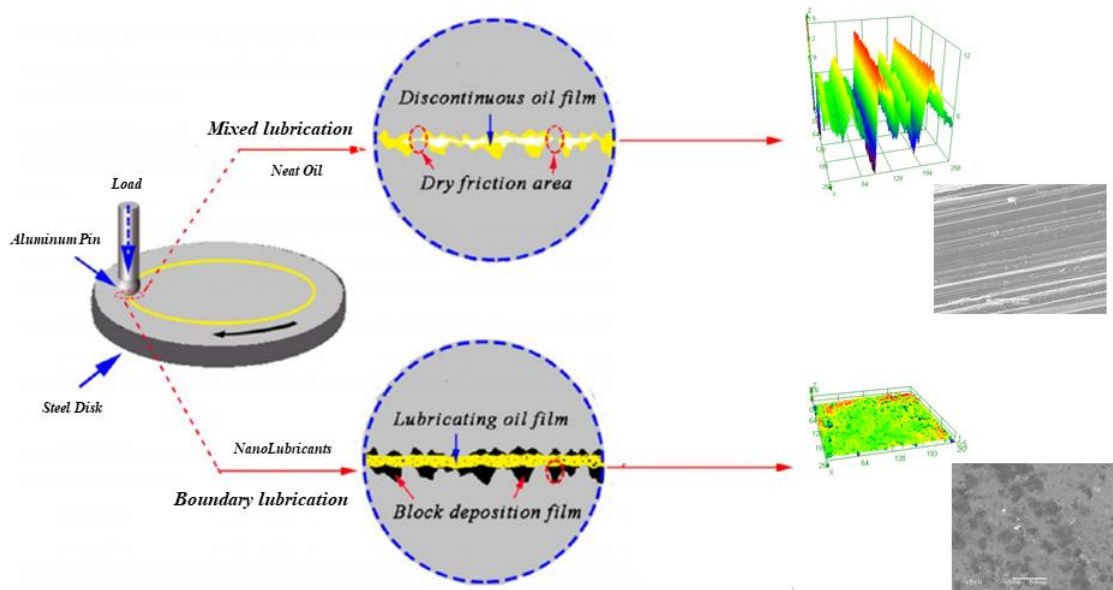
Figure 35 Schematic of the lubricating models of the neat oil and the nanolubricants
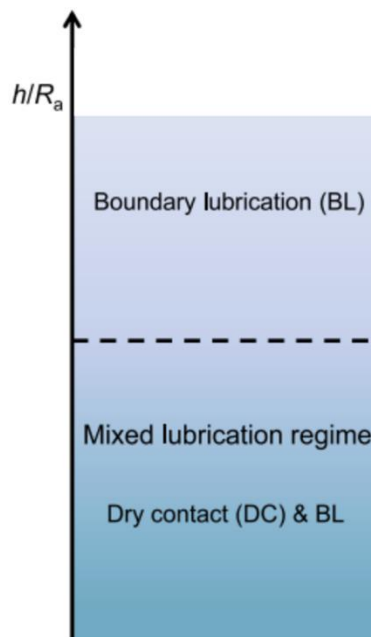
Figure 36 Lubrication regime transition

As the graphene is the absorbent of oil, it can be suggested that the graphene can absorb base oil, which thickens the oil film and prevents the friction pairs from direct contact. As a result, the lubrication state in the graphene dispersed oil has transferred to

good boundary lubrication from the mixed lubricating in the neat oil, which leads to a significant improvement in friction reduction and antiwear ability [101].

In summary, it can be explained by two important roles of graphene nanoplatelets: Firstly, the graphene nanosheets enter the contact with the oil and roll between the two contact surfaces. Secondly, during the sliding, because of the high contact pressure creating stressed zones of traction/compression and then lead to the formation of a thin physical tribofilm on the pin, as shown in Figure 37 - Figure 39. The physical tribofilms could not only bear the load but also prevent from direct contact of two metal surfaces. Therefore, the antiwear ability of the oil with graphene nanoplatelets was improved, and the friction coefficient and wear are decreased significantly.

Element	Weight%	Atomic%
C	7.32	15.39
O	2.15	3.40
Mg	1.06	1.10
Al	82.46	77.21
Mn	1.11	0.51
Fe	0.61	0.28
Cu	5.29	2.10
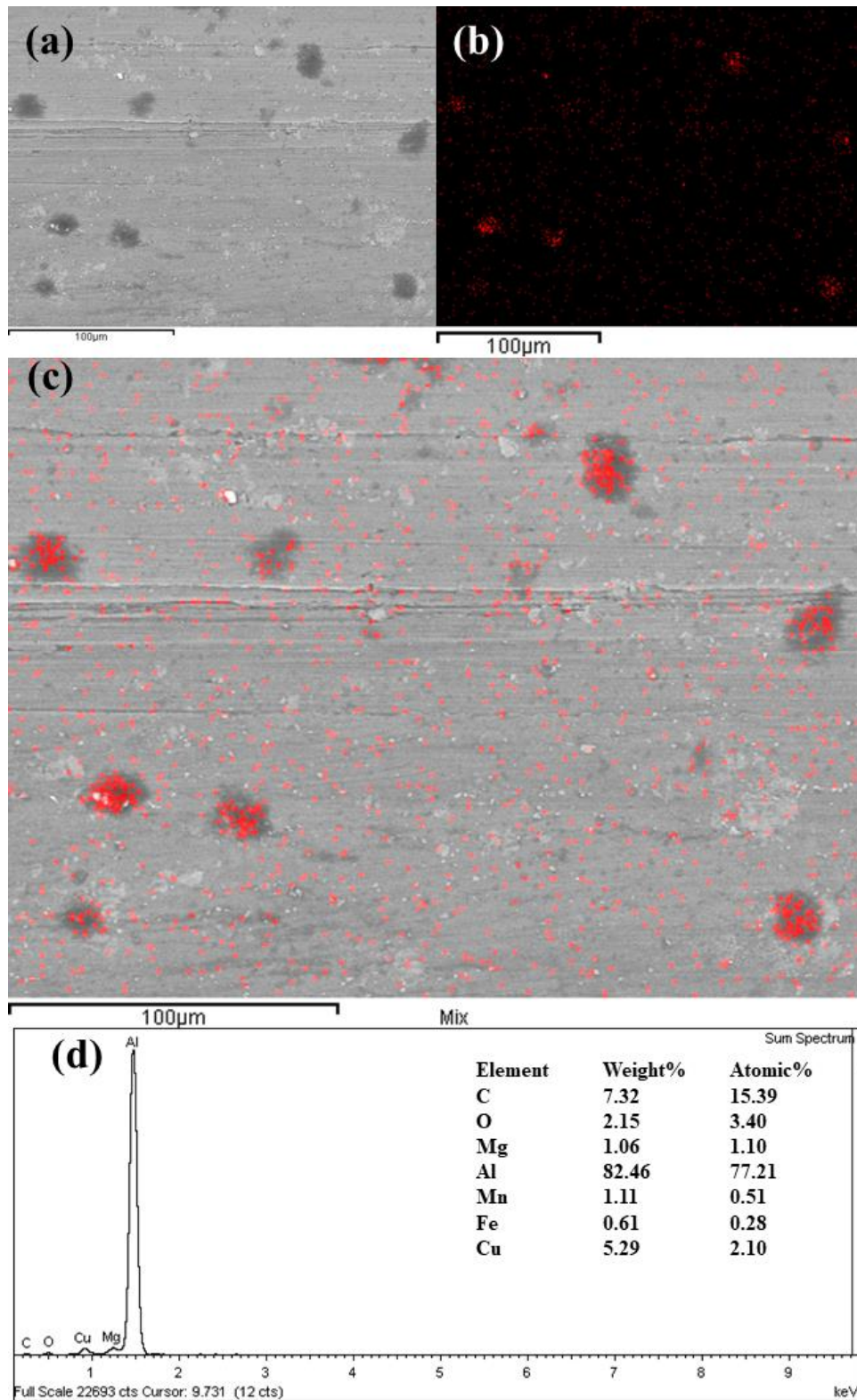
Figure 37 SEM image and elemental mapping for the surfaces tested with 0.10

vol.% nanolubricant at 15N and its material composition using EDX.

76

Element	Weight%	Atomic%
C	11.21	22.89
O	3.25	4.99
Mg	0.86	0.86
Al	72.78	66.16
Cr	3.77	1.78
Mn	0.98	0.44
Fe	2.13	0.93
Cu	5.04	1.94
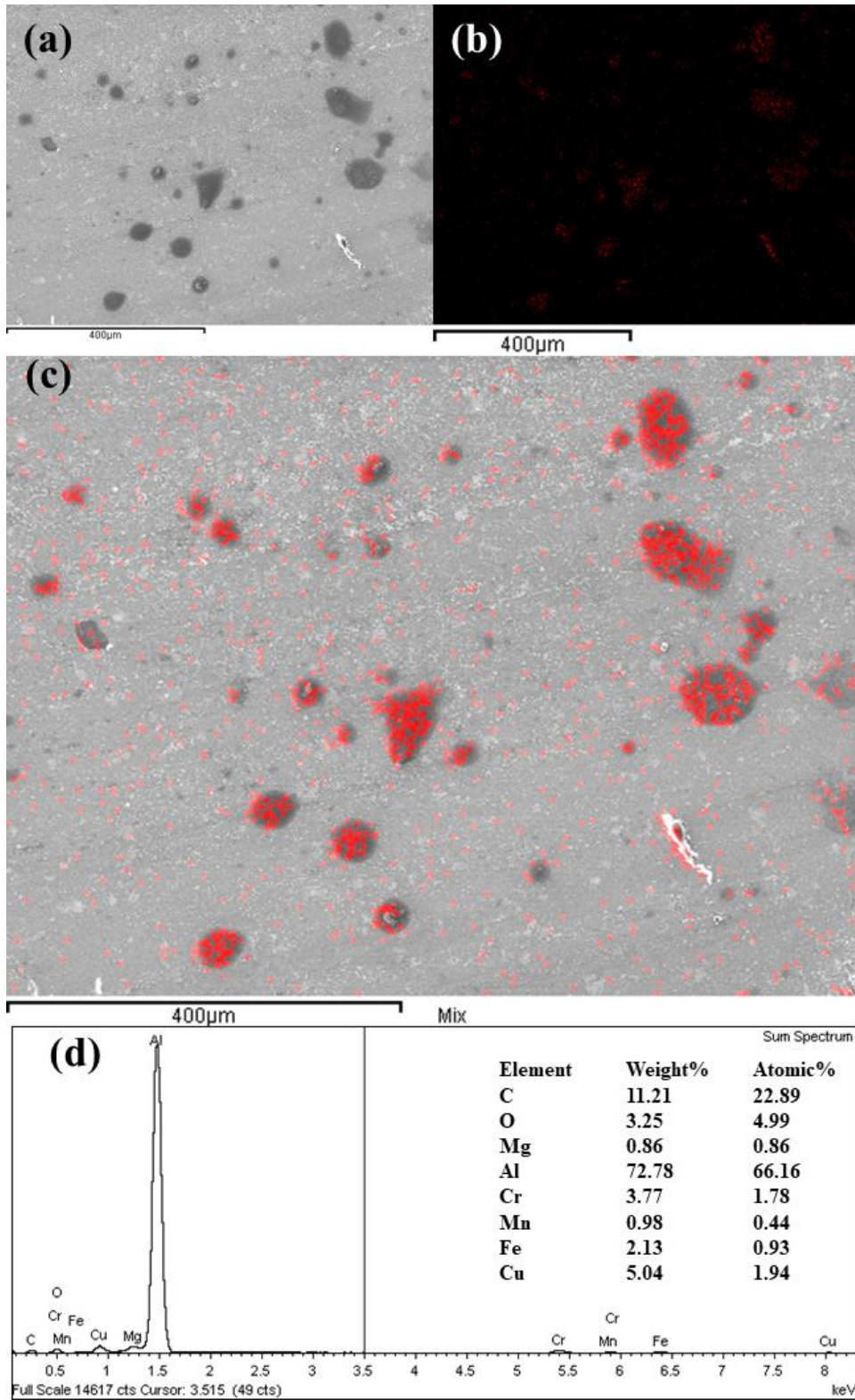
Figure 38 SEM image and elemental mapping for the surfaces tested with 0.20

vol.% nanolubricant at 20N and its material composition using EDX.

77

Element	Weight%	Atomic%
	14.61	29.11
O	3.59	5.37
Mg	0.69	0.68
Al	65.61	58.20
Cr	6.61	3.04
Mn	0.90	0.39
Fe	3.83	1.64
Cu	4.16	1.57
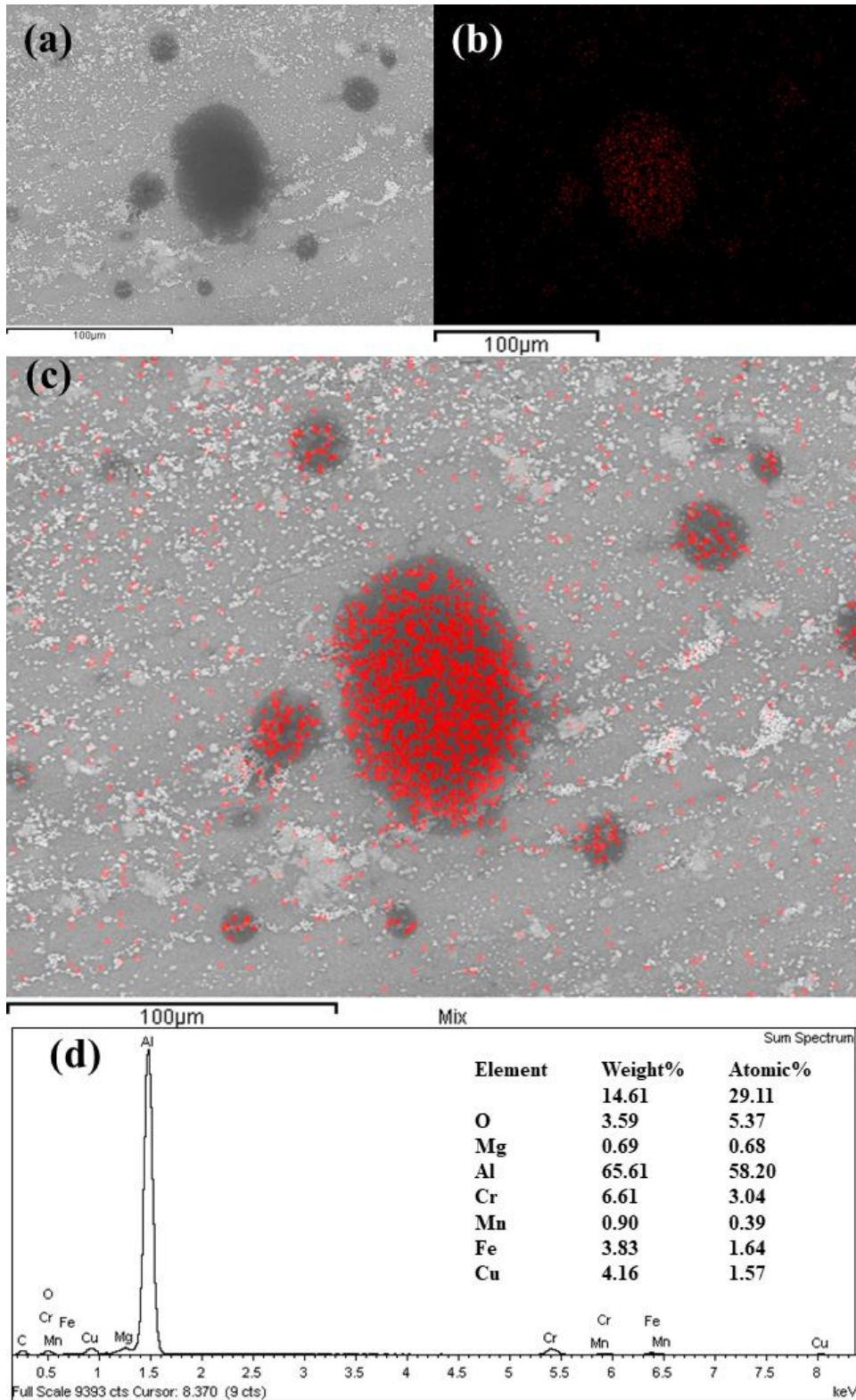
*Figure 39 SEM image and elemental mapping for the surfaces tested with 0.30 vol.% nanolubricant at 10N and its material composition using EDX.*

78

1.5 CONCLUSION

Graphene nanoplatelets (GNPs) were added to neat canola oil with several volume percentages. The results for the nanolubricants were then compared to the results of a neat oil. A pin-on-disk friction tribometer was used to test nanolubricants in the boundary lubrication region. The values of the coefficient of friction (COF) and steady state temperature are then recorded for different applied normal load. Results indicate that COF decreases by adding GNPs where the COF improve 14%, 27%, 52% and 33% by adding just 0.05 vol.% graphene at 5, 10, 15 and 20N, respectively. Increasing the concentration of graphene can decrease the COF. The friction coefficient decreases by 83%, 79%, 84% and 83% for the GNPs concentrations of 0.3 vol.% at 5, 10, 15 and 20N, respectively. The steady state temperature is also lower for nanolubricants which could be the result of the higher thermal performance of nanolubricants and/or the lower friction of the nanolubricants. There is no change in the viscosity by adding the GNPs. The viscosities of the nanolubricants decreases by increasing the load. The Stribeck curve was introduced which consolidates the friction and the viscosity results in one curve. Wear volume shows improvement by adding GNPs in based oil. There is an optimum point of concentration of GNPs where the wear rate is in lowest value. By increasing the load, the wear rate of aluminum in presence of nanolubricants decreased while the wear rate of neat oil increases.

The worn surfaces of the samples examined to find the role of graphene particles in the nanolubricants as well as the wear mechanism. The worn surface texture and surface roughness value show that lubricated surface with nanolubricants are smoother since narrower and shallower grooves exist. There is a direct correlation between wear

79

rate and surface roughness. Wear scar's diameters for each sample was measured and it has been shown that they decreased by increasing the volume percentage of graphene up to 0.30 vol.%. Then the wear scar diameters increase by increasing the concentration above 0.30 vol. %. The SEM/EDX analysis identified the elements on the surface samples tested with the nanolubricants. EDX results show that aluminum is the dominant element of worn surface and a trace of iron and chromium on the surface was observed and there is no significant trace of the carbon while the worn surfaces of lubricated with nanolubricant show that carbon presents on the surface due to the formation of tribofilm. To confirm that tribofilm is lubricant graphene film, Raman Spectroscopy was employed. The wear track nanolubricant exhibits strong D- and G-band of graphene in the Raman spectrum that confirms worn surface covered with GNPs. Therefore, the result verifies the deposition of graphene nanoplatelets on the worn surface during the wear process. Based on the results and characterization of worn surfaces, different possible enhancing mechanisms were discussed and the reduction of the real area of contact by forming lubricant graphene tribofilm was proposed as the dominant mechanism in this work. The proposed mechanism is compatible with the friction and wear experimental data.

2 CHAPTER II: EFFECT OF GRAPHENE AS A REINFORCEMENT

2.1 INTRODUCTION

A composite material is the combination of two or more dissimilar materials to form another material having superior properties. In the industries such as automotive, aerospace and sports, the requirements for high-performance materials to meet challenging demands keeps increasing. It is more difficult for conventional metals and alloys to need such demands since they have limited properties based on reinforcing metals with suitable reinforcement, Metal Matrix Composites (MMCs) provide alternative materials with enhanced properties to satisfy the challenging demands. Composite materials can be more easily tailored to have specific properties such as being lightweight, having high specific strength, high specific stiffness, high wear resistance, low coefficient of friction, high hardness, tailored thermal conductivity, low coefficient of thermal expansion, high energy absorption, and high damping capacity.

MMC's have been investigated by many researchers and create improvement in properties are observed for the same volume fraction of reinforcements when the size of the reinforcement is decreased. With recent advances in producing particles below 100 nm, it is expected that significant improvements can result from the incorporation of nanoparticles in metals. A nanocomposite is a combination of two phases, at least one of which is in the order of nano size (less than 100 nm) at least in one dimension. Accordingly, a metal matrix composite reinforced with a nanosized particle can be termed as a metal matrix nanocomposites (MMNCs). It is expected that by scaling down the particle size in MMC's and going down to the range of nanosized, some of the shortcomings

82

such as poor ductility, poor machinability, and reduced fracture toughness may be overcome. Generally, the size of reinforcement influences the mechanical properties such as strength, ductility, and fracture of MMCs. MMCs are produced to have superior properties when the reinforcement size is in the nano range. There are a few common different mechanisms for increase in strength in metal matrix composites; (1) Orowan strengthening from dislocation bowing by reinforced particles, (2) Hall–Petch strengthening from grain refinement, (3) Forest strengthening resulting from the Coefficient of Thermal Expansion (CTE) mismatch between matrix and particles, and (4) Taylor strengthening by modulus mismatch between matrix and particles. MMNCs will benefit from the Orowan mechanism only if a dispersed second phase of nanosized could be attained since the strengthening increase at the interface. Hall–Petch strengthening will in general one of the most active mechanisms which improve the strength in MMNCs by incorporation of nanoparticles which leads a decrease in grain size. The addition of nanoparticles refines grains or confines grain growth. CTE and modulus mismatch is considered to be negligible when compared to strengthening due to Orowan and grain refinement in several recent studies [102-105].

Among various reinforcements, recent emerging materials, carbonous materials, are found to have many favorable attributes such as high thermal conductivity, low coefficient of thermal expansion, high damping capacity and good self-lubricant property[102]. Considerable amount of research has been done to study the influences of embedding graphite particles into the metal matrix on the tribological properties of aluminum alloys [106-108]. Metal matrix composites embedded by graphite or carbon fibers have exhibit self-lubricating behavior since

graphite act as a solid lubricant [109]. In this regard, solid lubricant as reinforcement tends to decrease the friction coefficient of MMCs and improve tribological properties of composite, compared to composites reinforced by ceramic particles like aluminum and SiC. The graphite size, which has commonly been used in MMCs fabrication and obtaining desired mechanical and self-lubricating properties are in the micron range [102, 103, 110-115].

Recently, research has been focused on nanosized carbonous materials, such as carbon nanotubes (CNTs) and nano-graphite or graphene [110] in order to attain enhanced mechanical, electrical, and tribological properties. Carbon nanotubes and graphene possess exceptional mechanical strength as well as excellent electrical and thermal conductivities, and their incorporation in metallic matrices can lead to composites with higher mechanical, electrical, and magnetic properties. This has led to an increasing interest in incorporating carbon nanotubes and graphene in MMCs the most effective reinforcement for synthesizing self-lubricating composites for structural and functional components [116-118]. Carbon nanotubes and graphene were observed to reduce the grain size in aluminum alloys, resulting in an additional higher strength.

Although the emerging research interest in smart materials such as self-lubricating composites inspires both academia and industry that the combination of these carbonous materials and metallic matrices could potentially create composites that have high thermal and mechanical properties as well as exceptional wear resistance, there is still a need of understanding the nature, processing, and tailoring of these composites.

84

2.1.1 SELF-LUBRICATING METAL COMPOSITES

Man-made self-lubricating materials primarily involve the creation of some type of composite materials. A composite is a coupling of two different materials designed to inherit the qualities of both materials. Self-lubricating composites take advantage of a hard structural matrix carefully combined with a lubricating phase [119, 120]. There are several ways to incorporate the lubricating phase. Dispersing solid lubricant particles or fibers throughout the matrix can be a simple and effective way to ensure that the material is constantly lubricated. The properties of the individual matrix and lubricant, the concentration of the lubricating phase, the distribution or order of the lubricating phase and the interactions between the lubricant and the matrix, are all variables that determine the quality of these types of composites. A schematic of the self-lubricating composite is shown in Figure 40. As shown in the figure, the material wears against the contact surface, new solid lubricant particles will be exposed to the surface thereby keeping the surface lubricated. A classic example of this type of composite is the grey cast iron; it utilizes a hard iron matrix with dispersed lubricating graphite flakes. Constructing a composite with alternating layers of the structural phase and the lubricating phase is also an effective way to engineer self-lubricating materials.

As mentioned earlier, the distinctive feature of self-lubricating composites is that the wear particles formed on the contact surface act as solid lubricants and it can reduce the friction coefficient and wear rate. For instance, under sliding conditions, the metal/graphite composite can form self-lubricating composite because of the transfer layer of graphite which formed on the tribosurfaces during

85

sliding and this transfer layer acts as solid lubricant film which prevents direct contact between the mating surfaces [121]. To have an effective lubricant layer, it is also important that the solid lubricant has a strong adhesion on the bearing surface; otherwise, this lubricant layer can be easily rubbed away and tends to very short service life.
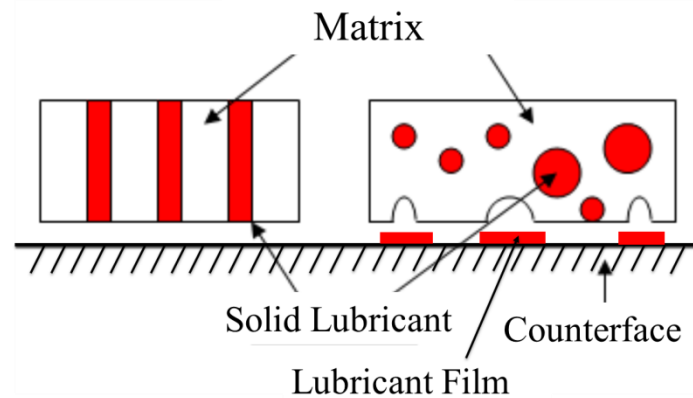
Figure 40 Schematic of self-lubricating composite and its mechanism

2.1.2 WHY SELF-LUBRICATING MATERIALS?

In most tribological applications, liquid or grease based lubricants are used to facilitate the relative motion of solid bodies by minimizing friction and wear between interacting surfaces. A lubricant made of lower shear strength layer between two contacting surfaces and the shear strength of this layer is less than the surface shear strength between the sliding surfaces[122]. Therefore, this lower shear strength lubricant layer reduces friction between the surfaces during relative motion [123]. In fact, lubricants can separate the surfaces with no actual contact between two metallic surfaces. This means that there is no formation of asperity junctions between the surfaces. However, in most cases, depending on the

thickness of the lubricant and testing conditions, asperities may have contacts and it is not possible to avoid asperity contacts completely; although lubricants are able to reduce asperity to asperity contact, they may also reduce the shear strength of the junctions formed [124, 125].

The challenges for liquid lubricants arise in extreme environmental conditions, such as very high or low temperatures, vacuum, radiation, and extreme contact pressure. At these conditions, solid lubricants may be the alternative choice which can help to decrease friction and wear without incorporating liquid lubricants. Generally, when solid lubricants are introduced at the contact interface, solid lubricants function in the same way as that of liquid lubricants. They are made of low shear strength layer that can shear easily between two surfaces and minimize direct contact between surfaces. Consequently, solid lubricants can lead to low friction and diminish wear damage between the sliding surfaces. Several well-known inorganic materials have lubrication properties in nature and they can provide excellent tribological performance during sliding. These solid lubricants include molybdenum disulfide, carbonous allotropes, hexagonal boron nitride, and boric acid [53, 110, 126, 127]. The key feature of solid lubricants is that they have a lamellar or layered crystal structure that can provide adequate lubricity. Graphite, hexagonal boron nitride, boric acid all have the layered crystal structures [1, 121, 128-130].

Challenges with solid lubricants are maintaining a continuous supply of solid lubricant on the contact surfaces to act as a lubricious layer between two sliding surfaces. Such a continuous supply of solid lubricant is more easily maintained in the case of liquid lubricants when compared to solid lubricants. The

most innovative development to ensure a continuous supply of solid lubricant at the contact surface during sliding is to introduce solid lubricant as reinforcement into the matrix of one of the sliding components. A self-lubricating material is one whose composition or structure facilitates low coefficients of friction and wear using a self-dispensed and self-regulated lubricant delivery system, such as graphite, MoS_2 etc. These materials are becoming more and more attractive as the world become increasingly conscious of our environmental protection and energy usage. Self-lubricating materials have the potential to effectively increase our energy efficiency through more efficiently operating system components.

Self-lubricating metal matrix composites can be processed by casting or powder metallurgy techniques [59, 131-143]. Almost all metals and alloys are being researched to develop self-lubricating composites. Self-lubricating composites have been used for a long time and are utilized rather widely by the industry to combat friction and wear in a variety of sliding, rolling, and rotating bearing applications. Recent studies exhibit that some wear particles produced at the interface are a solid lubricant and they can form a thin film layer of solid lubricant on the contact surfaces of materials. This lubricious layer causes to decrease the friction coefficient and wear rate and enhance tribological properties. Therefore, composites reinforced by solid lubricant become self-lubricating due to the lubricant film developed at the interface, which prevents direct contact between the mating surfaces. Thus, self-lubricating composite eliminates usage of any types of external lubricants by reducing friction and wear due to self-lubricating nature of the materials. This lubricant film does not present initially, and it forms only later as a result of surface wear and subsurface deformation. They are continuously

88

replenished by embedded solid lubricant particles in the matrix [103, 113]. For example, aluminum/graphite composites show an improvement in lubricity, durability, and resistance to seizure under both dry and lubricated conditions[113].

2.1.3 TRIBOLOGY OF ALUMINUM ALLOYS AND COMPOSITES

Aluminum alloys have a high wear rate because of their low hardness. Among aluminum alloys, eutectic Al-Si alloys have a high strength to weight ratio, good tribological behavior, and a low coefficient of thermal expansion that make them good candidates for many industrial components. In recent years, these materials have potential applications in the areas of automobile and aerospace [144]. In general, there are various ways to improve the tribological behavior of aluminum alloys including[145]:

1. *Morphology Modification:* Substituting of coarse α-Al with fine equiaxed α-Al (a.k.a. grain refinement) or replacing coarse fibrous/globular eutectic Si with the finer eutectic structure of plate/needle-like Si

2. *Reinforcement modification:* Embedding ceramic particles in aluminum alloys to make composites[110]. In general, reinforcements in the metal matrix increase the strength [146] and wear resistance of MMCs[147]. The composition and microstructure of MMCs, size, volume fraction, particles distribution, and properties of the interface between the metal matrices and the reinforcements

89

are important factors which can determine the performance of MMCs.

3. *Alloying:* Producing aluminum alloys from pure aluminum by adding Si, Cu, Ni, Mg, Fe, etc., followed by a proper heat treatment. Alloying decreases the wear rate and also increases mild to severe wear transition load during the process [148, 149], which is mainly attributed to material hardening [150, 151]. Addition of about 4-24% Si to aluminum improves wear resistance by at least two times [152]. Because of their high strength to weight ratio and high wear resistance, eutectic Al-Si alloys are good candidates for tribological applications.

4. *Surface modification:* Applying a solid lubricant on polished surfaces of aluminum alloys, which creates a soft lubricating film on the surface and/or on the counter face and reduces surface interactions.

Among all the techniques used to improve the tribological behavior of aluminum alloys, the reinforcement of aluminum matrix with ceramic materials, not only helps to achieve higher tribological performance, but also leads to achieve enhanced properties, such as high specific strength and modulus, high stiffness, increased fatigue resistance, good wear resistance at elevated temperatures, excellent corrosion resistance, and high temperature durability. In general, reinforcement particles improve COF of composites [153-155]. Replacement of cast iron components with aluminum-based composite castings is a proper strategy for reduction of weight, fuel consumption, emissions, and cost in automotive and

aerospace industry. Furthermore, aluminum matrix embedded by solid lubricants possess attractive properties, such as high damping capacity, good machinability, good corrosion resistance and higher fatigue life than the surface coated aluminum alloys [144, 147, 156, 157]. All these advantages in solid lubricant reinforced aluminum matrix composites cause an increase in the popularity of Al/Gr composites compared to other types of enhanced materials such as coated metals.

2.1.4 SELF-LUBRICATED ALUMINUM COMPOSITES

Self-lubrication is the ability of material to transfer embedded solid lubricants [158, 159], such as graphite [26, 55, 59, 107, 121, 129, 133, 134, 138, 139, 141, 160-170] to the contact surface to decrease wear rate and COF in the absence of an external lubricant [110, 121, 126, 129]. Aluminum reinforced with carbon-based materials, such as graphite, is known as a self-lubricating aluminum matrix composite. Graphite particles act as a solid lubricant at the contact interface, which enhances the tribological properties of these composites compared to unreinforced aluminum alloys or aluminum alloys reinforced by non-carbonous ceramic particles [171-173]. In general, solid lubricants to fabricate self-lubricating composites are solid carbon (carbon fibers [174-176], graphite particles [177-181], CNTs, graphene), molybdenum disulfide, and hexagonal boron nitride [110, 126, 157]. Low friction coefficient and low wear rate are the key properties of self-lubricating materials as well as their high seizure resistance.

The greatest challenge in introducing aluminum graphite composites in industrial components is the negative effect of graphite on mechanical properties

91

of composites. By increasing the amount of graphite in the matrix, the mechanical properties of aluminum matrix composite reinforced by graphite decreases [59, 106, 144]. There are many approaches to reducing the damaging effect of graphite particles on the deterioration of mechanical properties. For example, using hybrid aluminum metal matrix composites containing ceramic particles and graphite particles shows better tribological behavior compared to aluminum alloys or Al/Gr composites. In these hybrid composites, graphite acts as a solid lubricant and ceramic particles have load bearing ability, which leads to decrease in wear rate.

Earlier studies show that properties such as excellent anti-seizure effect[182], low thermal expansion[183], high damping capacity[184], low friction and wear[185], and reduced temperature rise at the worn contact surface are the key factors that make self-lubricating Al/Gr composites an attractive alternative to aluminum alloys in applications where tribology is dominant[106]. Al/Gr composites have superior tribological behavior, which is the most desirable factor for automotive industries for making components such as engine pistons, bearings, and bushings [110].

2.1.5 TRIBOLOGY OF SELF-LUBRICATING MATERIALS

In general, the addition of carbonous particles as reinforcement to an aluminum matrix enhances tribological properties compared to aluminum composite reinforced with other ceramic particles such as Al_2O_3 and SiC[157]. There is a significant reduction in friction and wear rate in self-lubricating

92

composites in comparison with unreinforced matrix alloys as a result of incorporation of graphite particles [53, 60, 185].

Ames et al. [55] show that the A356/10%Gr/20%SiC composites made by the molten metal mixing technique have about 100 times lower wear rate than unreinforced A356 alloy at a constant normal load of 110 N. The average size of graphite and SiC is 76.8 and 11.5 μm, respectively. The tribofilm established during sliding provides adequate lubrication between contact surfaces. Furthermore, the addition of graphite particles decreases the friction heat generated at the interface by its intrinsic lubrication behavior. This will consequently increase wear resistance due to the reduction in friction force[110].

Aluminum-silicon alloys consisting of graphite particulates can be of considerable interest for applications where properties such as wear resistance and seizure resistance are important, such as piston and cylinder liner materials in the automotive industry[186]. Das et al. [187] investigated the tribological behavior of Al-Si alloy/graphite composites and observed a significant improvement in the tribological behavior of composites due to the combined presence of graphite particles and silicon phase in the composite[163].

Improvement of wear resistance in self-lubricating composites primarily depends on the type[188], size[189] and distribution[190] of the reinforcing phase as well as the manufacturing technique of the composite. The interface between the matrix and graphite is a key parameter affecting mechanical properties and tribological behavior of Al/Gr composites[176, 191]. Several test parameters, such as load and sliding velocity also influence the wear and friction behavior of self-lubricating Al/Gr composites. The basic parameters that control the tribological

behavior of self-lubricating aluminum matrix composites can be classified into three general categories [110, 192]:

1. **Material variables:** These are the factors that change intrinsic properties of the material undergoing surface interaction. Parameters such as the type of reinforcement, reinforcement size, the shape of reinforcement, reinforcement volume fraction, and type and microstructure of the matrix.

2. **Test or service variables:** Factors such as normal load, sliding velocity, and sliding distance that depend on the test and working condition.

3. **Environmental variables:** Physical factors such as temperature and humidity that influence the testing conditions.

2.2 LITERATURE REVIEW

2.2.1 SYNTHESIZING MMNCS BY POWDER METALLURGY METHOD

Powder metallurgy method is one of the popular methods of producing MMCs and MMNCs. Pure aluminum and aluminum alloys are one of the most widely used materials in MMCs and MMNCs as a matrix from research and industrial viewpoints. This is due to their outstanding properties, such as lightweight, high strength, high specific modulus, low thermal expansion coefficient, and good wear resistance[193]. For processing of aluminum matrix

94

composites (AMCs) and aluminum matrix nano-composites (AMNCs), different types of milling including Planetary ball mill[194], attritor mill[193], Spex high energy ball mill [195] and cryomill [196] are using in different researches. Each method has its own advantages and disadvantages. Different types of materials can be used as reinforcement in AMCs and AMNCs. The common reinforcement materials which have been used in aluminum matrices are Al_2O_3[197], B_4C[198], SiC[199], AlN[200], CNTs[201, 202], etc. Recently, some researchers are using graphene as reinforcements for aluminum matrices[203-207]. In these researches, powder metallurgy method was used to produce AMNCs.

2.2.2 GRAPHENE PROPERTIES

It has emerged as a new material in the 21st century and received worldwide attention in nearly every field of science and engineering because of its exceptional optical, mechanical, charge transport and thermal properties. Properties of graphene are presented in Table 3. Graphene is two-dimensional single atomic carbon sheet of sp2-bounded in which atoms densely packed in a honeycomb lattice. Graphite, the most common form of carbon, is a stack of several graphene sheets along the c-axis with an interlayer spacing of 0.34 nm. The bonding between carbon atoms is very strong while there are weak van der Waals interactions between the layers. In terms of thermodynamics, it was thought that exfoliation of layered graphite to freestanding atomic layer would not be possible [208]. However, recently different approaches have been developed for synthesizing graphene in large quantities, including thermal evaporation of silicon carbide

95

[209, 210], chemical vapor deposition (CVD) of graphene on metal carbides or metal surfaces [211, 212], and wet chemical synthesis of graphene oxides followed by reduction [213, 214].

The yield strength predicted for a single graphite layer using MD simulation has reached an extreme value of 0.912 TPa [215]. Another study employed quantum mechanical approach revealed that the elastic modulus for armchair graphene and zigzag graphene are 1.086 and 1.05 TPa, respectively [216]. The Young's modulus and intrinsic tensile strength of graphene monolayer were experimentally tested by using nanoindentation of the atomic force microscope (AFM). The Young's modulus and intrinsic tensile strength obtained using these techniques are 1.1.02 TPa and 130 GPa, respectively [217]. By using the same method, mechanical properties of graphene bilayer and trilayer have been determined where Young's modulus is 1.04 and 0.98 TPa and intrinsic tensile strength is 126 and 101 GPa, respectively [63]. These supreme mechanical properties of graphene along with extreme thermal conductivity (5000 W m-1 K-1) [218], and super charge-carrier mobility (200,000 cm2 V-1 s-1) [219] makes them an attractive material for researchers in the last decade to employ them as reinforcement into a metal matrix. The graphene has a plate shape; dispersion in any kind of matrices is easier in comparison with CNTs. Hence, the graphene is a good substitution for CNTs as reinforcement for metal matrix composites [220]. Although graphene is defined as graphite single layers, graphene nanoplatelets (GNPs) or graphene nanosheets (GNSs) which are short stacks of platelet-shaped graphene sheets with an average thickness of the 5-100 nanometers are very common in the fabrication of metal matrix composites. Since graphene in its single

96

layer form cannot easily be stable in the free state, usually, GNPs are used as reinforcement and then the sheets are exfoliated to achieve a single layer dispersed graphene in a matrix. This inexpensive material possesses good thermal conductivity, electrical conductivity, mechanical strength and more surface area than the expensive carbon nanotubes (CNTs).

Table 3. Physical and mechanical properties of Graphene.

Property	Unit	Data	Reference
Specific surface area	m^2g^{-1}	2630	[221]
Electron mobility	$cm^2V^{-1}s^{-1}$	1500	[222]
Electron resistivity	$\Omega.cm$	10^{-6}	[222]
Thermal conductivity	$Wm^{-1}K^{-1}$	5.3×10^3	[222]
The coefficient of thermal expansion	K^{-1}	-8×10^{-4}	[223]
Elastic modulus	TPa	0.5-1	[224]
Tensile strength	GPa	130	[224]

The most common method to produce graphene is exfoliation method. Writing with a graphite pencil is the first exfoliation method to produce graphene from graphite. However, by this method, the thickness of graphene sheets is not controllable. Andre Geim's group in Manchester [62] produced a single layer of graphene to investigate its properties. They showed that by gently rubbing or pressing freshly cleaved graphite crystal on a silicon oxide wafer, a single atomic layer of graphene flake forms and visible under an optical microscope due to thin film interference effects[225]. However, this method is good to investigate the properties of graphene. For the case of using graphene in other researches

97

including using graphene as reinforcement in metal matrices, this method of exfoliation is not applicable.

Recently, researchers exfoliate graphene with some new methods (chemically, mechanically or combination of these two) and use the exfoliated graphene as reinforcement in metals[205]. Mina Bastwros et. al.[205] have used a method called modified Brodie's method to exfoliate graphite and produce graphene oxide. In this method, they mixed 10 g of graphite, 160 ml of nitric acid, and 85 g of sodium chlorate at room temperature. The mixture was stirred for 24 hours. Then, they washed the slurry for four times with 5% hydrochloric acid and distilled water. By this method, they produce intercalated graphite through sedimentation. Then, they dry the solution at 60°C. Finally, the intercalated graphite was exfoliated to a monolayer or few layers of graphene oxide by using ultrasonic power [205].

In another research by Ting He et. al. [226], they have used a mechanical method to exfoliate graphite and produce alumina/ graphene composites. In this method, wet milling was used to mechanically exfoliate graphite. Pure alumina with an average particle size of 150 nm and natural graphite powder were mixed and milled in ethanol by a planetary ball mill. The BPR and the rotation speed in the research were 30:1 and 250 rpm, respectively. Hot pressed in vacuum at 1100°C and 60 MPa has been used to consolidate the alumina/graphene composite [226].

Weifeng Zhao et. al. [227] have used a method which is a combination of a chemical and mechanical method to exfoliate graphene. In this method, 0.02 g of graphite nanosheets with a thickness of 30-80 nm were dispersed in 80 ml of

98

anhydrous N, Ndimethylformamide (DMF) solvent. Then, the slurry was milled for 30 hours by a planetary ball mill with the speed of 300 rpm. During milling, the dominant force which applies to the nanosheets should be shear force to exfoliate graphite and produce graphene. Graphite layers have the weak van der Waals bonding and DMF-graphene has a strong bond. As a result, the shear force during milling can exfoliate graphite nanosheets into graphene. Then, the result slurry was centrifuged at 10000 rpm for 20 minutes to separate exfoliated graphene from unexfoliated and partially exfoliated graphite nanosheets. In the last step, the DMF was evaporated from the supernatant under vacuum and the graphene powders were washed with ethanol[227].

Qianqian Li et. al. [228] have used a block copolymer Disperbyk-2150 (BYK Chemie GmbH) in ethanol to disperse MultiWalled Carbon Nanotubes (MWCNTs) for 15 minutes in an ultrasonic bath. The ratio of the block copolymer to MWCNTs was 1:1. Then, the solution was stirred for 30 minutes at 250 rpm [228]. These are the methods which are applicable to exfoliate graphene and used the exfoliated graphene as reinforcement in metal matrices.

2.2.3 SELF-LUBRICATING NANOCOMPOSITES

2.2.3.1 Mechanical Properties of MMNCs reinforced by Graphene

As mentioned earlier, graphene has special mechanical and electrical properties and because of these properties, researchers have used graphene as reinforcement to improve the properties of composite materials. Polymers usually have low electrical conductivity and mechanical properties. By adding Graphene

99

to polymer matrices, the mechanical and electrical properties of Polymer Matrix Composites (PMCs) improve significantly [229, 230]. Most metals have a good electrical conductivity and improving the electrical properties of metals may be difficult by adding graphene. As a result, researchers usually do not investigate the electrical properties of MMNCs reinforced by graphene. However, mechanical properties of metals especially light metals such as aluminum and magnesium are improvable. As a result, the main purpose of adding graphene to metal matrices is to improve mechanical properties of MMNCs and investigating the strengthening mechanisms. The mechanical properties of MMNCs reinforced by graphene has been summarized as follow.

Mechanical properties of MMNCs reinforced by graphene have been investigated by hardness measurements[204], tensile test[203], compression test[206] and flexural stress[205]. In addition, a few theoretical works have been done on mechanical properties of MMNCs reinforced by graphene[231].

It is expected that by adding graphene nanoplatelets to a metal matrix, the mechanical and tribological properties would be enhanced. In literature, only limited researches on metal matrix composites reinforced by graphene are available [208, 232-239]. To the authors' knowledge, so far, aluminum matrix composite reinforced by graphene has successfully produced only by powder metallurgy method [232, 233, 240]. Recently, Wang et al. [241] have shown that by adding 0.3 wt.% Graphene nano-sheets to the aluminum matrix, the tensile strength of composite increased by about 62%. However, Bartolucci et al. [233] have shown that the tensile strength and strain at failure of aluminum matrix composites reinforced by 0.1 wt.% graphene platelets are less than its pure

aluminum matrix. In addition to these two types of research, Chen et al. [234] have produced magnesium matrix composite reinforced by graphene nano-platelets. They employed a novel method combining liquid state ultrasonic processing and solid state stirring to fabricate the composites. By using this novel method, they reported that the graphene nanoplatelets (GNPs) could be dispersed uniformly into magnesium matrix. The results showed that the microhardness of magnesium matrix composite reinforced by GNPs has been increased by 78% compared to that of pure Mg prepared under the same processing condition. They have also shown that the GNPs show an excellent strengthening effect on the magnesium matrix composite [234, 237, 242-245].

In some studies, the Vickers hardness of MMNCs increased with weight fraction of graphene[204, 246]. Rashad et. al. [246]showed a significant increase in the Vickers hardness of Mg matrix composites reinforced by graphene nanoplatelets. The hardness of pure Mg with Mg matrix composites including 0.5-1.5 wt.% Al and 0.18wt.% GNP was compared. In the case of composites, the matrix is not pure Mg and it is Mg alloy. As a result, this comparison could be wrong and the increase in the hardness of these samples could be because of alloying element and solid solution strengthening [247] not because of graphene nanoplatelets. In some studies, the Vickers hardness slightly decreased or increased by adding graphene nanoplatelets into the metal matrices[206, 207]. However, Bartolucci et. al.[204] showed that by adding graphene to the aluminum matrix, the strength of the composite significantly decreased.

Fracture strength of a perfect single layer of graphene is about 125 GPa[224]. Wang et. al.[203] have used the rule of the mixture to estimate the

101

mechanical properties of aluminum matrix composites reinforced by Graphene. By adding 0.3wt.% (about 0.5vol.%) of GNSs to the aluminum matrix, the improvement in tensile strength of the composite should be around 500 MPa. However, this improvement has not been reached in the literature and there are some reasons for that. First of all, it assumes that all of the graphene nanoplatelets are a single layer of graphene which are homogenously distributed in the metal matrices. However, in the real world, the graphene reinforcements in the metal matrices are not a single layer. As a result, the fracture strength of multilayers of graphene is not 125 GPa. Secondly, the strength of GNPs in different directions are not the same. The in-plane strength of GNPs is much higher compared to the out-of-plane strength of GNPs. Graphene nanoplatelets are randomly distributed in all directions in the metal matrices. As a result, the out-of-plane GNPs in the metal matrices cannot act as an in-plane GNPs. Moreover, the distribution of GNPs in the metal matrices and bonding between the GNPs and metal matrices has a significant effect on the mechanical properties of these MMNCs. However, the homogenous distribution of GNPs and a perfect bonding between GNPs and metal matrices are not practically achievable. Because of these reasons, the theoretical strength of these MMNCs has not been reached.

There are well-known strengthening mechanisms for metal matrix nanocomposites. These mechanisms are including grain refinement, Orowan looping, solid solution strengthening, precipitation strengthening, load bearing, Coefficient of Thermal Expansion (CTE) mismatch and modulus mismatch strengthening[247]. Different explanation and strengthening mechanisms have

been used in the literature to explain the mechanical behavior of MMNCs reinforced by graphene.

During the powder processing of the MMNCs reinforced by GNPs, plastic deformation and strain hardening due to the ball occurs. As a result of the processing method, the grain size of the metal matrices decreased. Due to the smaller grain size, grain refinement strengthening which shows by Hall-Petch equation[203, 205, 231, 247] is one of the main strengthening mechanisms in the MMNCs reinforced by GNPs.

In addition, because of the strain hardening, dislocation density increased in the composite samples. Increasing the dislocation densities in the sample also causes to strengthening the MMNCs reinforced by GNPs[206, 246, 248]. Moreover, CTE mismatch between the metal matrices and GNPs can cause to increase the dislocation density and increasing the strength of the composite samples. However, the existence of the CTE mismatch strengthening in MMNCs with very small size reinforcements is in doubt[249, 250]. Since the size of the GNPs in one direction is very small, it could be possible that the CTE mismatch does not applicable to MMNCs reinforced by GNPs. It has been shown that the thickness of flaky shape metal matrices are thousand times larger than the GNPs thickness and a very small portion of the metal matrices was affected by the GNPs. In this study, the same grain size and amount of dislocation density were reported for Al/GNPs and unreinforced Al samples. These results approve that there is no CTE mismatch strengthening in this MMNCs reinforced by GNPs[203]. As a result, the CTE mismatch strengthening in the MMNCs reinforced by GNPs depends on the size and geometry of the metal matrices and reinforcements.

The other possible strengthening mechanism for MMNCs reinforced by GNPs is Orowan looping. Rashad et. al. [206, 246]have claimed that one of the strengthening mechanism in the MMNCs reinforced by GNPs is Orowan looping. The Orowan mechanism requires that unshearable particles be located within the grains. As a result, the size of grains and reinforcements are very important to get the Orowan strengthening in the MMNCs. Graphene is a two-dimensional material. In one dimension, the size of graphene is in the order of micron. Since the size of GNPs in one dimension is bigger than the size of grains in the metal matrix, it is almost impossible to get the Orowan strengthening in these MMNCs.

Since GNPs is a two-dimensional material, load bearing or load transfer strengthening mechanism could be one of the main strengthening mechanism in MMNCs reinforced by GNPs[203, 206, 231, 246, 248]. The load which is applied to the MMNCs may transfer to the reinforcements from the metal matrices through shear stresses along the interface between matrix and reinforcements. The interfacial area (S) and reinforcement's cross-sectional area (A) play an important role in the load transfer strengthening mechanism. There are different models to show the mechanical properties of MMCs.

2.2.3.2 Tribological Behavior of Self-lubricating Nanocomposites

During relative motion of two surfaces, different types of wear mechanisms, including adhesive wear, abrasive wear, delimitation wear, erosive wear, fretting wear, fatigue wear, and corrosive/oxidative wear may occur. The nature of wear mechanisms can be understood by studying the worn surfaces of materials. At low

loads and sliding speeds, abrasion is the dominant wear mechanism while at higher loads, the wear mechanism changes to delamination. Presence of grooves on the worn surfaces of the composites in the sliding direction at low normal loads shows that the abrasion wear mechanism becomes dominant.

Graphite is well-known reinforcement for metal matrix composites which acts as a solid lubricant and makes the composite as self-lubricating composites [102, 110, 113, 118, 121, 129]. When graphite is embedded into a metal matrix, the friction and wear behavior of metal/graphite composite significantly improves compared to unreinforced metal which leads to their increased industrial applications where tribological properties are dominant. Damage accumulation will be reduced in the presence of graphite particles and hence decrease the wear rate of metal matrix insignificant extent. MMCs reinforced by graphite particles or fibers are potential structural materials for aerospace and automotive owe to their excellent tribological properties.

Among many alloys, aluminum-based composites are extensively used in various industries because of high strength to weight ratio, superior tribological properties, and good corrosion resistivity. The explanation for the superior tribological properties of aluminum/graphite composites can be explained by the wear mechanisms which occur in these systems. Aluminum alloys have low yield stress and deform extensively during sliding contact while graphite particles in aluminum/graphite composite improve the deformation and fragmentation of the surface and sub-surface by providing a continuous film of graphite on the contact surfaces after a short running-in period. The graphite film hinders direct metal to metal contact and hence prevents seizure. Despite good tribological behavior of

105

metal/graphite composite, poor mechanical properties are the disadvantage in the graphite reinforced MMCs. These composites sometimes have lower mechanical properties than unreinforced alloy [59, 110]. In addition, graphite has a reverse effect on electrical conductivity when copper alloys are reinforced by micron-sized graphite due to be hindering effect of particles in the continuous copper matrix network, though it has a moderate electrical conductivity. Another feature that causes to reduce electrical conductivity of copper–graphite composite is the poor interface bonding between copper and graphite particles which leads to more electron scattering [118]. Due to these shortcomings in using graphite as reinforcement in metals, incorporation of nano-sized carbonous materials sought to be promising.

In general, it is desirable in terms of mechanical properties to have matrix grain size in the range of nanometer to achieve enhanced hardness, yield strength, and tribological properties such as wear resistance and friction coefficient [251]. Using nanosized particles as reinforcement also enhances both Young's modulus and tensile strength of composites as well as improving tribological performance. Due to the fact that nanocarbonous materials have superior physical and mechanical properties, they have recently employed as a novel reinforcement for self-lubricating metal matrix nanocomposite. Superior properties of MMNCs reinforced by carbon nanomaterials is due to metallurgical factors, such as Hall–Petch effect by grain size refinement, Orowan looping, and dislocation generation resulting from a thermal mismatch between the matrix and reinforcements [208]. Previous studies revealed that the MMCs with smaller size reinforcements exhibit a lower coefficient of friction and wear rate, thus, it was concluded that the MMNCs

106

have excellent tribological properties rather than metal matrix micro-composites, as it is also experimentally confirmed [110, 252, 253]. More specifically, the composite reinforced by nanoparticles (graphene) has lower COF than the composite reinforced by microparticles (graphite). Also, the hardness of composites reinforced by graphene is found to be higher than the composite reinforced by CNTs [102]. Worn surface observation suggested that the dominant wear mechanism for non-reinforced pure Al specimen has been delaminating wear accompanied by some adhesive wear mechanism. However, worn surfaces of the nano-particle reinforced composites were smoother and the total depth of deformations was smaller, grooves were finer than the unreinforced aluminum alloy matrix specimens [254, 255].

There is a great challenge in introducing carbon-based materials in metal matrices. Generally, molten aluminum is not able to wet carbonous materials, such as carbon fibers (CFs), graphite particles, carbon nanotubes (CNTs) and graphene where the contact angle of molten aluminum with graphite is between 140° and 160° [175]. The reason for high contact angle between carbonous materials and molten aluminum is due to the high surface tension of aluminum in a liquid state. The surface tension of molten aluminum and carbon nanotubes are 955 mN/m and 45.3 mN/m, respectively [256]. The very high value of the surface tension of molten aluminum compared to carbon nanotubes makes a synthesis of aluminum matrix composite reinforced with carbonaceous materials a challenging task. One of a typical way to improve wetting behavior of molten aluminum on carbonous materials is by forming metallic coatings, such as copper and nickel on reinforcements to reduce its contact angle [257, 258]. The formation of Al_3Ni,

107

Al$_3$Ni$_2$, and CuAl$_2$ as an intermetallic compound plays a key role in achieving good wettability between aluminum with copper and nickel [116, 259]. In the following sections, self-lubricating metal/CNT and Metal/ Graphene (single layer or nanoplatelets) nanocomposites have been introduced and their mechanical properties are discussed.

Usually to avoid friction and consequently, deterioration of material under wear, liquid or solid lubricants are employed. However, in cases such as high vacuum environment, high-speed conditions, high applied loads, and very low or high temperatures, liquid and grease type lubricants are undesirable. In such a tribological system the common liquid and grease type lubricants do not show desired performance or durability [208]. Another approach is replacing the liquid and grease type lubricants with solid lubricant coatings that they are used to decrease the coefficient of friction and wear rate. The coatings are applied on the surface of materials by depositing via chemical or physical vapor deposition techniques to form a coating layer [260, 261]. The disadvantages of solid lubricant coating are a limited lifetime, difficulty in replenishment, oxidation and aging-related degradation, and poor adhesion. Therefore, to avoid the drawbacks of both the liquid and grease type lubricants and the solid lubricant coatings, embedding carbonous materials in the metal matrix seems promising.

Generally, metal matrix composites have a lower coefficient of friction (COF) compared to the unreinforced matrix [102, 110, 262-265]. Furthermore, adding ceramic particles to the metal matrices lead to an increase in wear resistance of the matrices [102, 110, 265-268]. The main reason for increasing of wear resistance of metal matrix composite is attributed to the low friction

coefficient of metal matrix composite compared to the unreinforced metals. For conventional metal matrix composites, the reinforcements act as load bearing components at contact surface which tend to protect the surface from plowing during sliding. Generally, the hardness of reinforcement greatly affects the wear loss and hence, the wear volume of MMCs. The wear loss of MMCs depends on several intrinsic properties such as the reinforcements dispersion state, distribution of reinforcement, size of reinforcing particles, and interfacial bond between matrix and particles [208]. When bonding between matrix and reinforcement is poor, the hard ceramic particles are easily pulled out from MMCs and then they will be trapped between the sliding surfaces and act as third body abrasives and help to increase worn surface damage and wear rate. Among the composites, composites reinforced by carbonous materials show better tribological properties compared to composites reinforced by ceramic reinforcements, such as SiC and Al_2O_3 due to the lubricative nature of carbonous materials that make them a potential reinforcement for self-lubricating composite. The conventional self-lubricating composites are embedded by graphite particles or carbon fibers [110].

The main reason for the significant decrease in COF and wear rate is due to the formation of a lubricant film between the contact surfaces because of the presence of a carbon-based solid lubricant in the MMCs. Thus, the lubricant film prevents direct contact between sliding surfaces and reducing wear [59]. In addition, due to the presence of lubricant film which prevents direct contact, the transfer of atoms from the asperities of softer surface to the asperities of harder surface will be reduced that hence, it leads to decrease in cold welding of atoms of softer materials with atoms of harder materials during sliding and then subsequent

fracture of atomic junctions [118]. As noted before, although the graphite particles in the metal matrix improve the tribological performance, it tends to reduce the mechanical properties of the composites. Hence, recently, the nano solid lubricants are used as the dominant reinforcement for the metal matrices in self-lubricating composites. This is because the metal matrix composite reinforced by nano solid lubricant has excellent self-lubricating behavior with a low coefficient of friction and wear rate as well as high mechanical properties [269].

High strength, lightweight and lubricating nature of graphene made it suitable as reinforcement for self-lubricating ultrahigh strength metal matrix nanocomposites. As this is fairly a novel material and it is difficult to uniformly disperse in metals as well as its complex microstructure, there are only a few studies which investigated the tribological properties of graphene in a metallic matrix. Ghazaly et al. [236] who have investigated the effect of weight percentage of graphene on mechanical properties, also studied its effect on the wear rate of self-lubricating AA2124 aluminum alloy matrix nanocomposites. The results showed that self-lubricating composite reinforced by 3 wt. % graphene has better tribological properties under dry wear test compared to the unreinforced and another amount of graphene reinforcement. SEM micrographs of worn surfaces of unreinforced aluminum alloy and Al/graphene nanocomposites clearly demonstrate the presence of longitudinal grooves in all samples. In addition, by comparing the worn surfaces, it is obvious that the scratches, craters, and delamination of AA2124/3wt.% graphene composite are less than that of the unreinforced alloy. Thus, unreinforced alloy and AA2124/3wt.% graphene composite are in the severe and mild wear regime, respectively. Shallow parallel

grooves and ridges formed on the worn surface of AA2124/0.5 and 5 wt.% graphene nanocomposites due to microploughing. Thus, the dominant wear mechanism is a severe plastic deformation of the matrix that results in high wear rate. Entrapped debris between delaminated surfaces was observed at high magnification on worn surfaces of unreinforced AA2124 alloy while there is no wear debris on the worn surfaces of nanocomposite. Alumina fragmented films or strain hardened particles are the two main sources of debris. This debris is from the heavily milled consolidated powders which were detached under the load during the wear test. By comparing the worn surfaces at high magnifications, it is obvious that the surface of nanocomposite containing 3% graphene is smoother than that of unreinforced alloy and the composite reinforced with 5wt.%graphene. Furthermore, the surface of AA2124/3 wt.% graphene composite was covered by lubricant films that result in reducing friction and wear due to the soft nature of the lubricant film. Conversely, deep grooves and severe damage exist on the worn surfaces of AA2124/5 wt.% graphene composites which delaminated in the direction of sliding that explains the significant increase in wear rates and weight loss.

Inasmuch as copper has good electrical and thermal conductivities and graphite has lubricious nature, copper/graphite composites have a variety of application in industries. Conversely, the mechanical properties of copper composites decrease in the presence of graphite reinforcement. To solve the impact of microsized graphite particles, Rajkumar et al. [118] employed powder mixing, compaction and microwave sintering methods to synthesize copper nanocomposite reinforced by nano-graphite (NG) particles with an average

111

particle size of 35 nm to form copper/5–20 vol% NG nanocomposites. The graphite particles were coated with copper using electrodeless plating method. The nano graphite particles have not been exfoliated in this investigation and cannot be considered as single or "few layers" graphene sheets. the nanocomposites had better hardness and electrical conductivity compared to microcomposites. As stated earlier, the volume percentage of nano-particles influences physical and mechanical properties of self-lubricating composites. The number of nanoparticles also influences the relative density. The relative density increases with increasing the volume percentage up to 15 vol.% of nano-graphite due to the ability of nanoparticles to fill up the porosity cavities. When the nano-graphite amount is increased over 15% volume fraction, the relative density and hardness reduced due to the reduction in the distance between particles, which consequently facilitate nanoparticles agglomeration.

Results revealed that, at constant volume fraction, embedding nano-particles decreases the coefficient of friction and wear rate compared to the composite reinforced by microsized graphite particles. Higher hardness, lower porosity and finer microstructure are the reason for the improved wear resistance of nano-graphite reinforced composites. Further, the nano-graphite particles reinforced composites are more effective on the degree of self-lubrication compared to micron-size graphite particles reinforced composites. The number of nano-graphite particles also influences the tribological properties of self-lubricating copper composites. The increase in volume percentage of nano-graphite up to 15 vol.% tends to decrease the wear rate and COF because of the formation of a uniform and continuous layer of solid lubricant film. This lubricant

112

film reduces the rate of deformation of the matrix and improves the tribological behavior. When the amount of reinforcement increases, the decrease in the COF is associated with increase in the availability and uniformity of lubricant layer. The lubricant layer causes to minimize the metal to metal contacts between the copper matrix composite and steel counter surface. In contrast, when the volume fraction of nano-graphite is more than 15 vol.%, a large amount of agglomeration was observed that tends to incomplete spreading of graphite at the contact zone, and hence, increases the wear rate. Increasing of COF at high volume fraction of nano-graphite is a result of increasing the deformation and fracture at the contact surface of copper matrix and increasing the amount of copper debris at contact surfaces.

the wear rate and coefficient of friction both increase with increasing applied load while the coefficient of friction decrease with increasing the sliding speed. Increasing normal load also increases the amount of copper wear debris at the contact zone and hence influences the rate of increase in the coefficient of friction with normal load. In these figures, it can be seen that the coefficient of friction of self-lubricating composite significantly decreases with increasing the sliding speed up to 1.77 m/s because of formation of uniform lubricant film. By increasing the sliding speeds beyond 1.77 m/s, the coefficient of friction slightly increases or become constant for 5 and 10-15 vol.%, respectively. This is due to peel off of the self-lubricating film on the contact surface at high sliding speed. Furthermore, sliding speed does not affect the coefficient of friction of copper/nano-graphite with high amount of nano-graphite content due to the contact surface that is uniformly covered with the highly adherent graphite layer. As shown in SEM micrograph of worn surface at different sliding speed, at constant

normal load, the lubricant film on copper/15 vol.% nano-graphite is not continuous at lower sliding speed. While increasing the sliding speed, a lubricant layer uniformly forms on the surface of composite that decreases COF as a direct result of a decrease in direct surface to surface contact. However, a gradual increase in COF was observed for 20 vol.% of nano-graphite composite by increasing the sliding speed that it leads to lower mechanical properties such as hardness due to increase in temperature at the interface. Further, it tends to more grain fracture during sliding. This phenomenon is more intensive at higher sliding speeds.

The mechanism of wear under normal loads suggested by Huang et al. [270]. Fine graphite particles form an adherent layer at the contact zone and under high normal loads; these GNPs from composite is squeezed out to the contact zone. Owe to their smaller size, nano graphite particles can penetrate deep inside the asperities of composite and counter surface during the sliding process. During sliding, the nano-graphite particles could have filled most of the asperities of the composite surface. So, a graphite layer form at the pin (composite) –disc (steel) interface. The layer formation process continues up to the formation of thick adherent graphite layer. In case of micron size graphite particles, they can also undergo similar process; however, due to their larger size, they are not able to penetrate the very narrow grooves which formed during the wear process or gaps between the asperities of sliding contact easily.

Additionally, when the size of graphite particles comes down in the range of nanosized, at the same volume fraction, the mean free path between the graphite particles also decreases (Figure 41a) compared to the same volume fraction of

114

micronsized graphite particles (Figure 41b). This will cause smaller size asperities and less space between the asperities compared to micro graphite reinforced composite (Figure 41d) during the wearing process which can be filled nano-graphite particles as shown in Figure 41c. The completely filled nanographite particles produce more uniform graphite layer that reduces the direct contact between the two wearing bodies and will cause a reduction in the frictional coefficient. As confirmed by SEM (Figure 41h and Figure 41f), nanocomposite reduces the wear debris size, as shown in Figure 41e when compared to microcomposites (Figure 41f) [118].
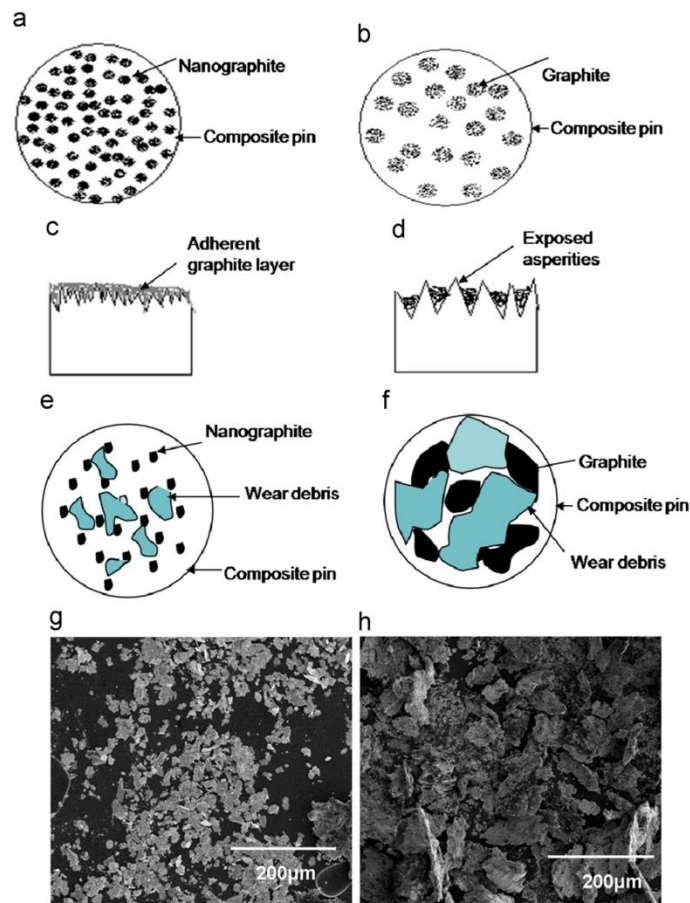
Figure 41 a) Distribution of nanographite in matrix, b) distribution of graphite in matrix, c) contact profile nanographite composite, d) contact profile of graphite

115

composite, e) and f) conceptual wear generation model for nanographite and graphite reinforced composite respectively, g) and h) typical wear debris at 48 N and 0.77 m/s for copper–nanographite and copper–graphite respectively[118].

2.2.4 SUMMARY

In section 1, metal-matrix composites and self-lubricating composite were reviewed. In particular, the potential use of aluminum self-lubricating matrix particulate reinforced composites presented. Applications of aluminum alloys are increasing in industries such as automotive and aerospace to reduce fuel usage and protect the environment, where they can successfully replace steel and cast iron parts. On the other hand, aluminum alloys have a disadvantage in that they have low mechanical properties and tribological behavior of aluminum alloys. In general, there are various ways to improve the tribological behavior of aluminum alloys including[145]: 1) Morphology Modification, 3) Alloying, 3) Surface modification and 4) Reinforcement modification. Making composites is a well-known method to enhance wear and friction properties. Then a brief introduction of tribological properties of self-lubricating aluminum matrix composites discussed. As a conclusion, solid lubricants play a dominant role in improving the tribological properties. Among various reinforcements, recent emerging material, carbon-based materials (graphite), is found to have many favorable attributes such as high thermal conductivity, low coefficient of thermal expansion, high damping capacity and good self-lubricant property [4]. Previous studies show that mechanical properties of aluminum matrix composites reinforced by graphite are low. Hence, recent studies tried to solve this problem by using nano-

116

reinforcements. Size of reinforcement generally influences the mechanical properties such as strength, ductility, and fracture of self-lubricating MMNCs. It is expected that by reducing the particle size in MMC's to the range of nanosized, some of the limitations such as poor ductility and elongation, poor machinability, and reduced fracture toughness of MMCs can be solved. The reason for significantly improved mechanical properties is due to the combined effect of Orowan strengthening and grain refining mechanisms and high temperature creep resistance properties could make metal matrix nanocomposites (MMNCs) very attractive, especially when lightweight aluminum matrix nanocomposites are used as the matrix material. The main conclusion which can be made is that nano-sized carbonous materials, such as nano-graphite or graphene, can simultaneously enhance mechanical and tribological properties. Therefore, embedding graphene to the aluminum matrix can improve both mechanical and tribological properties.

In section 2, work is done on synthesizing of metal/graphene composites and their mechanical and tribological properties to date have been reviewed. Most of the researches used powder metallurgy technique to fabricate self-lubricating metal matrix nanocomposites. In some studies, the Vickers hardness slightly decreased or increased by adding graphene nanoplatelets into the metal matrices[206, 207]. However, Bartolucci et. al.[204] showed that by adding graphene to the aluminum matrix, the strength of the composite significantly decreased. As a result, the mechanical behavior of MMNCs reinforced by graphene is not completely understood. During the powder processing of the MMNCs reinforced by GNPs, plastic deformation and strain hardening due to the ball occurs. As a result of the processing method, the grain size of the metal matrices

117

decreased. Due to the smaller grain size, grain refinement strengthening which shows by Hall-Petch equation[203, 205, 231, 247] is one of the main strengthening mechanisms in the MMNCs reinforced by GNPs.

For conventional metal matrix composites, the reinforcements act as load bearing components at contact surface which tend to protect the surface from plowing during sliding. Generally, the hardness of reinforcement greatly affects the wear loss and hence, the wear volume of MMCs. Among the composites, composites reinforced by carbonous materials show better tribological properties compared to composites reinforced by ceramic reinforcements, such as SiC and Al_2O_3 due to the lubricative nature of carbonous materials that make them a potential reinforcement for self-lubricating composite. The main reason for the significant decrease in COF and wear rate is due to the formation of a lubricant film between the contact surfaces because of the presence of a carbon-based solid lubricant in the MMCs. Thus, the lubricant film prevents direct contact between sliding surfaces and reducing wear. In addition, due to the presence of lubricant film which prevents direct contact, the transfer of atoms from the asperities of softer surface to the asperities of harder surface will be reduced that hence, it leads to decrease in cold welding of atoms of softer materials with atoms of harder materials during sliding and then subsequent fracture of atomic junctions. The results showed that self-lubricating composite reinforced by graphene has better tribological properties under dry wear test compared to unreinforced. Besides, adding more graphene can generally decrease COF due to the lubricant transfer layer is thicker and the real contact area between surfaces is less, therefore, COF of self-lubricating composites reduced by increasing amount of graphene.

118

2.3 MATERIALS AND EXPERIMENTS

Looking at the current state of knowledge and the shortcomings in the existing research streams, the research goal is to investigate properties of self-lubricating metal matrix nanocomposites and characterize them. The main objectives of this work are to synthesize and investigate the tribological properties of aluminum self-lubricating nanocomposites by addition of graphene as a reinforcement. As the hardness is an important parameter in wear, embedding another hard ceramic particle such as Al_2O_3 and making hybrid self-lubricating MMNCs will also be discussed.

This experimental work is carried out in 3 phases:

1. Study the tribological properties of self-lubricating aluminum/graphene and aluminum/alumina/graphene nanocomposites.

2. Investigate the effect of weight percentage of reinforcement and applied load on the wear and friction behavior of composites

3. Characterize worn surface of nanocomposites to find wear mechanism and characterize the tribofilm on the surface to understand the reason for the change in wear and COF.

Several factors which can influence the tribological properties including materials parameters (weight percentage of graphene and alumina) and test parameters (applied load). Any change in these parameters can result is a change in tribological properties. In this study, a selected number of factors were designated to evaluate the optimal parameters. For aluminum/graphene composites, the weight percentage of graphene will be 0.5, 1, 1.5, 2 and 3.

119

Therefore, the self-lubricating aluminum/graphene composites are Al/0.5GNPs (aluminum reinforced by 0.5 wt.% graphene), Al/1GNPs (aluminum reinforced by 1 wt.% graphene), Al/1.5GNPs (aluminum reinforced by 1.5 wt.% graphene), Al/2GNPs (aluminum reinforced by 2 wt.% graphene) and Al/3GNPs (aluminum reinforced by 3 wt.% graphene). For hybrid nanocomposites, the summation of weight percentage of reinforcement is constant (3%) and the ratio of graphene:alumina will be changed. The self-lubricating aluminum/graphene composites investigated were Al/0.5GNPs/2.5Al$_2$O$_3$ (aluminum reinforced by 0.5 wt.% graphene and 2.5 wt.% alumina), Al/1GNPs/2Al$_2$O$_3$ (aluminum reinforced by 1 wt.% graphene and 2 wt.% alumina), Al/1.5GNPs/1.5Al$_2$O$_3$ (aluminum reinforced by 1.5 wt.% graphene and 1.5 wt.% alumina), Al/2GNPs/1Al$_2$O$_3$ (aluminum reinforced by 2 wt.% graphene and 1 wt.% alumina), Al/2.5GNPs/0.5Al$_2$O$_3$ (aluminum reinforced by 2.5 wt.% graphene and 0.5 wt.% alumina). The test parameters that were selected include 5, 10, 15 and 20N of normal load and the sliding speed is constant, and it is 25 mm/s.

2.3.1 MATERIALS AND FABRICATION

The materials used in this investigation are a) 99% pure Al powder (Acros Organics, Waltham, MA) with an average particle size of 75 μm, b) Al$_2$O$_{3np}$ powder (Nanophase, Romeoville, IL) with an average particle size of 47 nm, and c) graphene nanoplatelets (GNP) nano27 (Asbury, Asbury, NJ) with average thickness of approximately 10 nm and average platelet diameter of ~1-2 μm.

To produce MMNCs, the reinforcements with various wt.% of ball milled graphene GNPs (see 1.4.1, Pg. 21) and as-received Al_2O_{3np} were dispersed in 99.9% benzene by ultrasonication. The aluminum powder and the reinforcement slurry were added to a Planetary Ball Mill PM 100 and milled for 6 hours at 500 rpm using a ball-to-powder weight ratio of 10:1 (5 and 20 mm diameter steel balls). The procedure to synthesize self-lubricating aluminum composites reinforced by graphene nanoplatelets (GNPs) and alumina (Al_2O_3) powders is schematically illustrated in Figure 42. The milled composite powders were dried at 135°C for 1 hour to remove the benzene in a vacuum oven to prevent oxidation of powders. The dried powders were consolidated by single action cold compaction in a steel mold with 200 MPa at room temperature followed by single action hot compaction in a steel mold with 500 MPa at 525°C in the air for 5 minutes such that a 25.4 mm diameter cylinder with a height of 10 mm was produced.
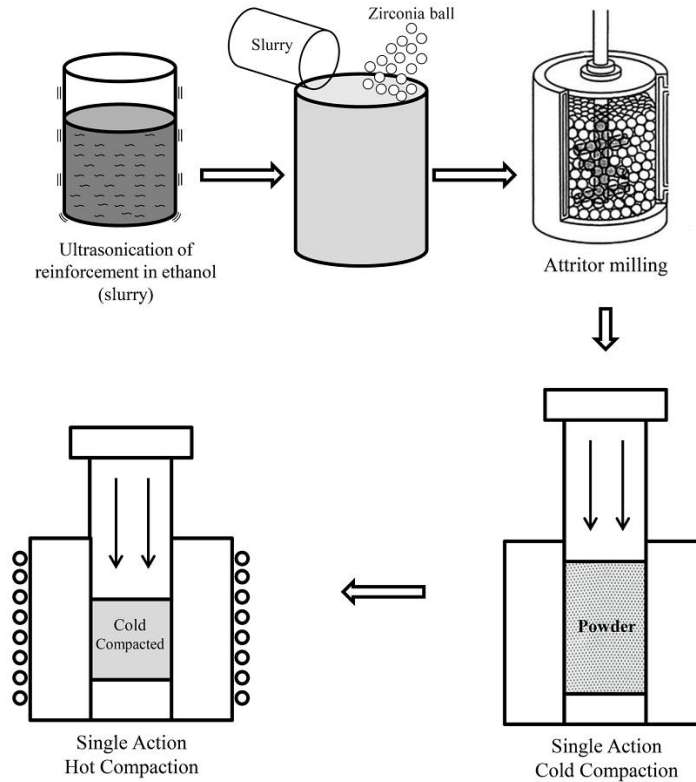
Figure 42 Schematic illustrations to show the attritor milling powder processing technique at room temperature

2.3.2 HARDNESS TEST

To investigate the mechanical properties of the samples Hardness Rockwell B were conducted on the samples. For hardness measurements, five independent Rockwell B Hardness (HRB) measurements were averaged for each sample at each stage of processing. The Rockwell hardness scale was chosen because it can capture the representative indentation behavior from a relatively large area of the MMNC sample surfaces.

2.3.3 TRIBOLOGICAL TESTS

To investigate the tribological behavior of the samples, pin-on-disk tests under dry condition were conducted. In the tests, cylindrical pins with a dimension of 6 mm in diameter and 8 mm in height were utilized from the hot compacted composite samples. The contact surface of composite pins is flat. The 440C stainless steel discs were prepared to act as the counter body in the wear test. To obtain the standard results, the standard counter body is used. The hardness of 440 steel is 62HRC. The commercial 440 stainless steel is machined and made into a disc as per the dimension of 55 mm in diameter and 10 mm in thickness. The pin-on-disk experiment was conducted for different normal loads (5, 10, 15 and 20 N) and constant sliding speed of 25 mm/s (or 120 rpm at 40 mm wear track) at a constant sliding distance of 1.5 km. The coefficient of friction (COF) and volume loss (wear rates) was measured during the wear tests. The pin and disk specimen were cleaned by acetone before and by hexane after each test.

The COF (coefficient of friction) value presented for each test was the average of the friction values. In addition, the linear wear-loss was acquired through a linear variable differential transducer (LVDT) with an encoder, which recorded the vertical displacement of the pin. The linear wear loss of each pin was converted into a volumetric wear loss using Eq. (1) derived from the geometry of a spherical cap.

$$V = \pi r^2 . h \qquad\qquad (2)$$

In Eq. (2), h is the linear displacement (mm) in the vertical (longitudinal) axis for the pin, r is the pin radius (6 mm), which is assumed to be constant

123

throughout the test, and *V* is the volumetric wear loss (mm³). For a given set of testing conditions, at least three repetitive tests were performed and the results of the average of three tests were presented.

2.3.4 CHARACTERIZATION

The worn surfaces of the samples were investigated to understand the wear mechanism. Comprehensive characterization tests were designed for the synthesized composites to understand and explain the relationship between processing, structure, and performance using the following techniques.

Two different scanning electron microscopes (SEM) (Hitachi S-4800 Ultra High-Resolution Cold Cathode Field Emission Scanning Electron Microscope (FE-SEM), JEOL JSM-6460 LV were used for characterization of the worn surfaces and. Elemental analysis is performed using an Oxford Energy Dispersive Spectroscopy detector attached to the SEM. The thin window silicon drift detector (SDD) allows the detection of the elements carbon and higher.

A FEI™ TEM200 Focused Ion Beam (FIB) with Gallium ion source was employed to obtain TEM thin foils. TEM was done by a Phillips CM-200 operating at 200 kV. STEM characterization was carried out using a FEI/Tecnai™ F30 300 kV TEM equipped with a Fischione™ high angle annular dark field (HAADF) detector and an X-ray Energy Dispersive Spectroscopy (XEDS) detector.

X-ray diffraction (XRD) data gathered by a D8 Bruker diffractometer with Cu Kα1 radiation (λ= 0.15406 nm) (scanning from $2\theta = 15°$ to $2\theta = 85°$, step size of 0.02°, counting time of 0.3s per step).

A LEXT OLS4100 3-D Laser Confocal Microscopy is used for 2-D and 3-D imaging and dimensional measurements with a surface feature observation resolution of 20 nm.

A Renishaw Inc. 1000B Raman spectroscopy (Helium neon laser (633nm)) is used to determine the formation of tribofilm on the worn surfaces.

2.4 RESULTS AND DISCUSSION

2.4.1 MICROSTRUCTURAL STUDIES

2.4.1.1 Ball Milling of Aluminum Powders

It has been well established that high-energy mechanical milling is one of the major techniques for producing powders with nanocrystalline structures [29]. In high energy milling, powder particles are subjected to severe plastic deformation through repetitive compressive loads arising from the impacts between the balls and the powder particles. As a result, new crystalline and amorphous materials could be produced with crystallite sizes at the nanometer scale [9]. Furthermore, the mechanical milling kinetics depends on the energy transferred to the powder from the balls during milling [10]. The energy transfer is governed by many parameters such as milling speed, size and size distribution of the balls, dry or wet milling and temperature and duration of milling [11]. High energy milling has advantages of being simple, relatively inexpensive to produce [12], applicable to any class of materials and easily scaled up to large quantities [13].

When a single-phase elemental powder or intermetallic compound powder is milled, the grain size of the powder particles continues to decrease until it reaches a minimum level—in the range of 3–25 nm.

For metallic and intermetallic powders, it is believed that fracturing and cold welding are not the major mechanisms for the reduction of the grain size. Instead, the reduction of the grain size is due to the localization of plastic deformation in the form of shear bands containing a high density of dislocations, the formation of subgrains or cells by the annihilation of dislocations and the conversion of subgrains/cells into grains through mechanically driven grain rotation and subgrain boundary sliding. In other words, the mechanism of forming nanosized grains during high-energy mechanical milling is very similar to the dynamic recrystallization which occurs during hot forming of metals and alloys, except the mechanical working temperature in milling is very low and limits the opportunities for the new grains to grow. The low temperature is essential in keeping the nanograins from further coarsening. The minimum grain size is determined by the balance between dislocation accumulation, and dynamic recovery through the formation of subgrain boundary and new grains.

Deviations from ideal crystallinity, such as finite crystallite size and strain (at the atomic level) lead to broadening of the diffraction lines in X-ray Diffraction spectra. By analyzing this broadening, it is possible to extract information about the microstructure of a material. However, various sources for the line broadening of X-Ray peaks exist. These include a) Instrumental Broadening (Non- ideal optics, Wavelength Dispersion, Sample Transparency, Axial Divergence, Flat Sample

126

Effect, Detector resolution (area det. & PSD's) b) Crystal size and Extended Defects Broadening, and c) Lattice Strain (microstrain).

A perfect crystal would extend in all directions to infinity, so we can say that no crystal is perfect due to it is finite size. This deviation from perfect crystallinity leads to a broadening of the diffraction peaks. However, above a certain size (~0.1 - 1 micron) this type of broadening is negligible. Crystallite size is a measure of the size of a coherently diffracting domain. Due to the presence of polycrystalline aggregates crystallite size is not generally the same thing as particle size in particulate materials. Therefore, in practice, the crystallite size analysis on a sample containing extended defects can be used to estimate the ordered domain size (the size of the region between defects). Scherrer (1918) first observed that small crystallite size could give rise to line broadening. He derived a well-known equation for relating the crystallite size to the broadening, which is called the "Scherrer Formula"[271].

$$D_v = \frac{K\lambda}{\beta\cos\theta}$$

D_v = Volume Weighted crystallite size

K = Scherrer constant, somewhat arbitrary value that falls in the range 0.87-1.0. I usually assume K = 1.

λ = The wavelength of the radiation

β = The integral breadth of a reflection (in radians 2θ) located at 2θ.

In crystals, there we can observe two types of strain a) Uniform strain b) Non-uniform strain. Uniform strain causes the unit cell to expand/contract in an isotropic way. This simply leads to a change in the unit cell parameters and shift of

127

the peaks. There is no broadening associated with this type of strain. On the other side, non-uniform strain leads to systematic shifts of atoms from their ideal positions and to peak broadening. The non-uniform strain arises from point defects (vacancies, site-disorder), plastic deformation (cold worked metals, thin films), and poor crystallinity. Stokes and Wilson (1944) first observed that strained or imperfect crystals containing line broadening of a different sort, then the broadening that arises from small crystallite size.

$$\varepsilon_{str} = \frac{\beta}{4\{\tan\theta\}}$$

ε_{str} = weighted average strain

β = The integral breadth of a reflection (in radians 2θ) located at 2θ.

Note that size and strain broadening show a different θ dependence.

This provides a way to separate the two effects.

To do an accurate analysis for size and/or strain effects one must accurately account for instrumental broadening. The manner of doing this differs depending upon the peak shape. Line broadening analysis is most accurate when the broadening due to crystallite size effects is at least twice the contribution due to instrumental broadening. If we use this criterion we can calculate the size range over which this technique will be the most accurate. We could also estimate a rough upper limit for reasonable accuracy by looking at the crystallite size that would lead to broadening equal to the instrumental broadening.

The width of a diffraction line can be estimated by more than one criterion. The two most common width parameters are, Full Width at Half Maximum (FWHM or Γ) - The width of the peak at 1/2 it's maximum intensity, and Integral

128

Breadth (β)- The width of a rectangle with the same height and area as the diffraction peak. The integral breadth (β) and FWHM (Γ) can be related for various peak shapes such as Lorentzian, Gaussian, and Voigt, Pseudo-Voigt. Therefore, differentiation of instrumental broadening and size/ strain broadening differs depending upon the peak shape (Figure 43). Following Lorentzian equation was used in our calculation.

$$\beta_{obs=}\beta_{size} + \beta_{strain} + \beta_{inst}$$

$$\{\beta_{obs-}\beta_{inst}\} = \beta_{strain} + \beta_{size}$$

Williamson and Hall (1953) proposed a method for deconvoluting size and strain broadening by looking at the peak width as a function of 2θ. Here. It is a Williamson-Hall relationship for the Lorentzian peak shape, but it can be derived in a similar manner for the Gaussian peak shape.

$$\{\beta_{obs-}\beta_{inst}\} = \frac{K\lambda}{D_v \cos\theta} + 4\varepsilon_{str}\{\tan\theta\}$$

$$\{\beta_{obs-}\beta_{inst}\}\cos\theta = \frac{K\lambda}{D_v} + 4\ \varepsilon_{str}\ \{\sin\theta\}$$

To make a Williamson-Hall plot, one need to plot $\{\beta_{obs-}\beta_{inst}\}\cos\theta$ on the y-axis (in radians 2θ) and 4sinθ on the x-axis. If you get a linear fit to the data, you can extract the crystallite size from the y-intercept of the fit and the strain from the slope of the fit. Simplified integral breadth methods work well if the peak shapes are either pure Gaussian or pure Lorentzian. It is generally necessary to correct for instrumental broadening and to use integral breadths (rather than FWHM) to obtain the most accurate analysis. Therefore, samples of high purity Aluminum

powder of initial particle size of approximately 40 μm was ball milled for different intensities and durations. Instrumental broadening and the peak shape were determined using a NIST SRM 640e standard silicon sample (Figure 44). The high energy ball mill process was carry out using a planetary ball mill with a hardened steel ball. Data from attritor mill were used to compare the type of milling process in final microstructural defects. The peak breadths of the (111), (200), (220) and (311) reflections, plotted according to W-H equation. After plotting $\{\beta_{obs-}\beta_{inst}\}\cos\theta$ on the y-axis and $4\sin\theta$ on the x-axis (Figure 45 and Figure 46), a linear fit to the data were used to extract the crystallite size from the y-intercept of the fit and the strain from the slope of the fit. Figure 47 shows the variation of crystallite size as a function of milling time and milling rpm. According to data in Figure 45, high energy ball mill at 600 rpm is the most effective technique in reducing the crystallite size in aluminum powder. Based on the results in Figure 46 the optimum milling time at 600rpm to obtain the smallest crystallite size is selected as 180 minutes. As it can be observed, the crystal size is decreasing and then reach a plateau by increasing the milling time, in which a higher rpm helps it to reach the plateau at shorter milling time.
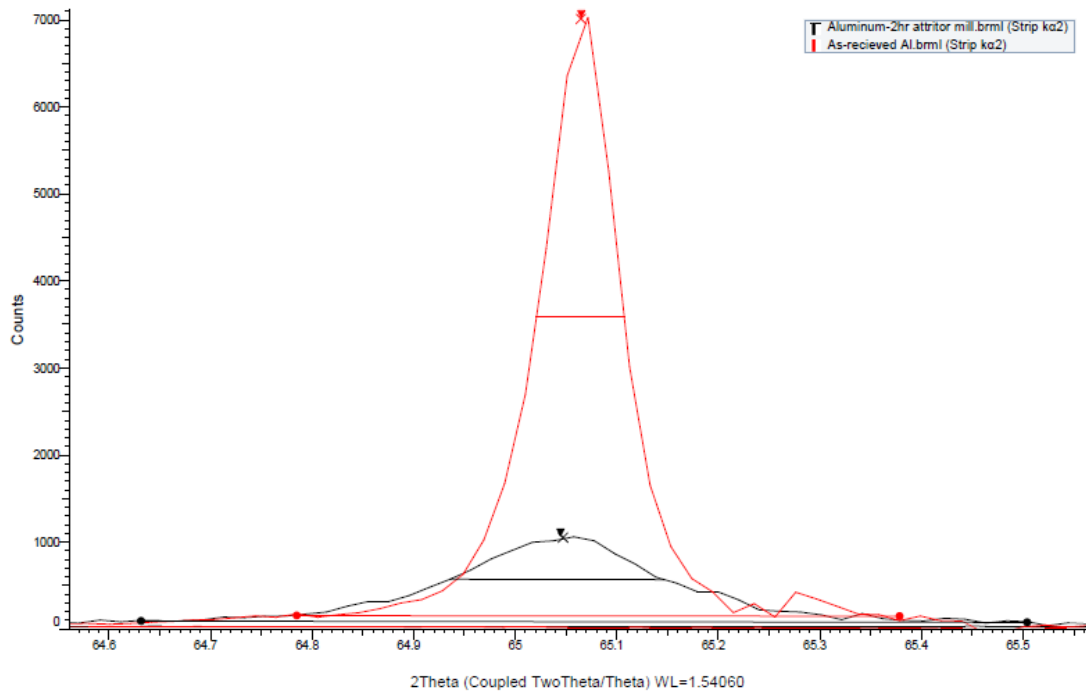
Figure 43 Illustration of FWHM comparison of (220) of as-received and milled aluminum

$$y = 9E-06x^2 - 0.0004x + 0.0541$$
$$R^2 = 0.8671$$
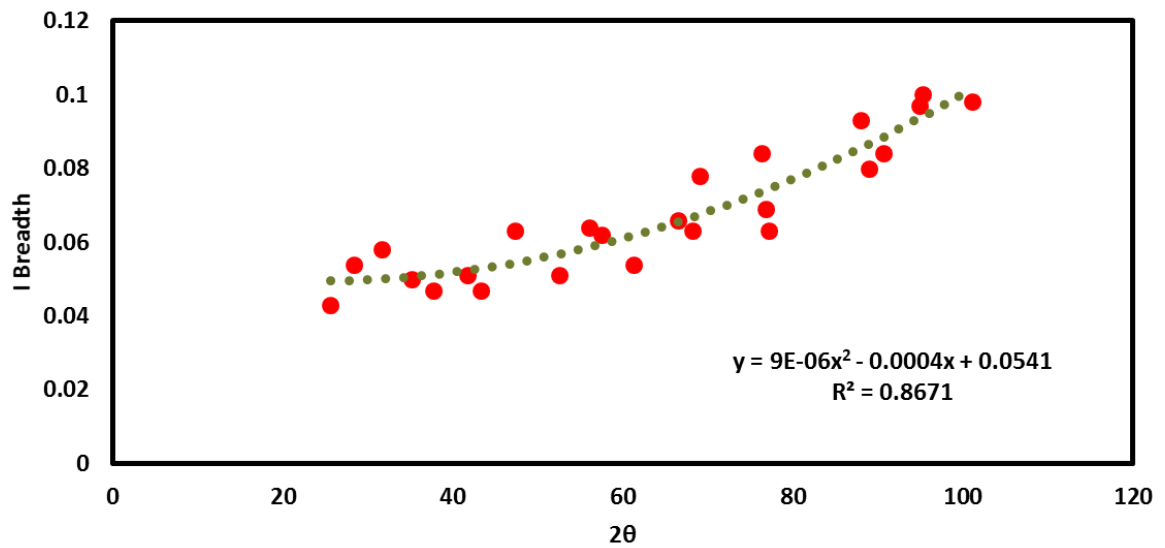
Figure 44 Determination of instrumental Broadening using a NIST SRM 640e standard silicon sample

131
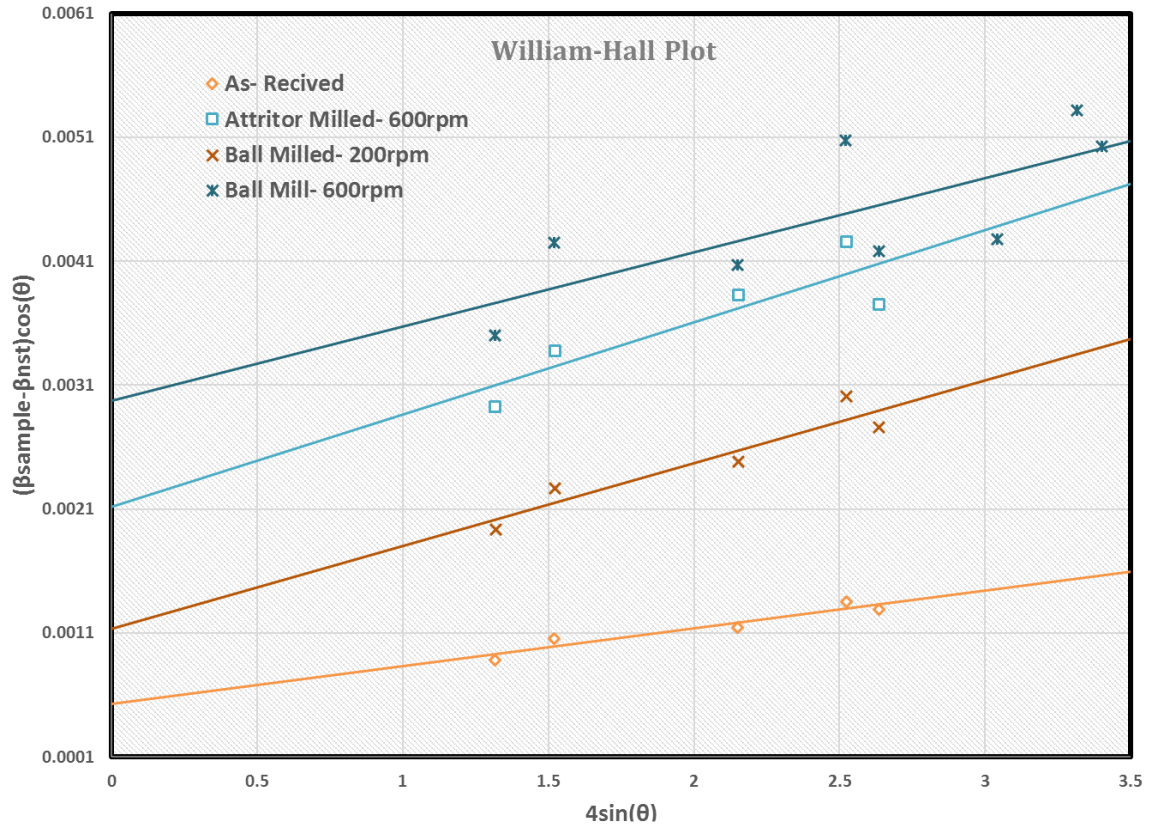
Figure 45 Williamson-Hall plot of as-received aluminum, ball milled Al at 200 rpm, ball milled Al at 600 rpm, and attritor milled Aluminum.
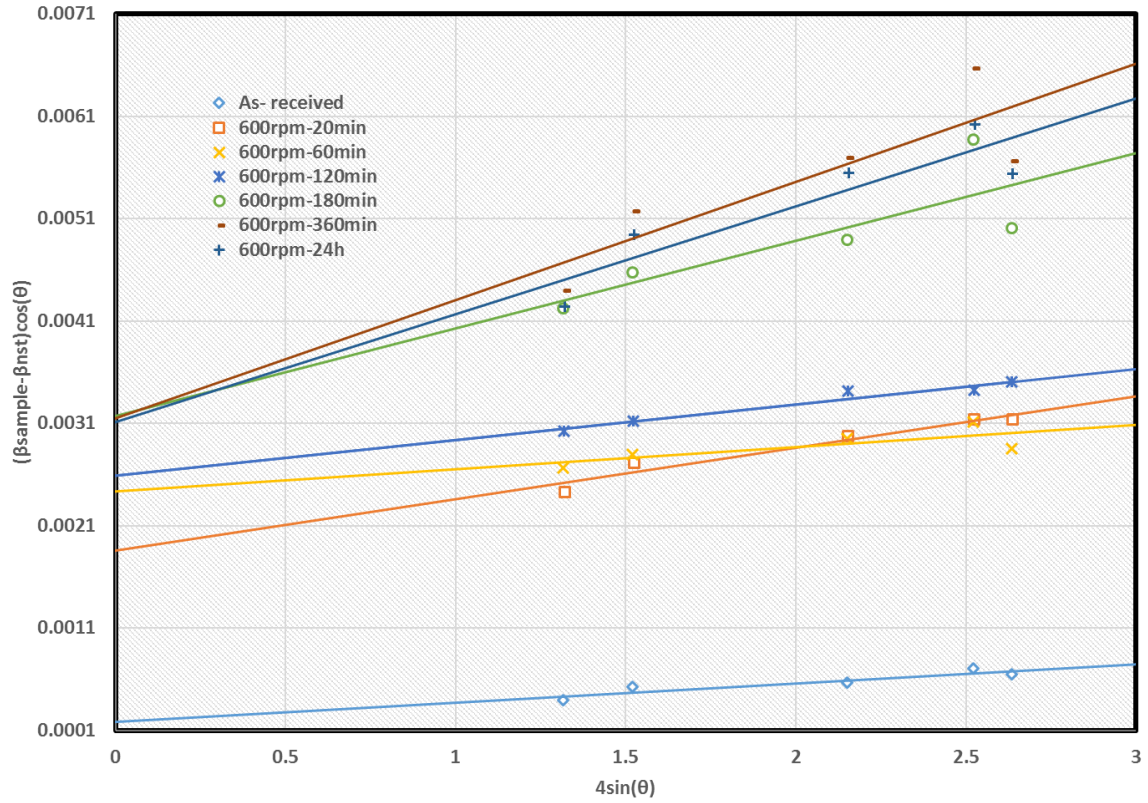
Figure 46 Williamson-Hall plot of as-received aluminum and ball milled

Aluminum at 600 rpm for 20, 60, 120, 180, 360, and 1440 minutes

2.4.1.2 Composites Synthesis

High Angle Annular Dark Field (HAADF) micrograph of Al/3GNPs powder depicts the presence of porosity/holes as shown in Figure 48. EDX analysis didn't reveal any compositional inhomogeneity and impurity. Figure 49 exhibit the electron diffraction pattern of Al/3GNPs composites. Figure 49(a) shows a typical electron diffraction pattern with no selected area aperture showing the presence of nanocrystalline grains. Figure 49b is the selected area electron diffraction pattern (SAEDP) showing the presence of diffraction spots from few aluminum grains, and Figure 49c shows the SAEDP from the areas where graphene can be possibly present in the aluminum matrix. Figure 50 corresponding to the bright field image of the spot indicated by red ring and arrow in Figure 49c. Diffraction spot within Al(111) ring help to identify the localized region in the sample where graphene can possibly be located. High-resolution HRTEM imaging was used to observe nanoscale features in the sample.

Figure 51 depicts the HAADF micrograph of Al/2GNP/1Al$_2$O$_3$ powder composite. Presence of Al$_2$O$_3$ nanoparticles is evident and confirmed by EDX as shown in Figure 52.
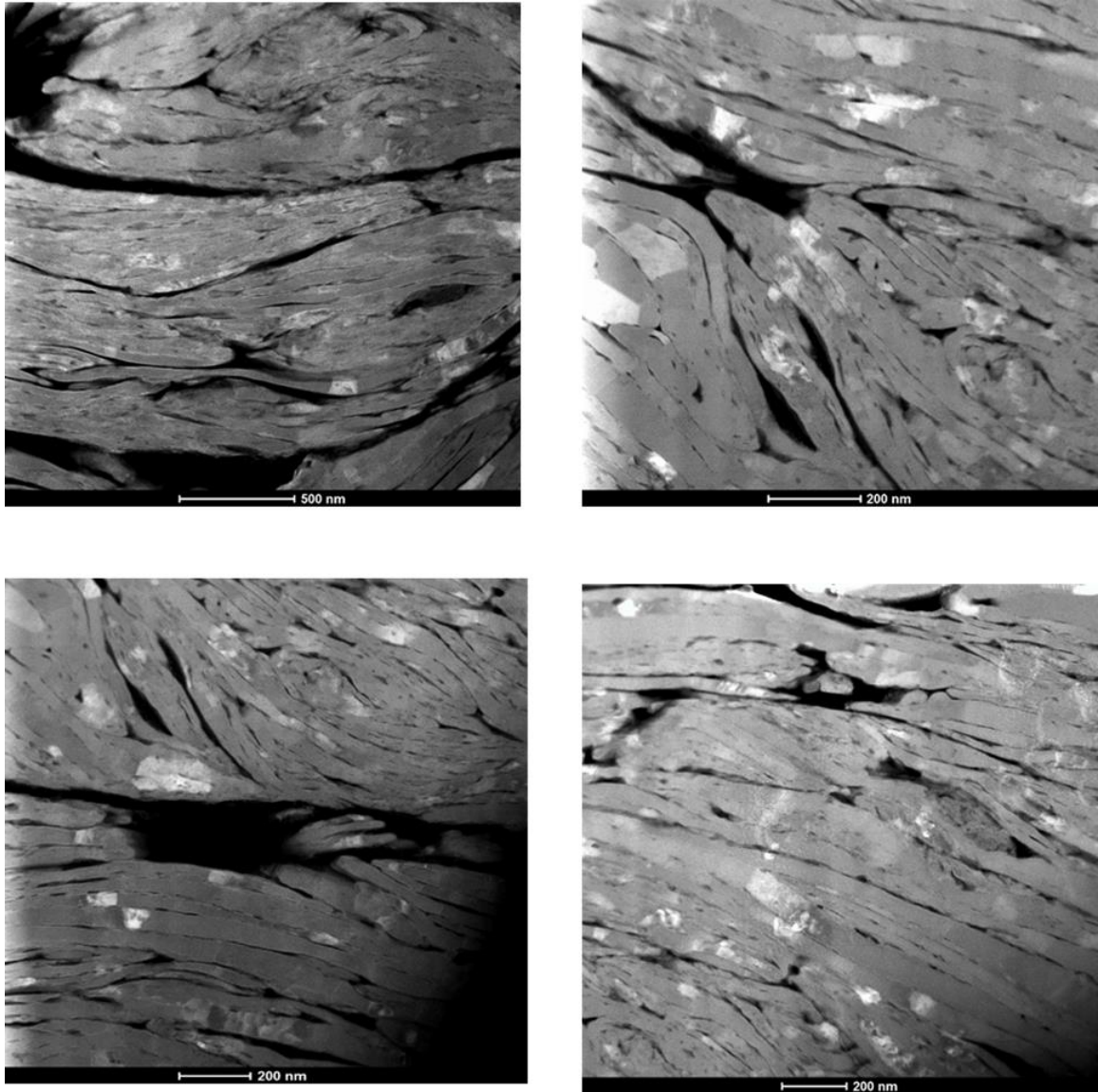
Figure 48 High Angle Annular Dark Field (HAADF) micrograph of Al/3GNP
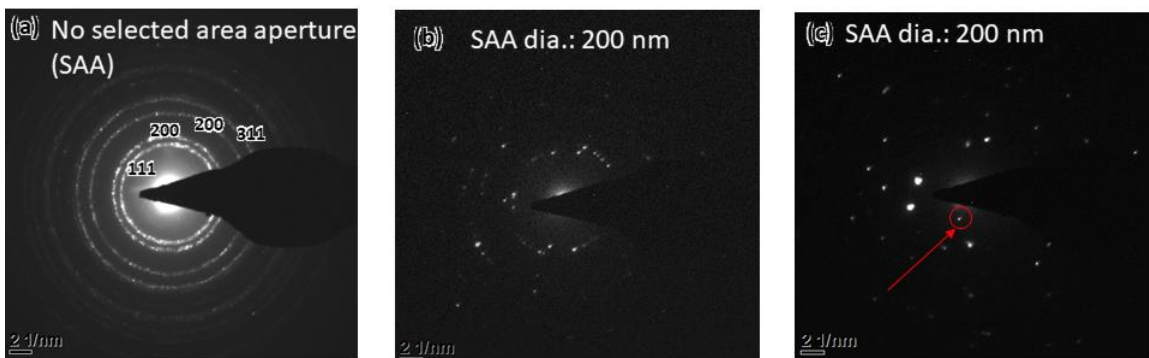
(powder composite)

Figure 49 Electron diffraction pattern of Al/3GNPs composites
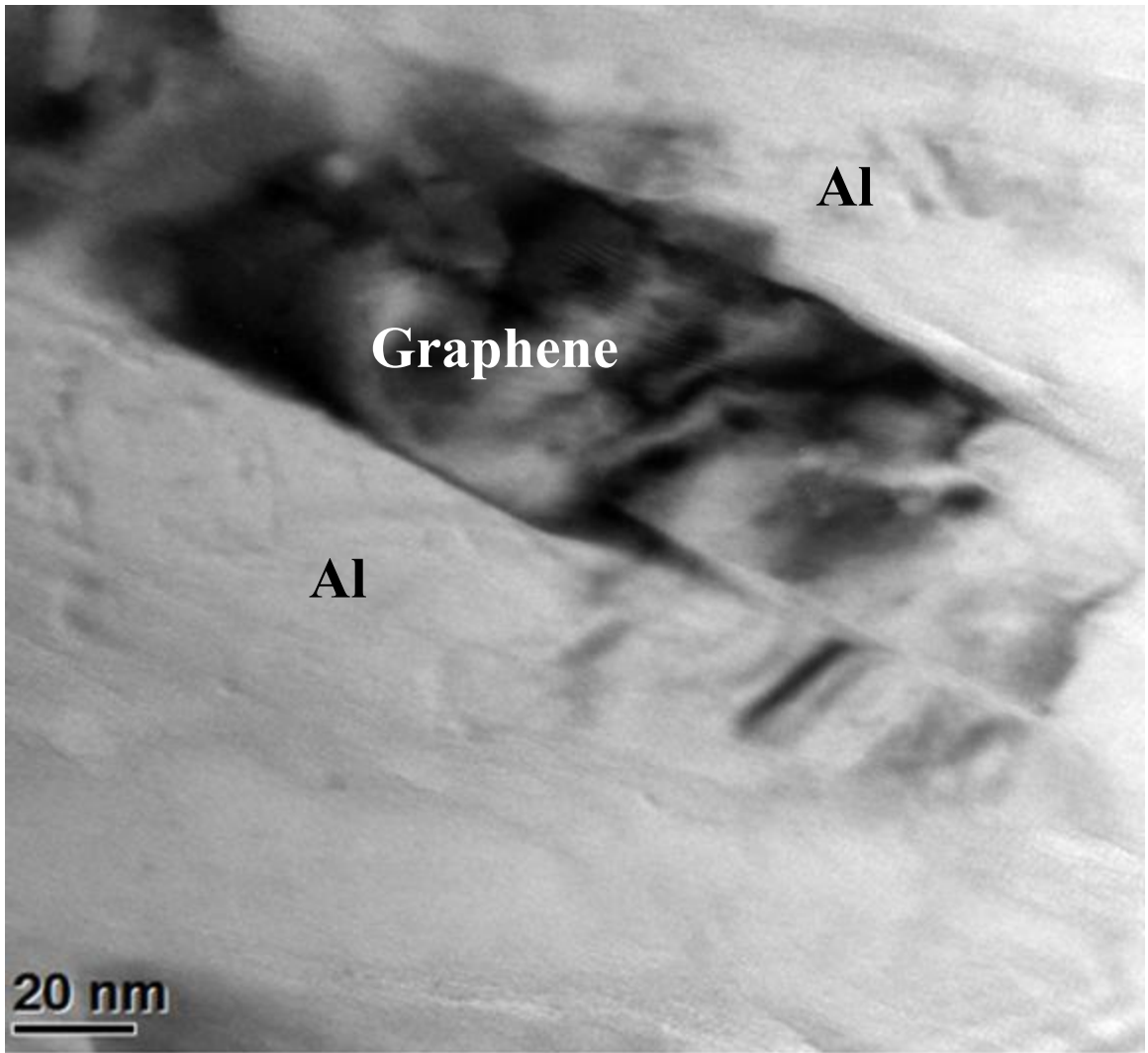
Figure 50 Typical bright field micrograph of Al/3GNP powder composite
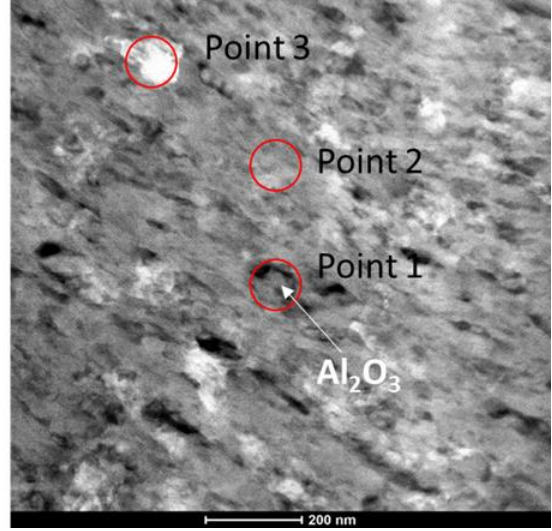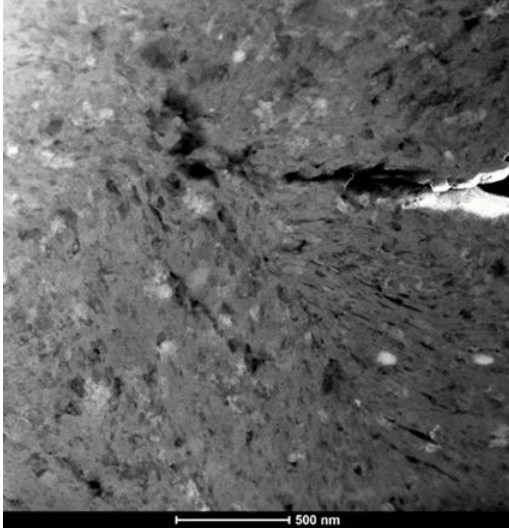
Figure 51 HAADF micrograph of Al/2GNP/1Al₂O₃ (powder composite)
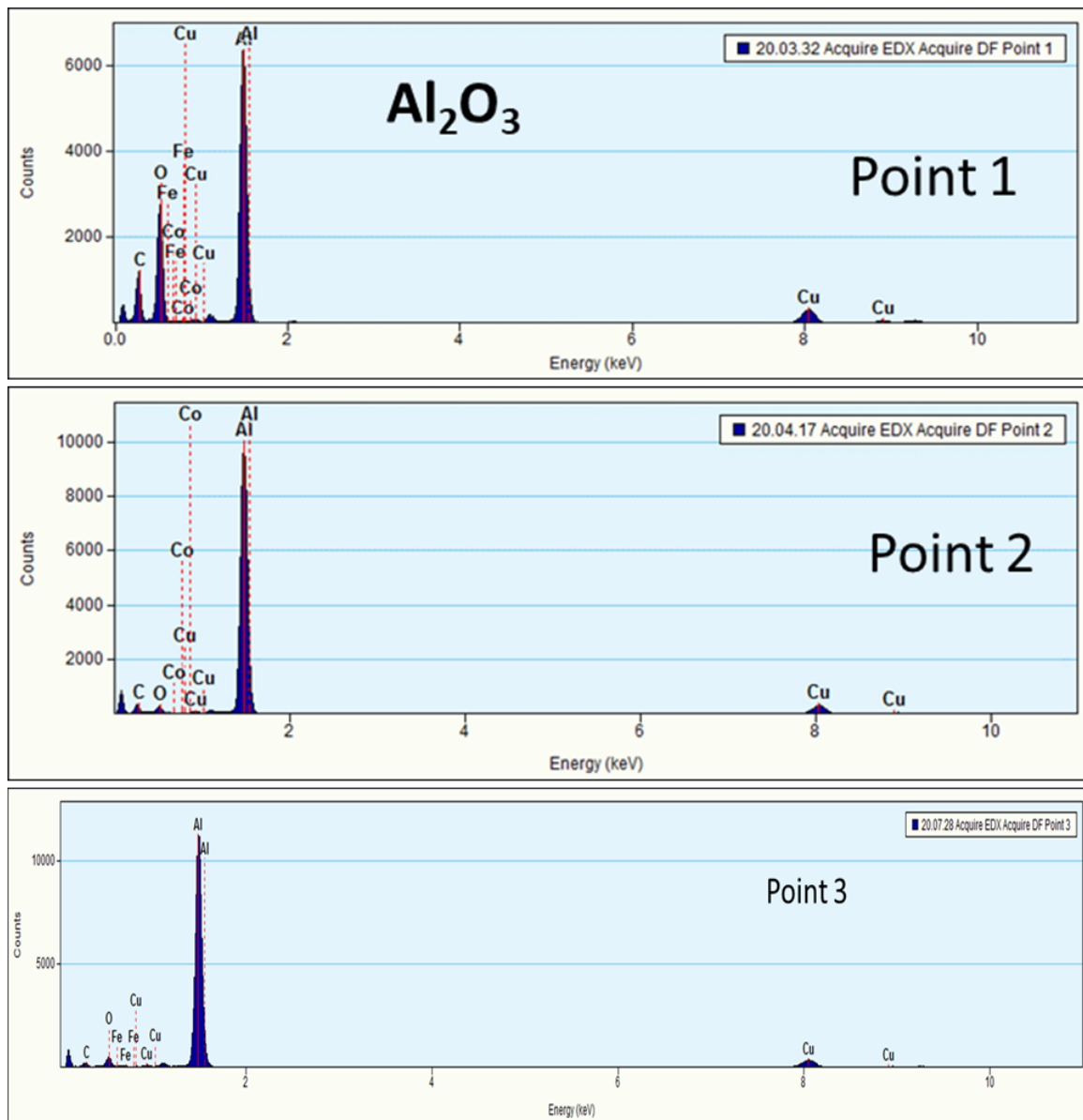
Figure 52 EDX of Al/2GNP/1Al₂O₃ on three points of Figure 51

Figure 53 - Figure 55 shows the HAADF micrograph of Al/1GNPs, Al/3GNPs, and Al/2GNP/1Al₂O₃ bulk composite, respectively. These figures show an anisotropic microstructure for composites. Figure 56 show diffraction pattern of TEM images of Al/1GNPs and Al/3GNPs. The diffraction pattern of bulk composites shows that oxide layers were formed on the surface of aluminum particles. Aluminum powders were heavily deformed during ball milling and

consolidation processing. Therefore, dislocations were generated during the powder metallurgy processing in the powders and led to increasing the mechanical properties.

In comparison between the microstructure of Al/1GNPs with Al/3GNPs, it can be mentioned that more porosity/holes/gaps appear on the Al/3GNPs composites which affect the mechanical properties and hardness of composites as will be discussed on 2.4.2 (Pg. 148). Figure 57 - Figure 59 shows the High-Resolution Transmission Electron Microscopy (HRTEM) with corresponding Fast Fourier transforms (FFT) for Al/1GNPs, Al/3GNPs, and Al/2GNP/1Al$_2$O$_3$ bulk composite, respectively. It can be concluded from these HRTEM images that graphene nanoplatelets were embedded between aluminum grains properly. In addition, it is evident that thickness of graphene is about 1-2 nm and confirms the good milling of graphene and aluminum powder and sintering condition to keep the graphene in nanosized range and nanocrystalline size of aluminum matrix. The distance between layers in the GNPs embedded in the aluminum was measured by the TEM images. The distance between layers of graphene in the composites sample calculated to about 0.346 nm. The same results have been reported by Chen et. al[248]. Besides, Figure 55 shows that the alumina nanoparticles are seated in between aluminum grains.
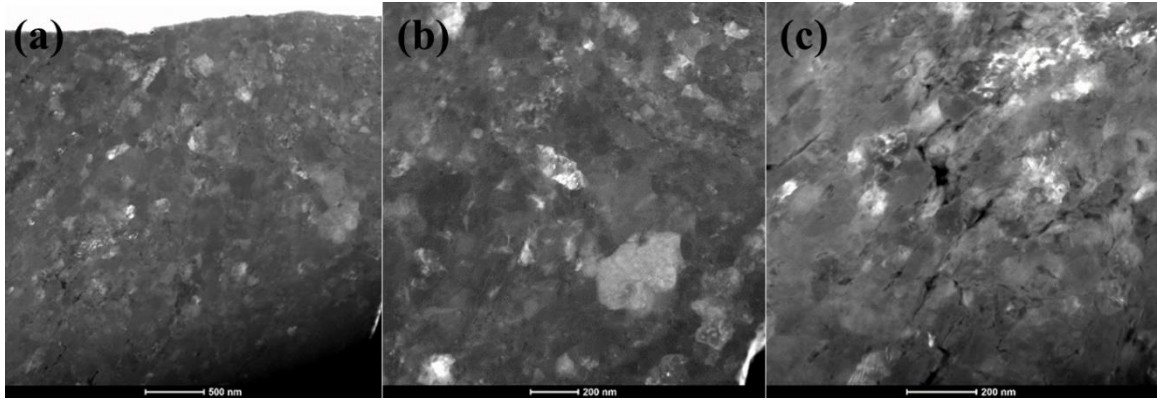
Figure 53 HAADF micrograph of Al/1GNPs bulk composite
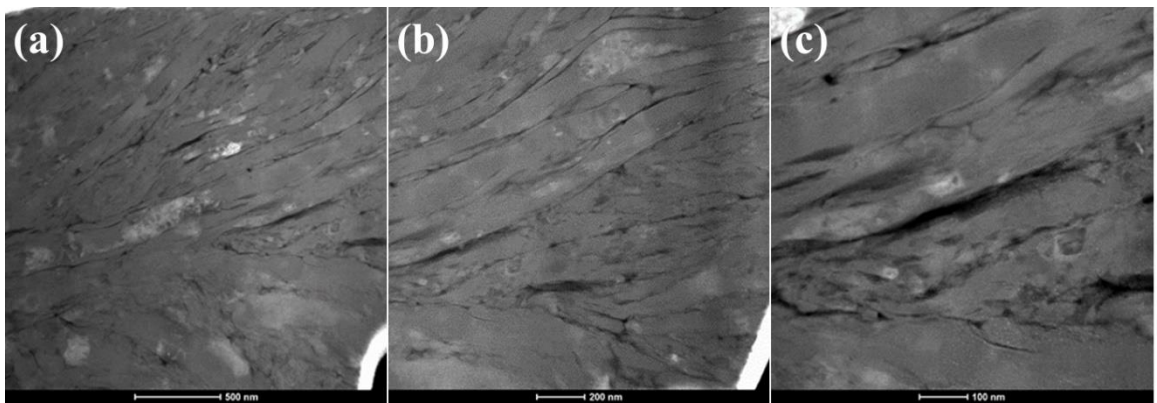
Figure 54 HAADF micrograph of Al/3GNPs bulk composite
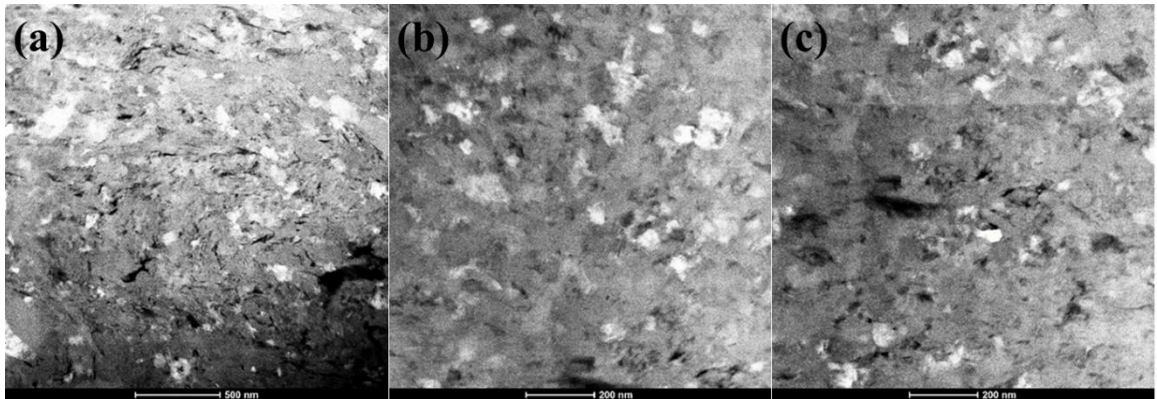
Figure 55 HAADF micrograph of 2GNP/1Al$_2$O$_3$ bulk composite

140
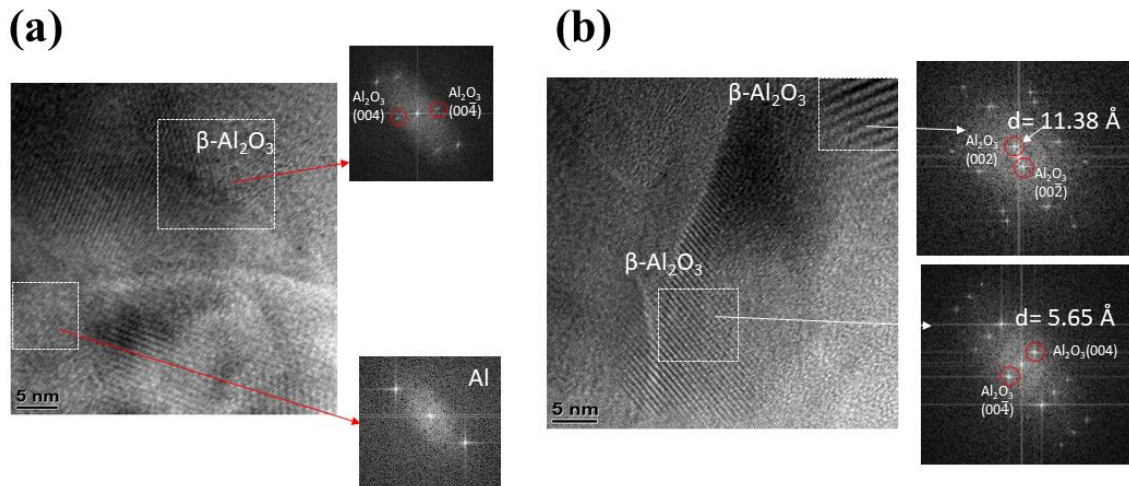
Figure 56 TEM images of a) Al/1GNPs and b) Al/3GNPs with oxygen enriched

locations
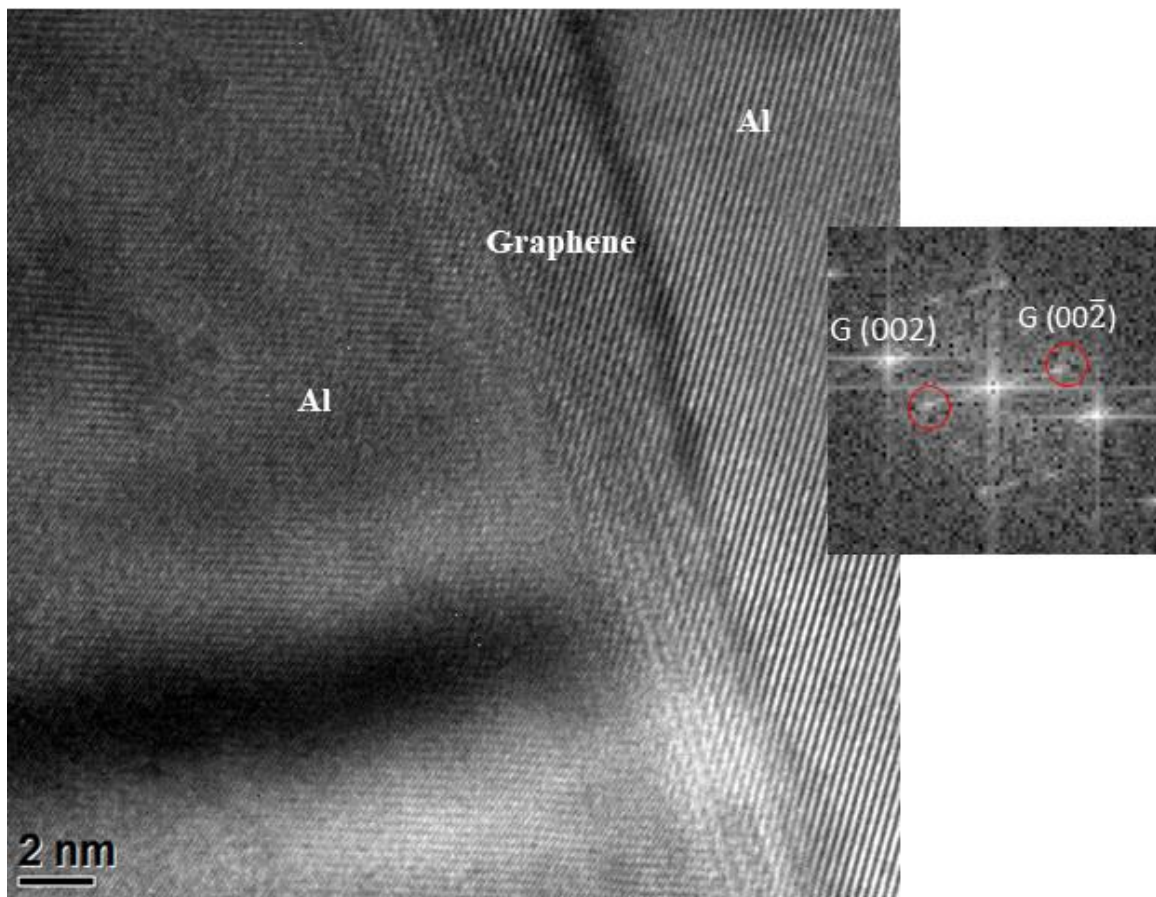
Figure 57 High-resolution Transmission electron microscopy (HR-TEM) with

corresponding Fast Fourier transforms (FFT) for Al/1GNPs

141
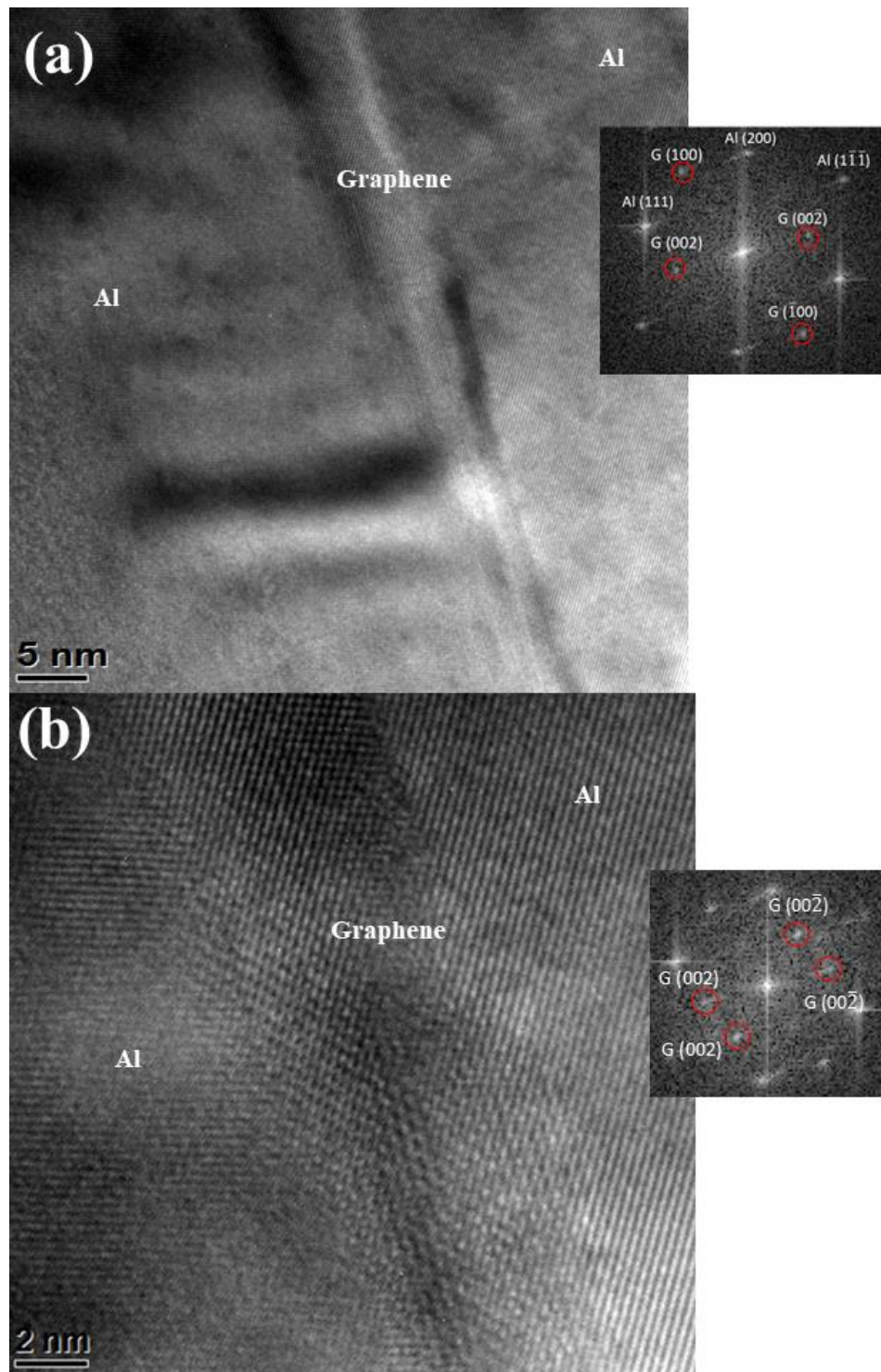
Figure 58 High-resolution Transmission electron microscopy (HR-TEM) with corresponding Fast Fourier transforms (FFT) for Al/3GNPs
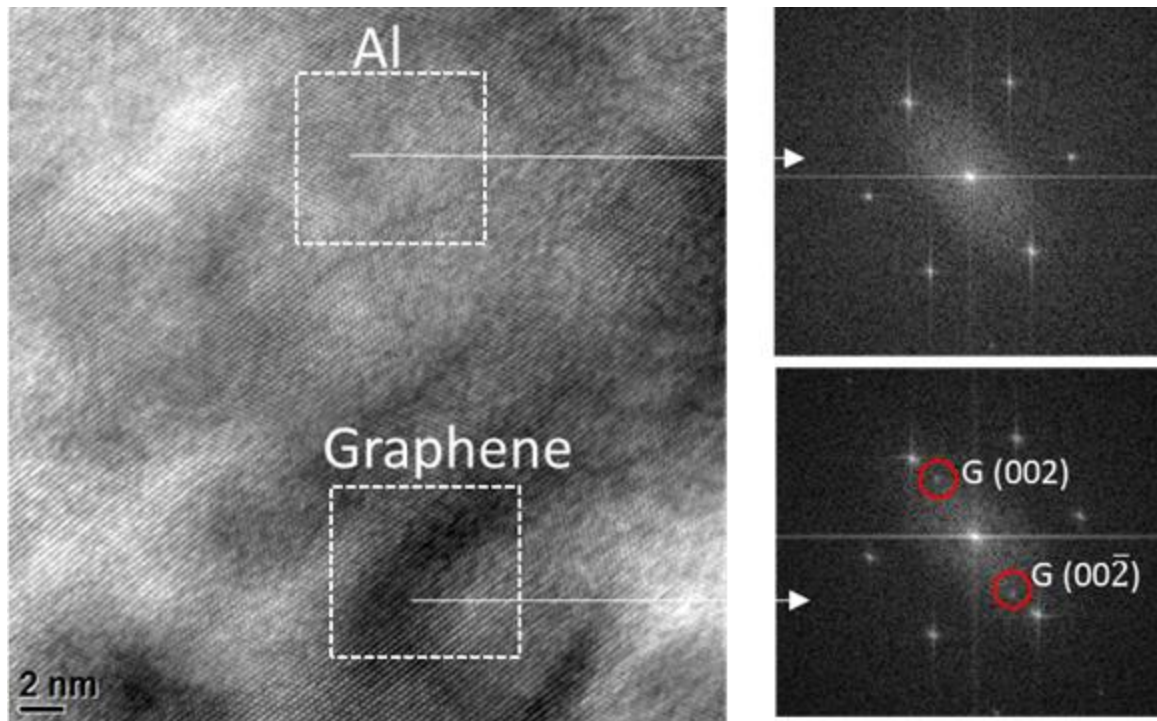
Figure 59 High-resolution Transmission electron microscopy (HR-TEM) with corresponding Fast Fourier transforms (FFT) for Al/2GNPs/1Al$_2$O$_3$

The XRD results for as received powders depicted in Figure 60 and Figure 61 where show the XRD results for the composite powders. In all the XRD spectrums, there are five peaks for aluminum. The 2θ measurement for these spectrums is approximately 38.4°, 44.6°, 65.0°, 78.2°, and 82.4°. Major aluminum peaks observed at 38.4° (111), 44.6° (200), 65.0° (220), 78.2° (311) and 82.4° (222). Figure 62 presents the XRD results on the selected bulk samples after consolidation processing. The XRD spectrum of the bulk samples are the same as the XRD spectrum of powders samples and show five major peaks of aluminum. These results prove that during consolidation processing, including single action cold compaction followed by single action hot compaction, there is no traceable undesirable reaction or formation of new phases. It can be concluded from the

143

XRD results different from the XRD results reported in [204] to exhibit peaks at $2\theta = 31.8, 55.0,$ and $72.5°$ to show the formation of aluminum carbide in Al-0.1 wt.% graphene composites. It is worth mentioning that the materials chosen for the milling media and the reservoir are highly wear-resistant and, therefore, the possibility of contamination is very low. As seen in XRD results, the chemical analysis identifies the presence of no contamination from milling media in the specimens produced in this study.

In Figure 63, the diffraction angle at the hkl values of (002), (100) and (004) corresponds to pure graphene phase. As graphene get embedded into the aluminum matrix, it is expected to observe GNPs diffraction peak at 2θ around $26°$ (Figure 63) in addition to the aluminum diffraction peaks. However, carbon reflections were not being observable for any of the samples due to the nanometric size and the low content of the reinforcement phase, which is below the detection limit of XRD for second phases [272].
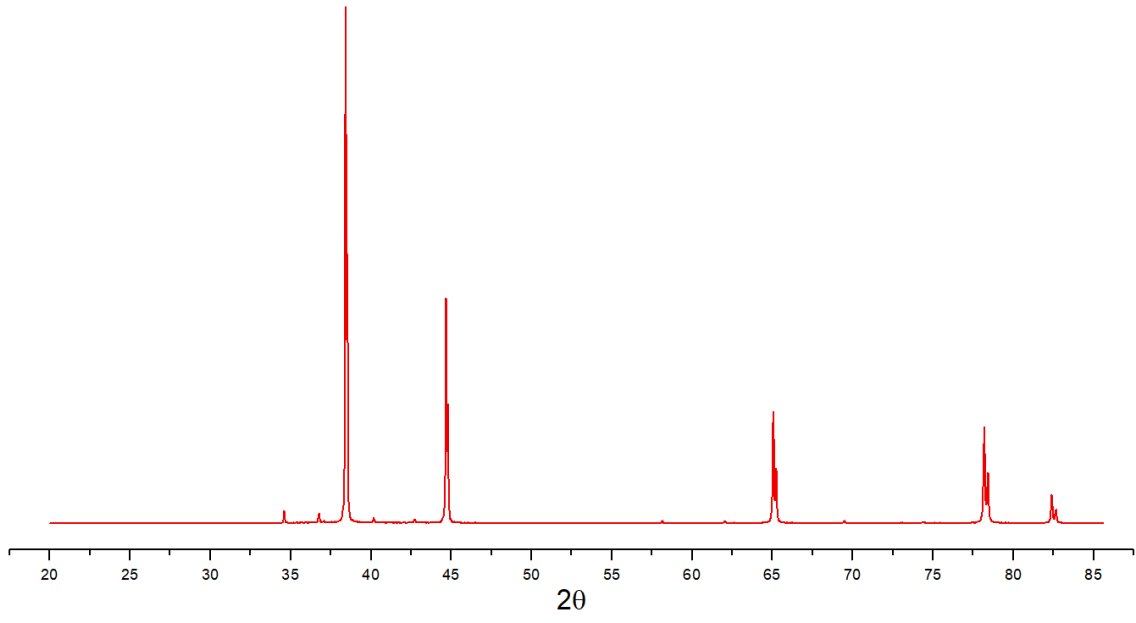
Figure 60 XRD spectrum of as-received aluminum powder
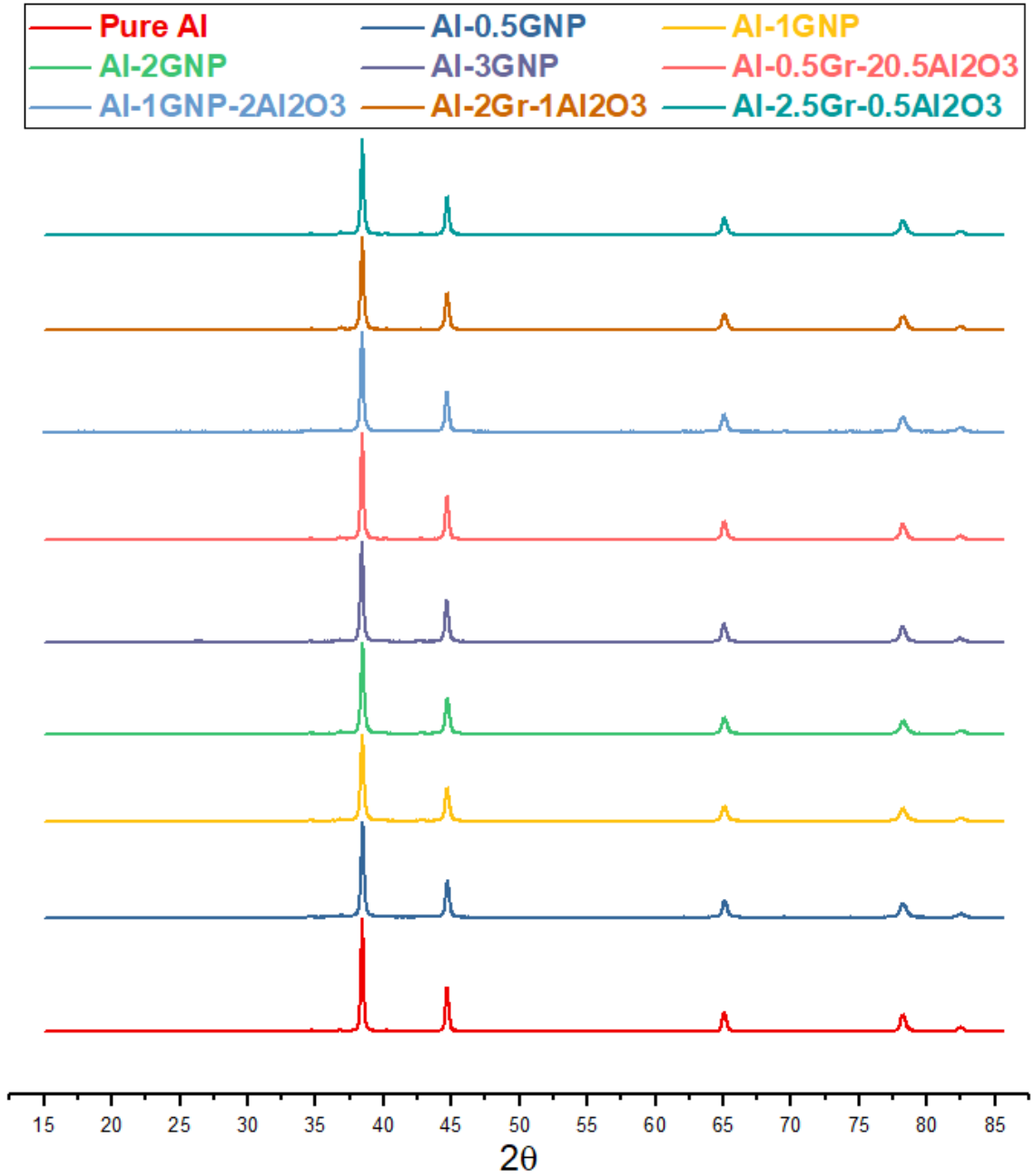
Figure 61 XRD spectrum of composite powders milled

146
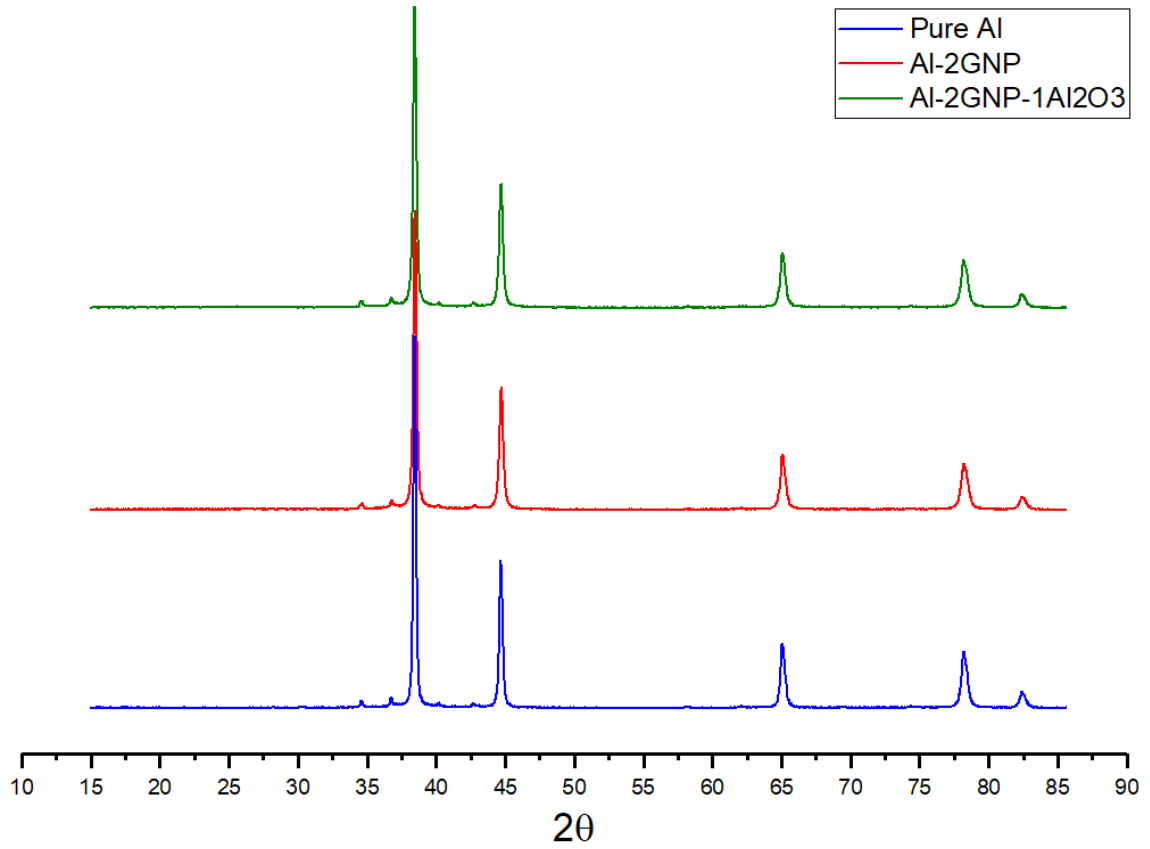
Figure 62 XRD spectrum of the bulk composite
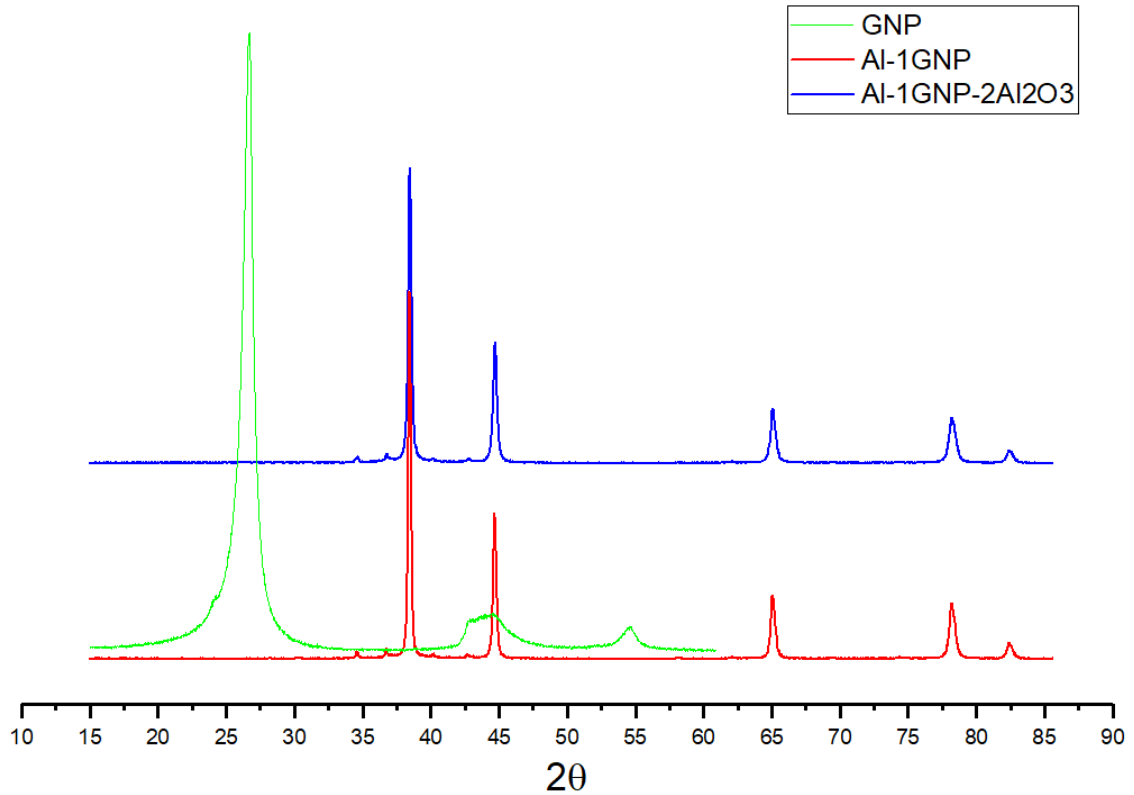
Figure 63 Comprising XRD spectrum of the bulk composite with graphene nanoplatelets

2.4.2 MECHANICAL PROPERTIES

Figure 64 shows the hardness Rockwell B (HRB) measurements for pure aluminum and aluminum matrix composites reinforced by graphene and Al_2O_3. Results clearly show that reinforcements increase the hardness of aluminum composites. Amongst composites, hybrid composites reinforced by graphene and alumina have a higher hardness than aluminum composites reinforced by graphene.

For Al/GNPs composites, the hardness of the composites initially increases with increasing graphene content and then decreases. Aluminum reinforced by 1

148

wt.% graphene nanoplatelets has the highest hardness among aluminum/GNPs composites. Bustamante et al. also reported that no clusters of graphene are observed in the reinforced composite with 1.0 wt.% of graphene under the condition of ball milling [207, 273]. Results show that   0.5 wt.% graphene is not enough to increase the hardness. Embedding graphene more than 1 wt.% (i.e. 2 and 3 wt.%) results in agglomeration and decrease in the hardness. Composites with higher graphene content show more porosity and gap which has a negative effect on the hardness of composites if one compares the microstructure of Al/1GNPs and Al/3GNPs composites in Figure 53 and Figure 54, respectively. It is evident that composites reinforced by 1 wt.% of graphene has less porosity and hole. Hence, the optimum weight percentage of graphene to increase the mechanical properties of aluminum is 1 wt.% where hardness increase from 74.8 HRB for pure aluminum to 90.1 HRB for Al/1GNPs composite and 20% improvement in hardness under otherwise identical experimental sample compaction and sintering conditions.

For aluminum hybrid composites, there is a synergetic effect of graphene and alumina particles to enhance mechanical properties [274, 275]. In a comparison of Al/GNPs and Al/GNPs/Al_2O_3 with the same weight percentage of graphene, the hardness of hybrid composites is higher. The hardness value increase from 90.1 HRB for Al/1GNPs to 94.4 HRB for Al/1GNPs/$2Al_2O_3$. It is attributed to the grain refinement of the matrix [276] and the influence of nanoparticles on strengthening of composite according to alumina nanoparticles act as obstacles to the motion of dislocation and Orowan mechanism is dominant [277, 278]. Moreover, lower porosity content of these samples has led to the higher

149

mechanical properties compared with Al/GNPs composites as will be discussed in microstructure [277].
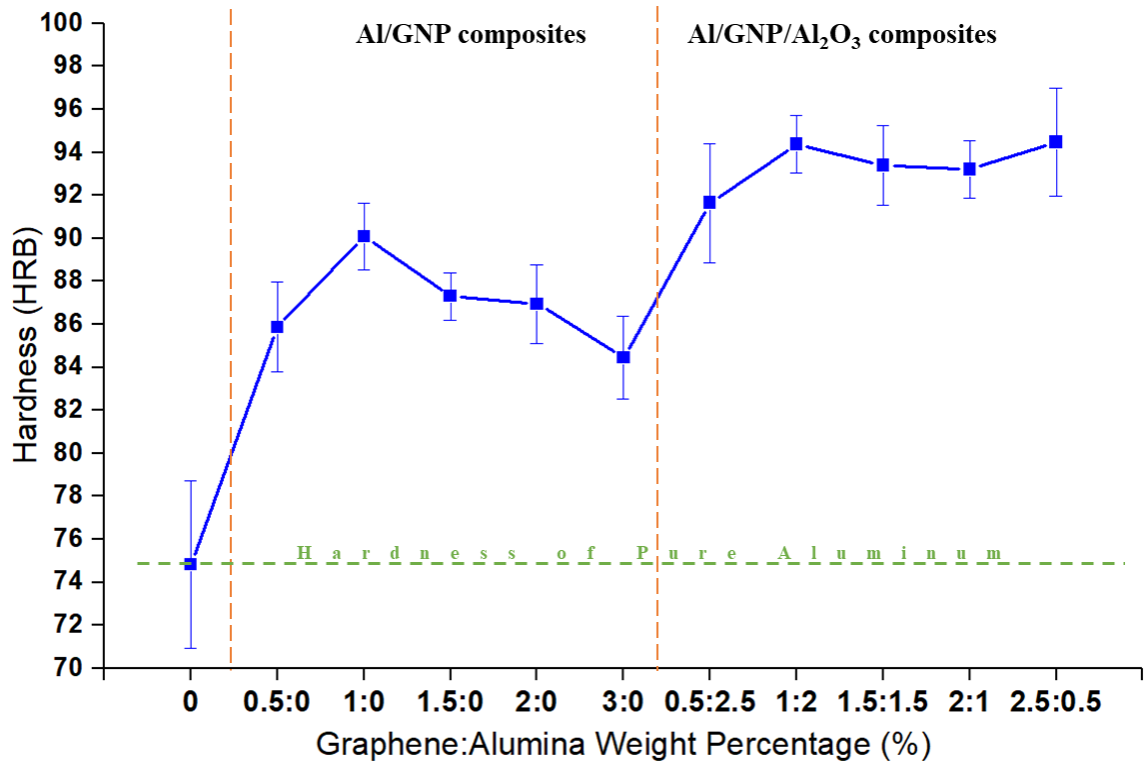
Figure 64 HRB measurements for pure aluminum and composite samples

2.4.3 TRIBOLOGICAL PROPERTIES

2.4.3.1 COF

The coefficient of friction (COF) is the critical parameter to obtain an indirect measurement of energy efficiency in industrial materials. Figure 65 exhibits the COF of aluminum and its composites. It is evident that embedding graphene nanoplatelets can decrease the coefficient of friction of aluminum due to

the presence of graphene as a solid lubricant which promotes the formation of lubricious tribofilm on the surface, therefore, reduce the surface-to-surface contact. Results show that adding graphene in loadings as low as 0.5 wt.% can decrease COF significantly. The reduction in coefficient of friction of the Al/Gr composites with increased graphene content is generally expected from the self-lubricating composites. This conclusion is consistent with that of aluminum/graphite composites reported by many investigators [103, 113, 279, 280].

Although the addition of 0.5 wt.% of GNPs to the aluminum matrix decrease the composites' COF, but the loading is sufficient enough to let the solid lubricant be fully available at the contact surface. The higher weight percentage of GNP (2 and 3 wt.%) decreased the COF of the composite sample significantly in comparison with other samples. Generally, as the number of graphene nanoplatelets between the contacting surfaces increases, the COF decreases owing to the lubricating tendency of the graphene nanoplatelets available at the sliding interface.

In comparison between Al/GNPs composites and aluminum hybrid composites, it is obvious that the COF of Al/GNPs/Al$_2$O$_3$ composites is lower than Al/GNPs composites. The reason for enhanced COF of hybrid composites is the presence of alumina particles and their rolling effect.

The effect of load on the COF of aluminum and its various composites was shown in Figure 66. In unreinforced aluminum, results show that COF increases by increasing the load. Therefore, higher COF was observed at higher load. On the contrary, in Al/GNPs and Al/GNPs/Al$_2$O$_3$ composites, there is a minor decrease

151

in the COF at higher loads. The possible explanation for this phenomenon may lay down in the lubricating behavior of the reinforcement and the fact that higher wear releases more solid lubricant into the contact area. In another word, when the applied load is higher, initially a substantial wear is happening. Consequently, the higher volume of worn composites releases a higher amount of lubricating graphene and alumina onto the contact surface. Therefore, these released particles can form a protective tribofilm. In summary, at higher normal loads, more graphene is projecting out from the pin surface due to plowing between pin and disk. Consequently, the direct contact between surfaces of the sample and disk is decreased by the graphene layer and this ultimately decreased the wear and COF.
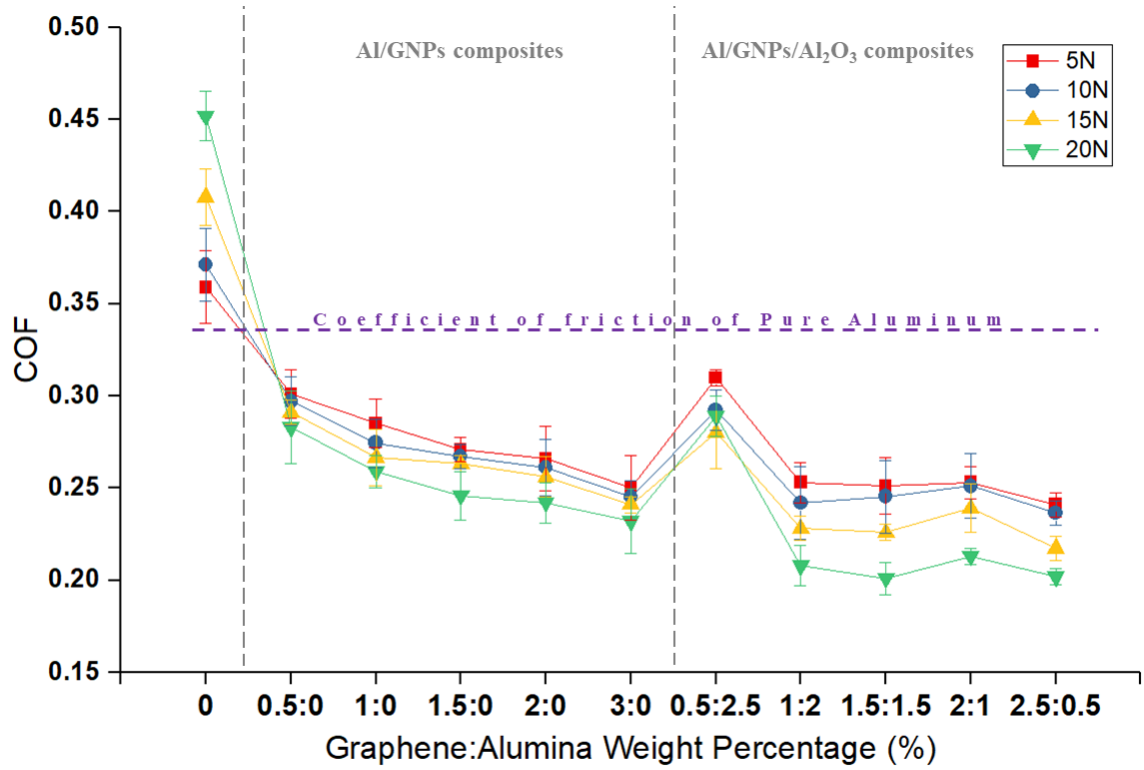
Figure 65 The variation of the COF for aluminum and its composites at different loads
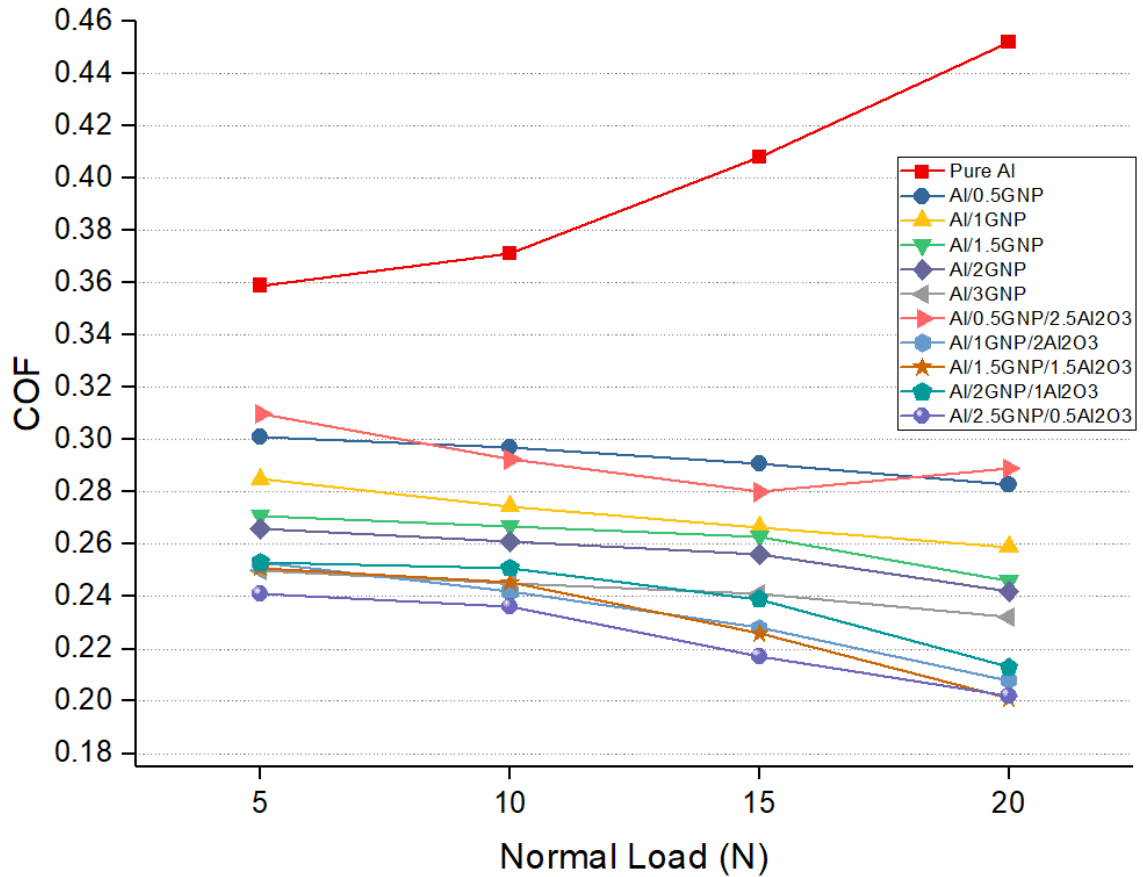
Figure 66 Effect of normal load on COF of various aluminum composites

2.4.3.2 Wear

Wear resistance of aluminum and its composites are reported in term of normalized wear rate where normalized wear rate is equal to volume loss divided by the sliding distance and applied normal load. Figure 67 shows the effect of particle types and the weight percentage of reinforcement on the wear rate. The wear rate of composites is lower than aluminum due to the presence of graphene and alumina embedded in aluminum. Consequently, the lifetime of the aluminum is significantly prolonged as the sliding surface is continuously supplied with lubricating particles.

154

The hardness of the material plays a key role to explain the wear behavior of materials. Generally, the softer the material is, the higher wear rates it has. Further, in the literature, it is well known that there is an inverse relation between wear rate and hardness of the materials. For this reason, Al/1GNPs and Al/1GNPs/2Al$_2$O$_3$ show the lowest wear rate among Al/GNPs and Al/GNPs/Al$_2$O$_3$, respectively compared to pure aluminum and other composites. According to Archard equation, the wear rate is inversely proportional to hardness. The sliding wear due to abrasion was given as:

$$V = \frac{kPL}{H}$$

where V is the volume loss, P is the applied load, L is the sliding distance, H is the hardness of the specimen, and k is the wear coefficient. Therefore, as it is expected from Archard equation, the wear rate decreases by graphene particles up to 1 wt.% graphene nanoplatelets due to increase in the hardness be embedding the graphene particles. Besides, the graphene nanoplatelets form a lubricant protective tribolayer on the worn surfaces, which consequently reduces the wear rate by lowering the real contact area between two mating surfaces. As seen earlier, adding more graphene above 1 wt.% has a negative effect on hardness possibly due to agglomeration, which in turn reduces wear resistance. In conclusion, under low GNPs contents up to 1 wt.%, the composites outperformed the pure aluminum; while the wear performance of the composite deteriorated at high GNPs contents of 3 wt.%. In addition, there is another effect of graphene nanoplatelets which improve the wear properties, and that is the ability of GNPs to play an important role in protecting the surface against oxygen and enhancing oxidation resistance.

155

In presence of oxygen, aluminum will oxidize on the surface and forms an oxide on the surface. This thin oxide layer can act as a third body abrasive.

If compare the wear rate of Al/GNPs composites with aluminum hybrid composites reinforced by graphene and alumina, it is obvious that the wear rate of self-lubricating aluminum hybrid composites is lower than Al/GNPs composites because the hardness of hybrid composites is higher than Al/GNPs and increase the ability of materials for less surface damage. For Al/GNPs and Al/GNPs/Al$_2$O$_3$ composites with the same weight percentage of graphene, hybrid aluminum composites have lower wear rate due to the synergetic effect of graphene and alumina. Alumina particles have two effects, 1) rolling effect and 2) compensating of wear surface. The alumina particles have a spherical shape that can roll between two surfaces and reduce the contact between surfaces. Alumina nanoparticles are hard particles and can act as a third abrasive party and make more wear on the surface and delamination of the graphene lubricant film. Thus, the optimum amount of alumina is required to reduce the wear rate. Therefore, less than optimum amount, there is not enough particles to roll between two surfaces and compensating the wear and more than the amount of optimum, more alumina particles present on the surface and can from a cluster of hard alumina particles and make more abrasive on the surface. Consequently, the optimum amount of alumina is 2 wt.% and aluminum composites reinforced with 1 wt.% graphene and 2 wt.% alumina where the wear rate has the lowest value of wear rate. The wear rates of aluminum composite reinforced by 1 wt.% graphene and 2 wt.% alumina (Al/1GNPs/2Al$_2$O$_3$) are 2.6, 1.4, 1.1 and 0.2 mm^3/N.m×10^{-5} in comparison with a wear rate of pure aluminum are 14.4, 15.7, 16.5 and 21.0 mm^3/N.m×10^{-5}, so, there

156

are 82%, 91%, 93% and 99% improvements of wear rate at 5N, 10N, 15N and 20N, respectively. By comparing the aluminum composite and hybrid composites, embedding 2 wt.% alumina nanoparticles in Al/GNPs can reduce the wear rate where the wear rate decreases from 9.3, 9.0, 5.6 and 4.2 mm³/N.m×10⁻⁵ for Al/GNPs to 2.6, 1.4, 1.1 and 0.2 mm³/N.m×10⁻⁵ for Al/1GNPs/2Al2O3 composites and there are 72%, 85%, 80% and 94% improvements of wear rate at 5N, 10N, 15N and 20N, respectively.

The effect of load on the wear rate of aluminum and its various composites was shown in Figure 68. The same trend of COF can be observed for wear rate where the wear rate of aluminum was increased by increasing the load while, on the contrary, the wear of composites including the Al/GNPs and Al/GNPs/Al$_2$O$_3$ decreases at higher load. The reason for lower wear at higher load is that more wear was occurred at starting of wear test and consequently, more graphene and alumina release onto the surface and these particles can form a protective tribofilm and therefore, the wear rate of composites reduces at higher load.
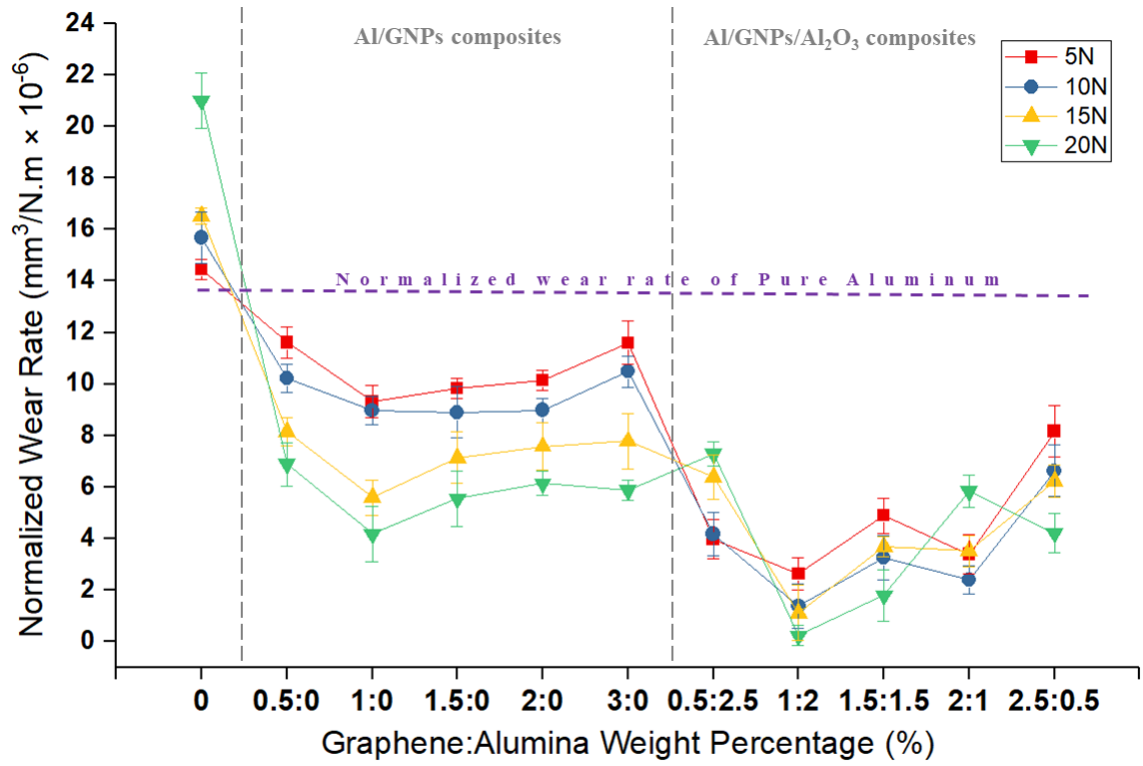
Figure 67 The variation of wear rate for aluminum and its composites at different loads
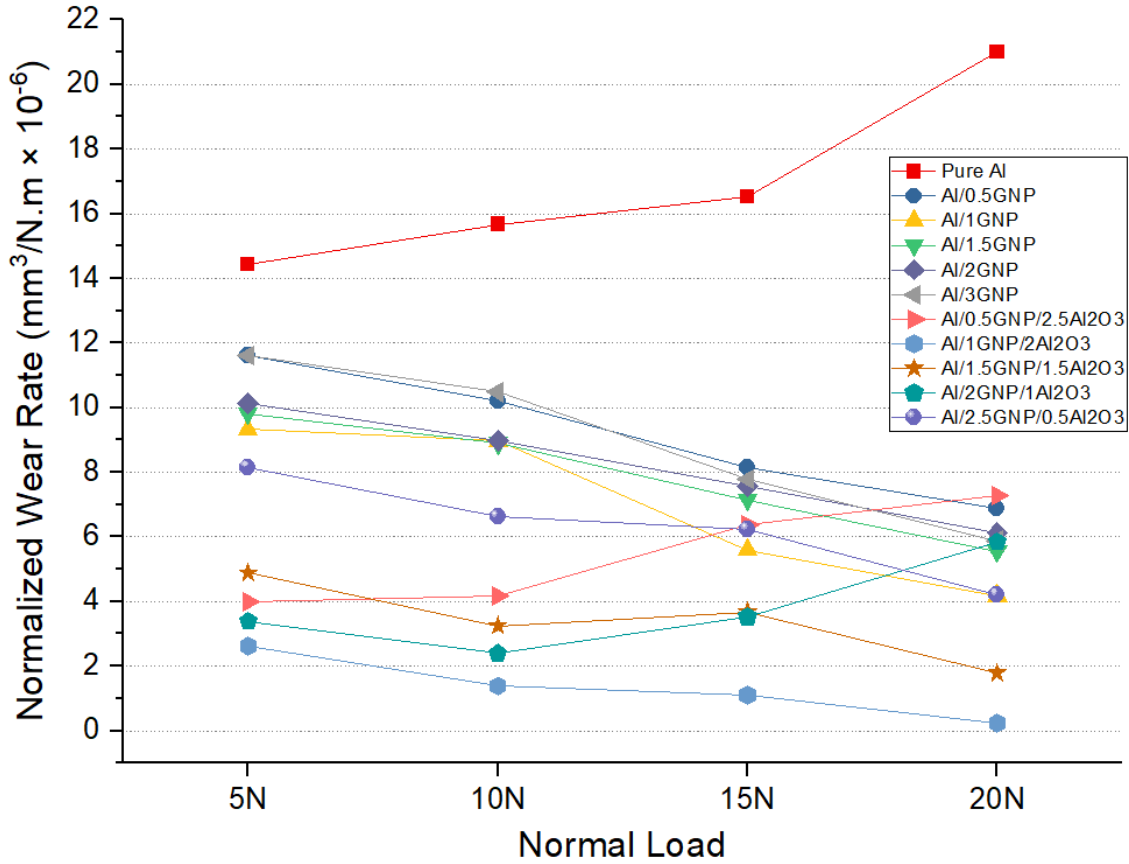
Figure 68 Effect of normal load on the wear rate of various aluminum composites

Figure 69 illustrate the relationship between COF, Wear rate and hardness at 15N with weight percentage of graphene nanoplatelets and alumina nanoparticles. Under low GNPs content up to 1 wt.%, there is a direct relationship between COF and wear rate. There is a sharp reduction in wear rate from 16.5 mm³/N.m×10⁻⁵ in pure aluminum to 5.6 mm³/N.m×10⁻⁵ in Al/1GNP while the COF reduced from 0.41 in pure aluminum to 0.27 in Al/1GNPs at 15N. The high GNPs composites in Al/3GNPs caused less friction between the stainless-steel disk and the Al/3GNPs composite surface, therefore, reduced the COF while the wear rate of composite increases. Meanwhile, the wear rate increment from 1 wt.% to 3 wt.% graphene is in line with the hardness reduction, from 90.1 HRB in Al/1GNPs to

84.5 HRB in Al/3GNPs. Therefore, the increased wear rate in Al/3GNPs is associated with its mechanical properties. It is believed that the low hardness of Al/3GNPs resulted in weak inter-granular strengths; therefore, more materials have been removed during the wear test, even though they have relatively low COF. Therefore, as shown in Figure 69, all samples are corresponding to an opposite relationship between wear rate and hardness.

160
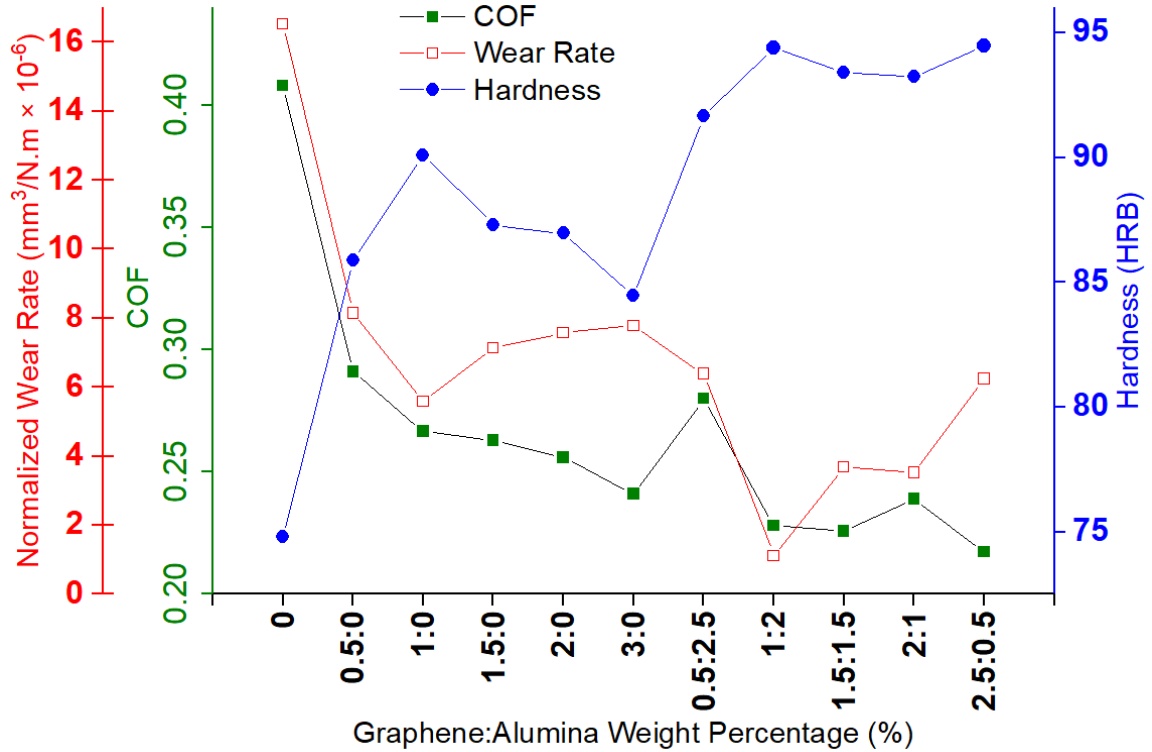
Figure 69 The relationship between COF, Wear rate, hardness and GNP content at

15N

2.4.3.3 Surface Studies

2.4.3.3.1   3D profilometry

An optical profilometer was employed to study the worn surfaces and measure surface roughness parameters of pure aluminum and composites' pins. Figure 70 - Figure 73 show three-dimensional images of worn surfaces of pure aluminum and its composites using an optical profilometer at different loads. Surface analysis show that adding reinforcement is effective to have smoother finished surfaced after tribotest. It is evident that the wear for aluminum is very severe where the wear track profile shows a typical body abrasion.

161

As discussed earlier, the wear rate of composites is less than pure aluminum possibly owes to its higher hardness. Therefore, it is expected to have less damage and wear on the surface, consequently, the surfaces of composites show narrower and shallower grooves. For example, for aluminum and its composites at 5N, the surface of aluminum (Figure 70a) is rougher than the surface of composites (Figure 70b-k). The wear of composites is mild abrasion while the surface of pure aluminum exhibits the severe abrasion.

Amongst the self-lubricating aluminum composites reinforced by GNPs nanoplatelets, the smoother surface belongs to aluminum reinforced by 1 wt.% GNPs (as shown earlier, the wear rate of Al/1GNPs is also lower than other Al/GNPs composites). Figure 71c which shows the worn surface of Al/1GNPs composite at 10 N applied load, is much smoother in comparison with the surface of all other Al/GNPs composites at the same applied load condition (Figure 71d-f).

If compare the worn surface of Al/GNPs with Al/GNPs/Al$_2$O$_3$ in Figure 70 - Figure 73, it is evident that surface of hybrid composites is smoother than Al/GNPs composites at the same applied load. This can be explained by the higher hardness of Al/GNPs/Al$_2$O$_3$ in comparison with Al/GNPs composites. For example, for composites with the same weight percentage of GNPs at 15N, the surface of Al/1GNPs (Figure 72c) is rougher than the surface of other Al/1GNPs/2Al$_2$O$_3$ composites (Figure 72h) and it is clearly shown that narrower and shallower grooves appear on the worn surface of hybrid composites. The smoother surface on the composites is also due to the fact that the major part of the applied load is carried by alumina nanoparticles which minimized the amount of plastic deformation and aid to the formation of lubricant film on the surface of

composites. In addition, there are interactions between dislocations and Al_2O_3 nanoparticles that ultimately resist the propagation of cracks during sliding wear. Moreover, the lubricant GNPs tribolayer can reduce the actual area of contact. These are the main reasons which lead to decrease in the wear rate of the composites containing GNPs and alumina phases.

If compare the worn surface of composites at different loads, it can be concluded that surface of composites is smoother at higher load. For example, for composites with 1 wt.% GNPs and 2 wt.% alumina, the worn surface at lower load (5 and 10N) as shown Figure 70(h) and Figure 71(h) is rougher than the surface of at higher load (15 and 20N) as illustrated in Figure 72(h) and Figure 73(h). Accordingly, less damage can be observed on the worn surface and less, narrower and shallower grooves are appeared on the surface at higher load. Therefore, wear rate at higher load indicates ultra-mild two-body abrasion while the mild two-body abrasion occurs at lower load.

Pure Aluminum

(a)

Al/GNPs

(b) **(c)** **(d)**

(e) **(f)**

Al/GNPs/Al₂O₃

(g) **(h)** **(i)**

(j) **(k)**
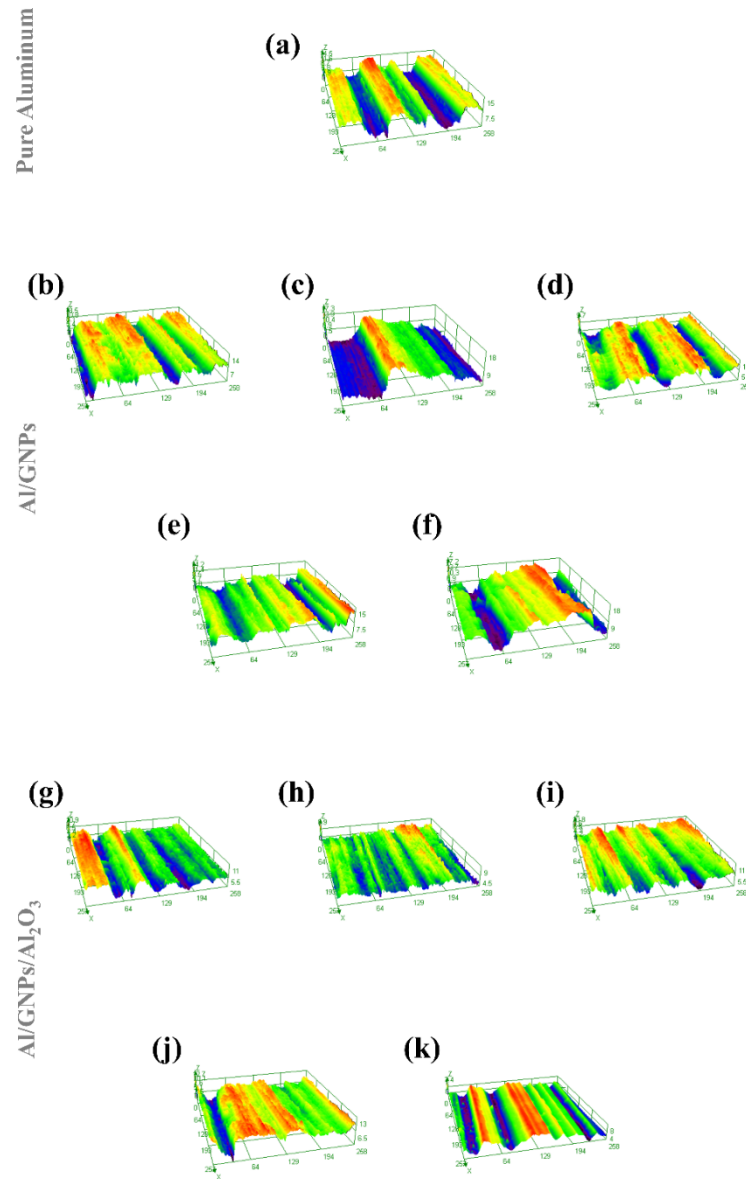
Figure 70 The 3D Optical profilometer images of worn surface of the pin at 5N for

a) pure aluminum, b) Al/0.5GNPs, c) Al/1GNPs, d) Al/1.5GNPs, e) Al/2GNPs, f)

Al/3GNPs, g) Al/0.5GNPs/2.5Al₂O₃, h) Al/1GNPs/2Al₂O₃, i) Al/1.5GNPs/1.5Al₂O₃, j)

Al/2GNPs/1Al₂O₃ and k) Al/2.5GNPs/0.5Al₂O₃

164

Pure Aluminum

(a)

Al/GNPs

(b)   (c)   (d)

(e)   (f)

Al/GNPs/Al$_2$O$_3$

(g)   (h)   (i)

(j)   (k)
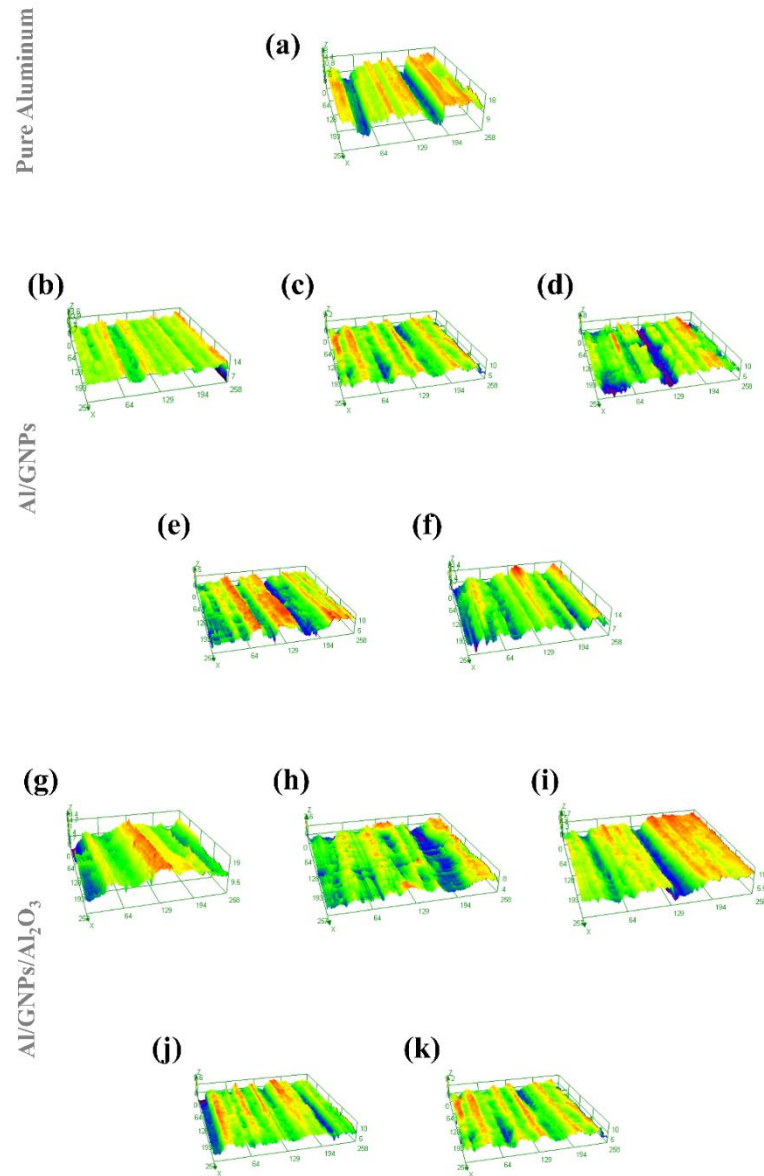
Figure 71 The 3D Optical profilometer images of worn surface of the pin at 10N for a) pure aluminum, b) Al/0.5GNPs, c) Al/1GNPs, d) Al/1.5GNPs, e) Al/2GNPs, f) Al/3GNPs, g) Al/0.5GNPs/2.5Al$_2$O$_3$, h) Al/1GNPs/2Al$_2$O$_3$, i) Al/1.5GNPs/1.5Al$_2$O$_3$, j) Al/2GNPs/1Al$_2$O$_3$ and k) Al/2.5GNPs/0.5Al$_2$O$_3$

165
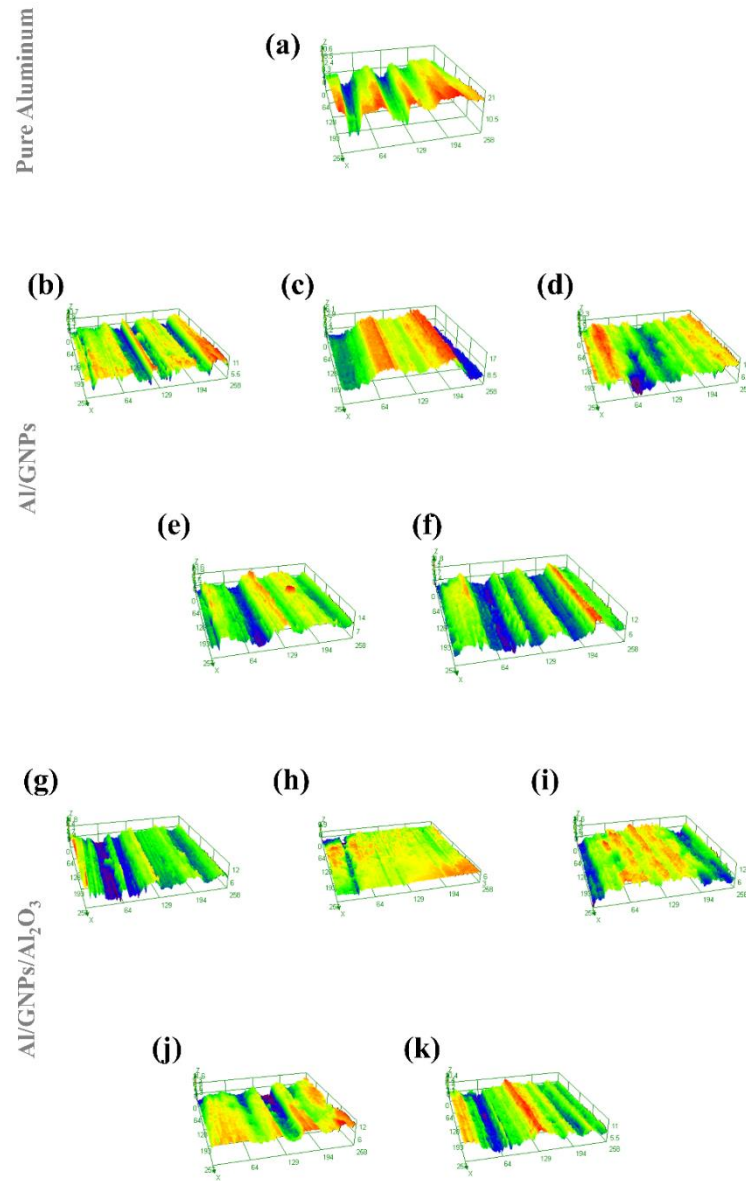
Figure 72 The 3D Optical profilometer images of worn surface of the pin at 15N for

a) pure aluminum, b) Al/0.5GNPs, c) Al/1GNPs, d) Al/1.5GNPs, e) Al/2GNPs, f)

Al/3GNPs, g) Al/0.5GNPs/2.5Al$_2$O$_3$, h) Al/1GNPs/2Al$_2$O$_3$, i) Al/1.5GNPs/1.5Al$_2$O$_3$, j)

Al/2GNPs/1Al$_2$O$_3$ and k) Al/2.5GNPs/0.5Al$_2$O$_3$
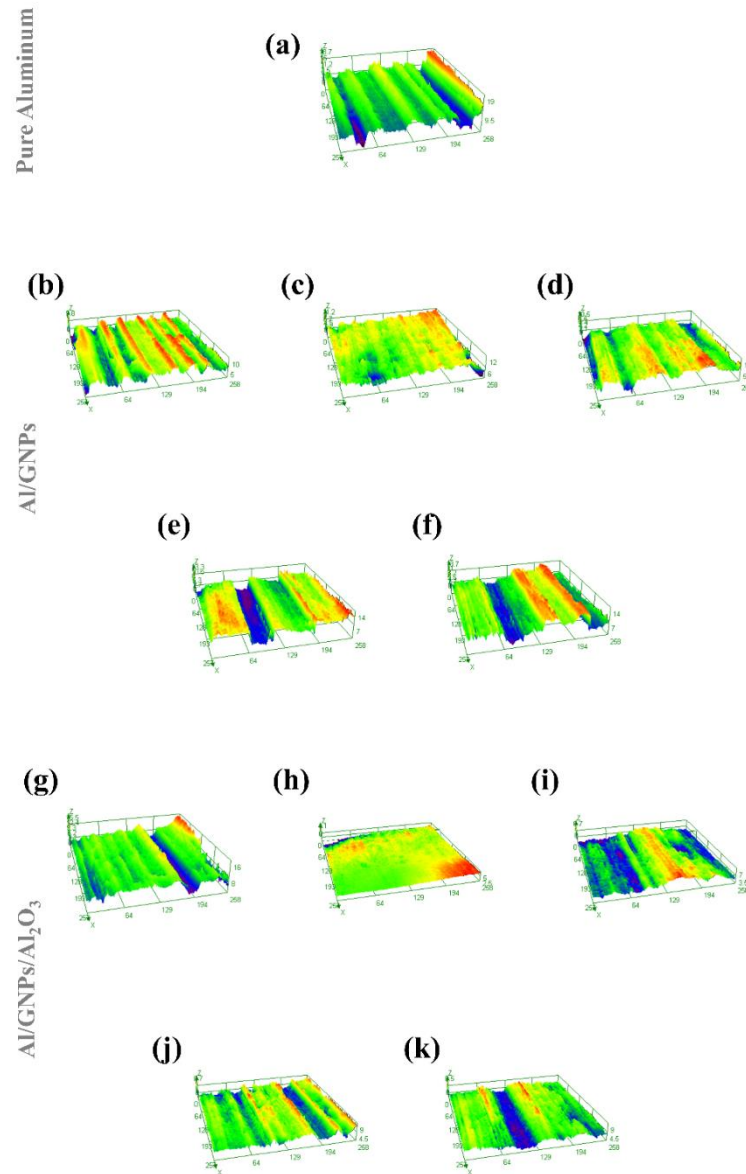
Figure 73 The 3D Optical profilometer images of worn surface of the pin at 20N for a) pure aluminum, b) Al/0.5GNPs, c) Al/1GNPs, d) Al/1.5GNPs, e) Al/2GNPs, f) Al/3GNPs, g) Al/0.5GNPs/2.5Al₂O₃, h) Al/1GNPs/2Al₂O₃, i) Al/1.5GNPs/1.5Al₂O₃, j) Al/2GNPs/1Al₂O₃ and k) Al/2.5GNPs/0.5Al₂O₃

Figure 74 shows the correlation of surface roughness (S_a) of worn surfaces of pure aluminum and self-lubricating composites pins at different loads. The

surface roughness of pins after test can confirm the results of wear rate. By comparing the roughness number of pure aluminum composites, it is obvious that embedding the GNPs and alumina as a reinforcement are effective to enhance the wear rate and have smoother finished surface. In addition, the surface roughness of hybrid composites is less than surface roughness of Al/GNPs composites where the wear rate of composites is less than wear rate of Al/GNPs (Figure 67) as discussed. In general, it can be found that the worn surface of pure aluminum is rougher with many thick and deep grooves while the worn surfaces of composites is comparably smoother, and the grooves are shallower. Besides, aluminum hybrid self-lubricating composites has less and shallow grooves in comparison with Al/GNPs composites. Figure 75 illustrate the relationship between Wear rate and surface roughness at 15N with weight percentage of GNPs nanoplatelets and alumina nanoparticles. There is a direct relationship between S_a and wear rate and a sharp reduction in wear rate and Sa by adding 0.5 wt.% GNPs. Moreover, the surface roughness increment from 1 wt.% to 3 wt.% GNPs is in line with the increasing wear rate. Therefore, all composite samples are corresponding to a direct relationship between wear rate and surface roughness.
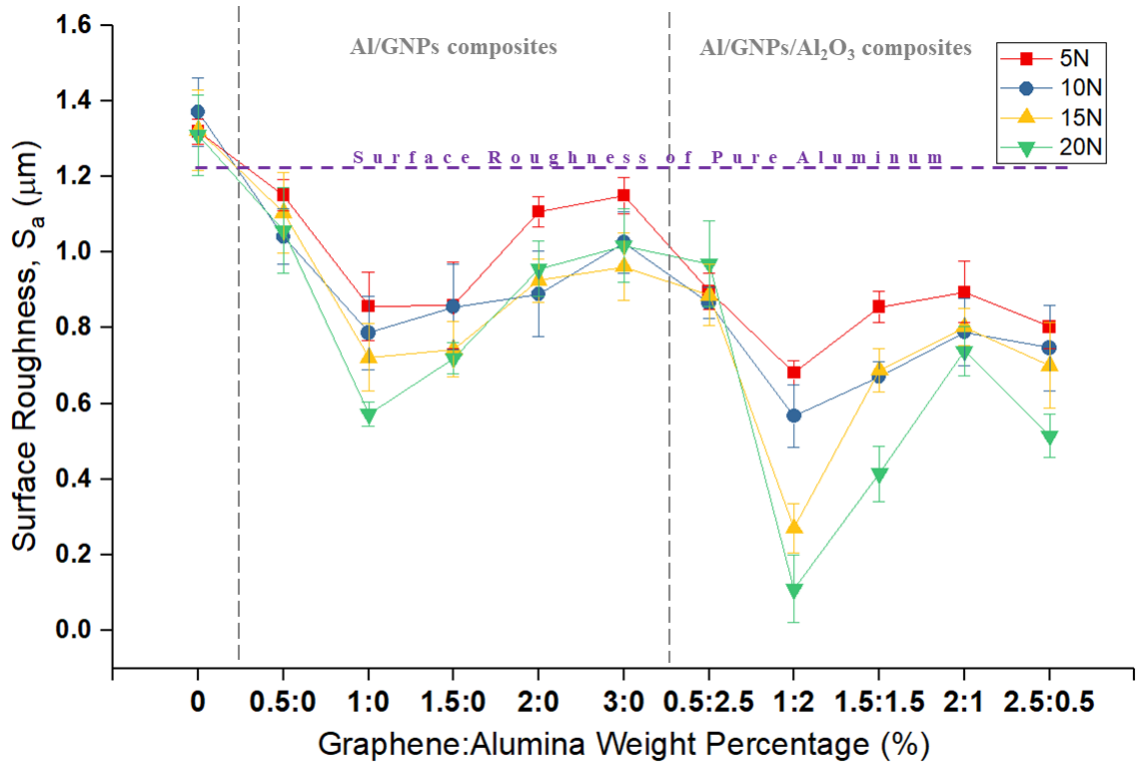
Figure 74 The surface roughness of worn surfaces of aluminum and its composites at different loads
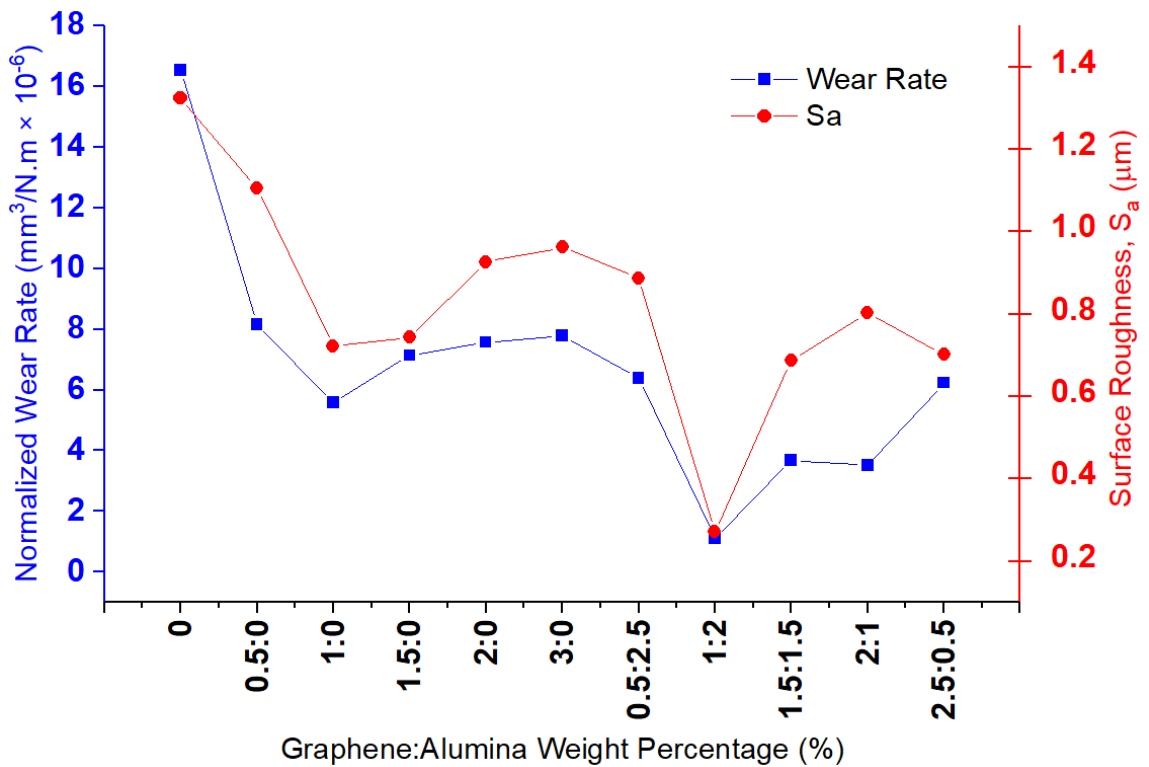
Figure 75 The relationship between Wear rate, surface roughness (S_a) and reinforcement content at 15N

2.4.3.3.2   SEM/EDS

The SEM/EDX was employed to study the worn surface and find its composition. Figure 76 - Figure 79 exhibit the SEM image of worn surface for various composites at different loads. By comparing the worn surface of pure aluminum and its composites, it is evident that more damages and delamination on the surface of pure aluminum appears where surface of composites have less number of grooves and debris. In addition, the grooves are narrower and shallower and the size of debris on the surface of composites is smaller. By comparing the Al/GNPs and Al/GNPs/Al$_2$O$_3$, the surface of hybrid composites reinforced by GNPs and alumina shows smoother surface and less debris. If compare Figure 76 - Figure 79 (b) with Figure 76 - Figure 79 (d), it can be concluded that the grooves become narrower and shallower on the worn surface of hybrid self-lubricating composites. Generally, the surface texture of worn surface can confirm the wear rate results where wear rate of aluminum is higher than its composites because of more damage and wear on the surface. Also, hybrid composites have better wear properties because of narrower and shallower grooves and less damages on the surfaces of hybrid composites in comparison with Al/GNPs composites. The surface of composites shows the trace of GNPs on the worn surfaces. In addition, SEM images also shows bigger clusters of GNPs sheets along the wear track at higher volume fraction of GNPs embedded into the composites.

170
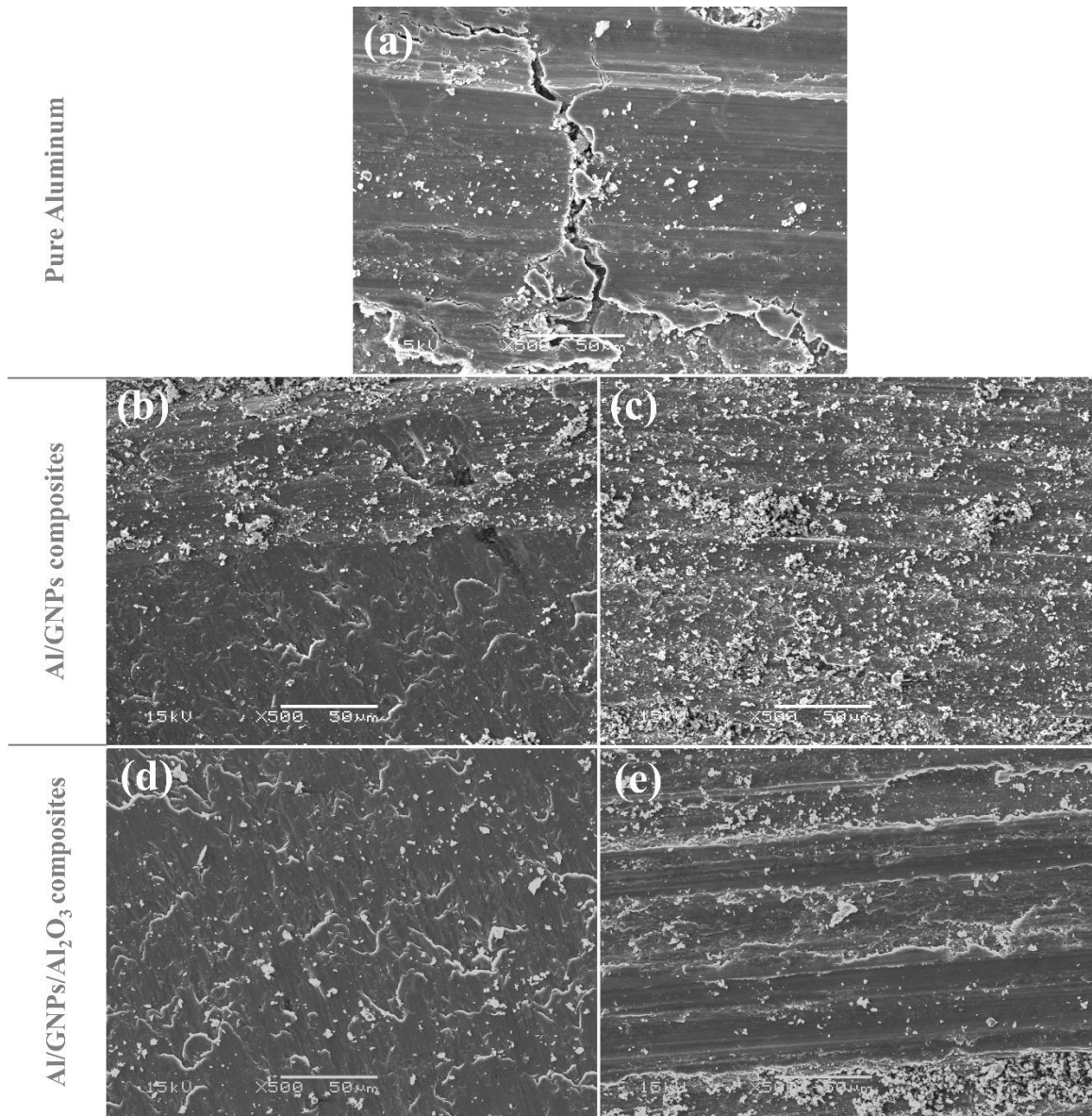
Figure 76 Scanning electron micrographs of worn pin surfaces at 5N for a) pure aluminum, b) Al/1GNPs, c) Al/3GNPs, d) Al/1GNPs/2Al₂O₃ and e) Al/2GNPs/1Al₂O₃

Pure Aluminum

Al/GNPs composites

Al/GNPs/Al$_2$O$_3$ composites
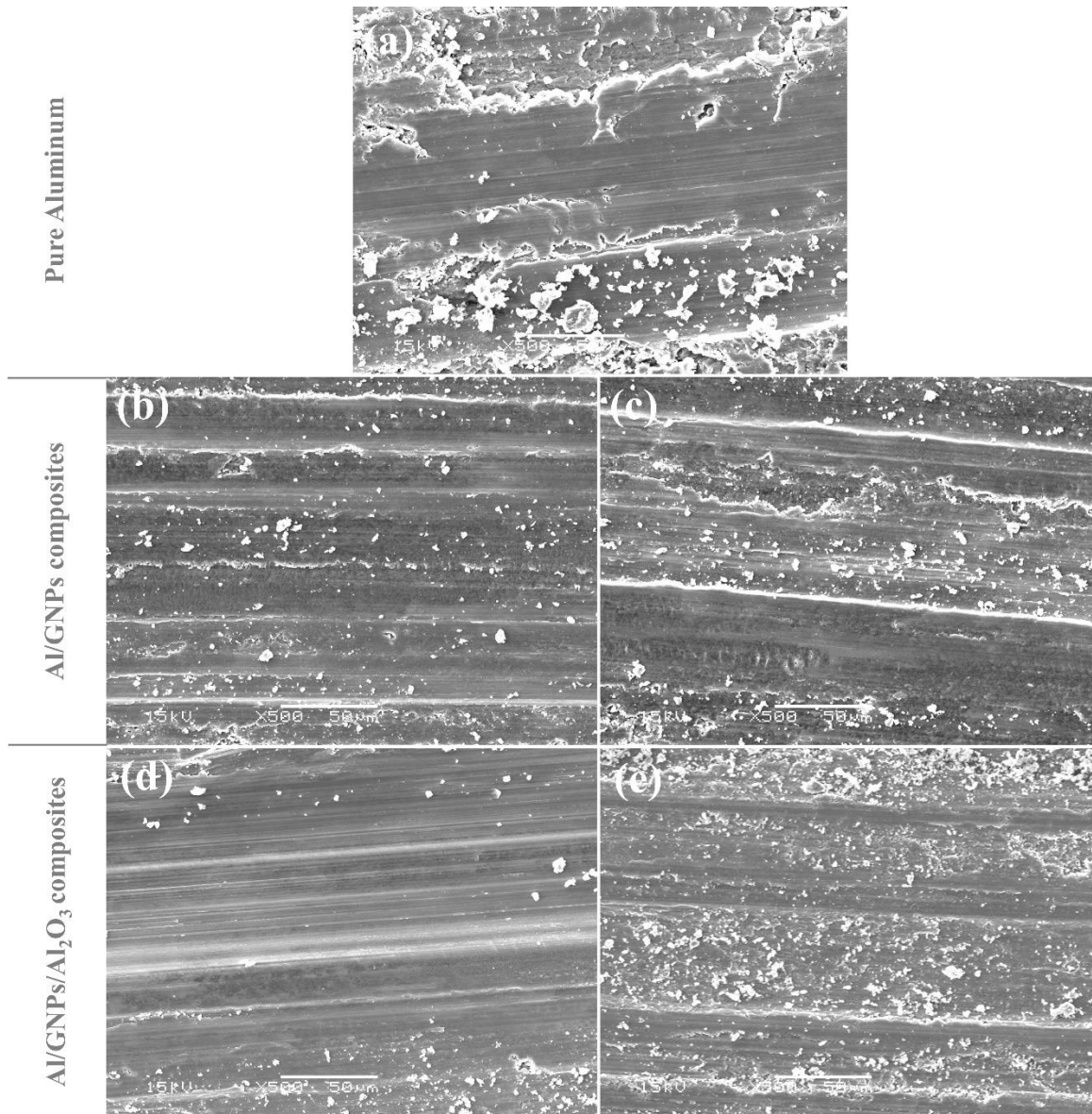
Figure 77 Scanning electron micrographs of worn pin surfaces at 10N for a) pure aluminum, b) Al/1GNPs, c) Al/3GNPs, d) Al/1GNPs/2Al$_2$O$_3$ and e) Al/2GNPs/1Al$_2$O$_3$
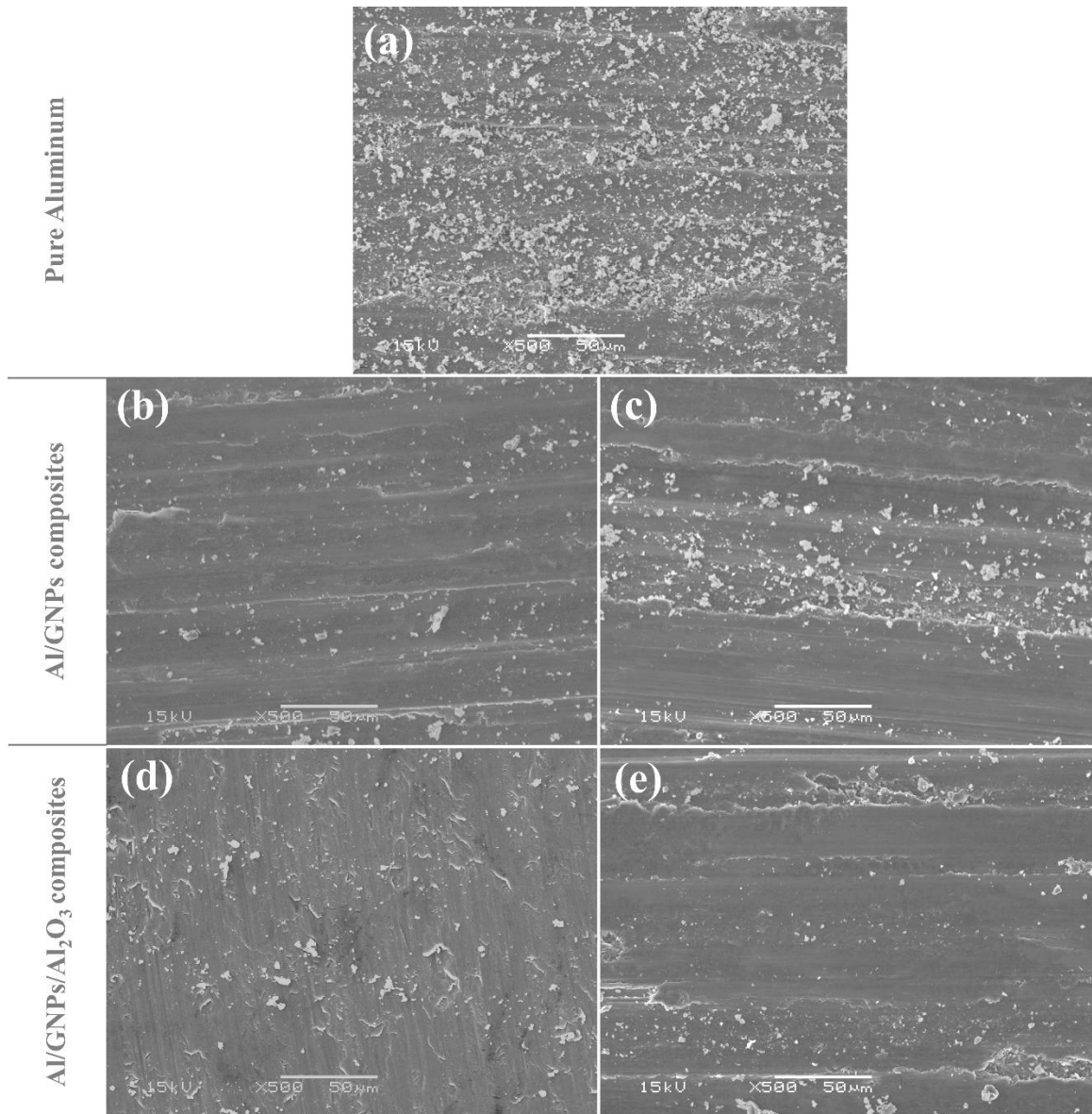
Figure 78 Scanning electron micrographs of worn pin surfaces at 15N for a) pure aluminum, b) Al/1GNPs, c) Al/3GNPs, d) Al/1GNPs/2Al₂O₃ and e) Al/2GNPs/1Al₂O₃
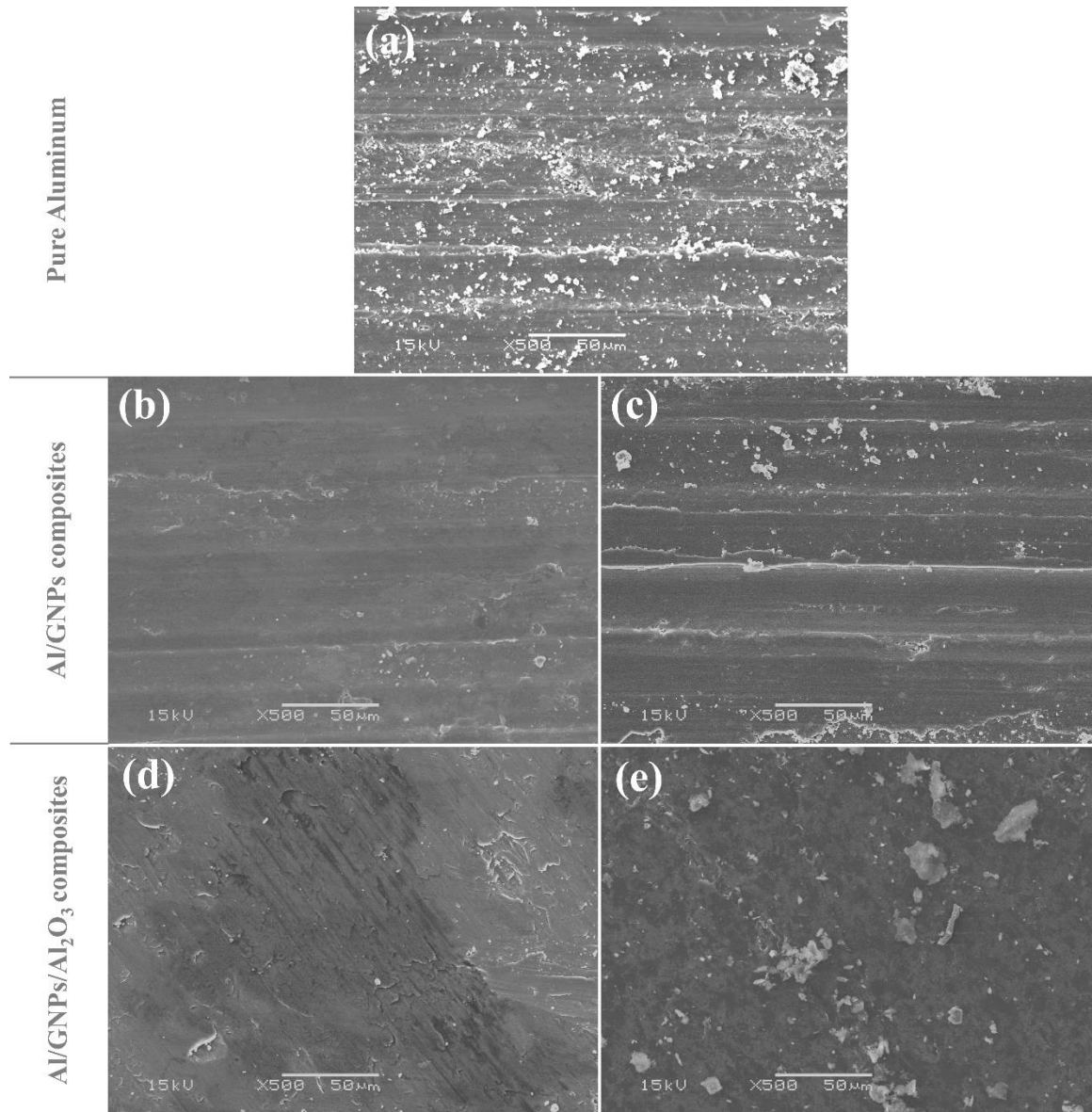
Figure 79 Scanning electron micrographs of worn pin surfaces at 20N for a) pure aluminum, b) Al/1GNPs, c) Al/3GNPs, d) Al/1GNPs/2Al₂O₃ and e) Al/2GNPs/1Al₂O₃

The worn surfaces have parallel grooves in the direction of sliding with varying groove width and depth that depend on several factors such as the normal load. The texture of the worn surfaces clearly depicts the load-dependent wear behavior in pure aluminum samples. As the applied load increased, the wear track became wider. Moreover, the lower applied loads (5 and 10N) produced relatively

smoother wear track surfaces (Figure 76a and Figure 77a), with hardly any grains being pulled-out. However, the 15N applied load caused a larger area of grain pull-out (Figure 78a), and the 20N load led to even severe damage to the wear surfaces, with traces of wear groves and large debris on the surface (Figure 79a). Such aluminum grain pull-outs under different applied loads produced a large amount of wear debris which in turn resulted in abrasive sliding wear. These types of grooves which show on the worn surfaces are due to abrasive wear during sliding conditions.

Figure 80 can exhibit the effect of load on the worn surface of Al/1GNPs and Al/1GNPs/2Al$_2$O$_3$ composites which are entirely dissimilar to the wear tracks of pure aluminum. by comparing the SEM images from top to bottom as shown increasing the normal load, it can be concluded that the worn surface of composites shows a smoother surface with fewer grooves and debris. It is confirmed the results of wear rate where wear rate of composites at higher load decreases by increasing the load.

Al/1GNPs Composites   **Al/1GNPs/2Al₂O₃ Composites**

5N

10N

15N

20N
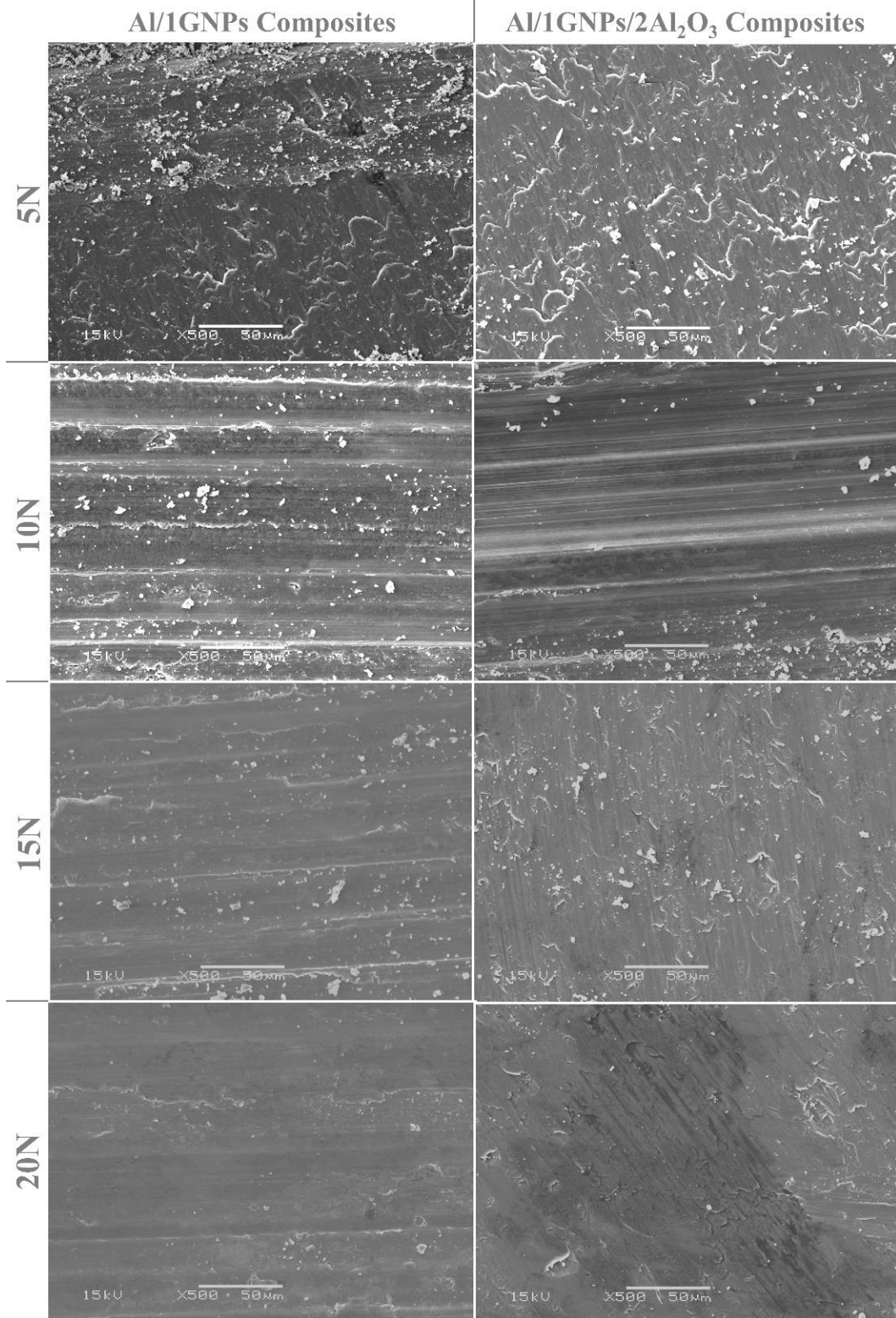
Figure 80 Effect of load on the worn surface of composites

As shown in SEM images, darker regions can be distinguished on the worn surfaces of composites. This confirms the presence of carbon sheets at least partly covering the surface. This appearance is very similar to SEM images from a tribological study on GNPs reinforced aluminum surfaces. To confirm that black regions are carbon-rich, EDX was conducted. Figure 81 shows the surface texture and surface composition of pure aluminum at different loads. The surface composition of the worn surface shows the trace of Fe and Cr that can be transferred from steel disk during contact between two surfaces of pins and disk. Majority of the surface is covered by aluminum and oxygen because the temperature goes up during the dry wear test and oxidation occur and the surface of the pin is aluminum oxide. If compare the composition of pure aluminum with Al/GNPs composites (Figure 82), the significant difference is the presence of carbon on the surface that comes from GNPs embedded into aluminum. The chemical composition of the worn surface of Al/GNPs was shown in Figure 82. As it is expected, carbon can be found on the surface of composites. therefore, it can be concluded that a layer of carbon is formed on the surface and this lubricant tribolayer can improve the friction and wear properties by reducing the contact between surfaces and forming a solid lubricant film on the surface. In addition, the surface of composites has less amount of Fe and Cr and it can be expressed that less transfer of Fe and Cr to the surface of pin happened. Hence, it is evident that contact between pin and disk reduces after forming the lubricant GNPs layer because of less transfer of Fe and Cr to the surface of composites pins.

In addition, there is another effect of GNPs nanoplatelets can be observed on the EDX results by reducing the amount of oxygen on the worn surface if

177

compare the O-content of pure aluminum with Al/GNPs (Figure 81 and Figure 82). It is confirmed the claim that GNPs prevent the oxygen diffusion in the surface and GNPs enhance oxidation resistance because in presence of oxygen alumina compound on the surface form and this brittle alumina compound can break and have more failure and make more debris that act as a third body abrasive and then increase the wear as well. Therefore, GNPs can reduce oxidation on the surface.

178
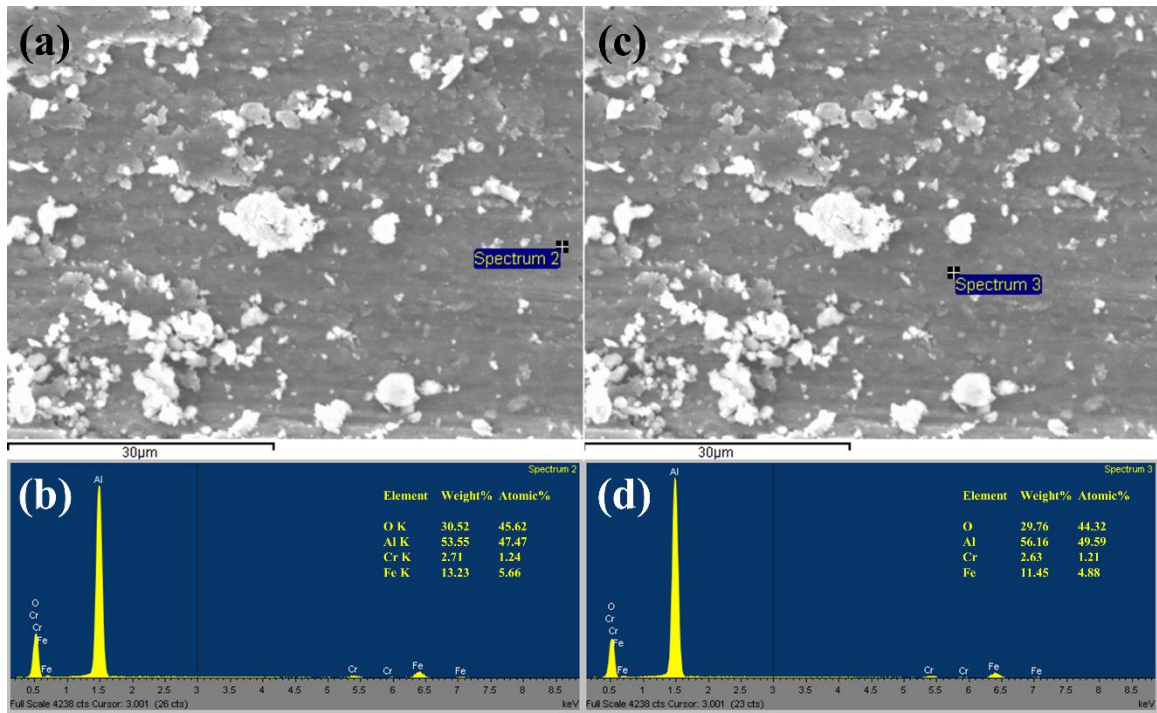
Figure 81 SEM/EDX of worn surface of pure aluminum at 15N
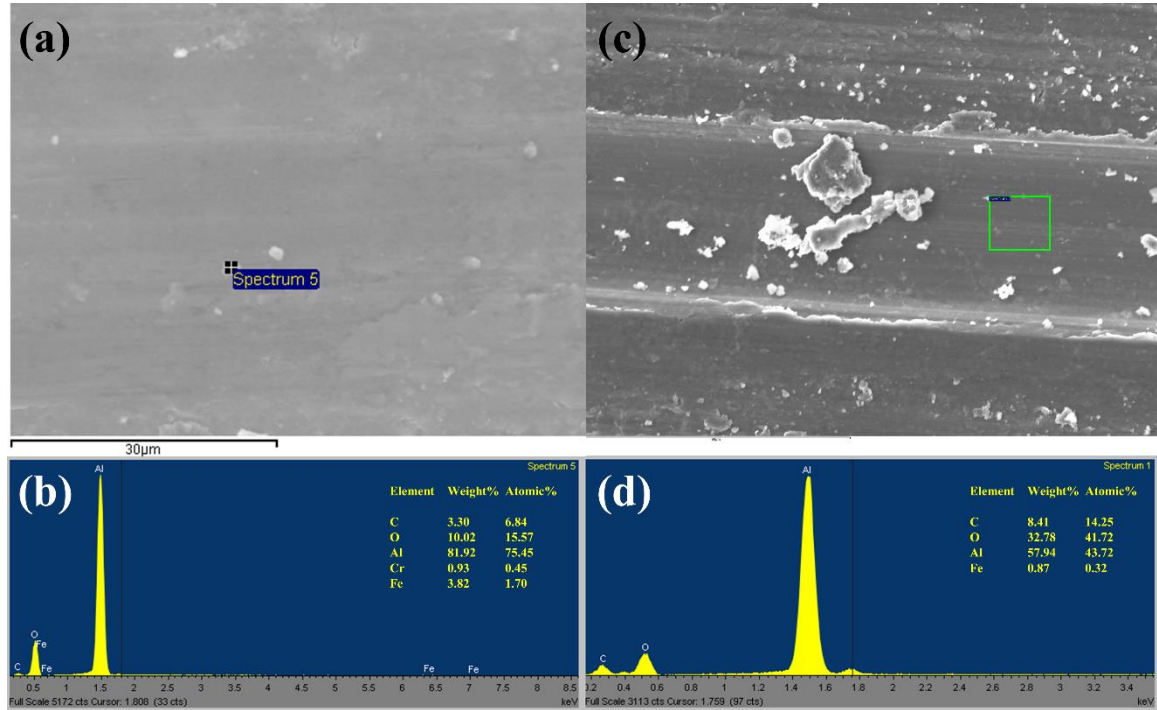
Figure 82 SEM/EDX of worn surface of a,b) Al/1GNPs and c,d) Al/3GNPs at 15N

179

On the surface of pure aluminum and composites, debris can be found. The big differences between the debris on the surface of pure aluminum and composites are size, volume fraction and composition. The characterization of debris is compared in Figure 83. It can be concluded that more area of the worn surface is covered by debris for pure aluminum in comparison with Al/3GNPs. Therefore, this debris act as a third body abrasive particles and higher wear and damage happen on the surface. Besides, the composition of debris for Al/3GNPs shows the trace of carbon on the debris. Therefore, the debris is self-lubricating composites and cause less wear.
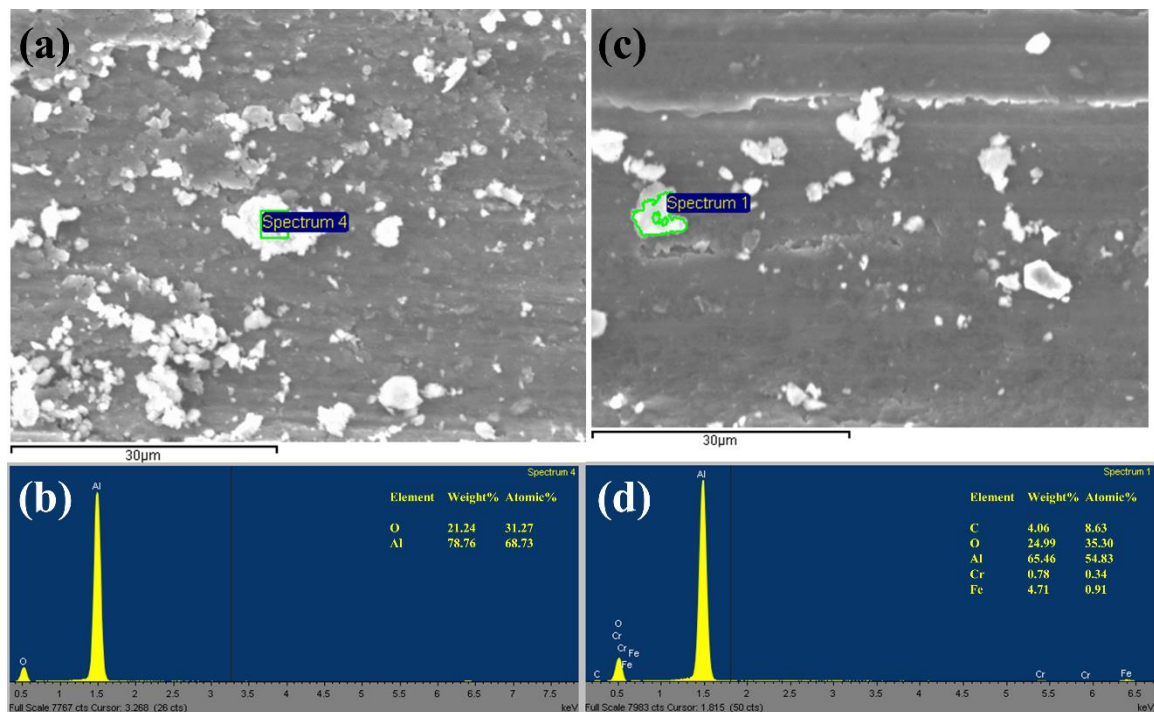
Figure 83 SEM/EDX of debris of a,b) pure aluminum and c,d) Al/3GNPs at 15N

Increasing carbon-content decreases wear rates, especially when higher hardness and lower porosity associated with a finer microstructure. It is suggested that the segregation and clumping of GNPs within the aluminum matrices resulted

180

in the release of the non-uniform GNPs thick tribofilms on the aluminum matrices. Such films were easily delaminated between the rubbing surfaces, which was evident in Figure 84 - Figure 87. As mentioned earlier, several black spots on the worn surfaces appeared on the surface of composites. It is expected to be GNPs particles that deposited on the worn surface and form lubricant film to improve the tribological properties by preventing surface-to-surface contact. Figure 84 - Figure 87 depicts SEM image and elemental mapping for the worn surfaces of selected composites at 10N. the EDX results show a trace of high weight percentage of carbon and confirm that a thick tribofilm of GNPs on the surface.

In addition, the SEM image and elemental mapping of worn surface shows that the more area of worn surface covered by GNPs tribolayer and have better distribution at higher weight percentage of GNPs of composites if compare Figure 84 and Figure 85 as the worn surface of Al/1GNPs and Al/3GNPs, respectively, where the worn surface of Al/3GNPs covers by more GNPs tribolayer. Therefore, the COF of Al/3GNPs is less than Al/1GNPs because of less contact between surface in Al/3GNPs covered by GNPs as shown in Figure 85.
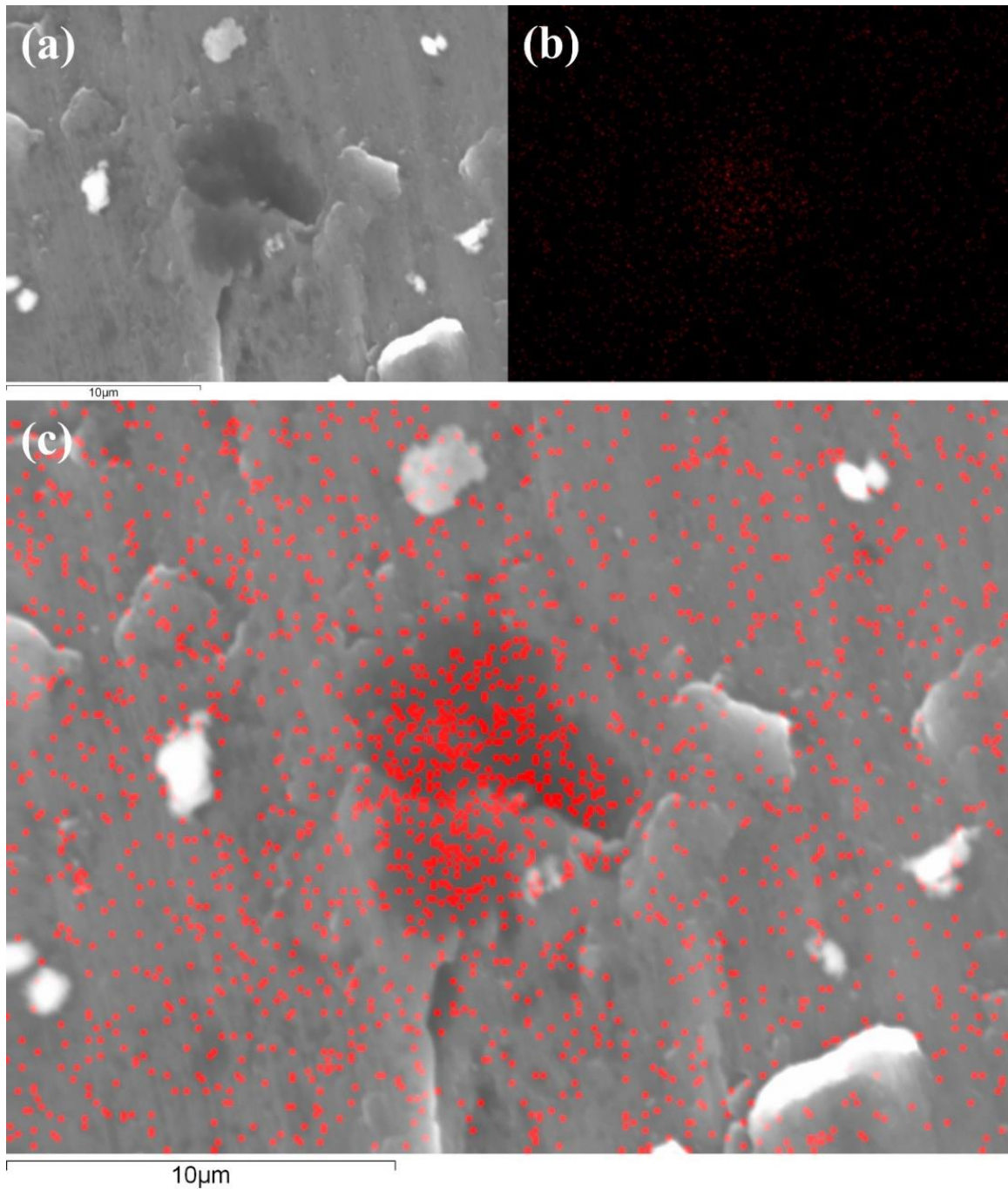
Figure 84 SEM image and elemental mapping for the worn surfaces of

Al/1GNPs at 10N using EDX at 1000X
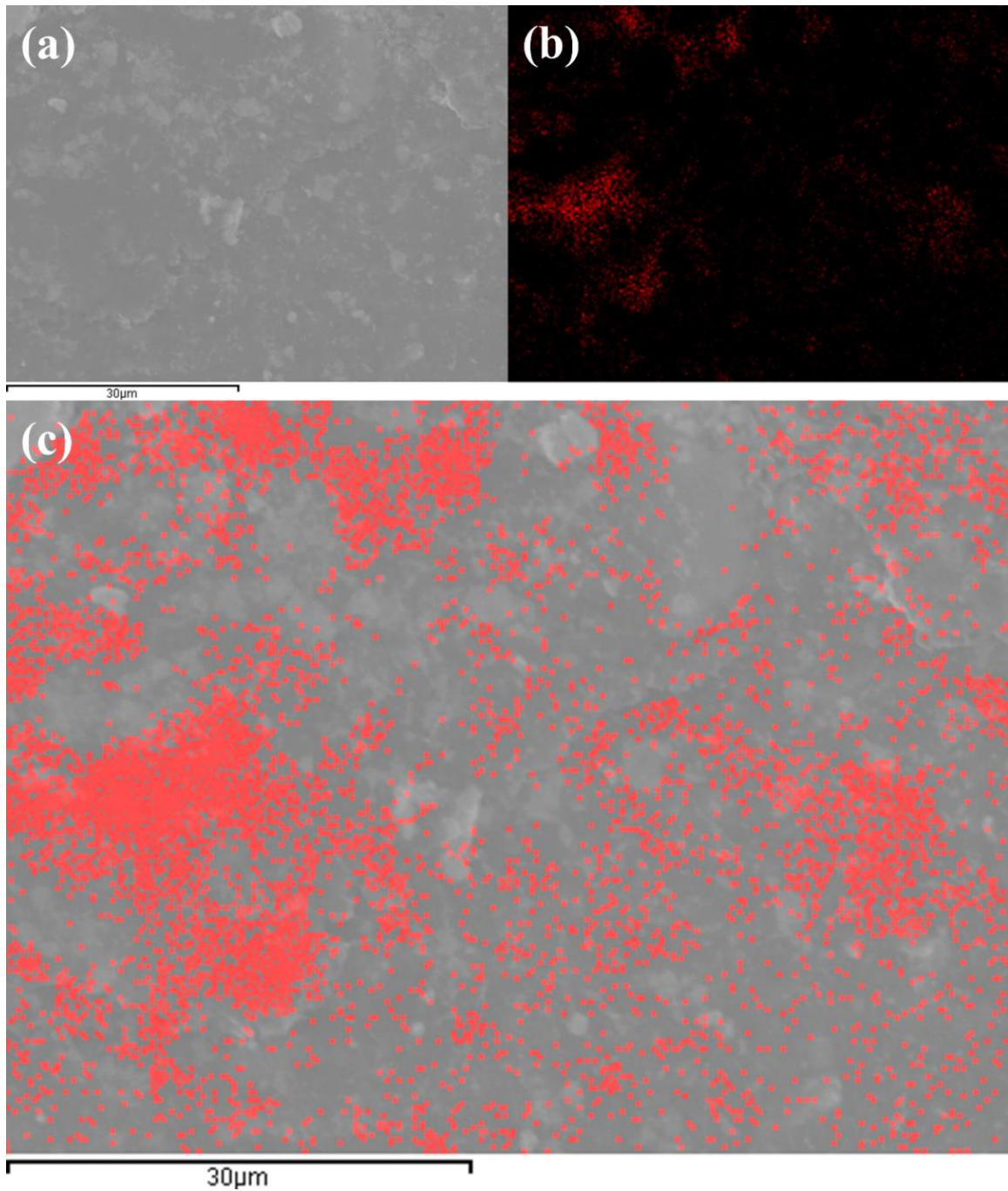
Figure 85 SEM image and elemental mapping for the worn surfaces of

Al/3GNPs at 10N using EDX at 1000X
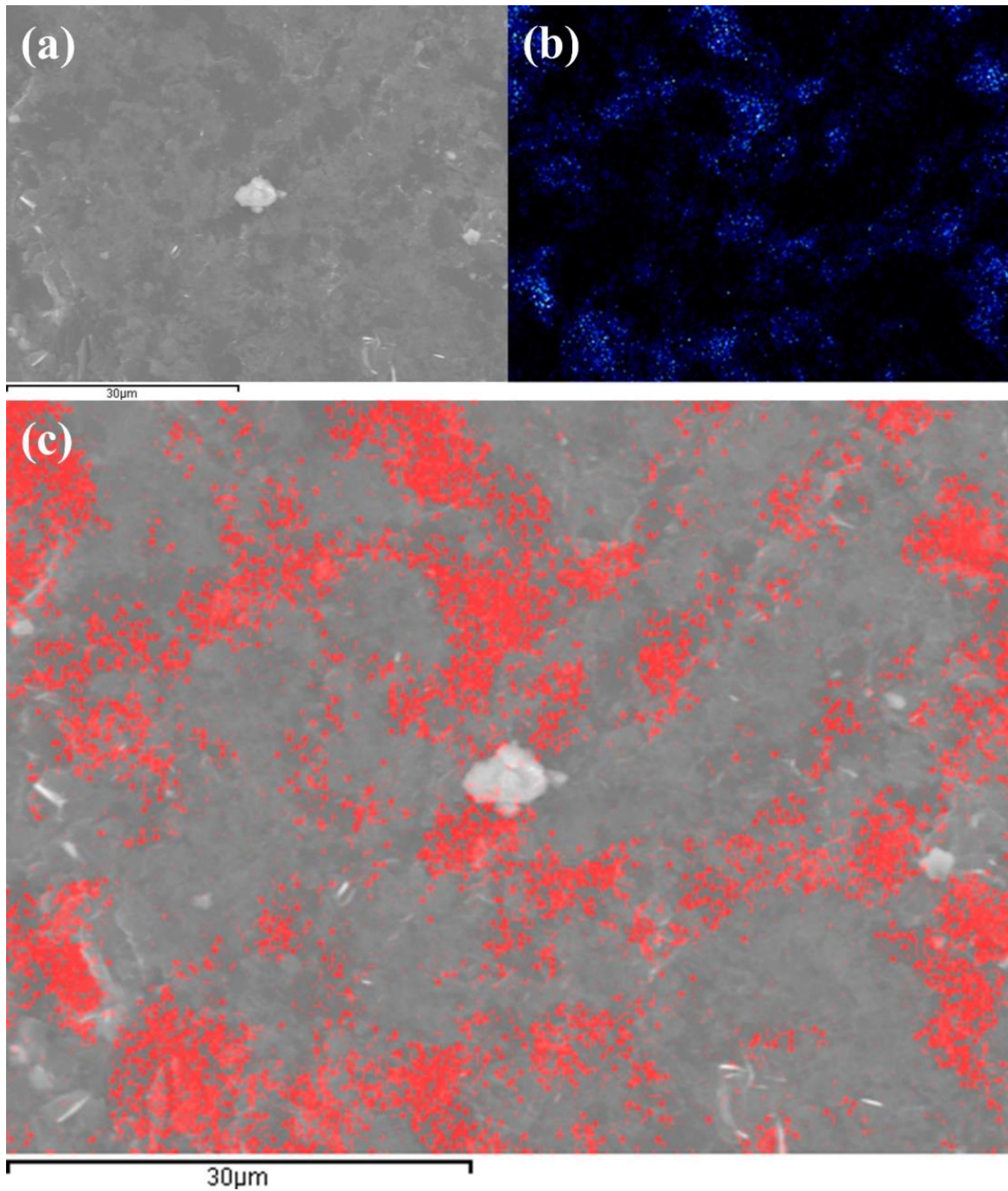
Figure 86 SEM image and elemental mapping for the worn surfaces of

Al/1GNPs/2Al$_2$O$_3$ at 10N using EDX at 1000X
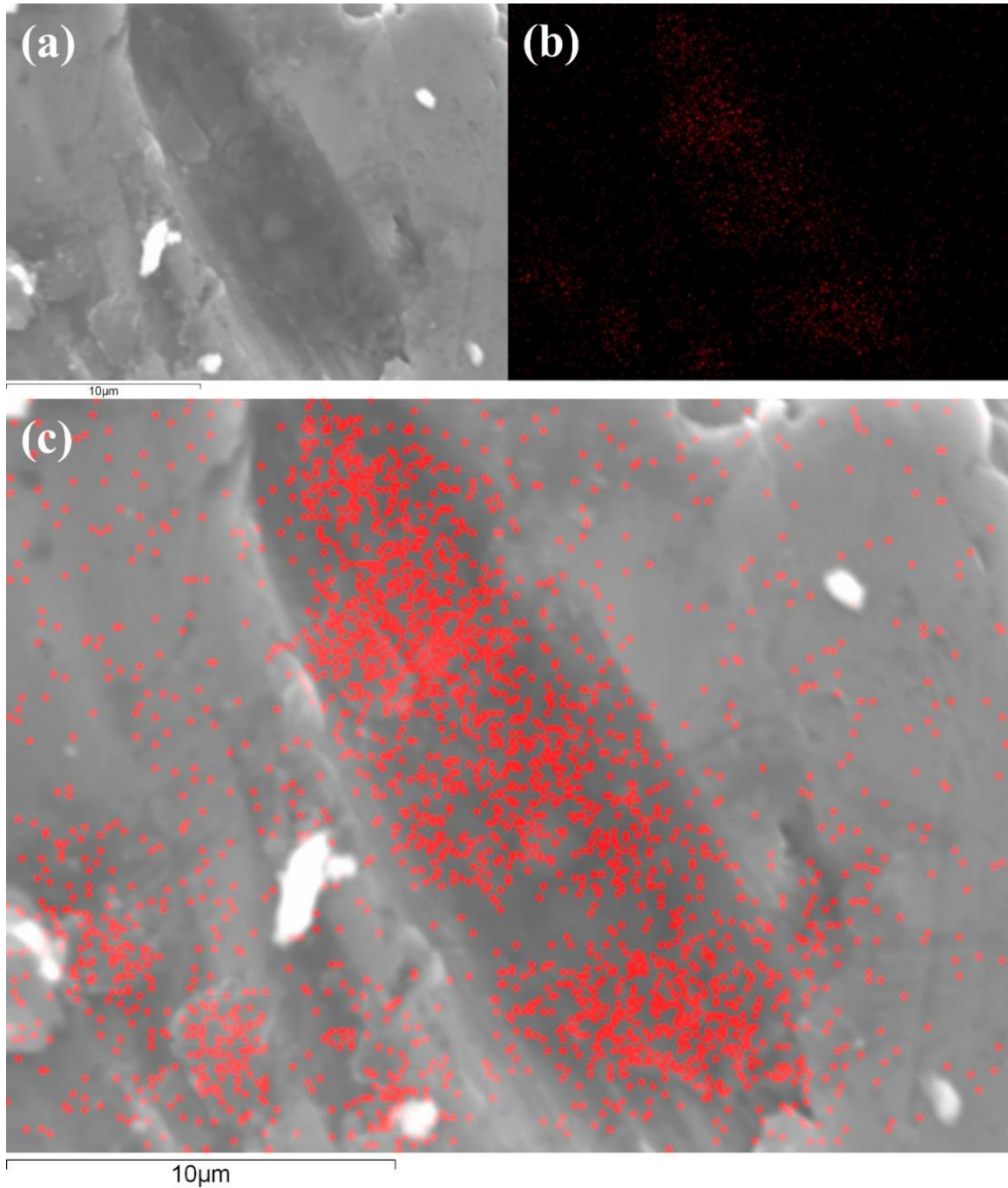
Figure 87 SEM image and elemental mapping for the worn surfaces of Al/2GNPs/1Al$_2$O$_3$ at 10N using EDX at 1000X

SEM/EDX analysis of worn surface at higher load at higher magnification (Figure 88 and Figure 89) shows that because of high applied load, more contact

between surfaces is expected and therefore more wear occurs and as shown in Figure 88 and Figure 89 at beneath of surface GNPs exist and more wear can release more GNPs on the surface and cover majority of worn surface and consequently, reduce the real contact area and improve friction and wear properties of composites. the elemental mapping studies show that into delamination caused by wear, GNPs appear and can reduce the contact between surface or release and form a lubricant tribolayer.
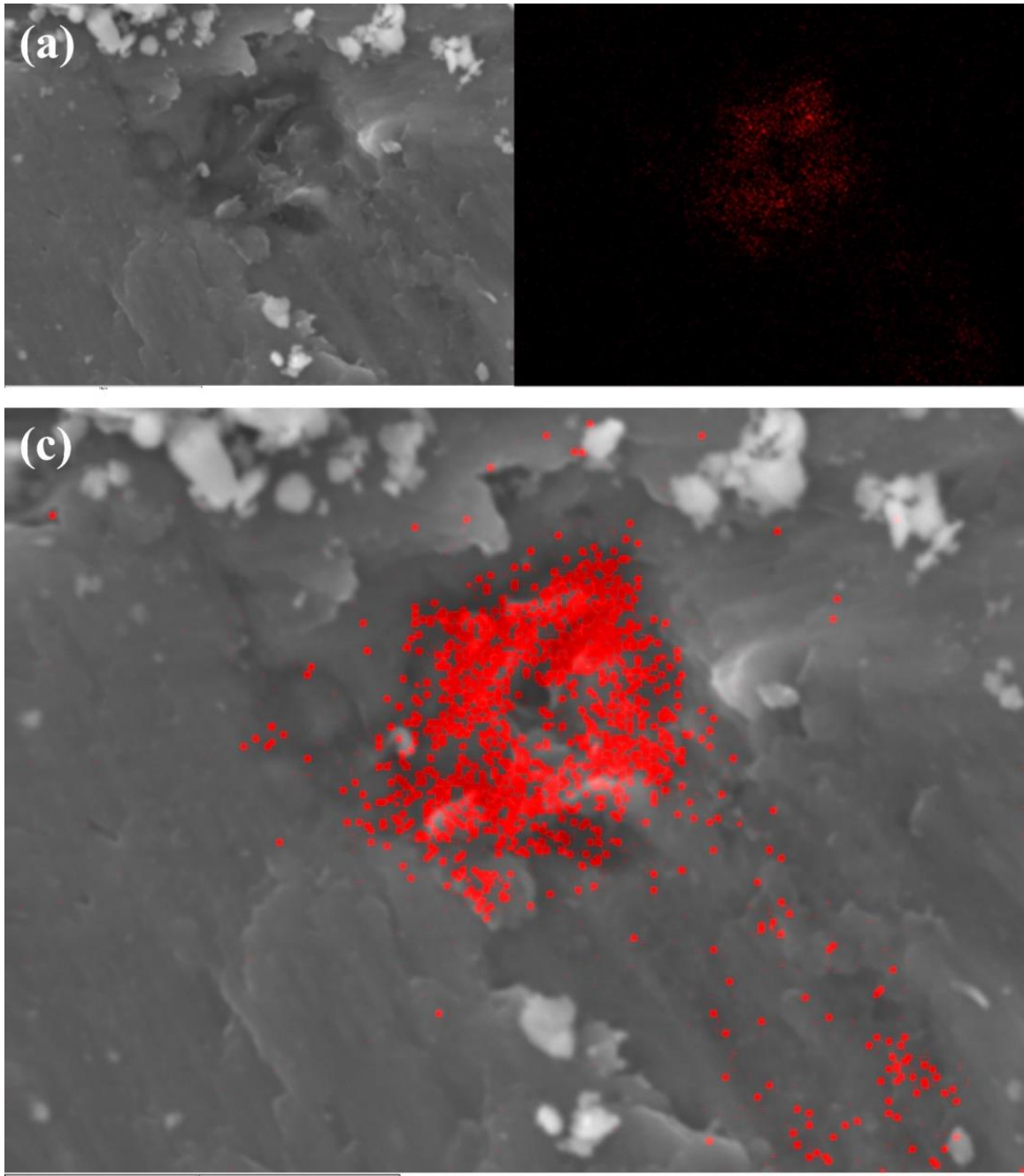
Figure 88 SEM image and elemental mapping for the worn surfaces of Al/3GNPs at 20N using EDX at 1000X
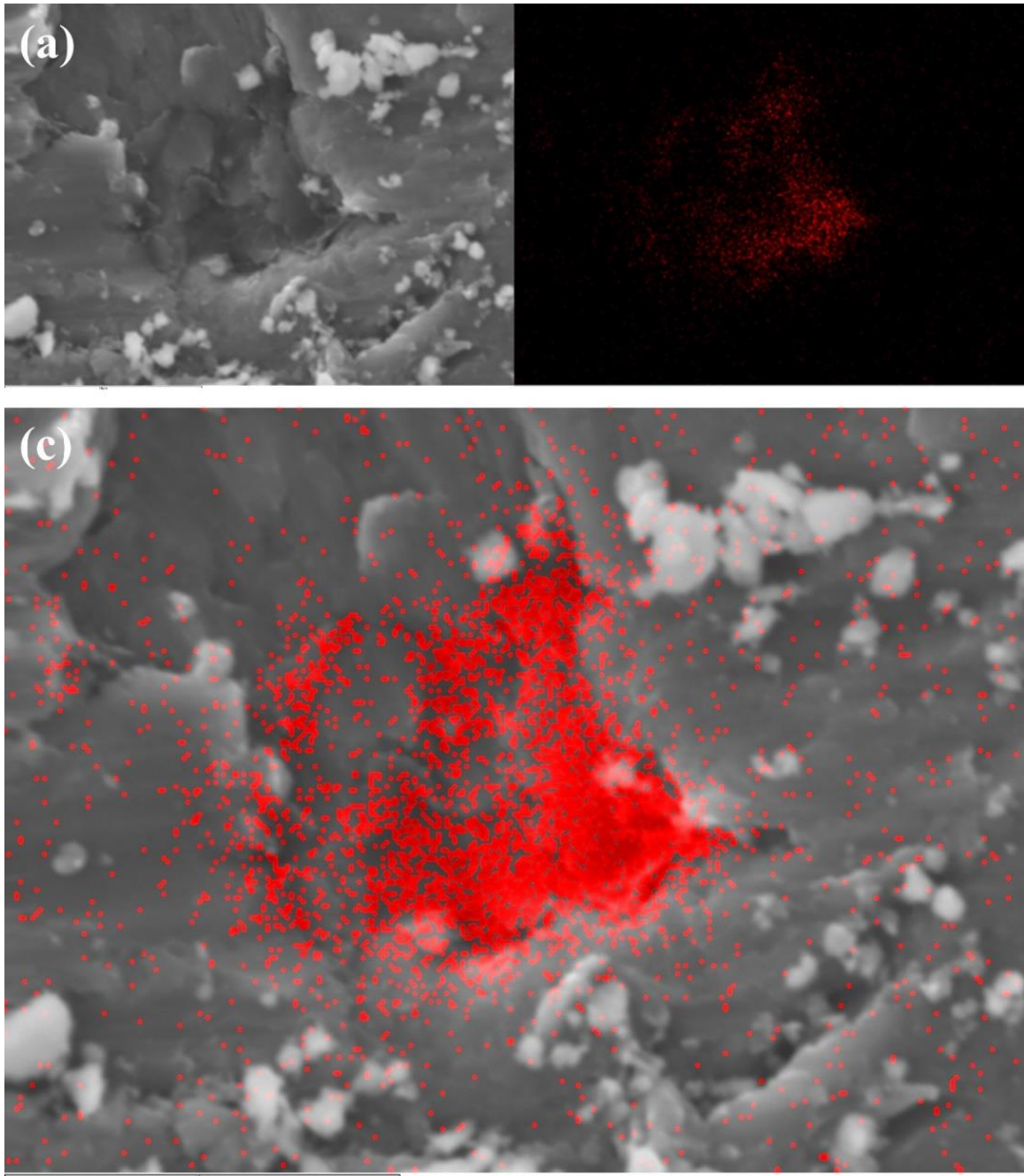
Figure 89 SEM image and elemental mapping for the worn surfaces of

Al/1GNPs/2Al2O3 at 20N using EDX at 1000X

2.4.3.3.3 Raman Spectra

To achieve a specific mechanical or tribological properties, the interface between GNPs and aluminum is of significant importance for the overall performance of composite materials. Researchers reported that the carbon reinforcements easily react with the aluminum and produce a mechanically and chemically unstable Al_4C_3 at the GNPs-matrix interface during the sintering. This reaction can be expressed as, $4Al+3C \rightarrow Al_4C_3$ at 750 °C the free energy of formation of Al_4C_3 is −168 kJ/mol [281].

Raman Spectroscopy was carried out to determine the formation of Al_4C_3 phase at the Al/GNPs interface after wear tests. The full Raman Spectra of worn surface of Al/3GNPs composite is shown in Figure 90. this proves that the surface of the wear track is at least partly covered with GNPs, however, with a disordered structure due to the presence of the D-peak in the Raman spectra as shown in Figure 90. Figure 91 compares the D- and G- band of ball milled GNPs for 3 hours and worn surface of Al/3GNPs composites. The ratio between the intensities of the D and G bands, I_D/I_G, is considered to be the ratio of structural defects and domain size in graphitic materials [282]. The I_D/I_G ratio increases significantly after wear test. Therefore, graphene nanoplatelets are thought to be damaged most during milling and wear because of the physical force applied during the process. In addition, the XRD results of the worn surface of Al/3GNPs shows the presence of GNPs on the worn surface due to G(002) peak at 26.6° is observed as shown in Figure 92.

Figure 93 shows the regional Raman spectrum of Al/3GNPs composite a) before wear test and b) at the wear tracks after wear test. As shown in this Figure

90 the characteristic peaks of GNPs were observed at ~1350 cm^{-1} (D Peaks), ~1670 cm^{-1} (G peaks). As shown in Figure 93b, a Raman peak exists at 865 cm^{-1} which correspond to metal-carbon bond in Al$_4$C$_3$. Obviously, the Al$_4$C$_3$ does not exist in the Al with GNPs composites in this research since the processing temperature was lower than the formation temperature of Al$_4$C$_3$. However, results show that the tribofilm consists of a GNPs tribofilm that chemically bonded to the aluminum matrix (Figure 93b).

The Al$_4$C$_3$ formation reaction could occur not only during the sintering processing but also during the subsequent heat treatment and/or in use under an elevated temperature environment. Li et al. [2] reported that the heat treatment promoted the Al$_4$C$_3$ formation and degraded the mechanical properties of the carbon/aluminum composites. The heterogeneous nucleation of the Al$_4$C$_3$ is associated with surface defects on carbon, such as exposed edges of graphite basal planes that exhibit carbon atoms with uncompensated high-energy electron bonds. The fact that Al/GNPs composites contain no Al$_4$C$_3$ (Figure 93a) indicates that aluminum is not reactive to GNPs at the exposed processing condition. The tribofilm forms after the wear test contain a small amount of Al$_4$C$_3$ (traceable by Raman at the interface and untraceable by the X-ray diffraction). This suggests that aluminum reacts with GNPs during wear test and forms Al$_4$C$_3$. This can be attributed to the raised local temperature during the wear test. Additionally, the wear test process may introduce extra structural defects to GNPs, which makes them more susceptible to react with the aluminum matrix and leads to a low activation energy. The TEM image of tribosurface of composites proves the formation of Al$_4$C$_3$ compound in the interface of GNPs and aluminum and make

190

tribolayer with chemical bonding. Figure 94 exhibit the TEM images of tribolayer for Al/1GNPs, Al/3GNPs, and Al/2GNPs/1Al$_2$O$_3$ composites.

The formation of Al$_4$C$_3$ in carbon-reinforced aluminum matrix composites can affect both mechanical and tribological properties of the composite [3,4,5]. Many kinds of literature reported that the formation of a ceramic Al$_4$C$_3$ phase at the C/Al interface can improve interfacial bonding to some extent [6, 7]. However, the formation of excessive Al$_4$C$_3$ is considered to be harmful due to its intrinsic brittleness, low thermal conductivity and strong tendency of hydrolysis [8, 9]. In other words, the properties and reliability of the C/Al composites significantly depend on the extent of the Al$_4$C$_3$-formed interfacial reaction. Therefore, it becomes a critical issue to correlate the properties with various processing conditions and interfacial reaction extent.

As being discussed in Figure 67, there is an optimum GNPs content in Al/GNPs composite that gives an enhancement to the wear resistance of the composites. Al$_4$C$_3$ has two effects on tribological properties, one may enhance, and one can deteriorate the wear characteristics. Formation of Metal-Carbon bonds at the tribosurface can enhance the hardness as well as create a strong chemical bond between aluminum and GNPs. In addition, carbide crystals can enhance the local hardness and therefore has a positive effect on the tribological properties. On the other hand, they are brittle and thus promote accelerated crack growth rates. Therefore, they can act as secondary hard abrasives when fall out of the metal as debris.

As can be seen in Figure 67 and, the addition of GNPs clearly gives a positive effect on wear and friction up to 1 wt.%. Higher loads will also enhance the

formation of metal-carbon bonds and therefore better tribological properties are expected. However, at higher GNPs contents, the negative effect of Al_4C_3 can be the deteriorating factor of wear characteristics [283-286].
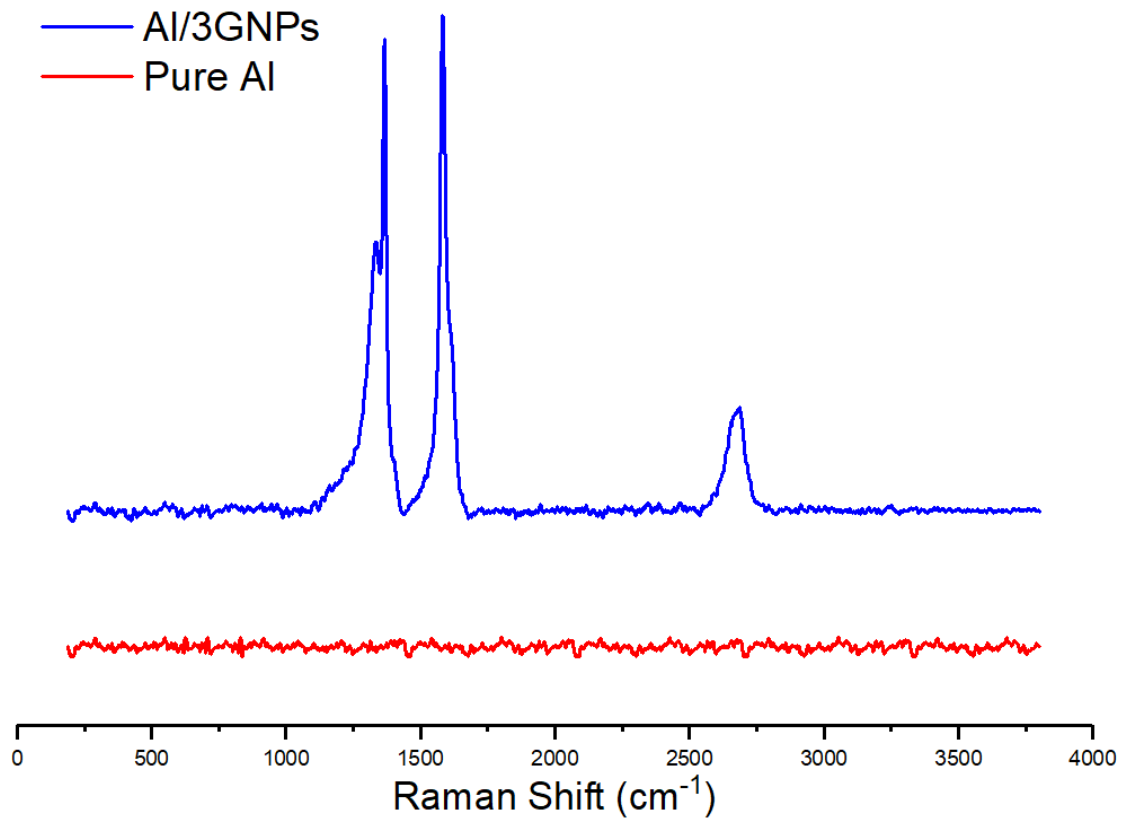
Figure 90 The Raman spectrum of the worn surface of Al/3GNPs composite
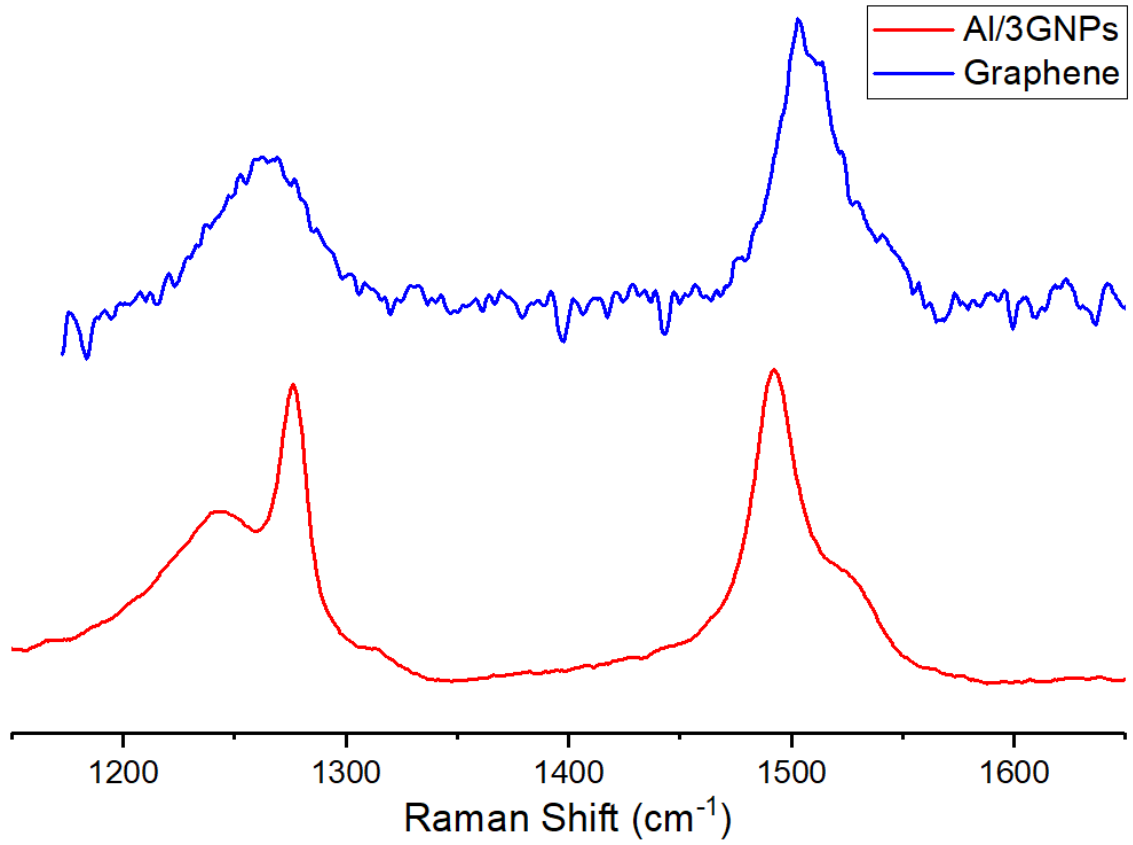
Figure 91 D- and G-band Raman spectrum of initial GNPs powder and Al/3GNPs composites
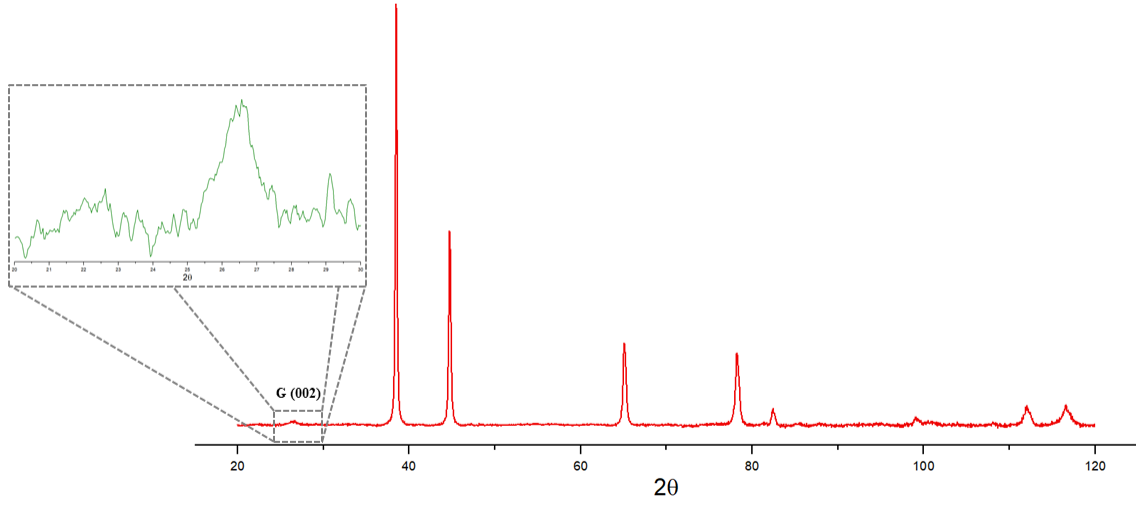
Figure 92 XRD of worn surface of Al/3GNPs composites at 20N
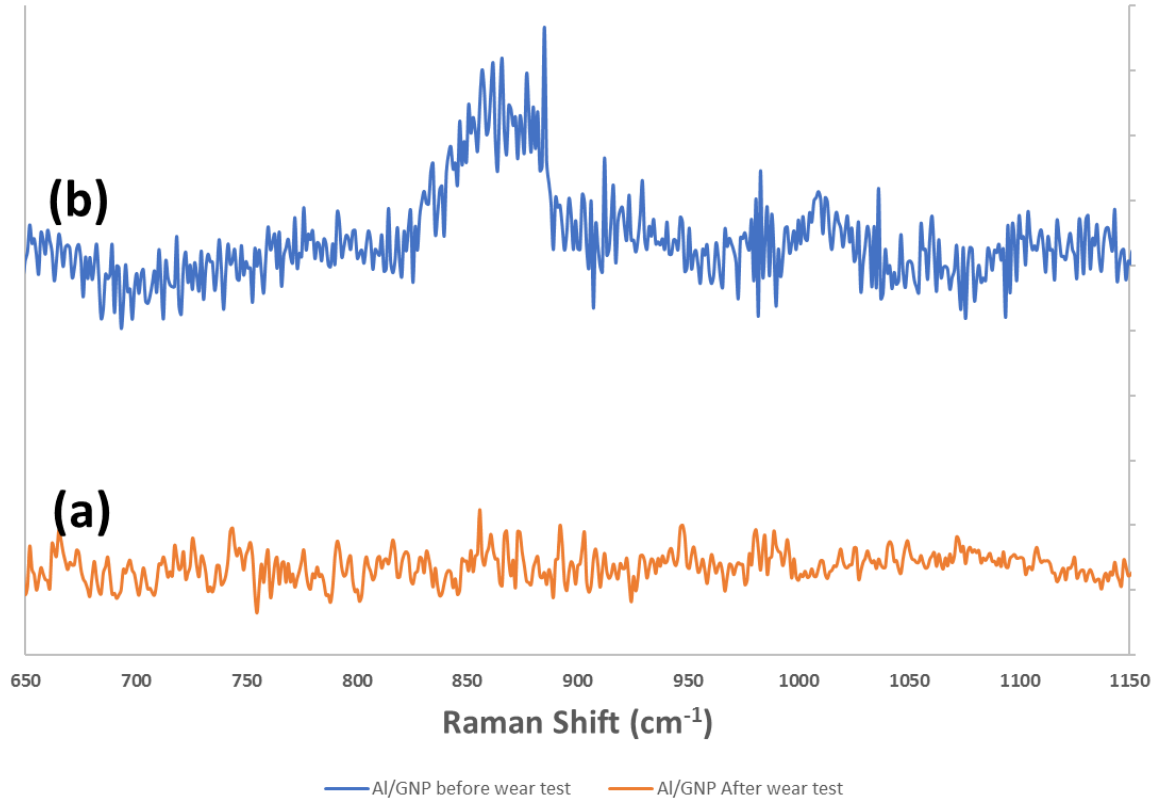
Figure 93 The Raman spectrum centered at 900 cm-1 of Al/GNPs composite a) before wear test and b) at the wear tracks after wear test

196
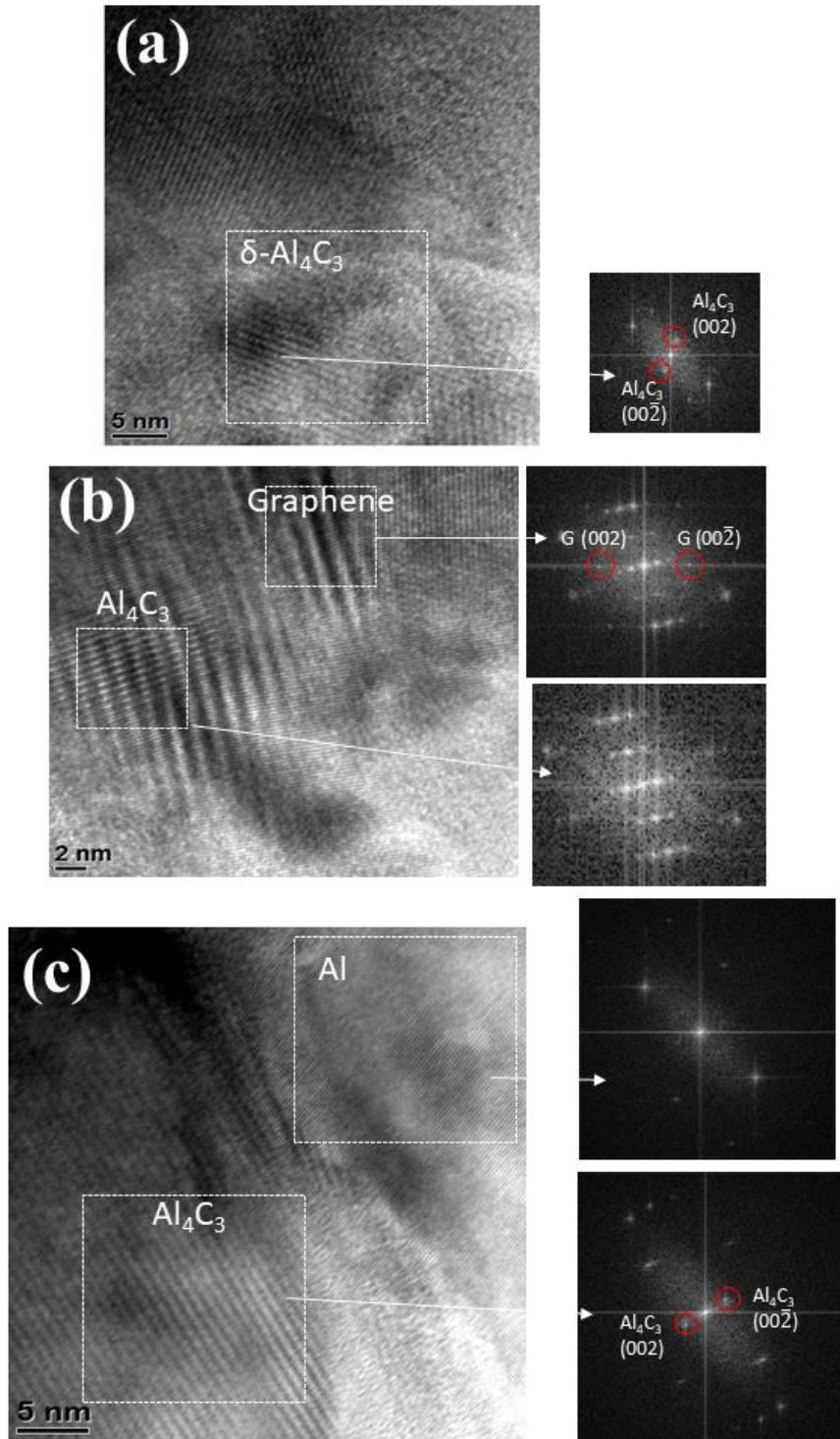
Figure 94 Cross-section TEM image of tribosurface of a) Al/1GNPs, b) Al/3GNPs and c) Al/2GNPs/1Al2O3 composites

2.4.4 WEAR MECHANISMS

A common type of wear in aluminum is adhesive wear [287] which occurs when two surfaces are initially rubbed against each other. However, due to localized heating and oxygen diffusion, the surface forms aluminum oxide layer which is brittle in nature and undergoes abrasive wear. It is expected that hard and brittle alumina phase will generate large particles of wear debris, thus increasing wear rate and COF. Figure 95 shows a schematic of wear mechanisms of pure aluminum. Therefore, the wear track of pure aluminum is very rough, and some cracks appear on the surface as shown in Figure 96. The surface of the wear track reveals crack formation. Strong aluminum-steel interactions contribute to a severe wear rate, with excessive material transfer and cladding of aluminum on the counter surface. The strong interactions and material transfer is the reason for the failure of the surface of aluminum samples that make debris and propagate crack on the worn surfaces. The large amount of material transfer and formation of debris is also another reason of high wear rate. The EDS shows high amount of oxygen. The brittle Al_2O_3, surface layer generates large amount of wear debris (Figure 97).
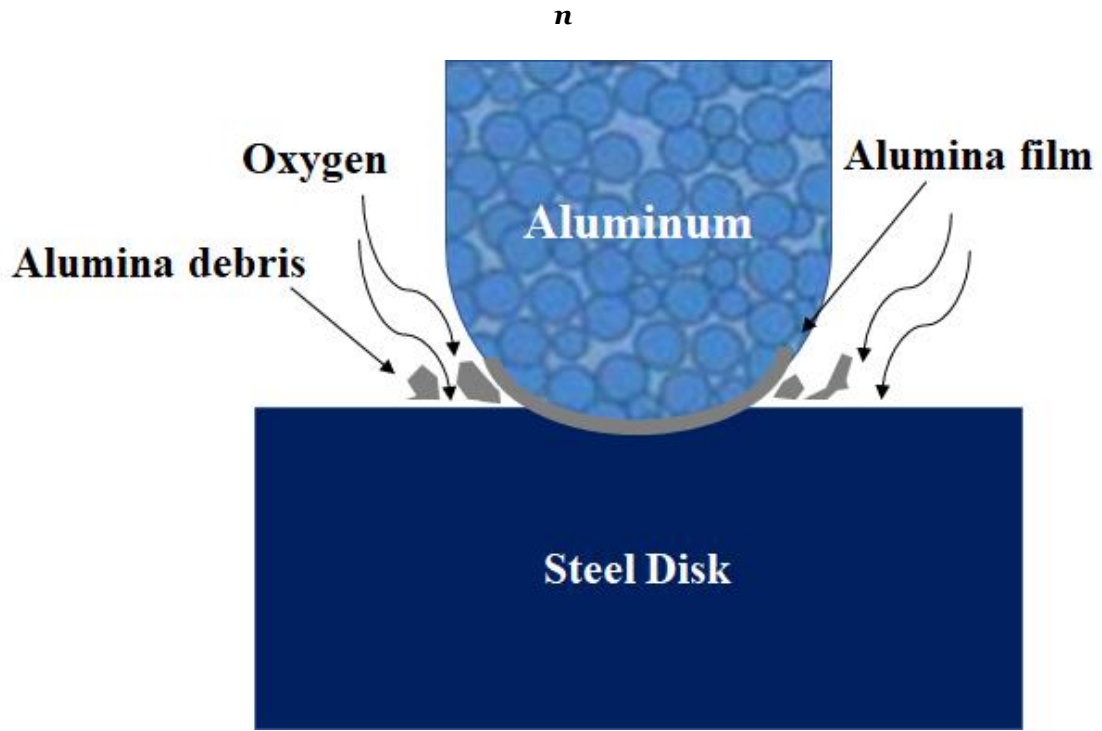
Figure 95 Schematic Representation of Behavior of Pure Al
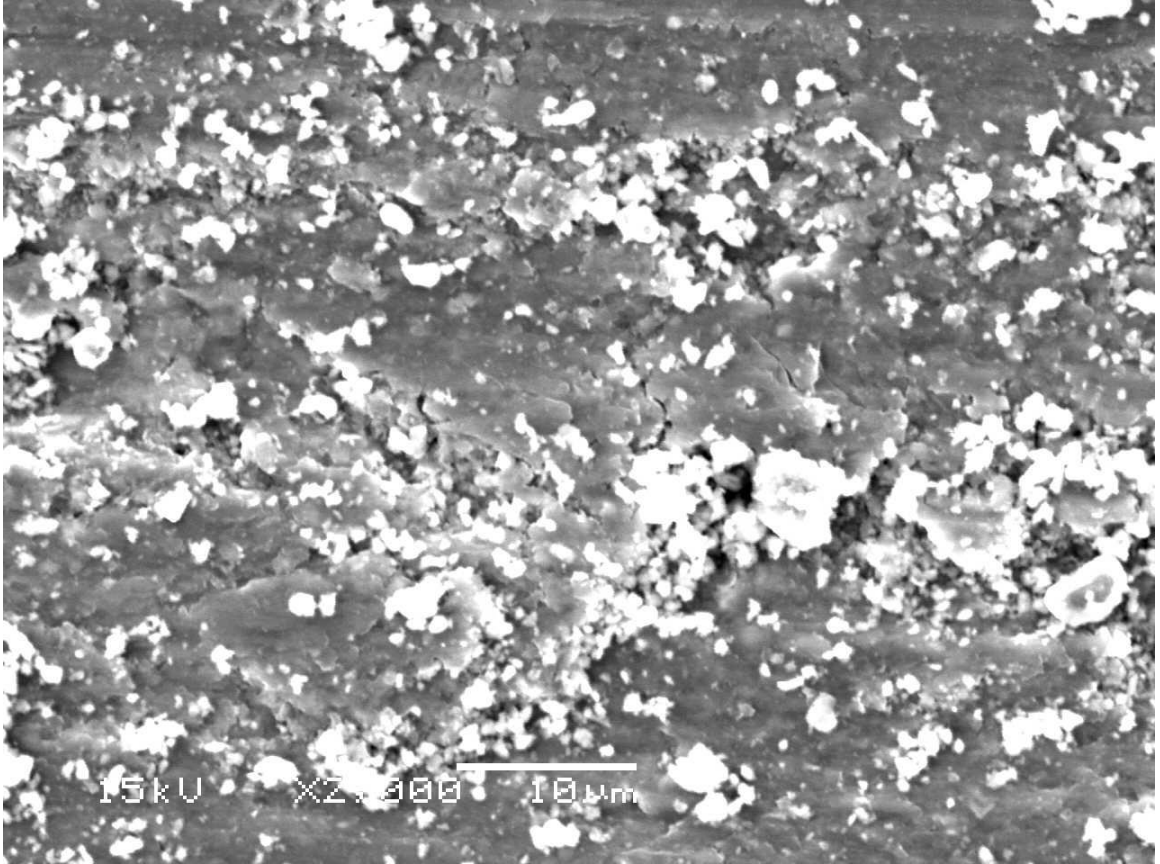
Figure 96 SEM image of the worn surface for pure aluminum at 15N at 2000X
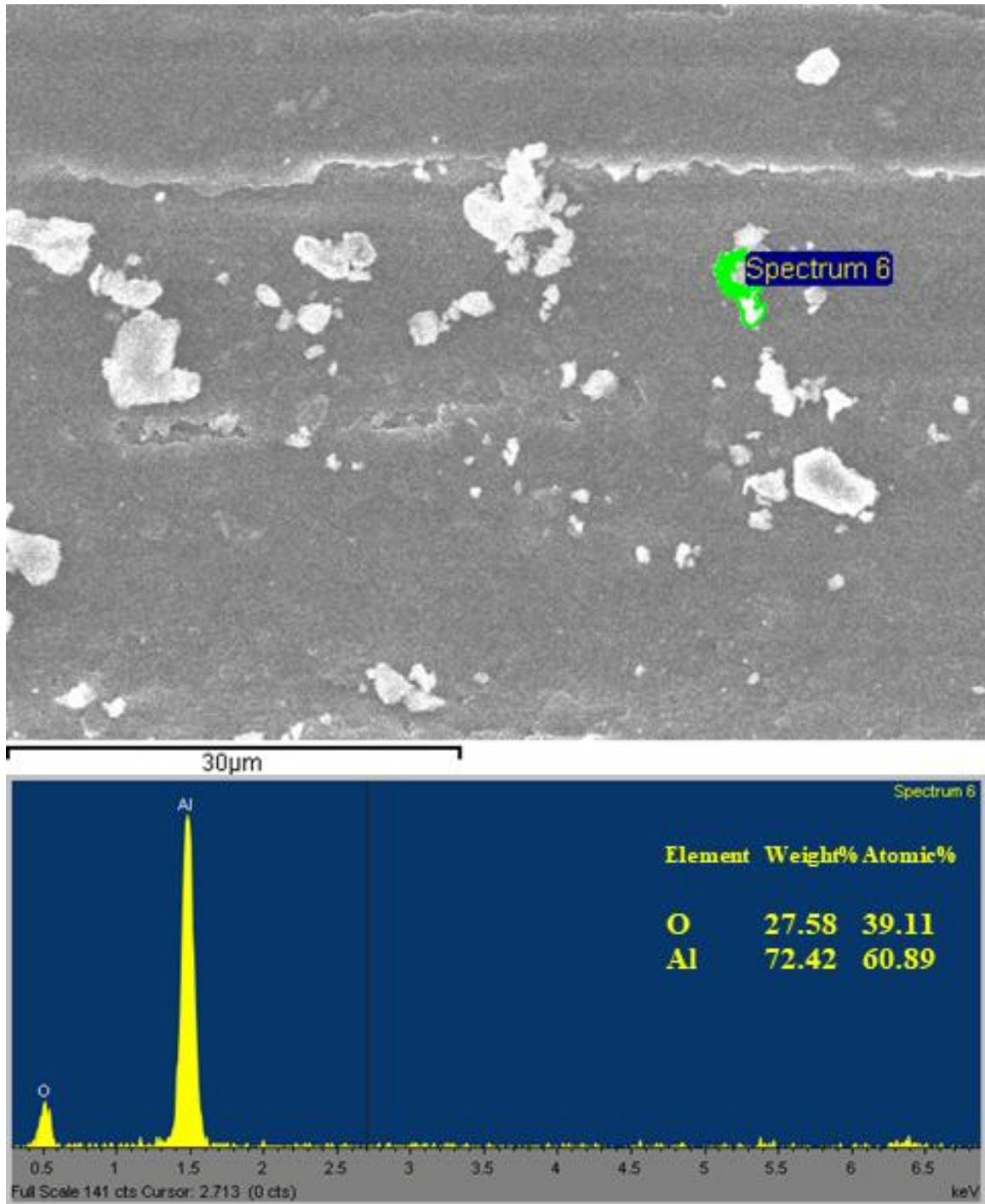
Figure 97 Chemical composition of debris on the worn surface of pure aluminum at 5N

The aluminum-steel pair forms a strong metallic bond which causes to transfer of aluminum at the steel surface when sliding against a stainless-steel disk.

While the aluminum-steel interactions are strong, the aluminum-carbon interactions are very weak. In this case, not only on the composite surfaces but also on the mating surfaces, a protective lubricant tribofilm is formed. In addition to the fact that almost all composites contain GNPs particles, GNPs sheets are easily sheared, the lubricating nature of GNPs and weak aluminum-carbon interactions contributes to an overall lowered friction.

Therefore, it is expected that uniform dispersion of GNPs would facilitate the formation of a uniform tribofilm, which will the reduction of COF and improved wear resistance. The stated hypothesis of GNPs in aluminum matrix expects to find lower wear rate and COF than for pure aluminum. Figure 98 shows a schematic of the proposed wear mechanism in Al/GNPs composites. Figure 99(a) shows the wear surface of Al/3GNPs composites. Some region indicates deposition of GNPs on the surface and forms a tribofilm. This tribofilm consists of carbon-rich as indicated in EDX shown in Figure 99(b). In addition, the EDS of the worn surface shows higher oxygen in comparison with pure aluminum (Figure 97). Another mechanism present in this sample is the ability of the GNPs to act as inhibitor preventing oxygen to go through the sample. Therefore, it is suggested that oxide formation occurs less due to preventing the action of GNPs nanoplatelets and GNPs tribolayer from diffusion of oxygen and consequently, reduce the wear rate and COF.

Several detachments are found as wear debris on the worn surface with less amount of debris in comparison with the worn surface of aluminum. Besides, no plastic deformation is observed in debris particle, suggesting that the wear debris is lifted up before plastic deformation. Also, the wear debris composition exhibits

the presence of GNPs (Figure 99d), therefore, the debris is self-lubricating and cause less wear and damage on the surface as third body abrasive particles.

This study confirmed that a tribolayer of GNPs is deposited on the worn surface. It appears that weak interlayer forces between GNPs layers enable sliding or layer buckling to reduce the stress; therefore, the COF decreases in presence of GNPs nanoplatelets attached to the surface. When a GNPs sheet experiences shear, the weak van der Waals forces break apart and few layers of GNPs tend to wrap the deformed material forming sheet-like structures that facilitate shear sliding with one another. Also, the GNPs provides the surface with the ability to deflect. It must be noted that this wrapping is possible for very thin GNPs and not thick graphite as the ability to wrap and deflect is more difficult to be achieved (Figure 100) when a large number of layers are present. A tribofilm is formed on the surface due to the breaking of the weak van der Walls forces that hold the C-C structure. Due to shear forces, a portion of the tribofilm is transferred on the pin surface. The wear occurs between transfer film and tribolayer providing lubrication properties and helping to reduce COF.

According to chapter 2.4.3.2, wear rate is dependent on increased GNPs content. This also applies to relative density and hardness. The Al/3GNP compact is less prone to resist the applied load, compared to the Al/1GNP composites. This is due to a higher porosity and lower hardness. The equilibrium between load and area becomes large to match the hardness of the mating material. This is an alternative explanation why worn volumes are higher, when increased GNPs content, after tests with similar parameters.

It is concluded that the addition of GNPs leads to reduce friction and wear. The composite with GNPs additives presents few wear debris with the smaller size. This demonstrated that GNPs nanoparticles can effectively provide lubricious and anti-wear properties in aluminum creating a tribofilm and a transferfilm. Moreover, SEM micrographs indicate that an overall wear mechanism is a combination of adhesive and abrasive wear the same as pure aluminum and the difference is the regime where for composites are low or mild abrasion. In addition, when self-lubrication or lubrication action is effective at the interface, basically the low sliding speed experiments represent that the tests were conducted under boundary lubricated regime. At this situation, the adhesion is minimized (if not eliminated) due to the presence of lubrication effect and thus the contribution of abrasive wear mode is the key factor.
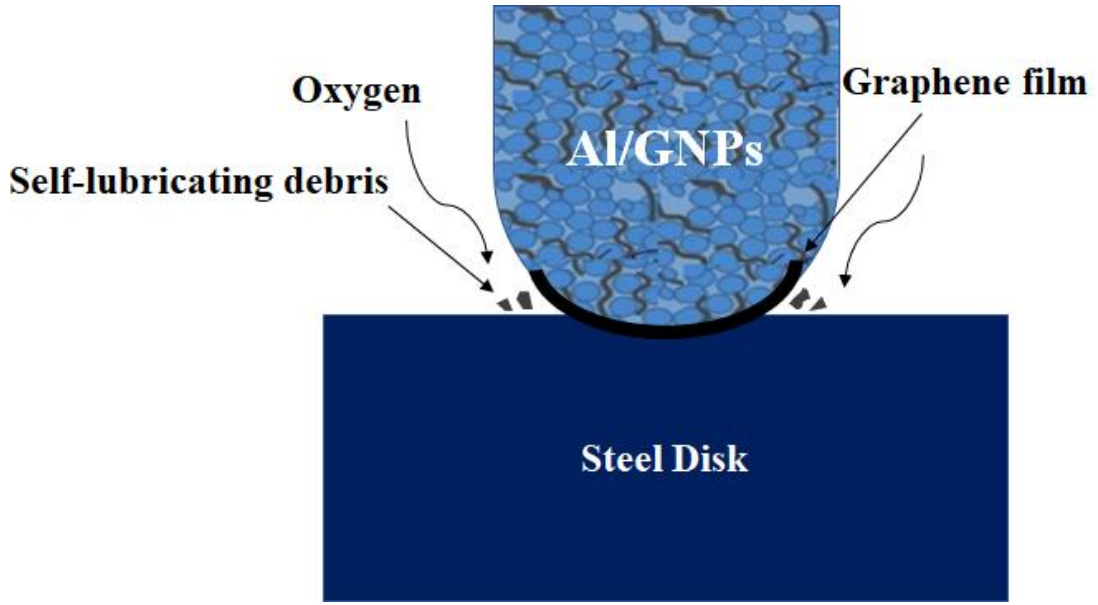
Figure 98 Schematic Representation of Behavior of Al/GNPs composites
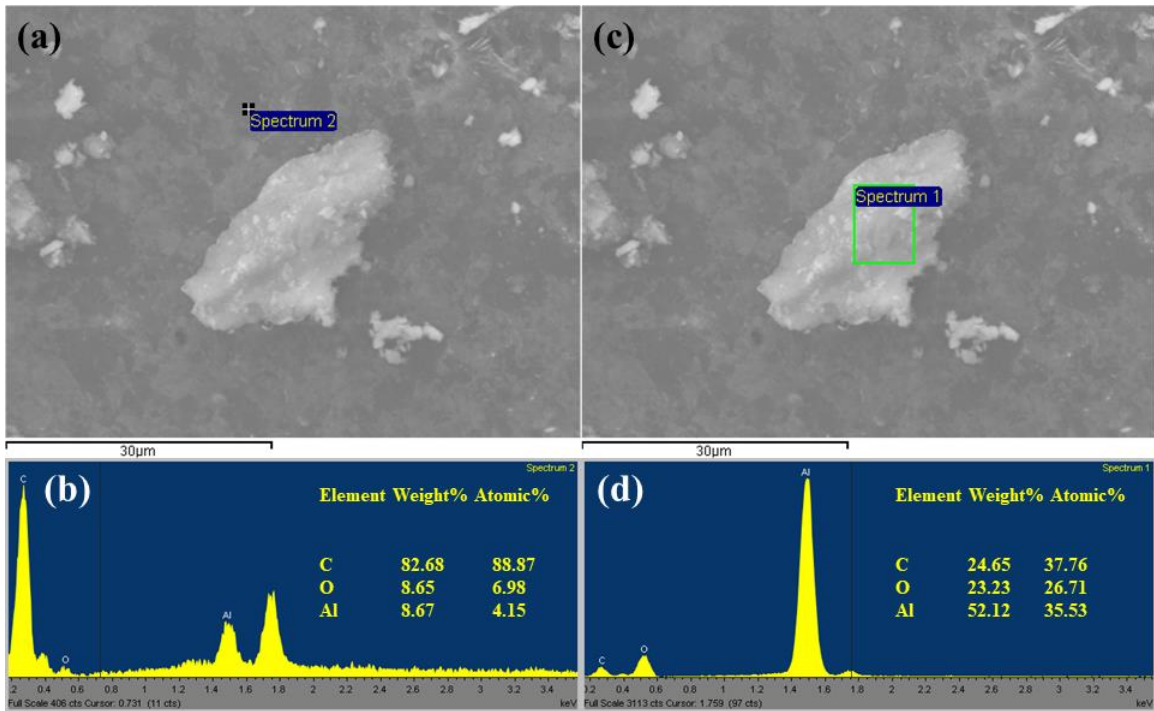
Figure 99 Chemical composition of worn surface and debris on the worn surface of

Al/3GNPs at 5N
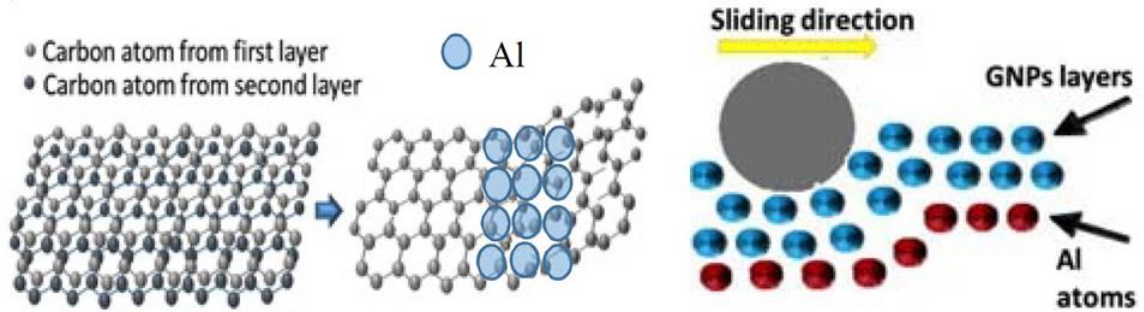
Figure 100 Schematic Representation of GNPs wear mechanism

2.5 CONCLUSION

Self-lubricating aluminum nanocomposites reinforced by GNPs nanoplatelets (GNPs) and alumina have been synthesized by powder metallurgy (PM) technique and using Hot-Pressing (HP). The effect of reinforcement weight percentage on structural features, mechanical properties, and tribological properties of the nanocomposites was investigated. Microstructural studies using TEM showed the presence of GNPs in the aluminum matrix without any undesired phases, which confirm the feasibility of PM and HP technique and parameters in synthesizing Aluminum matrix nanocomposites. The XRD spectrums of the bulk samples show five major peaks of aluminum which prove no undesirable reaction or formation of new phases occurs during self-lubricating aluminum nanocomposites fabrication. The carbon element did not detect in any of the nanocomposites due to the nanometric size and the low content of the reinforcement phase. The hardness of the Al/GNPs composites increased with the increase of the content of GNPs up to 1 wt.% and then decreased where hardness increases from 74.8 HRB for pure aluminum to 90.1 HRB for Al/1GNPs composite. The reason for the reduction in hardness can

206

be found in the microstructure of composites, where more agglomeration occurs more porosity appears (confirmed in the TEM analysis). The hardness of hybrid nanocomposites is higher than pure aluminum and as well as Al/GNPs composites; the hardness increases from 74.8 HRB for pure aluminum to 94.4 HRB for Al/1GNPs/2Al$_2$O$_3$ composite.

Reduced coefficients of friction and improved wear resistance have been observed in self-lubricating nanocomposites at several loads. At 15N applied loads, Addition of 1 wt.% GNPs in the self-lubricating composites caused a remarkable reduction in wear rate and COF value. The wear rate and COF decreased by 66% and 35% in comparison with the unreinforced aluminum. Similarly, in Al/1GNPs/2Al$_2$O$_3$ 93% reduction in the wear rates and 44% reduction in COF value in comparison with the pure aluminum were recorded. It is obvious that tribological properties of self-lubricating hybrid aluminum composites reinforced by GNPs and alumina are improved possibly due their hardness. In all composites, there is an opposite relationship between wear rate and hardness. There is an optimum weight percentage of reinforcement where the wear rate is minimum, and the hardness is maximum. This optimum value was obtained at 1 wt.% GNPs for Al/GNPs composites and 1 wt.% GNPs/2 wt.% Al$_2$O$_3$ for hybrid composites. It is worth noting that unlike unreinforced aluminum, self-lubricating composites has lower wear rate and COF at higher loads.

Worn surfaces and surface roughness parameters were studied by an optical profilometer. Surface texture and roughness values measured in self-lubricating composites are in line with the observed wear rate and COF values. To study the surface of worn surface and find the composition of worn surfaces, SEM/EDX was

conducted. Black spots on the worn surface were detected where EDX data suggests the presence of GNPs tribofilm. In addition, the lower oxygen content on the worn surface in presence of GNPs suggests the ability of GNPs in reducing oxygen diffusion and therefore, hinder the formation of brittle oxides on the surface. Raman Spectroscopy was carried out to determine the nature of tribofilm. Raman shows D- and G- band that confirms the worn surface is covered with GNPs tribofilm. In addition, an Al_4C_3 peak was observed at tribosurface. even the Al_4C_3 does not exist in the synthesized Al/GNPs composites. Results show that the tribofilm consists of GNPs tribofilm that are chemically bonded to the aluminum matrix. TEM image of the tribosurface of composites confirms the formation of Al_4C_3 compound at the interface of GNPs and aluminum. This formation of Al_4C_3 can lead to chemical bond between the matrix and the tribolayer.

The dominant wear mechanism to explain the improved wear characteristics in the composite is "reduction on real contact area" by the formation of GNPs tribofilm and preventing the oxidation of the worn surface. In addition, the layered GNPs structure is exposed at the contact surface and then keeps the surface lubricated. In hybrid composites, in addition to this mechanism, alumina particles added to Al/GNPs nanocomposites have a load bearing as well as rolling effect. Surface studies clearly show that narrower and shallower grooves appear on the worn surface of hybrid composites compared to pure aluminum and Al/GNPs nanocomposites. The major part of the applied load is carried by alumina nanoparticles. This will minimize the amount of plastic deformation and therefore, helps the formation of lubricant film at the interface. In addition, there are

208

interactions between dislocations and Al_2O_3 nanoparticles that ultimately resist the propagation of cracks during sliding wear.

FUTURE WORK

The objective of this dissertation was to explore the feasibility of using graphene for tribological applications for nanolubricants and self-lubricating nanocomposites.

It is suggested to make nanolubricants with several thicknesseses of graphene nanoplatelets to investigate the effect of a number of layers on tribological properties of nanolubricants. In addition, it is required to characterize the cross-section of the worn surface by TEM. As the canola oil is not a commercial lubricant, it is possible to investigate the graphene efficacy for engine oil or finding a way to improve other properties such as stability to commercialize it. The effect of nanoparticles on the real area of contact and contact force can be investigated using an analytical model. It should be developed such a contact model and relate the contact parameters to measurable parameters such as friction and wear. The approach should try to identify, quantify and evaluate the most influential contact parameters affecting the system into a model that can illuminate the mechanisms behind the friction and wear behavior of nano-lubricants.

For nanocomposites, although preliminary information was obtained regarding the microstructure, properties, and the processing conditions, future work will focus on TEM and SEM investigation to show how the nanoparticles are distributed along and within the grain boundaries at different processing condition. Also, more characterization is required to identify the AL_2O_3 and graphene particles by EBSD and lattice imaging. Experimental studies are required to investigate the variation in cooling rate and the particle size and

content on their engulfment. The use of this technique to synthesize master alloys for subsequent re-melting and dispersion in a larger melt can be explored. Future work will also focus on alloy selection so that higher mechanical properties can be obtained. Synthesize the nanocomposites with aluminum alloys with higher initial mechanical properties such A365 and A206 may lead to utilization of the full potential of these materials. However, a careful study is required to investigate the possible reaction models of the reactant and the alloying elements. Computational analysis of the effect of graphene on reducing the contact area and the mechanism of wear reduction.

REFERENCES

1.   Reeves, C.J., et al. *Evaluating the tribological performance of green liquid lubricants and powder additive based green liquid lubricants*. in *Proceedings of 2012 STLE Annual Meeting & Exhibition, STLE*. 2012.

2.   Bhushan, B., *Principles and applications of tribology*. 2013: John Wiley & Sons.

3.   Erhan, S.Z., et al., *Lubricant base stock potential of chemically modified vegetable oils*. Journal of agricultural and food chemistry, 2008. **56**(19): p. 8919-8925.

4.   Lovell, M., et al., *Increasing formability in sheet metal stamping operations using environmentally friendly lubricants*. Journal of materials processing technology, 2006. **177**(1-3): p. 87-90.

5.   Li, W., et al., *Green waxes, adhesives and lubricants*. Phil. Trans. R. Soc. A, 2010. **368**(1929): p. 4869-4890.

6.   Grushcow, J. *High oleic plant oils with hydroxy fatty acids for emission reduction*. in *World Tribology Congress III*. 2005. American Society of Mechanical Engineers.

7.   Jayadas, N., K.P. Nair, and G. Ajithkumar. *Vegetable Oils as Base Oil for Industrial Lubricants: Evaluation Oxidative and Low Temperature Properties Using TGA, DTA and DSC*. in *World Tribology Congress III*. 2005. American Society of Mechanical Engineers.

8.   Coscione, A.R. and W.E. Artz, *Vegetable oil stability at elevated temperatures in the presence of ferric stearate and ferrous octanoate*. Journal of agricultural and food chemistry, 2005. **53**(6): p. 2088-2094.

9.   Sharma, B.K., et al., *One-pot synthesis of chemically modified vegetable oils*. Journal of agricultural and food chemistry, 2008. **56**(9): p. 3049-3056.

10.   Hwang, H.-S. and S.Z. Erhan, *Modification of epoxidized soybean oil for lubricant formulations with improved oxidative stability and low pour point*. Journal of the American Oil Chemists' Society, 2001. **78**(12): p. 1179-1184.

11.   Li, S., et al., *Linear sulphonate detergents as pour point depressants*. Lubrication Science, 2004. **16**(2): p. 127-137.

12.   Adamczewska, J. and D. Wilson, *Development of ecologically responsive lubricants*. Lubrication Science, 1997. **14**(2): p. 129-142.

13.   Ouyang, Q. and K. Okada, *Nano-ball bearing effect of ultra-fine particles of cluster diamond*. Applied surface science, 1994. **78**(3): p. 309-313.

14.   Chen, L., et al., *Nanofluids containing carbon nanotubes treated by mechanochemical reaction*. Thermochimica Acta, 2008. **477**(1-2): p. 21-24.

15.   Wu, Y.-Y. and M.-J. Kao, *Using TiO2 nanofluid additive for engine lubrication oil*. Industrial Lubrication and Tribology, 2011. **63**(6): p. 440-445.

16.   Godet, M., *The third-body approach: a mechanical view of wear*. Wear, 1984. **100**(1-3): p. 437-452.

17.   Tao, X., Z. Jiazheng, and X. Kang, *The ball-bearing effect of diamond nanoparticles as an oil additive*. Journal of Physics D: Applied Physics, 1996. **29**(11): p. 2932.

18. Zhou, J., et al., *Tribological behavior and lubricating mechanism of Cu nanoparticles in oil.* Tribology Letters, 2000. **8**(4): p. 213-218.

19. Hong, R., et al., *Synthesis and surface modification of ZnO nanoparticles.* Chemical Engineering Journal, 2006. **119**(2-3): p. 71-81.

20. Hu, Z., J. Dong, and G. Chen, *Study on antiwear and reducing friction additive of nanometer ferric oxide.* Tribology international, 1998. **31**(7): p. 355-360.

21. Zhou, X., et al., *Study on the tribological properties of surfactant-modified MoS2 micrometer spheres as an additive in liquid paraffin.* Tribology International, 2007. **40**(5): p. 863-868.

22. Yu, H., et al., *Effect of thermal activation on the tribological behaviours of serpentine ultrafine powders as an additive in liquid paraffin.* Tribology International, 2011. **44**(12): p. 1736-1741.

23. Zhang, Z., et al., *The effect of LaF3 nanocluster modified with succinimide on the lubricating performance of liquid paraffin for steel-on-steel system.* Tribology International, 2001. **34**(2): p. 83-88.

24. Lince, J. and P. Fleischauer, *Solid Lubrication for Spacecraft Mechanisms*. 1997, AEROSPACE CORP EL SEGUNDO CA TECHNOLOGY OPERATIONS.

25. Rittenhouse, J.R. and J.B. Singletary, *Space materials handbook*. 1968, LOCKHEED MISSILES AND SPACE CO PALO ALTO CALIF MATERIALS SCIENCES LAB.

26. Clauss, F.J., *Solid lubricants and self-lubricating solids*. 2012: Elsevier.

27. Duzcukoglu, H. and Ö.S. ŞAHIN, *Investigation of wear performance of canola oil containing boric acid under boundary friction condition.* Tribology Transactions, 2010. **54**(1): p. 57-61.

28. Hu, Z., et al., *Preparation and tribological properties of nanoparticle lanthanum borate.* Wear, 2000. **243**(1-2): p. 43-47.

29. Tarasov, S., et al., *Study of friction reduction by nanocopper additives to motor oil.* Wear, 2002. **252**(1): p. 63-69.

30. Liu, G., et al., *Investigation of the mending effect and mechanism of copper nano-particles on a tribologically stressed surface.* Tribology Letters, 2004. **17**(4): p. 961-966.

31. Rapoport, L., et al., *Mechanism of friction of fullerenes.* Industrial lubrication and tribology, 2002. **54**(4): p. 171-176.

32. Rapoport, L., et al., *Tribological properties of WS2 nanoparticles under mixed lubrication.* Wear, 2003. **255**(7-12): p. 785-793.

33. Zhang, M., et al., *Performance and anti-wear mechanism of CaCO3 nanoparticles as a green additive in poly-alpha-olefin.* Tribology International, 2009. **42**(7): p. 1029-1039.

34. Battez, A.H., et al., *CuO, ZrO2 and ZnO nanoparticles as antiwear additive in oil lubricants.* Wear, 2008. **265**(3-4): p. 422-428.

35. Huang, H., et al., *An investigation on tribological properties of graphite nanosheets as oil additive.* Wear, 2006. **261**(2): p. 140-144.

36. Zhou, J., et al., *Study on an antiwear and extreme pressure additive of surface coated LaF3 nanoparticles in liquid paraffin.* Wear, 2001. **249**(5-6): p. 333-337.

37.	Dong, J. and Z. Hu, *A study of the anti-wear and friction-reducing properties of the lubricant additive, nanometer zinc borate.* Tribology international, 1998. **31**(5): p. 219-223.

38.	Greenberg, R., et al., *The effect of WS2 nanoparticles on friction reduction in various lubrication regimes.* Tribology Letters, 2004. **17**(2): p. 179-186.

39.	Huang, H., et al., *Friction and wear properties of IF–MoS 2 as additive in paraffin oil.* Tribology Letters, 2005. **20**(3): p. 247-250.

40.	Xu, T., et al., *Study on the tribological properties of ultradispersed diamond containing soot as an oil additive©.* Tribology transactions, 1997. **40**(1): p. 178-182.

41.	Liu, W. and S. Chen, *An investigation of the tribological behaviour of surface-modified ZnS nanoparticles in liquid paraffin.* Wear, 2000. **238**(2): p. 120-124.

42.	Chen, S., W. Liu, and L. Yu, *Preparation of DDP-coated PbS nanoparticles and investigation of the antiwear ability of the prepared nanoparticles as additive in liquid paraffin.* Wear, 1998. **218**(2): p. 153-158.

43.	Xue, Q., W. Liu, and Z. Zhang, *Friction and wear properties of a surface-modified TiO 2 nanoparticle as an additive in liquid paraffin.* Wear, 1997. **213**(1): p. 29-32.

44.	Wo, H.-z., K.-h. Hu, and X.-g. Hu, *Tribological Properties of MoS~ 2 Nanoparticles as Additive in a Machine Oil.* TRIBOLOGY-BEIJING-, 2004. **24**(1): p. 37-40.

45.	Thakre, A.A., A. Thakur, and J. Taylor, *Study of behaviour of aluminium oxide nanoparticles suspended in SAE20W40 oil under extreme pressure lubrication.* Industrial Lubrication and Tribology, 2015. **67**(4).

46.	Jeng, Y.-R., et al., *Tribological Performance of Oil-Based Lubricants with Carbon-Fe Nanocapsules Additive.* Tribology Transactions, 2015(just-accepted): p. 00-00.

47.	Nunn, N., et al., *Tribological properties of polyalphaolefin oil modified with nanocarbon additives.* Diamond and Related Materials, 2015. **54**: p. 97-102.

48.	Hu, X., *On the size effect of molybdenum disulfide particles on tribological performance.* Industrial Lubrication and Tribology, 2005. **57**(6): p. 255-259.

49.	Lee, C.-G., et al., *A study on the tribological characteristics of graphite nano lubricants.* International journal of precision engineering and manufacturing, 2009. **10**(1): p. 85-90.

50.	Lin, J., L. Wang, and G. Chen, *Modification of graphene platelets and their tribological properties as a lubricant additive.* Tribology Letters, 2011. **41**(1): p. 209-215.

51.	Omrani, E., et al., *Influences of graphite reinforcement on the tribological properties of self-lubricating aluminum matrix composites for green tribology, sustainability, and energy efficiency—a review.* The International Journal of Advanced Manufacturing Technology, 2015: p. 1-22.

52.	Moghadam, A.D., et al., *Mechanical and tribological properties of self-lubricating metal matrix nanocomposites reinforced by carbon nanotubes (CNTs) and graphene–A review.* Composites Part B: Engineering, 2015. **77**: p. 402-420.

53.	Moghadam, A.D., et al., *Functional metal matrix composites: self-lubricating, self-healing, and nanocomposites-an outlook.* JOM, 2014. **66**(6): p. 872-881.

54.	Eswaraiah, V., V. Sankaranarayanan, and S. Ramaprabhu, *Graphene-based engine oil nanofluids for tribological applications.* ACS applied materials & interfaces, 2011. **3**(11): p. 4221-4227.

55. Ames, W. and A. Alpas, *Wear mechanisms in hybrid composites of Graphite-20 Pct SiC in A356 Aluminum Alloy (Al-7 Pct Si-0.3 Pct Mg).* Metallurgical and Materials Transaction A, 1995. **26**(1): p. 85-98.

56. Riahi, A. and A. Alpas, *The role of tribo-layers on the sliding wear behavior of graphitic aluminum matrix composites.* Wear, 2001. **251**(1-12): p. 1396-1407.

57. Guo, M.T. and C.-Y. Tsao, *Tribological behavior of aluminum/SiC/nickel-coated graphite hybrid composites.* Materials Science and Engineering: A, 2002. **333**(1-2): p. 134-145.

58. Igartua, A., et al., *Tribological tests to simulate wear on piston rings*, in *Critical component wear in heavy duty engines*. 2011, John Wiley & Sons Ltd Singapore. p. 167-195.

59. Akhlaghi, F. and A. Zare-Bidaki, *Influence of graphite content on the dry sliding and oil impregnated sliding wear behavior of Al 2024–graphite composites produced by in situ powder metallurgy method.* Wear, 2009. **266**(1-2): p. 37-45.

60. Omrani, E., et al., *Effect of graphite particles on improving tribological properties Al-16Si-5Ni-5Graphite self-lubricating composite under fully flooded and starved lubrication conditions for transportation applications.* The International Journal of Advanced Manufacturing Technology, 2016. **87**(1-4): p. 929-939.

61. Aranganathan, N. and J. Bijwe, *Comparative performance evaluation of NAO friction materials containing natural graphite and thermo-graphite.* Wear, 2016. **358**: p. 17-22.

62. Novoselov, K.S., et al., *Electric Field Effect in Atomically Thin Carbon Films.* Science, 2004. **306**: p. 666-669.

63. Lee, C., et al., *Elastic and frictional properties of graphene.* Physica Status Solidi (b), 2009. **246**(11-12): p. 2562.

64. Shin, Y.J., et al., *Frictional characteristics of exfoliated and epitaxial graphene.* Carbon, 2011. **49**(12): p. 4070-4073.

65. Sandoz-Rosado, E.J., O.A. Tertuliano, and E.J. Terrell, *An atomistic study of the abrasive wear and failure of graphene sheets when used as a solid lubricant and a comparison to diamond-like-carbon coatings.* Carbon, 2012. **50**(11): p. 4078-4084.

66. Marchetto, D., et al., *Friction and wear on single-layer epitaxial graphene in multi-asperity contacts.* Tribology Letters, 2012. **48**(1): p. 77-82.

67. Berman, D., A. Erdemir, and A.V. Sumant, *Few layer graphene to reduce wear and friction on sliding steel surfaces.* Carbon, 2013. **54**: p. 454-459.

68. Zen, A.G. and R. G.W., *Tribological Evaluation of nano graphene Platelets as an additive to biolubricant base fluid*, in *EURECA* 2013.

69. Zhang, W., et al., *Tribological properties of oleic acid-modified graphene as lubricant oil additives.* Journal of Physics D: Applied Physics, 2011. **44**(20): p. 205303.

70. Choudhary, S., H.P. Mungse, and O.P. Khatri, *Dispersion of alkylated graphene in organic solvents and its potential for lubrication applications.* Journal of Materials Chemistry, 2012. **22**(39): p. 21032-21039.

71. Gansheimer, J. and R. Holinski, *Molybdenum disulfide in oils and greases under boundary conditions.* Journal of Lubrication Technology, 1973. **95**(2): p. 242-246.

72.	Rapoport, L., N. Fleischer, and R. Tenne, *Applications of WS 2 (MoS 2) inorganic nanotubes and fullerene-like nanoparticles for solid lubrication and for structural nanocomposites.* Journal of Materials Chemistry, 2005. **15**(18): p. 1782-1788.

73.	Kimura, Y., et al., *Boron nitride as a lubricant additive.* Wear, 1999. **232**(2): p. 199-206.

74.	Nosonovsky, M. and B. Bhushan, *Green tribology: biomimetics, energy conservation and sustainability.* 2012: Springer.

75.	Smolyanitsky, A., J.P. Killgore, and V.K. Tewary, *Effect of elastic deformation on frictional properties of few-layer graphene.* Physical Review B, 2012. **85**(3): p. 035412.

76.	Lee, C., et al., *Frictional characteristics of atomically thin sheets.* science, 2010. **328**(5974): p. 76-80.

77.	Paton, K.R., et al., *Scalable production of large quantities of defect-free few-layer graphene by shear exfoliation in liquids.* Nature materials, 2014. **13**(6): p. 624.

78.	Chen, X., J.F. Dobson, and C.L. Raston, *Vortex fluidic exfoliation of graphite and boron nitride.* Chemical Communications, 2012. **48**(31): p. 3703-3705.

79.	Cancado, L., et al., *Measuring the degree of stacking order in graphite by Raman spectroscopy.* Carbon, 2008. **46**(2): p. 272-275.

80.	Ferrari, A.C., *Raman spectroscopy of graphene and graphite: disorder, electron–phonon coupling, doping and nonadiabatic effects.* Solid state communications, 2007. **143**(1-2): p. 47-57.

81.	Xing, T., et al., *Disorder in ball-milled graphite revealed by Raman spectroscopy.* Carbon, 2013. **57**: p. 515-519.

82.	Kaniyoor, A. and S. Ramaprabhu, *A Raman spectroscopic investigation of graphite oxide derived graphene.* Aip Advances, 2012. **2**(3): p. 032183.

83.	Nguyen, C., et al., *Viscosity data for Al2O3–water nanofluid—hysteresis: is heat transfer enhancement using nanofluids reliable?* International Journal of Thermal Sciences, 2008. **47**(2): p. 103-111.

84.	Rashidi, A., et al., *Thermal and rheological properties of oil-based nanofluids from different carbon nanostructures.* International Communications in Heat and Mass Transfer, 2013. **48**: p. 178-182.

85.	Kole, M. and T. Dey, *Investigation of thermal conductivity, viscosity, and electrical conductivity of graphene based nanofluids.* Journal of Applied Physics, 2013. **113**(8): p. 084307.

86.	Heine, D.R., M.K. Petersen, and G.S. Grest, *Effect of particle shape and charge on bulk rheology of nanoparticle suspensions.* The Journal of Chemical Physics, 2010. **132**(18): p. 184509.

87.	Williams, J., *Engineering tribology.* 2005: Cambridge University Press.

88.	Jackson, R. and I. Green, *The behavior of thrust washer bearings considering mixed lubrication and asperity contact.* Tribology Transactions, 2006. **49**(2): p. 233-247.

89.	Lee, C.-H. and A.A. Polycarpou, *Static friction experiments and verification of an improved elastic-plastic model including roughness effects.* Journal of Tribology, 2007. **129**(4): p. 754-760.

90.	Lee, C.-H., M. Eriten, and A.A. Polycarpou, *Application of elastic-plastic static friction models to rough surfaces with asymmetric asperity distribution.* Journal of Tribology, 2010. **132**(3).

91. Kogut, L. and I. Etsion, *A static friction model for elastic-plastic contacting rough surfaces.* Journal of Tribology, 2004. **126**(1): p. 34-40.

92. Etsion, I., et al., *Experimental investigation of the elastic–plastic contact area and static friction of a sphere on flat.* Journal of Tribology, 2005. **127**(1): p. 47.

93. Lahouij, I., et al., *In Situ TEM Observation of the Behavior of an Individual Fullerene-Like MoS_2 Nanoparticle in a Dynamic Contact.* Tribology Letters, 2011. **42**(2): p. 133-140.

94. Ou, J., et al., *Tribology Study of Reduced Graphene Oxide Sheets on Silicon Substrate Synthesized via Covalent Assembly.* Langmuir, 2010. **26**(20): p. 15830–15836.

95. Miura, K. and M. Ishikawa, *C60 Intercalated Graphite as Nanolubricants.* Materials 2010. **3**(9).

96. Berman, D., et al., *Extraordinary macroscale wear resistance of one atom thick graphene layer.* Advanced Functional Materials, 2014. **24**(42).

97. Filleter, T., et al., *Friction and Dissipation in Epitaxial Graphene Films.* PHYSICAL REVIEW LETTERS, 2009. **102**.

98. Lee, H., et al., *Comparison of frictional forces on graphene and graphite.* Nanotechnology, 2009. **20**(32): p. 325701.

99. Zhang, T., X. Li, and H. Gao, *Fracture of graphene: a review.* International Journal of Fracture, 2015. **196**: p. 1-31.

100. Dhar, P., et al., *The role of percolation and sheet dynamics during heat conduction in poly-dispersed graphene nanofluids.* Applied Physics Letters, 2013. **102**.

101. Meng, Y., F. Su, and Y. Chen, *Au/Graphene Oxide Nanocomposite Synthesized in Supercritical CO_2 Fluid as Energy Efficient Lubricant Additive.* ACS applied materials & interfaces, 2017. **9**(45): p. 39549–39559.

102. Dorri-Moghadam, A., et al., *Functional Metal Matrix Composites: Self-lubricating, Self-healing, and Nanocomposites-An Outlook.* JOM, 2014. **66**(6): p. 872-881.

103. Liu, Y., et al., *Friction and wear of aluminium-graphite composites: the smearing process of graphite during sliding.* Wear, 1992. **159**(2): p. 201-205.

104. Ferguson, J., et al., *On the strength and strain to failure in particle-reinforced magnesium metal-matrix nanocomposites (Mg MMNCs).* Materials Science and Engineering: A, 2012. **558**: p. 193-204.

105. Vogt, R., et al., *The absence of thermal expansion mismatch strengthening in nanostructured metal–matrix composites.* Scripta Materialia, 2009. **61**(11): p. 1052-1055.

106. Baradeswaran, A. and E. Perumal, *Wear and mechanical characteristics of Al 7075/graphite composites.* Composites: Part B, 2014. **56**: p. 472–476.

107. Baradeswaran, A. and A.E. Perumal, *Study on mechanical and wear properties of Al 7075/Al2O3/Graphite hybrid composites.* Composites: Part B, 2014. **56**: p. 464–471.

108. Iacob, G., et al., *Studies on wear rate and micro-hardness of the Al/Al 2 O 3/Gr hybrid composites produced via powder metallurgy.* Composites Part B: Engineering, 2015. **69**: p. 603-611.

109. Liu, X.-B., et al., *Effects of temperature and normal load on tribological behavior of nickel-based high temperature self-lubricating wear-resistant composite coating.* Composites Part B: Engineering, 2013. **53**: p. 347-354.

217

110. Rohatgi, P.K., et al., *Tribology of metal matrix composites*, in *Tribology for scientists and engineers*. 2013, Springer. p. 233-268.

111. Kestursatya, M., J. Kim, and P. Rohatgi, *Wear performance of copper–graphite composite and a leaded copper alloy.* Materials Science and Engineering: A, 2003. **339**(1): p. 150-158.

112. Liu, Y., P. Rohatgi, and S. Ray, *Tribological characteristics of aluminum-50 vol pct graphite composite.* Metallurgical Transactions A, 1993. **24**(1): p. 151-159.

113. Rohatgi, P., S. Ray, and Y. Liu, *Tribological properties of metal matrix-graphite particle composites.* International Materials Reviews, 1992. **37**(1): p. 129-152.

114. Krishnan, B., et al., *Performance of an Al-Si-graphite particle composite piston in a diesel engine.* Wear, 1980. **60**(1): p. 205-215.

115. Badia, F. and P. Rohatgi, *Dispersion of graphite particles in aluminum castings through injection of the melt.* 1969.

116. Bakshi, S., D. Lahiri, and A. Agarwal, *Carbon nanotube reinforced metal matrix composites - a review.* International Materials Reviews, 2010. **55**(1): p. 41-64.

117. Deng, C.F., et al., *Processing and properties of carbon nanotubes reinforced aluminum composites.* Materials Science and Engineering A, 2007. **444**(1-2): p. 138.

118. Rajkumar, K. and S. Aravindan, *Tribological behavior of microwave processed copper–nanographite composites.* Tribology International, 2013. **57**: p. 282.

119. Omrani, E., et al., *New emerging self-lubricating metal matrix composites for tribological applications*, in *Ecotribology*. 2016, Springer. p. 63-103.

120. Omrani, E., P.L. Menezes, and P. Rohatgi, *Tribology and Applications of Self-Lubricating Materials*. 2017: CRC Press.

121. Menezes, P.L., P.K. Rohatgi, and M.R. Lovell, *Self-Lubricating Behavior of Graphite Reinforced Metal Matrix Composites*, in *Green Tribology*. 2012, Springer. p. 445-480.

122. Menezes, P.L., C.J. Reeves, and M.R. Lovell, *Fundamentals of lubrication*, in *Tribology for Scientists and Engineers*. 2013, Springer. p. 295-340.

123. Menezes, P.L., et al., *Friction and wear*, in *Tribology for Scientists and Engineers*. 2013, Springer. p. 43-91.

124. Ludema, K.C., *Friction, wear, lubrication: a textbook in tribology*. 2010: CRC press.

125. Stachowiak, G.P., G.W. Stachowiak, and P. Podsiadlo, *Automated classification of wear particles based on their surface texture and shape features.* Tribology International, 2008. **41**(1): p. 34-43.

126. Reeves, C.J., et al., *Tribology of Solid Lubricants*, in *Tribology for Scientists and Engineers*. 2013, Springer. p. 447-494.

127. Rohatgi, P.K., et al. *Addition of Solid Lubricants to Metal Matrices and Liquid Lubricants to Improve Tribological Performance*. in *ASIATRIB - 2014*. 2014.

128. Menezes, P.L., et al., *Green lubricants: role of additive size*, in *Green Tribology*. 2012, Springer. p. 265-286.

129. Menezes, P.L., et al., *Self-lubricating behavior of graphite-reinforced composites*, in *Tribology for Scientists and Engineers*. 2013, Springer. p. 341-389.

130. Mannekote, J.K., et al., *Tribology of Green Lubricants*, in *Tribology for Scientists and Engineers*. 2013, Springer. p. 495-521.

131. Patnaik, S., et al., *Wear Characteristics of Aluminium-Graphite Composites Produced by Stir Casting Technique.* Journal of Materials & Metallurgical Engineering, 2014. **4**(3): p. 13-20.

132. Dwivedi, S.K. and S. Patel, *EVALUATION OF HARDNESS OF ALUMINIUM/GRAPHITE PARTICULATE COMPOSITE FABRICATED BY STIR CASTING ROUTE.* EVALUATION, 2014. **3**(01): p. 26-28.

133. Shanmughasundaram, P. and R. Subramanian, *Wear behaviour of eutectic Al-Si alloy-graphite composites fabricated by combined modified two-stage stir casting and squeeze casting methods.* Advances in Materials Science and Engineering, 2013. **2013**.

134. Wu, L.L., et al. *Wear Resistance of Graphite/Aluminium Composites that Prepared by Stirring Casting.* in *Advanced Materials Research.* 2013. Trans Tech Publ.

135. Baghani, A., et al., *Investigation on the Effect of Mold Constraints and Cooling Rate on Residual Stress During the Sand-Casting Process of 1086 Steel by Employing a Thermomechanical Model.* Metallurgical and Materials Transactions B, 2014. **45**(3): p. 1157-1169.

136. Baghani, A., et al., *Application of Computational Fluid Dynamics to study the effects of Sprue Base Geometry on the Surface and Internal Turbulence in gravity casting.* Proceedings of the Institution of Mechanical Engineers, Part L: Journal of Materials Design and Applications, 2013: p. 1464420713500182.

137. Etter, T., et al., *Strength and fracture toughness of interpenetrating graphite/aluminium composites produced by the indirect squeeze casting process.* Materials Science and Engineering: A, 2004. **386**(1): p. 61-67.

138. Zeren, A., *Effect of the graphite content on the tribological properties of hybrid Al/SiC/Gr composites processed by powder metallurgy.* Industrial Lubrication and Tribology, 2015. **67**(3): p. 262-268.

139. Ravindran, P., et al., *Tribological behaviour of powder metallurgy-processed aluminium hybrid composites with the addition of graphite solid lubricant.* Ceramics International, 2013. **39**(2): p. 1169-1182.

140. Chen, J. and I. Huang, *Thermal properties of aluminum–graphite composites by powder metallurgy.* Composites Part B: Engineering, 2013. **44**(1): p. 698-703.

141. Mahdavi, S. and F. Akhlaghi, *Effect of the graphite content on the tribological behavior of Al/Gr and Al/30SiC/Gr composites processed by in situ powder metallurgy (IPM) method.* Tribology Letters, 2011. **44**(1): p. 1-12.

142. Akhlaghi, F. and S. Mahdavi, *Effect of the SiC Content on the Tribological Properties of Hybrid Al/Gr/SiC Composites Processed by In Situ Powder Metallurgy (IPM) Method.* Advanced Materials Research, 2011. **264-265**: p. 1878-1886.

143. Hashemabad, S.G. and T. Ando, *Ignition characteristics of hybrid Al–Ni–Fe 2 O 3 and Al–Ni–CuO reactive composites fabricated by ultrasonic powder consolidation.* Combustion and Flame, 2015. **162**(4): p. 1144-1152.

144. Shanmughasundaram, P. and R. Subramanian, *Wear Behaviour of Eutectic Al-Si Alloy-Graphite Composites Fabricated by Combined Modified Two-Stage Stir Casting and Squeeze Casting Methods.* Advances in Materials Science and Engineering, 2013: p. 1-8.

219

145.   Goto, H., C.V. Suciu, and T. Inokuchi, *Friction and Wear Properties of Aluminum-Silicon Alloy Impregnated Graphite Composite (ALGR-MMC) under Lubricated Sliding Conditions.* Tribology Transactions, 2009. **52**: p. 331-345.

146.   Tabandeh-Khorshid, M., S.A. Jenabali-Jahromi, and M.M. Moshksar, *Mechanical properties of tri-modal Al matrix composites reinforced by nano- and submicron-sized Al2O3 particulates developed by wet attrition milling and hot extrusion.* Materials & design, 2010. **31**(8): p. 3880-3884.

147.   Rohatgi, P. and M. Surappa, *Deformation of graphite during hot extrusion of cast aluminum-silicon-graphite particle composites.* Materials Science and Engineering, 1984. **62**(2): p. 159-162.

148.   Rao, A.K.P., et al., *Microstructural and wear behavior of hypoeutectic Al–Si alloy (LM25) grain refined and modified with Al–Ti–C–Sr master alloy.* Wear, 2006. **261**(2): p. 133-139.

149.   Dwivedi, D.K., *Wear behaviour of cast hypereutectic aluminium silicon alloys.* Materials & design, 2006. **27**(7): p. 610-616.

150.   Chen, M., T. Perry, and A.T. Alpas, *Ultra-mild wear in eutectic Al–Si alloys.* Wear, 2007. **263**(1): p. 552-561.

151.   Vencl, A., I. Bobić, and Z. Mišković, *Effect of thixocasting and heat treatment on the tribological properties of hypoeutectic Al–Si alloy.* Wear, 2008. **264**(7): p. 616-623.

152.   Bai, B. and S. Biswas, *Characterization of dry sliding wear of Al-Si alloys.* Wear, 1987. **120**(1): p. 61-74.

153.   Shafiei-Zarghani, A., S.F. Kashani-Bozorg, and A. Zarei-Hanzaki, *Microstructures and mechanical properties of Al/Al$_2$O$_3$ surface nano-composite layer produced by friction stir processing.* Materials Science and Engineering A,, 2009. **500**: p. 87.91.

154.   Ghasemi-Kahrizsangi, A. and S.F. Kashani-Bozorg, *Microstructure and mechanical properties of steel/TiC nano-composite surface layer produced by friction stir processing.* Surface & Coatings Technology, 2012.

155.   Sharma, S.C., *The sliding wear behavior of Al6061–garnet particulate composites.* Wear, 2001. **249**: p. 1036-1045.

156.   Elmadagli, M., T. Perry, and A.T. Alpas, *A parametric study of the relationship between microstructure and wear resistance of Al–Si alloys.* Wear, 2007. **262**(1-2): p. 79-92.

157.   Moghadam, A.D., et al., *Functional Metal Matrix Composites: Self-lubricating, Self-healing, and Nanocomposites-An Outlook.* JOM, 2014: p. 1-10.

158.   Dorri Moghadam, A., et al., *Mechanical and tribological properties of self-lubricating metal matrix nanocomposites reinforced by carbon nanotubes (CNTs) and graphene–A review.* Composites Part B: Engineering, 2015. **77**: p. 402-420.

159.   Omrani, E., et al., *Mechanical and Tribological Properties of Self-Lubricating Bio-based Carbon-Fabric Epoxy Composites Made Using Liquid Composite Molding.* Tribology International, 2015. **10.1016/j.triboint.2015.06.007**.

160.   Deaquino-Lara, R., et al., *Tribological characterization of Al7075–graphite composites fabricated by mechanical alloying and hot extrusion.* Materials & Design, 2015. **67**: p. 224-231.

161.   Baradeswaran, A. and A. Elaya Perumal, *Effect of graphite on Tribological and mechanical properties of AA7075 composites.* Tribology Transactions, 2015. **58**(1): p. 1-6.

162.   Wu, L.L., et al., *Wear Resistance of Graphite / Aluminium Composites that Prepared by Stirring Casting.* Advanced Materials Research, 2013. **683**: p. 333-338.

163.   Radhika, N., et al., *Dry sliding wear behaviour of aluminium/alumina/graphite hybrid metal matrix composites.* Industrial Lubrication and Tribology, 2012. **64**(6): p. 359-366.

164.   Radhika, N., R. Subramanian, and S.V. Prasat, *Tribological behaviour of Aluminium/Alumina/Graphite hybrid metal matrix composite using taguchi's techniques.* Journal of Minerals and Materials Characterization and Engineering, 2011. **10**(05): p. 427.

165.   Rajaram, G., S. Kumaran, and T.S. Rao, *Fabrication of Al–Si/graphite composites and their structure–property correlation.* Journal of Composite Materials, 2011. **45**(26): p. 2743-2750.

166.   Baradeswaran, A. and A. Elayaperumal, *Wear characteresitic of Al6061 reinforced with graphite under different loads and sppeds.* Advanced Materials Research, 2011. **287-290**: p. 998-1002.

167.   Suresha, S. and B.K. Sridhara, *Wear characteristics of hybrid aluminium matrix composites reinforced with graphite and silicon carbide particulates.* Composites Science and Technology, 2010. **70**(11): p. 1652-1659.

168.   Jinfeng, L., et al., *Effect of Graphite paticle reinforcment on dry sliding wear of SiC/Gr/Al Composites.* Rare Metal Materials and Engineering, 2009. **38**(11): p. 1894-1898.

169.   Fuentes, R., et al., *Wear behavior of a self-lubricating aluminum/graphite composite prepared by powder metallurgy.* Industrial Lubrication and Tribology, 2003. **55**(4): p. 157-161.

170.   Guo, M.L.T. and C.-Y.A. Tsao, *Tribological behavior of self-lubricating aluminium/SiC/graphite hybrid composites synthesized by the semi-solid powder-densification method.* Composites Science and Technology, 2000. **60**(1): p. 65-74.

171.   Mahdavi, S. and F. Akhlaghi, *Effect of the SiC particle size on the dry sliding wear behavior of SiC and SiC–Gr-reinforced Al6061 composites.* Journal of Materials Science, 2011. **46**(24): p. 7883-7894.

172.   Saheb, D.A., *Aluminum Silicon Carbide and Aluminum Graphite Particulate Composites.* ARPN Journal of Engineering and Applied Sciences, 2011. **6**(10).

173.   Srivastava, S., et al., *Study of the wear and friction behavior of immiscible as cast-Al-Sn/Graphite composite.* International Journal of Modern Engineering Research, 2012. **2**(2): p. 25-42.

174.   Shams, S.S. and R.F. El-Hajjar, *Effects of scratch damage on progressive failure of laminated carbon fiber/epoxy composites.* International journal of mechanical sciences, 2013. **67**: p. 70-77.

175.   Oh, S.-I., et al., *Fabrication of carbon nanofiber reinforced aluminum alloy nanocomposites by a liquid process.* Journal of Alloys and Compounds, 2012. **542**(25): p. 111.

176. Nayeb-Hashemi, H. and J. Seyyedi, *Study of the interface and its effect on mechanical properties of continuous graphite fiber-reinforced 201 aluminum.* Metallurgical Transactions A, 1989. **20**(4): p. 727-739.

177. Kiran, T., et al., *Effect of heat treatment on tribological behavior of zinc aluminum alloy reinforced with graphite and SIC particles for journal bearing.* Industrial Lubrication and Tribology, 2015. **67**(4).

178. Mitrović, S., et al., *Tribological Potential of Hybrid Composites Based on Zinc and Aluminium Alloys Reinforced with SiC and Graphite Particles.* Tribology in Industry, 2012. **34**(4): p. 177-185.

179. Kestursatya, M., J. Kim, and P. Rohatgi, *Friction and wear behavior of a centrifugally cast lead-free copper alloy containing graphite particles.* Metallurgical and Materials transactions A, 2001. **32**(8): p. 2115-2125.

180. Rohatgi, P. and B. Pai, *Seizure resistance of cast aluminium alloys containing dispersed graphite particles of various sizes.* Wear, 1980. **59**(2): p. 323-332.

181. Rohatgi, P. and B. Pai, *Seizure resistance of cast aluminum alloys containing dispersed graphite particles of different sizes.* Journal of Tribology, 1979. **101**(3): p. 376-380.

182. Prasad, B., T. Dan, and P. Rohatgi, *Pressure-induced improvement in interfacial bonding between graphite and the aluminium matrix in graphitic-aluminium particle composites.* Journal of materials science letters, 1987. **6**(9): p. 1076-1078.

183. Vedula, M., R. Pangborn, and R. Queeney, *Fibre anisotropic thermal expansion and residual thermal stress in a graphite/aluminium composite.* Composites, 1988. **19**(1): p. 55-60.

184. Rohatgi, P., et al., *Improved damping capacity and machinability of graphite particle-aluminum alloy composites.* Materials Science and Engineering, 1976. **26**(1): p. 115-122.

185. Rohatgi, P., S. Ray, and Y. Liu, *Tribological properties of metal matrix-graphite particle composites.* International Materials Reviews, 1992. **37**: p. 129-152.

186. Yang, J.B., et al., *The tribological characteristics of A356.2Al alloy/Gr(p) composites.* Wear, 2004. **257**: p. 941-952.

187. Das, S., V. Prasad, and T. Ramachandran, *Microstructure and wear of cast (Al-Si alloy)-graphite composites.* Wear, 1989. **133**: p. 173-187.

188. Roy, M., et al., *The effect of participate reinforcement on the sliding wear behavior of aluminum matrix composites.* Metallurgical Transactions A, 1992. **23**(10): p. 2833-2847.

189. Alpas, A. and J. Zhang, *Effect of microstructure (particulate size and volume fraction) and counterface material on the sliding wear resistance of particulate-reinforced aluminum matrix composites.* Metallurgical and Materials Transactions A, 1994. **25**(5): p. 969-983.

190. Van Acker, K., et al., *Influence of tungsten carbide particle size and distribution on the wear resistance of laser clad WC/Ni coatings.* Wear, 2005. **258**(1): p. 194-202.

191. Tokisue, H. and G. Abbaschian, *Friction and wear properties of aluminum-particulate graphite composites.* Materials Science and Engineering, 1978. **34**(1): p. 75-78.

192. A.P. Sannino, H.J.R., *Dry sliding wear of discontinuously reinforced aluminum composites: review and discussion.* Wear, 1995. **189**(1-2): p. 1-19.

193. Tabandeh Khorshid, M., S.A. Jenabali Jahromi, and M.M. Moshksar, *Mechanical properties of tri-modal Al matrix composites reinforced by nano- and submicron-sized Al2O3 particulates developed by wet attrition milling and hot extrusion.* Materials and Design, 2010. **31**: p. 3880-3884.

194. Kollo, L., et al., *Investigation of planetary milling for nano-silicon carbide reinforced aluminium metal matrix composites.* Journal of Alloys and Compounds, 2010. **489**: p. 394-400.

195. Rodrigues de Araujo, E., et al., *Preparation of Metal Matrix Aluminum Alloys Composites Reinforced by Silicon Nitride and Aluminum Nitride through Powder Metallurgy Techniques.* Materials Science Forum, 2012. **727-728**: p. 259-262.

196. Hofmeister, C., et al., *Composition and structure of nitrogen-containing dispersoids in trimodal aluminum metal–matrix composites.* Journal of Materials Science, 2010. **45**: p. 4871-4876.

197. Derakhshandeh Haghighi, R., et al., *A Comparison Between ECAP and Conventional Extrusion for Consolidation of Aluminum Metal Matrix Composite.* Journal of Materials Engineering and Performance, 2012. **21**: p. 1885-1892.

198. Li, Y., et al., *Deformation twinning in boron carbide particles within nanostructured Al 5083/B4C metal matrix composites.* Philosophical Magazine, 2010. **90**: p. 783-792.

199. Knowles, A.J., et al., *Microstructure and mechanical properties of 6061 Al alloy based composites with SiC nanoparticles.* Journal of Alloys and Compounds, 2014: p. http://dx.doi.org/10.1016/j.jallcom.2014.01.134.

200. Kondoh, K., J. Umeda, and R. Watanabe, *Cavitation resistance of powder metallurgy aluminum matrix composite with AlN dispersoids.* Materials Science and Engineering A, 2009. **499**: p. 440-444.

201. Saheb, N., et al. *Carbon Nanotube reinforced Al6061 AND Al2124 nanocomposites.* in *ECCM15-15TH European Conference on Composite Materials*. 2012. Venice, Italy.

202. Esawi, A.M.K., et al., *The influence of carbon nanotube (CNT) morphology and diameteron the processing and properties of CNT-reinforced aluminium composites.* Composites: Part A, 2011. **42**: p. 234–243.

203. Wang, J., et al., *Reinforcement with graphene nanosheets in aluminum matrix composites.* Scripta Materialia, 2012. **66**: p. 594-597.

204. Bartolucci, S.F., et al., *Graphene–aluminum nanocomposites.* Materials Science and Engineering A, 2011. **528**: p. 7933-7937.

205. Bastwros, M., et al., *Effect of ball milling on graphene reinforced Al6061 composite fabricated by semi-solid sintering.* Composites: Part B, 2014. **60**: p. 111-118.

206. Rashad, M., et al., *Effect of Graphene Nanoplatelets addition on mechanical properties of pure aluminum using a semi-powder method.* Progress in Natural Science: Materials International, 2014. **24**: p. 101-108.

207. Pérez-Bustamante, R., et al., *Microstructural and hardness behavior of graphene-nanoplatelets/aluminum composites synthesized by mechanical alloying.* Journal of Alloys and Compounds, 2014: p. http://dx.doi.org/10.1016/j.jallcom.2014.01.225.

208. Tjong, S.C., *Recent progress in the development and properties of novel metal matrix nanocomposites reinforced with carbon nanotubes and graphene nanosheets.* Materials Science and Engineering R, 2013. **74**(10): p. 281–350.

209. Berger, C., et al., J. Phys. Chem. B, 2004. **108**.

210. Berger, C., et al., *Electronic Confinement and Coherence in Patterned Epitaxial Graphene.* Sience, 2006. **312**: p. 1191-1196

211. Reina, A., et al., *Layer Area, Few-Layer Graphene Films on Arbitrary Substrates by Chemical Vapor Deposition.* Nano letters 2009. **9**(8): p. 3087.

212. Li, X., et al., *Large-Area Synthesis of High-Quality and Uniform Graphene Films on Copper Foils.* Science, 2009. **324**(5932): p. 1312.

213. Li, X., et al., *Evolution of Graphene Growth on Ni and Cu by Carbon Isotope Labeling.* Nano Letter, 2009. **9**(12): p. 4268.

214. Zhao, L., et al., *Influence of copper crystal surface on the CVD growth of large area monolayer graphene.* Solid State Communications, 2011. **151**(7): p. 509.

215. Tsai, J.-L. and J.-F. Tu, *Characterizing mechanical properties of graphite using molecular dynamics simulation.* Materials & Design, 2010. **31**(1): p. 194.

216. Zheng, Q., et al., *Effects of functional groups on the mechanical and wrinkling properties of graphene sheets.* Carbon, 2010. **48**(15): p. 4315.

217. Lee, C., et al., *Measurement of the Elastic Properties and Intrinsic Strength of Monolayer Graphene.* Science, 2008. **321**(5887): p. 385.

218. Balandin, A.A., et al., *Superior Thermal Conductivity of Single-Layer Graphene.* nano Letter, 2008. **8**(3): p. 902-907.

219. Bolotin, K.I., et al., *Ultrahigh electron mobility in suspended graphene.* Solid State Communications, 2008. **146**(9-10): p. 351-355.

220. Wang, J., et al., *Reinforcement with graphene nanosheets in aluminum matrix composites.* Scripta Materialia, 2012. **66**(8): p. 594.

221. Zhu, Y., et al., *Graphene and Graphene Oxide: Synthesis, Properties, and Applications.* Advanced Materials 2010. **22**: p. 1-19.

222. Choi, W., et al., *Synthesis of Graphene and Its Applications: A Review.* Critical Reviews in Solid State and Material Sciences, 2010. **35**: p. 52-71.

223. Yoon, D., Y.-W. Son, and H. Cheong, *Negative Thermal Expansion Coefficient of Graphene Measured by Raman Spectroscopy.* Nano Letters, 2011. **11**: p. 3227-3231.

224. Lee, C., et al., *Measurement of the elastic properties and intrinsic strength of monolayer graphene.* Science, 2008. **321**: p. 385-388.

225. Novoselov, K.S., et al., *Two-dimensional atomic crystals.* Proceedings of the National Academy of Sciences of the United States of America, 2005. **102**: p. 10451-10453.

226. He, T., et al., *Preparation and Consolidation of Alumina/Graphene Composite Powders.* Materials Transactions, 2009. **50**: p. 749-751.

227. Zhao, W., et al., *Preparation of graphene by exfoliation of graphite using wet ball milling.* Journal of Materials Chemistry, 2010. **20**: p. 5817-5819.

228. Li, Q., et al., *Improved processing of carbon nanotube/magnesium alloy composites.* Composites Science and Technology, 2009. **69**: p. 1193-1199.

229. Rafiee, M.A., et al., *Buckling resistant graphene nanocomposites.* Applied Physics Letters, 2009. **95**: p. 223103-1-3.

230. Zheng, D., et al., *In situ thermal reduction of graphene oxide for high electrical conductivity and low percolation threshold in polyamide 6 nanocomposites.* Composites Science and Technology, 2012. **72**: p. 284-289.

231. Shin, S.E., et al., *Strengthening behavior of few-layered graphene/aluminum composites.* Carbon, 2015. **82**: p. 143-151.

232. Wang, J., et al., *Reinforcement with graphene nanosheets in aluminum matrix composites.* Scripta Materialia, 2012. **66**: p. 594-597.

233. Bartoluccia, S.F., et al., *Graphene–aluminum nanocomposites.* Materials Science and Engineering A, 2011. **528**: p. 7933-7937.

234. Chen, L.-Y., et al., *Novel nanoprocessing route for bulk graphene nanoplatelets reinforced metal matrix nanocomposites.* Scripta Materialia, 2012. **67**: p. 29-32.

235. Bastwros, M., et al., *Effect of ball milling on graphene reinforced Al6061 composite fabricated by semi-solid sintering.* Composites Part B: Engineering, 2014. **60**: p. 111-118.

236. Ghazaly, A., B. Seif, and H.G. Salem, *Mechanical and Tribological Properties of AA2124-Graphene Self Lubricating Nanocomposite.* Light Metals 2013, 2013: p. 411-415.

237. Rafiee, M.A., et al., *Enhanced mechanical properties of nanocomposites at low graphene content.* ACS nano, 2009. **3**(12): p. 3884-3890.

238. Stankovich, S., et al., *Graphene-based composite materials.* Nature, 2006. **442**(7100): p. 282-286.

239. Xu, C., X. Wang, and J. Zhu, *Graphene− metal particle nanocomposites.* The Journal of Physical Chemistry C, 2008. **112**(50): p. 19841-19845.

240. Tabandeh-Khorshid, M., et al., *Tribological performance of self-lubricating aluminum matrix nanocomposites: role of graphene nanoplatelets.* Engineering Science and Technology, an International Journal, 2016. **19**(1): p. 463-469.

241. !!! INVALID CITATION !!! .

242. Sengupta, R., et al., *A review on the mechanical and electrical properties of graphite and modified graphite reinforced polymer composites.* Progress in Polymer Science, 2011. **36**(5): p. 638-670.

243. Zhao, X., et al., *Enhanced mechanical properties of graphene-based poly (vinyl alcohol) composites.* Macromolecules, 2010. **43**(5): p. 2357-2363.

244. Wang, X., et al., *In situ polymerization of graphene nanosheets and polyurethane with enhanced mechanical and thermal properties.* J. Mater. Chem., 2011. **21**(12): p. 4222-4227.

245. Song, P., et al., *Fabrication of exfoliated graphene-based polypropylene nanocomposites with enhanced mechanical and thermal properties.* Polymer, 2011. **52**(18): p. 4001-4010.

246. Rashad, M., et al., *Improved strength and ductility of magnesium with addition of aluminum and graphene nanoplatelets (Al + GNPs) using semi powder metallurgy method.* Journal of Industrial and Engineering Chemistry, 2014: p. http://dx.doi.org/10.1016/j.jiec.2014.08.024.

247. Ferguson, J.B., et al., *On the superposition of strengthening mechanisms in dispersion strengthened alloys and metal-matrix nanocomposites: Considerations of stress and energy.* Metals and Materials International, 2014. **20**: p. 375-388.

225

248. Chen, L.-Y., et al., *Novel nanoprocessing route for bulk graphene nanoplatelets reinforced metal matrix nanocomposites.* Scripta Materialia, 2012. **67**: p. 29-32.

249. Vogt, R., et al., *The absence of thermal expansion mismatch strengthening in nanostructured metal–matrix composites.* Scripta Materialia 2009. **61**: p. 1052-1055.

250. Ferguson, J.B., et al., *On the strength and strain to failure in particle-reinforced magnesium metal-matrix nanocomposites (Mg MMNCs).* Materials Science & Engineering A, 2012. **558**: p. 193-204.

251. Pérez-Bustamante, R., et al., *Novel Al-matrix nanocomposites reinforced with multi-walled carbon nanotubes.* Journal of Alloys and Compounds, 2008. **450**(1-2): p. 323-326.

252. Cizaire, L., et al., *Mechanisms of ultra-low friction by hollow inorganic fullerene-like MoS2 nanoparticles.* SurfaceandCoatingsTechnology, 2002. **160**: p. 282-287.

253. Jun, Q., A. Linan, and P.J. Blau, *Sliding friction and wear characterristics of Al2O3 Al nanocomposites*, in *STLE/ASME 2006 International Joint Tribology Conference*. 2006: San Antonio, Texas, USA. p. 59-60.

254. Nemati, N., et al., *Investigation of microstructure, hardness and wear properties of Al–4.5 wt.% Cu–TiC nanocomposites produced by mechanical milling.* Materials & design, 2011. **32**(7): p. 3718-3729.

255. Sameezadeh, M., M. Emamy, and H. Farhangi, *Effects of particulate reinforcement and heat treatment on the hardness and wear properties of AA 2024-MoSi 2 nanocomposites.* Materials & design, 2011. **32**(4): p. 2157-2164.

256. Nuriel, S., et al., *Direct measurement of multiwall nanotube surface tension.* Chemical Physics Letters, 2005. **404**(4-6): p. 263.

257. So, K.P., et al., *SiC formation on carbon nanotube surface for improving wettability with aluminum.* Composites Science and Technology, 2013. **74**: p. 6.

258. Lim, J.-Y., et al., *Effects of CNF dispersion on mechanical properties of CNF reinforced A7xxx nanocomposites.* Materials Science & Engineering A, 2012. **556**: p. 337.

259. Neubauer, E., et al., *Potential and challenges of metal-matrix-composites reinforced with carbon nanofibers and carbon nanotubes.* Composites Science and Technology, 2010. **70**(16): p. 2228.

260. Donnet, C. and A. Erdemir, *Historical developments and new trends in tribological and solid lubricant coatings.* Surface & Coatings Technology, 2004. **180-181**: p. 76.

261. Donnet, C. and A. Erdemir, *Solid Lubricant Coatings: Recent Developments and Future Trends.* Tribology Letters, 2004. **17**(3): p. 389.

262. Bhattacharjee, D., K. Muthusamy, and S. Ramanujam, *Effect of load and composition on friction and dry sliding wear behavior of tungsten carbide particle reinforced iron composites.* Tribology Transactions, 2013(just-accepted).

263. Bastwros, M.M.H., A.M.K. Esawi, and A. Wifi, *Friction and wear behavior of Al–CNT composites.* Wear, 2013. **307**(1-2): p. 164-173.

264. Alidokht, S., A. Abdollah-zadeh, and H. Assadi, *Effect of applied load on the dry sliding wear behaviour and the subsurface deformation on hybrid metal matrix composite.* Wear, 2013. **305**(1): p. 291-298.

265. Suresh, S., et al., *Mechanical behavior and wear prediction of stir cast Al–TiB< sub> 2</sub> composites using response surface methodology.* Materials & Design, 2014. **59**: p. 383-396.

266. Desai, R.S., D. Girish, and G. Ravindra Babu, *Effect of wear load and sliding velocity on wear transition behaviour of Al/TiO2 metal matrix composites.* International Journal of Science Research, 2013. **1**(4): p. 237-244.

267. Banerji, A., H. Hu, and A. Alpas, *Sliding wear mechanisms of magnesium composites AM60 reinforced with Al$_2$O$_3$ fibres under ultra-mild wear conditions.* Wear, 2013. **301**(1): p. 626-635.

268. Umanath, K., K. Palanikumar, and S. Selvamani, *Analysis of dry sliding wear behaviour of Al6061/SiC/Al$_2$O$_3$ hybrid metal matrix composites.* Composites Part B: Engineering, 2013. **53**: p. 159-168.

269. Choi, H.J., S.M. Lee, and D.H. Bae, *Wear characteristic of aluminum-based composites containing multi-walled carbon nanotubes.* Wear, 2010. **270**(1-2): p. 12.

270. Huang, H., et al., *An investigation on tribological properties of graphite nanosheets as oil additive.* Wear, 2006. **261**: p. 140-144.

271. Patterson, A., *The Scherrer formula for X-ray particle size determination.* Physical review, 1939. **56**(10): p. 978.

272. Suryanarayana, C., E. Ivanov, and V. Boldyrev, *The science and technology of mechanical alloying.* Materials Science and Engineering: A
2001. **304-306**: p. 151-158.

273. DU, X.M., R.Q. CHEN, and F.G. LIU, *Investigation of Graphene Nanosheets Reinforced Aluminum Matrix Composites.* Digest Journal of Nanomaterials and Biostructures, 2017. **12**(1): p. 37-45.

274. Moghadam, A.D., et al., *Effect of in-situ processing parameters on the mechanical and tribological properties of self-lubricating hybrid aluminum nanocomposites.* Tribology Letters, 2016. **62**(2): p. 25.

275. Moghadam, A.D., et al., *Strengthening in hybrid alumina-titanium diboride aluminum matrix composites synthesized by ultrasonic assisted reactive mechanical mixing.* Materials Science and Engineering: A, 2017. **702**: p. 312-321.

276. Sajjadi, S.A., H.R. Ezatpour, and M.T. Parizi, *Comparison of microstructure and mechanical properties of A356 aluminum alloy/Al2O3 composites fabricated by stir and compo-casting processes.* Materials & Design, 2012. **34**: p. 106-11.

277. Akbari, M.K., H.R. Baharvandi, and O. Mirzaee, *Nano-sized aluminum oxide reinforced commercial casting A356 alloy matrix: Evaluation of hardness, wear resistance and compressive strength focusing on particle distribution in aluminum matrix.* Composites Part B: Engineering, 2013. **52**: p. 262-268.

278. Mazahery, A., H. Abdizadeh, and H.R. Baharvandi, *Development of high-performance A356/nano-Al$_2$O$_3$ composites.* Materials Science and Engineering: A, 2009. **518**(1-2): p. 61-64.

279. Das, S., S.V. Prasad, and T.R. Ramachandran, *Tribology of Al/Si alloy-graphite composites: triboinduced graphite films and the role of silicon morphology.* Materials Science and Engineering: A
1991. **138**(1): p. 123-132.

280. Hocheng, H., et al., *Fundamental turning characteristics of a tribology-favored graphite/aluminum alloy composite material.* Composites Part A: Applied Science and Manufacturing, 1997. **28**(9-10): p. 883-890.

281. Etter, T., et al., *Aluminium carbide formation in interpenetrating graphite/aluminium composites.* Materials Science and Engineering: A, 2007. **448**(1-2): p. 1-6.

282. Antunes, E., et al., *Comparative study of first- and second-order Raman spectra of MWCNT at visible and infrared laser excitation.* Carbon, 2006. **44**(11): p. 2022-2211.

283. Lin, R., *Interface Evolution in Aluminum Matrix Composites During Fabrication.* Key Engineering Materials, 1995. **104-107**: p. 507-522.

284. Li, H., et al., *Mechanical properties and interfacial analysis of aluminum matrix composites reinforced by carbon nanotubes with diverse structures.* Materials Science and Engineering: A, 2013. **577**: p. 120-124.

285. Bakshi, S.R. and A. Agarwal, *An analysis of the factors affecting strengthening in carbon nanotube reinforced aluminum composites.* Carbon, 2011. **49**(2): p. 533-544.

286. Johnson, W.B. and B. Sonuparlak, *Diamond/Al metal matrix composites formed by the pressureless metal infiltration process.* Journal of Materials Research, 1993. **8**(5): p. 1169-1173.

287. Suh, N.P., *An overview of the delamination theory of wear.* Wear, 1977. **44**(1): p. 1-16.

CURRICULUM VITAE

EDUCATION

ABD	PhD.	Materials Science and Engineering, University of Wisconsin-Milwaukee
2010	M.S.	Materials Science and Engineering, , K.N. Toosi University of Technology - Iran
2007	B.S.	Metallurgical Engineering, Ferdowsi University of Mashhad- Iran

POSITIONS HELD

2017	**Associate Lecturer,** Mechanical Engineering Technology, University of Wisconsin-Green Bay
2015- Present	**Research Assistant/ Lab manager**, University of Wisconsin-Milwaukee
2015- Present	**Teaching Assistant**, Management Sciences, University of Wisconsin-Milwaukee
2009-2011	**Adjunct Instructor**, College of Engineering, University of Applied Science and Technology, Iran
2007-2011	**Research Engineer**, Iranian Welding Research & Engineering Centre, Iran

TEACHING EXPERIENCE

"Chemistry for Engineers", Associate Lecturer, Mechanical Engineering Technology, University of Wisconsin-Green Bay.

"Engineering Composites", Teaching Assistant, Department of Mechanical Engineering, University of Wisconsin- Milwaukee.

"Supply Chain Management", Teaching Assistant, Department of Business Administration, University of Wisconsin- Milwaukee.

"Introduction to Supply Chain Management", Teaching Assistant, Department of Business Administration, University of Wisconsin- Milwaukee.

"Operations Planning and Control", Teaching Assistant, Department of Business Administration, University of Wisconsin- Milwaukee.

"Supply Chain Technology and Simulation", Teaching Assistant, Department of Business Administration, University of Wisconsin- Milwaukee.

"Basic Engineering Thermodynamics", Instructor, University of Applied Science and Technology, Iran.

"Mechanical Properties of Materials", Instructor, University of Applied Science and Technology, Iran.

"Physical Properties of Materials", Instructor, University of Applied Science and Technology, Iran.

"Friction and Wear", Teaching Assistant, Department of Mechanical Engineering, University of Wisconsin- Milwaukee.

Summary of Research Publications

h-Index = 11, Citations ~ 580; Books – 2; Chapters - 4; Journal articles – 17; Conference presentation – 11

Peer Reviewed Papers (First Author: 10)

1. Moghadam, Afsaneh Dorri, Emad Omrani, Hugo Lopez, Le Zhou, Yongho Sohn, and Pradeep K. Rohatgi. "Strengthening in Hybrid Alumina-Titanium Diboride Aluminum Matrix composites synthesized by Ultrasonic Assisted Reactive Mechanical Mixing." Materials Science and Engineering: A (2017).

2. Balali, Mohammad Hasan, Narjes Nouri, Emad Omrani, Adel Nasiri, and Wilkistar Otieno. "An overview of the environmental, economic, and material developments of the solar and wind sources coupled with the energy storage systems." International Journal of Energy Research (2017).

3. Etemadi, R., B. Wang, K. M. Pillai, B. Niroumand, E. Omrani, and P. Rohatgi. "Pressure Infiltration Processes to Synthesis Metal Matrix Composites-A Review of Metal Matrix Composites, the Technology and Process Simulation." Materials and Manufacturing Processes just-accepted (2017).

4. Emad Omrani, Ahmad P. Tafti, Mojtaba F. Fathi, Afsaneh Dorri Moghadam, Pradeep Rohatgi, Roshan M. D'Souza, and Zeyun Yu. "Tribological study in microscale using 3D SEM surface reconstruction." Tribology International 103 (2016): 309-315.

5. Emad Omrani, Bamdad Barari, Afsaneh Dorri Moghadam, Pradeep L. Menezes, Krishna M. Pillai, and Pradeep K. Rohatgi. "Mechanical, physical and tribological characterization of nano-cellulose fibers reinforced bio-epoxy

231

composites: An attempt to fabricate and scale the 'Green'composite." Carbohydrate polymers 147 (2016): 282-293.

6.   Emad Omrani, Afsaneh Dorri Moghadam, Pradeep L. Menezes, and Pradeep K. Rohatgi. "Effect of in-situ processing parameters on the mechanical and tribological properties of self-lubricating hybrid aluminum nanocomposites." Tribology Letters 62, no. 2 (2016): 1-10.

7.   Emad Omrani, Afsaneh Dorri Moghadam, Pradeep L. Menezes, and Pradeep K. Rohatgi. "Influences of graphite reinforcement on the tribological properties of self-lubricating aluminum matrix composites for green tribology, sustainability, and energy efficiency—a review." The International Journal of Advanced Manufacturing Technology 83, no. 1-4 (2016): 325-346.

8.   Emad Omrani, Afsaneh Dorri Moghadam, Mahmoud Algazzar, Pradeep L. Menezes, and Pradeep K. Rohatgi. "Effect of graphite particles on improving tribological properties Al-16Si-5Ni-5Graphite self-lubricating composite under fully flooded and starved lubrication conditions for transportation applications." The International Journal of Advanced Manufacturing Technology (2016): 1-11.

9.   Emad Omrani, Pradeep L. Menezes, and Pradeep K. Rohatgi. "State of the art on tribological behavior of polymer matrix composites reinforced with natural fibers in the green materials world." Engineering Science and Technology, an International Journal 19, no. 2 (2016): 717-736.

10.   Tabandeh-Khorshid, Meysam, Emad Omrani, Pradeep L. Menezes, and Pradeep K. Rohatgi. "Tribological performance of self-lubricating aluminum matrix nanocomposites: role of graphene nanoplatelets." Engineering Science and Technology, an International Journal 19, no. 1 (2016): 463-469.

11.   Emad Omrani, Afsaneh Dorri Moghadam, Pradeep L. Menezes, and Pradeep K. Rohatgi. "Mechanical and tribological properties of self-lubricating metal matrix nanocomposites reinforced by carbon nanotubes (CNTs) and graphene–a review." Composites Part B: Engineering 77 (2015): 402-420.

12.   Emad Omrani, Bamdad Barari, Afsaneh Dorri Moghadam, Pradeep K. Rohatgi, and Krishna M. Pillai. "Mechanical and tribological properties of self-lubricating bio-based carbon-fabric epoxy composites made using liquid composite molding." Tribology International 92 (2015): 222-232.

13.   Moghadam, Afsaneh Dorri, Benjamin F. Schultz, J. B. Ferguson, Emad Omrani, Pradeep K. Rohatgi, and Nikhil Gupta. "Functional metal matrix composites: self-lubricating, self-healing, and nanocomposites-an outlook." JOM 66, no. 6 (2014): 872-881.

14.   Etaati, A., Ali Shokuhfar, Emad Omrani, P. Movahed, H. Bolvardi, and H. Tavakoli. "Study on homogenization time and cooling rate on microstructure and hardness of Ni-42.5 wt% Ti-3wt% Cu alloy." In Defect and Diffusion Forum, vol. 297, pp. 489-494. Trans Tech Publications, 2010.

15.   Emad Omrani, Ali Shokuhfar, A. Etaati, M. Dorri, and A. Saatian. "The effects of homogenization time and cooling environment on microstructure and transformation temperatures of Ni-42.5 wt% Ti-7.5 wt% Cu alloy." In Defect and Diffusion Forum, vol. 297, pp. 344-350. Trans Tech Publications, 2010.

16.   A. Dorri M., H. Izadi, E. Omrani, "Study on the Failure of Stage 1 Nozzles in the Gas Turbine", Published in Iranian Scientific, Research and Industrial Welding Quarterly, Vol. 33, P. 46.

233

17.   E. Omrani, "Corrosion of Stainless Steel Used For Marine Structure and the Ways to Prevent It", Published in Iranian Scientific, Research and Industrial Welding Quarterly, Vol. 32, P. 14.

Books and Chapters Publication

1.   Emad Omrani, Pradeep L. Menezes, and Pradeep K. Rohatgi, "Tribology of Self-lubricating Materials and Applications." CRC Press.

2.   Emad Omrani, Pradeep L. Menezes, and Pradeep K. Rohatgi, "Advances in Self Lubricating composites." Springer.

3.   Emad Omrani, Afsaneh Dorri Moghadam, Pradeep L. Menezes, and Pradeep K. Rohatgi. "New emerging self-lubricating metal matrix composites for tribological applications." In Ecotribology, pp. 63-103. Springer International Publishing, 2016.

4.   Rohatgi, Pradeep K., Meysam Tabandeh-Khorshid, Emad Omrani, Michael R. Lovell, and Pradeep L. Menezes. "Tribology of metal matrix composites." In Tribology for scientists and engineers, pp. 233-268. Springer New York, 2013.

5.   General Metallurgy and Material Selection, Education Ministry of Iran, 2010, ISBN 964-05-1879-4.

6.   Comprehensive problems in Materials Science and Engineering, Modaresan Sharif Press, 2nd Edition, 2010, ISBN 978-964-187-107-1.

Conference Presentations

1. Omrani, Emad; Dorri Moghadam, Afsaneh; Menezes, Pradeep; Rohatgi, Pradeep, Role of Graphene Nanoplatelets on Tribological Properties of Self-lubricating Aluminium Matrix Nanocomposites, MS&T'17, Oct 8-12, 2017, David L. Lawrence Convention Centre, Pittsburgh, PA USA

2. Omrani, Emad; Dorri Moghadam, Afsaneh; Rohatgi, Pradeep, Lightweight Self-lubricating Aluminum Matrix Composites Reinforced by Graphene, MS&T'17, Oct 8-12, 2017, David L. Lawrence Convention Centre, Pittsburgh, PA USA

3. Omrani, Emad; Dorri Moghadam, Afsaneh; Menezes, Pradeep; Rohatgi, Pradeep, "Challenge Between Aluminum Matrix Nanocomposites and Microcomposites for Tribological Applications", 71st Annual Meeting & Exhibition of the Society of Tribologists and Lubrication Engineers, May 15-19, 2016, Bally's Las Vegas Hotel and Casino, Las Vegas, Nevada USA.

4. Omrani, Emad; Menezes, Pradeep; Rohatgi, Pradeep, "Carbon Allotropes as an Oil Additives, Which One Is More Effective?", 71st Annual Meeting & Exhibition of the Society of Tribologists and Lubrication Engineers, May 15-19, 2016, Bally's Las Vegas Hotel and Casino, Las Vegas, Nevada USA.

5. Omrani, Emad; Dorri Moghadam, Afsaneh; Menezes, Pradeep; Rohatgi, Pradeep, "Effect of in-situ processing parameters on the mechanical and tribological properties of hybrid aluminum nanocomposites", STLE Tribology Frontiers, October 2015, Grand Hyatt Denver, Denver, Colorado.

6. Omrani, Emad; Reeves, Carlton; Menezes, Pradeep; Rohatgi, Pradeep, "Tribological properties of micro- and nano-sized solid lubricant (graphite and

graphene) as lubricant oil additives", STLE Tribology Frontiers, October 2015, Grand Hyatt Denver, Denver, Colorado.

7.   H. Sabetghadam, A. Araee, E. Omrani, G.R. Shirazi, "The effect of bonding temperature on properties of 410SS/Cu diffusion-bonded joint", Proceeding of The International Institute of Welding (IIW) Congress on Welding & Joining, Tehran, Iran.

8.   H. Adgi, A. Halvaee, E. Omrani, A. Hadian, "The effects of testing time and temperature of low vacuum diffusion welding on microstructure and mechanical properties of SiCp/A356 Al MMC", Proceeding of The International Institute of Welding (IIW) Congress on Welding & Joining, Tehran, Iran.

9.   G.R. Shirazi, F. Malek, H. Sabetghadam, E. Omrani, "Weld defects assessment basis on workmanship and Fitness-For-Purpose", Proceeding of The International Institute of Welding (IIW) Congress on Welding & Joining, Tehran, Iran.

10.   E. Omrani, A. Shokuhfar, A. Etaati, A. Dorri M., A. Saatian, "The Effects of Annealing Time and Cooling Environment on Microstructure and Transformation Temperatures of Ni-42.5wt%Ti-7.5wt%Cu Alloy", Proceeding of 5th international conference of DSL, 2009, Rome, Italy.

11.   Etaati, A. Shokuhfar, E. Omrani, P. Movahed, H. Bolvardi, H.Tavakoli, "Study on Homogenization Time and Cooling Rate on Microstructure and Transformation Temperatures of Ni-42.5wt%Ti-3wt%Cu Alloy", Proceeding of 5th international conference of DSL, 2009, Rome, Italy.

Professional Service Activities

- Journal Reviewer: RSC Advances, Critical Review in Solid State and Materials Sciences, Composites Part B: Engineering, Journal of Composite Materials, Tribology Transactions, Lubricants, Journal of Adhesion, Advances in Applied Ceramics, Rare Metals, Chemical Papers, Technologies, Scientific World Journal, Indian Journal of Materials Science, Journal of Mining and Metallurgy, Section B: Metallurgy

- Conference Organizer: MS&T 2016 (Materials Tribology) and MS&T 2017 (Advanced Coatings for Wear and Corrosion Protection)

- Conference Reviewer: MS&T 2016 (Materials Tribology) and MS&T 2017 (Advanced Coatings for Wear and Corrosion Protection)

- Conference Session Chair: MS&T 2016 (Materials Tribology)

- Chapters Reviewer: Advances in Self Lubricating composites

- Project/Grant Reviewer: National Foundation for Science and Technology Development

Collaborations

- Pradeep Rohatgi, Materials Science and Engineering, University of Wisconsin-Milwaukee, WI

- Pradeep Menezes, Mechanical Engineering, University of Nevada-Reno

- Krishna Pillai, Mechanical Engineering, University of Wisconsin-Milwaukee, WI

- Benjamin Schultz, Materials Science and Engineering, University of Wisconsin-Milwaukee, WI

- Nikhil Gupta, Mechanical and Aerospace Engineering, New York University

- Zeyun Yu, Computer Science, University of Wisconsin-Milwaukee, WI

- Ali Shokuhfar, Mechanical Engineering. K.N. Toosi University of Technology